

**CHARACTERIZATION OF MITE-ASSOCIATED VIRUSES IN PLANT
PATHOSYSTEMS OF HAWAII**

**A DISSERTATION SUBMITTED TO THE GRADUATE DIVISION OF THE
UNIVERSITY OF HAWAII AT MĀNOA IN PARTIAL FULFILLMENT OF THE
REQUIREMENTS FOR THE DEGREE OF**

DOCTOR OF PHILOSOPHY

IN

TROPICAL PLANT PATHOLOGY

Fall 2021



BY

ALEJANDRO OLMEDO-VELARDE

DISSERTATION COMMITTEE:

MICHAEL J. MELZER (CHAIRPERSON)

JOHN S. HU

MOHAMMAD ARIF

MICHAEL SHINTAKU

RICHARD MANSHARDT

DEDICATED TO MY FAMILY
AND THE MEMORY OF SARITA, MY MOTHER

ACKNOWLEDGEMENTS

I am deeply thankful to my thesis advisor, Dr. Michael Melzer, for his patience, guidance, continuous support, and encouragement to pursue my professional goals. Mike has been a great advisor and a friend that always shared good advice and transmitted his good vibe and energetic attitude. I am very fortunate to have had the chance to join the Agrosecurity Laboratory and have worked under his tutelage. These last five years have been fantastic and full of great experiences and learning.

Also, I am thankful to Dr. John S. Hu for his guidance and for providing beneficial and wise advice about my future scientific career. He was also a key component of my success during my graduate studies. Many thanks to Dr. Mohammad Arif for all the support, friendship, and willingness to provide some advice or help so that I can succeed in my scientific career.

I am also thankful to the rest of my committee members: Dr. Michael Shintaku and Dr. Richard Manshardt, for their kind patience and input on my PhD research. I am very thankful to past and present Agrosecurity lab members: Asoka, Allie, Tomie, Nelson, Shizu, Jarin, Lisa, and Brandi, for all their help during my five years in the lab. I am also thankful to all the PEPS faculty whose teaching and courses made me the plant pathologist and virologist that I am now. I am grateful to Dr. Shefali Dobhal and the Plant Bacteriology Lab for always being willing to help me and let me borrow any reactive or equipment. I am also grateful to Dr. Wayne Borth for his help and guidance for plant virus purification. His plant virus purification lessons were a key for me to obtain another valuable skill as a plant virologist. Many thanks to Ms. Tina Carvalho for her help and guidance on the TEM and SEM.

I am deeply thankful to all the collaborators of the Agrosecurity lab: Dr. Avijit Roy from USDA ARS NEA BARC, for providing technical help, advice, and support in the citrus leprosis viruses sequencing and any other project. Dr. Ronald Ochoa from USDA ARS Systematic Entomology Laboratory for his kind help, valuable discussions, and advice on identifying brevipalpus mites. I am very thankful and indebted to Dr. Francisco Ochoa-Corona from Oklahoma State University, who introduced me to the lovely world of plant virology during my undergrad internship. Although he was not directly involved with my PhD research, he always guided me and cared for me during my graduate studies.

Last but not least, I would like to thank and acknowledge my family. Adriana, the love of my life, for being patient, always supportive, and being there for me with her unconditional love. My scientific success would not have been possible without you and your love. My father, for always caring for Adriana and me and

allocating his time on our weekend WhatsApp calls. My brothers, Carlos and Pablo, for always being supportive. The Larrea-Sarmiento family, for being like my second family for me, being patient and supportive, and loving me. The Velarde family, for being supportive and always being there for me.

ABSTRACT

Although mites' ability to vector plant viruses was demonstrated long ago, there remains a significant knowledge gap for these viruses and their interactions with their plant host and mite vector compared to other arthropod-vectoring plant viruses. Most mite-transmitted plant viruses are vectored by mites that belong to the superfamily Eriophyoidea and the genus *Brevipalpus* (Acari: Tenuipalpidae). Viruses transmitted by eriophyid mites belong to at least seven genera, but *Emaravirus* members (family *Fimoviridae*) are considered emergent plant viruses of agricultural importance. The viruses transmitted by brevipalpus mites, also known as *Brevipalpus*-transmitted viruses (BTVs), belong to three genera classified within two families, *Dichorhavirus* (family *Rhabdoviridae*) and *Cilevirus* and *Higrevirus* (family *Kitaviridae*). The goal of this study is to lessen the knowledge gap for this group of plant viruses by further characterizing the genomics and biology of new and existing mite-associated viruses. In this work, we identify passionfruit (*Passiflora edulis*) as a new host for the BTV citrus leprosis virus C2 (genus *Cilevirus*). Also, after more than 60 years of absence, we report citrus leprosis in the US and determined it is caused by an orchid strain of the BTV orchid fleck virus (genus *Dichorhavirus*). This discovery has led to an eradication effort for this federally-actionable pest. A new BTV, named hibiscus yellow blotch virus (HYBV), was characterized, and provisionally placed within the genus *Cilevirus*. HYBV represents an evolutionary lineage between cileviruses and higrevirus and was detected in *Brevipalpus yothersi*, representing this new virus's potential vector. New hibiscus and citrus isolates of hibiscus green spot virus 2 (HGSV-2; genus *Higrevirus*) were characterized and found to possess low genetic diversity. The foundation for a reverse genetics system for BTVs was established through the development of an infectious clone of HGSV-2 that was capable of establishing infection in several natural and experimental plant hosts. This represents the first infectious clone developed for a BTV and a critical tool for future research in this arena. Finally, the transmission of HGSV-2 was demonstrated using *B. azores* mites. This is the first report of *B. azores*, having the capability to transmit viruses, and confirms HGSV-2's status as a BTV. The virome of populations of flat mites collected from several plant hosts from two Hawaiian Islands was found to be predominated by picornavirids. Kita and Kita-like viruses were also found and supported a possible evolutionary scenario in which kitavirids emerged from arthropod-specific viruses such as negevirus. A partial sequence of a putative new cile-like virus was found in tenuipalpid mites collected from pineapple. This virome study warrants further examination of flat mite populations from different hosts and geographic origins to surveil for and understand the diversity of BTV and BTV-like agents. Finally, ti ringspot-associated virus (TiRSaV) was characterized and found to contain at least five genomic segments, which could be detected in symptomatic ti plants

(*Cordyline fruticosa*) only. TiRSaV was also detected in two putatively novel species of eriophyid mites recovered from symptomatic plants.

TABLE OF CONTENTS

Content	Page
ACKNOWLEDGEMENTS	3
ABSTRACT	5
TABLE OF CONTENTS	7
LIST OF TABLES	12
LIST OF FIGURES	13
LIST OF ABBREVIATIONS	14
CHAPTER I	18
INTRODUCTION AND LITERATURE REVIEW	18
1.1 Plant virus vectors	18
1.2 Mite pests of agricultural importance	19
1.3 Plant viruses transmitted by mites	20
1.4 Spider mites (Tetranychidae)	20
1.4.1 Plant viruses transmitted by spider mites (Tetranychidae)	21
1.5 Eriophyid mites (Eriophyoidea)	21
1.5.1 Plant viruses transmitted by eriophyid mites (Eriophyoidea)	22
1.6 Flat mites (Tenuipalpidae)	24
1.6.1 Plant viruses transmitted by flat mites (Tenuipalpidae)	25
1.7 <i>Rhabdoviridae</i> -Plant rhabdoviruses	26
1.7.1 <i>Rhabdoviridae-Dichorhavirus</i>	28
1.8 <i>Kitaviridae</i>	29
1.8.1 Higrevirus	32
1.8.2 <i>Cilevirus</i>	34
1.9 Reverse genetics	35
1.10 Infectious clones of RNA viruses	36
1.11 Second and third generation sequencing	38
1.12 LITERATURE CITED	40
OBJECTIVES	52
CHAPTER II	53
CITRUS LEPROSIS VIRUSES IN HAWAII	53

2.1 INTRODUCTION	53
2.2 MATERIALS AND METHODS	54
2.2.1 BTV-C- and BTV-N-specific primer design	54
2.2.2 PCR Annealing Temperature Optimization	55
2.2.3 Tissue collection	55
2.2.4 Virus Detection	56
2.2.5 Genome sequencing	57
2.2.6 Phylogenetic Analyses	58
2.2.7 Barcoding and virus detection in flat mites	58
2.3 RESULTS	58
2.3.1 BTV-specific primers and PCR assay optimization	58
2.3.2 Detection of BTVs in citrus and passion fruit samples	62
2.3.3 Molecular characterization of OFV in citrus and CiLV-C2 in passion fruit in Hawaii	65
2.3.4 BTVs are present as mixed virus infections	65
2.3.5 Phylogenetic relationships of OFV and CiLV-C2	66
2.3.6 Flat mites barcoding and CiLV-C2 detection	67
2.4 DISCUSSION	68
2.5 REFERENCES	72
CHAPTER III	77
MOLECULAR CHARACTERIZATION OF A NEW KITAVIRID INFECTING HIBISCUS IN HAWAII	77
3.1 INTRODUCTION	77
3.2 MATERIALS AND METHODS	78
3.2.1 Tissue collection and virus indexing	78
3.2.2 Genome sequencing	79
3.2.3 Genomic and Proteomic Analyses	81
3.2.4 Phylogenetic Analyses	81
3.2.5 Transmission Electron Microscopy	82
3.2.6 Virus Detection	82
3.2.7 Mite barcoding and virus detection in flat mites	83
3.3 RESULTS	84
3.3.1 Symptom monitoring and virus indexing	84
3.3.2 Molecular characterization of hibiscus yellow blotch virus	84

3.3.3 Transmission electron microscopy	88
3.3.4 Phylogenetic placement of hibiscus yellow blotch virus	89
3.3.5 Protein comparisons between genera in the Kitaviridae family	92
3.3.6 Analyses of untranslated regions of kitavirids	92
3.3.7 Hibiscus yellow blotch virus detection in flat mites	94
3.3.8 Natural mixed infections in hibiscus	95
3.4 DISCUSSION	97
3.5 LITERATURE CITED	101
CHAPTER IV	107
FURTHER MOLECULAR AND BIOLOGICAL CHARACTERIZATION OF HIBISCUS GREEN SPOT VIRUS 2	107
4.1 INTRODUCTION	107
4.2 MATERIALS AND METHODS	108
4.2.1 Virus source and nucleic acid extraction	108
4.2.2 Genome sequencing	108
4.2.3 Construction of a full-length cDNA clone of HGSV-2	111
4.2.4 Preparation and transformation of competent cells	114
4.2.5 Agroinfiltration assays	114
4.2.6 Partial purification, observation and mechanical transmission of the recombinant HGSV-2	115
4.2.7 Establishment of an isoline colony of <i>Brevipalpus</i> sp. mites	116
4.2.8 Transmission assays using <i>Brevipalpus</i> sp. mites	116
4.2.9 (DNase)-RT-PCR and (DNase)-RT-qPCR assays	117
4.2.10 Mite identification using molecular barcoding and scanning electron microscopy, and virus acquisition status	118
4.3 RESULTS	119
4.3.1 HGSV-2 presents distinct genome organization within isolates that have low overall genomic sequence diversity	119
4.3.2 Construction of a full-length cDNA clone of HGSV-2	121
4.3.3 35SRbz-HGSV-2-RNA1/2/3 are infectious in <i>P. vulgaris</i> , <i>N. benthamiana</i> , <i>N. tabacum</i> and <i>H. arnottianus</i> plants	123
4.3.4 Further evidence of the infectivity of 35SRbz-HGSV-2-RNA1/2/3	127
4.3.5 Identification of <i>Brevipalpus</i> specimens used in transmission assays and virus acquisition status	129
4.3.6 <i>B. azores</i> transmits HGSV-2	130

4.4 DISCUSSION	133
4.5 LITERATURE CITED	138
CHAPTER V	143
THE VIROME OF TENUIPALPID MITES IN HAWAII, WITH AN EMPHASIS ON KITA- AND KITA-LIKE VIRUSES	143
5.1 INTRODUCTION	143
5.2 MATERIALS AND METHODS	144
5.2.1 Flat mite specimen collection	144
5.2.2 Nucleic acid extraction	144
5.2.3 Determination of the virome in the tenuipalpid mite samples	145
5.2.4 Virus nomenclature	146
5.2.5 Mite barcoding, virus detection and HTS results confirmation in individual mite samples	146
5.2.6 Genomic and Proteomic Analyses	146
5.2.7 Phylogenetic Analyses	147
5.3 RESULTS	147
5.3.1 Molecular identification of mite samples	147
5.3.2 Analysis of the virome present in tenuipalpid mites	148
5.3.3 Confirmation of virus presence in individual mite samples	152
5.3.4 Molecular characterization of virus contig sequences similar to kitavirids and negevirus	154
5.3.5 Phylogenetic relationships of the tenuipalpid mite populations and putative new negevirus and kitavirids found within the tenuipalpid-associated virome	157
5.4 DISCUSSION	162
5.5 LITERATURE CITED	168
CHAPTER VI	176
MOLECULAR AND BIOLOGICAL CHARACTERIZATION OF A NEW EMARAVIRUS MEMBER LIKELY TRANSMITTED BY ERIOPHYID MITES INFECTING <i>CORDYLINA FRUTICOSA</i> IN HAWAII	176
6.1 INTRODUCTION	176
6.2 MATERIALS AND METHODS	177
6.2.1 Tissue collection and virus source	177
6.2.2 Emaravirus and TiRSaV detection	177
6.2.3 Double-stranded RNA isolation and sequencing	178
6.2.4 Genome assembly	178

6.2.5 Sequence and phylogenetic analyses	179
6.2.6 Mechanical transmission to experimental herbaceous hosts	180
6.2.7 Detection of TiRSaV in eriophyid mites	180
6.3 RESULTS	181
6.3.1 Genome sequencing	181
6.3.2 Genome organization and phylogenetic analyses	184
6.3.3 Mechanical transmission to experimental herbaceous hosts	188
6.3.4 Eriophyid mites and detection of TiRSaV	189
6.4 DISCUSSION	190
6.5 LITERATURE CITED	193
CHAPTER VII	197
CONCLUSIONS AND FUTURE RESEARCH DIRECTIONS	197

LIST OF TABLES

Table 2.1 Cilevirus/Higrevirus-specific, dichorhavirus-specific, and kitavirid-specific primer sets designed using multiple nucleotide sequence alignments and Primaclade (Gadberry et al., 2005)	64
Table 3.1 Primers used in this study for 5' and 3' RACE, genomic sequence validation, and detection of hibiscus yellow blotch virus (HYBV)	85
Table 3.2 Percent amino acid identities between orthologous proteins of hibiscus yellow blotch virus (HYBV) and <i>Kitaviridae</i> members	92
Table 3.3 Kitavirus intra-species nucleotide composition analysis of the 5' and 3' untranslated regions (UTR), and 5' and 3' conserved termini among the genomic segments of each virus species	98
Table 4.1 PCR primers used for the sequencing and detection of citrus and hibiscus isolates of hibiscus green spot virus 2 (HGSV-2), and construction of 35SRbz-HGSV-2-RNA1/2/3 as part of a reverse genetics system for HGSV-2	115
Table 4.2 PCR conditions for linearization of vector pJL89 and pJL89-Fragment1 as well as amplification of Fragments 1 and 2 of HGSV-2-RNA1 and HGSV-2-RNA2 and 3	118
Table 4.3 List of amino acid substitutions found in RNA 1, 2 and 3 of the full-length cDNA clone of HGSV-2 (35SRbz-HGSV-2-RNA1/2/3)	130
Table 4.4 Agroinfiltration experiments of the cotyledonary leaves of <i>P. vulgaris</i> plants using the full-length cDNA clone of HGSV-2	132
Table 4.5 Agroinfiltration results using both the full-length cDNA clone of HGSV-2 ((35SRbz-HGSV-2-RNA1/2/3)) and pJL89 (control) on the cotyledonary and true leaves of <i>H. arnottianus</i> , and the true leaves of <i>N. benthamiana</i> and <i>N. tabacum</i>	133
Table 5.1 Location, identity of the tenuipalpid mites, number of HTS reads and contigs generated for determination of the virome present in each mite sample collected from Oahu and Hawaii Islands	156
Table 5.2 RT-PCR assays results for virus presence confirmation	160
Table 6.1 Primers designed and used in this study for symptom association, specific detection of the 5 TiRSaV RNAs, bridging sequence gaps and RACE	190
Table 6.2 Number of high-throughput sequencing reads and depth of coverage values for the five RNAs that comprise the ti ringspot associated virus (TiRSaV) genome	191
Table 6.3 Percent amino acid identities between orthologous proteins of ti ringspot-associated virus (TiRSaV) and members and putative members of the genus <i>Emaravirus</i>	194

LIST OF FIGURES

Figure 1.1 Diagram summarizing knowledge of plant virus-vectors relationships	22
Figure 1.2 Two-spotted spider mite (<i>Tetranychus urticae</i> , body length ~0.5mm) on common bean leaf	24
Figure 1.3 Wheat curl mites (<i>Aceria tosichella</i>) feeding on wheat leaves	26
Figure 1.4 Genomic organization and virion of emaraviruses	27
Figure 1.5 Flat mites shapes and colors	29
Figure 1.6 Symptoms caused by Brevipalpus-transmitted viruses (BTV) in citrus, hibiscus, orchids, coffee, passionfruit, <i>Solanum violaeifolium</i> and <i>Clerodendrum</i> spp. BTV-C and BTV-N cause a cytopathological effect in cytoplasm and nucleus, respectively	31
Figure 1.7 Comparative genome organization of plant rhabdoviruses and dichorhavirus virion	32
Figure 1.8 Maximum Likelihood phylogenetic tree of the full-length L protein sequences of plant rhabdoviruses	35
Figure 1.9 Phylogenetic relationships of Kitaviridae members	36
Figure 1.10 Genomic organization of cile- and higreviruses	37
Figure 1.11 Cilevirus virion and Higrevirus viroplasms	38
Figure 1.12 Requirements for the development of virus infectious clones	41
Figure 2.1 (A-C) Citrus leprosis (CL) symptoms observed in the leaves	57
Figure 2.2 (A-C) Viral-like symptoms of passion fruit samples collected from three Community Gardens located in Honolulu, Oahu	58
Figure 2.3 Representation of multiple nucleotide sequence alignments for the RNA-dependent RNA polymerase (RdRp) (A) and SP24 (B) genes of BTV-C (cileviruses and higrevirus), and for the RdRp gene (C) of kitavirids (cileviruses, higrevirus and blunerviruses)	63
Figure 2.4 Representation of multiple sequence alignments for the nucleoprotein (N) gene (A) and polymerase (L) gene (B) of dichorhavirus	63
Figure 2.5 Gradient PCR for Cile/Higre-R1-F/R, Cile/Higre-R2-F/R and Kitavirids-F/R within six temperatures ranging from 45°C to 55°C (1 = 45 °C, 2 = 47 °C, 3 = 49 °C, 4 = 51 °C, 5 = 53 °C, 6 = 55 °C). Positive control cDNA preparations for the hibiscus strain of citrus leprosis virus C2 (CiLV-C2) and hibiscus green spot virus (HGSV-2) were used for the assays	64
Figure 2.6 RT-PCR assay for detection of BTV-N RNA 1 (N gene, ~350 bp) and RNA 2 (L gene, ~500 bp) on the pool of RNAs of the citrus samples from Hawaii Island	65
Figure 2.7 RT-PCR assays for detection of BTV-C RNA 1 (RdRp, 280-310 bp) and RNA 2 (p24 gene, 198 bp), and kitavirids RNA 1/2 (RdRp, 411 bp) on the passion fruit leaf samples from Oahu	65
Figure 2.8 RT-PCR assays for detection of OFV using OFV-specific primer sets (OFV-Orc-GPF/GPR and OFV-R2-GF1/GR; Roy et al., 2020) on the citrus leprosis samples from the Hawaii Island	66

Figure 2.9 RT-PCR assays for detection of CiLV-C2 on 19 passion fruit leaf samples from the Ala Wai community garden	67
Figure 2.10 Multiple dsRNA bands observed following resolution by 1X TBE agarose gel electrophoresis	68
Figure 2.11 Phylogenetic relationship of orchid fleck virus (OFV) isolated from Hawaiian citrus with other OFV isolates infecting citrus (Cit1 and Cit2) and orchids (Orc1 and Orc2) based on the concatenated full genomic sequences of RNA 1 and 2	68
Figure 2.12 Phylogenetic relationship of CiLV-C2 (hibiscus isolate of CiLV-C2) infecting passion fruit in Hawaii with other cileviruses based on the RdRp domain nucleotide sequences	69
Figure 2.13 DRT-PCR assays for detection of CiLV-C2 on single brevipalpus (B1-B8) mite specimens	70
Figure 3.1 Variation in lesion symptoms displayed by Hibiscus rosa-sinensis leaves infected by hibiscus yellow blotch virus	83
Figure 3.2 Agarose gel electrophoresis of dsRNAs extracted from hibiscus yellow blotch virus (HYBV)-infected Hibiscus rosa-sinensis leaves (right lane)	88
Figure 3.3 Genome organization comparison between hibiscus yellow blotch virus (HYBV) and Cilevirus and Higreivirus members	89
Figure 3.4 Pairwise protein sequence similarity matrix of the replication-associated polyprotein, p24 and putative movement protein of hibiscus yellow blotch virus (HYBV) with their homologs of Cilevirus, Higreivirus and Blunervirus members using sequence demarcation tool (SDT) 1.2	91
Figure 3.5 Structural alignment results of hibiscus yellow blotch virus (HYBV) p10 and hibiscus green spot virus 2 (HGSV-2) p10 using the Expresso algorithm implemented in T-Coffee	91
Figure 3.6 Panel (A): Electron micrographs of hibiscus yellow blotch virus-infected Hibiscus rosa-sinensis leaves containing aggregates of electron dense spherical structures (arrowheads) typically between 50-60nm in diameter	93
Figure 3.7 Phylogenetic relationships among members of the families Kitaviridae, Virgaviridae, Bromoviridae, Closteroviridae and negeviruses based on an RNA-dependent RNA polymerase (RdRp) multiple protein alignment using CLUSTAL and inferred using Maximum Likelihood algorithm implemented in MEGA 7.0.25	94
Figure 3.8 Phylogenetic placement of hibiscus yellow blotch virus (HYBV) with other viruses possessing conserved proteins	95
Figure 3.9 Agarose gel electrophoresis of 28S rRNA, hibiscus yellow blotch (HYBV) RNA 1 and RNA 2 amplicons using direct RT-PCR (DRT-PCR) assays described by Druciarek et al. (2019)	98
Figure 3.10 Leaves collected from symptomatic Hibiscus spp. plants growing within 1.6 kilometers of the hibiscus yellow blotch virus (HYBV)-infected <i>H. rosa-sinensis</i> plant	100
Figure 3.11 Detection of hibiscus yellow blotch virus (HYBV), citrus leprosis virus C2 (CiLV-C2), and hibiscus green spot virus 2 (HGSV-2) in Hibiscus spp. samples by RT-qPCR (A) and RT-PCR (B) assays	100
Figure 4.1 Symptoms of hibiscus green spot virus 2 infection on <i>Hibiscus arnottianus</i> (left) and <i>Citrus sinensis</i> (right) characterized by the presence of green blotches surrounded by a chlorotic halo	112

Figure 4.2 Schematic diagram of the strategy adapted from Matsumura et al. (2019) to clone the HGSV-2-RNA 1 (8,369 bp) into pJL89	118
Figure 4.3 Set up for the transfer of <i>Brevipalpus</i> sp. mites from an isolate colony to a detached <i>C. sinensis</i> leaf presenting HGSV-2 symptoms and maintained in a 1.5 mL tube containing distilled water	122
Figure 4.4 Genomic organization (A) and diversity (B) of the HGSV-2 isolates sequenced in this study and compared to the original citrus isolate of HGSV-2 (HQ852052-4, Melzer et al., 2012)	125
Figure 4.5 Important sequence differences found in RNA 2 between the original citrus isolate of HGSV-2 (HQ852053) and the HGSV-2 isolates from this study	126
Figure 4.6 Important sequence differences in RNA 3 between the original citrus isolate of HGSV-2 (HQ852054) and the HGSV-2 isolates from this study	126
Figure 4.7 Symptoms caused by the full-length cDNA clone of HGSV-2 (35SRbz-HGSV-2-RNA1/2/3) agroinfiltrated into <i>P. vulgaris</i> cotyledonary leaves	128
Figure 4.8 Symptoms of the accelerated senescence and hypersensitive-response (HR)-like phenotype observed in the <i>P. vulgaris</i> cotyledonary leaves agroinfiltrated with the full-length cDNA clone of HGSV-2 (35SRbz-HGSV-2-RNA1/2/3) after 17-21 dpi (left) and 23-30 dpi (center), and compared to a control leaf inoculated with pJL89 empty vector (right)	128
Figure 4.9 Symptoms caused by 35SRbz-HGSV-2-RNA1/2/3 in the cotyledonary and true leaves of <i>H. arnottianus</i> and the true leaves of <i>N. benthamiana</i> and <i>N. tabacum</i>	131
Figure 4.10 Partially purified virion preparations of the virus progeny from the full-length cDNA clone of HGSV-2 and results of diagnostic DNase-RT-PCR assays	132
Figure 4.11 Necrotic local lesions putatively caused by recombinant HGSV-2 (rHGSV-2) virions mechanically inoculated on <i>N. benthamiana</i> leaves (center)	132
Figure 4.12 DRT-qPCR (left) and DRT-PCR (right) assays for mite barcoding (28S rRNA; upper right) and detection of RNA 1, 2, (left) and 3 (lower right), of HGSV-2	133
Figure 4.13 Physiological characteristics of <i>Brevipalpus azores</i> females used in this study (A and B) and observed with a Hitachi S-4800 Field Emission Scanning Electron Microscope at an accelerating voltage of 5.0 kV	135
Figure 4.14 Symptoms caused by HGSV-2 on a single <i>C. reticulata</i> leaf 21-120 days after exposure to viruliferous <i>B. azores</i> mites	135
Figure 4.15 Transmission of a citrus isolate of HGSV-2 to <i>Hibiscus arnottianus</i> by <i>Brevipalpus azores</i>	136
Figure 5.1 Map detailing plant host and growing location and hosts from which flat mite specimens were collected on the islands of Oahu and Hawaii	151
Figure 5.2 SPAdes de novo assembled contigs with matches to sequences with putative viral origin organized by taxonomical classification (families and order)	156
Figure 5.3 Raw sequence reads of viral origin generated from flat mite libraries are organized by taxonomical order or family	158

Figure 5.4 Genome organization of the BTVs-C, citrus leprosis virus C2 (CiLV-C2) and hibiscus green spot virus 2 (HGSV-2), and the putative new viruses that show relationship to the Kitaviridae family and the unofficial negevirus taxon	163
Figure 5.5 Phylogenetic relationships using partial 28S rRNA gene sequences from several tenuipalpid mites classified within <i>Brevipalpus</i> , <i>Raioella</i> and <i>Dolichotetranychus</i>	165
Figure 5.6 Phylogenetic relationships using partial cytochrome oxidase I (COI) gene sequences from several tenuipalpid mites classified as <i>Brevipalpus</i> , <i>Raioella</i> , <i>Dolichotetranychus</i> and <i>Larvacarus</i>	166
Figure 5.7 Phylogenetic relationships inferred using the RNA-dependent RNA polymerase (RdRp) conserved domain found in the contig sequences of the putative new negeviruses and kitavirids in tenuipalpid mite samples	167
Figure 5.8 Phylogenetic relationships inferred using helicase (HEL) conserved domain found in the contig sequences of the putative new negeviruses and kitavirids in tenuipalpid mite samples	169
Figure 5.9 Phylogenetic relationships inferred using the methyltransferase (MET) conserved domain found in the contig sequences of the putative new negeviruses and kitavirids in tenuipalpid mite samples	169
Figure 6.1 Ringspot symptoms on the leaves of common green ti variety (<i>Cordyline fruticosa</i>)	185
Figure 6.2 Agarose gel electrophoresis of RT-PCR products using primer set specific to putative TiRSaV RNAs (see Table 6.1) to determine if these RNAs were associated with Ti ringspot symptoms and TiRSaV infection	192
Figure 6.3 Genome organization of Ti ringspot associated virus. Shaded boxes represent the predicted open reading frame (ORF) for each RNA	193
Figure 6.4 Phylogenetic placement of Ti ringspot-associated virus (TiRSaV) within the genus Emaravirus using the A) RNA-dependent RNA polymerase (RdRp), B) glycoprotein precursor (GP), C) nucleocapsid (NC), and D) movement protein (MP) sequences	195
Figure 6.5 RT-PCR assays using TiRSaV-RdRp F/R and TiRSaV-NC F2/R2 on systemic leaves of <i>Nicotiana benthamiana</i> and <i>N. tabacum</i> mechanically inoculated with ti ringspot-associated virus (TiRSaV) 30 dpi	196
Figure 6.6 Symptoms on leaves of <i>Nicotiana tabacum</i> infected by ti ringspot-associated virus (TiRSaV)	197
Figure 6.7 28S, ITS regions and TiRSaV genome partial segments amplification from mite cDNA	197

LIST OF ABBREVIATIONS

aa	amino acids
AAP	acquisition access period
AcCRaV	Actinidia chlorotic ringspot-associated virus
ASGPB	Advanced Studies in Genomics, Proteomics, and Bioinformatics Laboratory at University of Hawaii at Manoa
BCMV	bean common mosaic virus
BLMaV	blackberry leaf mottle-associated virus
BMB	binary movement block
BMV	brome mosaic virus
BNRBV	blueberry necrotic ring blotch virus
bp	base pairs
BTV	Brevipalpus-transmitted virus
BTV-C	Brevipalpus-transmitted virus, cytoplasmic type
BTV-N	Brevipalpus-transmitted virus, nuclear type
CaMV	cauliflower mosaic virus
CiCSV	citrus chlorotic spot virus
CiLV-C	citrus leprosis virus C
CiLV-C2	citrus leprosis virus C2
CiLV-C2H	citrus leprosis virus C2, hibiscus strain
CiLV-N	citrus leprosis virus N
CaCV	Capsicum chlorosis orthospovirus
CL	citrus leprosis
ClCSV	Clerodendrum chlorotic spot virus
CMV	cucumber mosaic virus
COI	cytochrome oxidase I
Contigs	contiguous sequences
CoRSV	coffee ringspot virus

CP	coat protein
C-Pro	cysteine protease
CTV	citrus tristeza virus
CVEV	citrus vein enation virus
DMB	double membrane bounded bodies
dpi	days post-inoculation
dsRNA	doubled-stranded RNA
DRT-PCR	direct reverse transcription polymerase chain reaction
DsMV	dasheen mosaic virus
EMARaV	European mountain ash ringspot-associated virus
FMV	fig mosaic virus
G	glycoprotein
GP	glycoprotein precursor
HCRSV	hibiscus chlorotic ringspot virus
HDV-Rbz	hepatitis delta virus ribozyme
HEL	helicase
HGSV-2	hibiscus green spot virus 2
HLFPV	hibiscus latent Fort Pierce virus
HPWMoV	High Plains wheat mosaic virus
HR	hypersensitive response
HTS	high throughput sequencing
HYBV	hibiscus yellow blotch virus
IAP	inoculation access period
ICTV	International Committee on Taxonomy of Viruses
ISEM	immunosorbent electron microscope
ITS	internal transcribed spacer
Kbp	kilobase pairs
L	polymerase
LBVaV	lettuce big vein-associated virus
LNyV	lettuce necrotic yellows virus

MP	movement protein
M	matrix protein
MES	(N-morpholino)-ethanesulfonic acid
MET	methyltransferase
ML	Maximum Likelihood
N or NC	nucleocapsid protein
nt	nucleotide
NTC	non-template control
OD	optical density
OFV	orchid fleck virus
ORF	open reading frame
P	phosphoprotein
PCR	polymerase chain reaction
PfGSV	passion fruit green spot virus
PPSVM 1	pigeonpea sterility mosaic virus 1
PPSVM 2	pigeonpea sterility mosaic virus 2
PRSV	papaya ringspot virus
PTA	phosphotungstic acid
PVBV	palo verde broom virus
PYDV	potato yellow dwarf virus
RACE	rapid amplification of complementary ends
RdRp	RNA-dependent RNA polymerase
rHGSV-2	recombinant hibiscus green spot virus 2
RLBV	raspberry leaf blotch virus
RNP	ribonucleoprotein
RRV	rose rosette virus
RT-PCR	reverse transcription polymerase chain reaction
RT-qPCR	reverse transcription quantitative polymerase chain reaction
RYRSaV	redbud yellow ringspot-associated virus
SDT	sequence demarcation tool

SEM	scanning electron microscope
sgRNA	sub genomic RNA
SP24	membrane protein of plant and insect viruses
ss	single-stranded
ssRNA	single-stranded RNA
SvRSV	Solanum violaeifolium ringspot virus
SYNV	Sonchus yellow net virus
TBSV	tomato bushy stunt virus
T	thymine
TCSV	tomato chlorotic spot orthospovirus
TEM	transmission electron microscope
TFBV	tomato fruit blotch virus
TGB	triple gene block
TiRSaV	ti ringspot-associated virus
TNA	total nucleic acids
TN93	Tamura-Nei
TPNRBV	tea plant necrotic ring blotch virus
TSWV	tomato spotted wilt orthospovirus
UA	uranyl acetate
UTR	untranslated regions
WMV	watermelon mosaic virus
w/v	weight/volume

CHAPTER I

INTRODUCTION AND LITERATURE REVIEW

1.1 Plant virus vectors

There are over 2000 recognized virus species infecting plants belonging to at least 21 families containing at least 92 genera and 2 unassigned genera (Hull 2014a; ICTV 2019). Most plant viruses causing diseases in crops have a positive-sense, single-stranded (ss) RNA genome (Hull 2014a). Over the last decade, virologists have discovered and characterized a tremendous and unprecedented number of viruses using high throughput sequencing (HTS), contributing enormously to our knowledge on the diversity of viruses in nature (Villamor et al., 2019). In fact, due to these numerous contributions, viruses are now the most biodiverse organisms on Earth (Greninger 2018). In the case of plant viruses, new species are being discovered every day and are responsible for up to 47% of the new and emerging diseases affecting crops (Anderson et al., 2004).

The majority of plant viruses rely on biological vectors for their survival, plant-to-plant transmission, and even long-distance spread. Plant virus vectors belong to many groups including insects, mites, nematodes, and zoospore-producing fungi, with plant-feeding insects being the largest class group transmitting plant viruses (Figure 1.1) (Hull 2014a; Dietzgen et al., 2016). Specific and complex virus-vector interactions varying in duration and specificity have evolved in a mutualistic symbiosis, and most of the time at the detriment of the plant (Bragard et al., 2013; Whitfield et al., 2015; Dietzgen et al., 2016).

Plant viruses code for structural proteins expressed on the surface of the virion which are essential for their transmission. In some cases, additional non-structural helper proteins are required to bridge the virion and the protein of the vector binding site. These viral proteins on the virion (also called determinants) bind to specific sites in (or on) the vectors and are retained until transmission is achieved (Dietzgen et al., 2016; Whitfield et al., 2015). Based on the ability of the virus to bind, circulate, or even propagate throughout its vector, three modes of transmission are observed: non-persistent, semi-persistent and persistent. Non-persistent viruses are retained in the vector stylet, semi-persistent viruses are internalized to the vector fore- and mid-gut, and persistent viruses can internalize into vector tissues and can also invade salivary glands. Persistent viruses can be further classified into circulative non-propagative and circulative-propagative based on their ability to replicate within their vector (Bragard et

al., 2013; Dietzgen et al., 2016). The vector transmission timeframes to acquire, retain and inoculate the virus into a new host, after feeding on an infected plant, last from seconds to minutes, hours to days, or days to weeks (or even whole life) for non-persistent, semi-persistent and persistent viruses, respectively (Bragard et al., 2013). Due to these interactions and conserved homology present in and among the protein determinants coded by viruses of the same family or genus, it has been demonstrated and can be inferred, most of the time, that within a given plant virus genus, all members utilize the same type of vector and have the same transmission relationship (Whitfield et al., 2015).

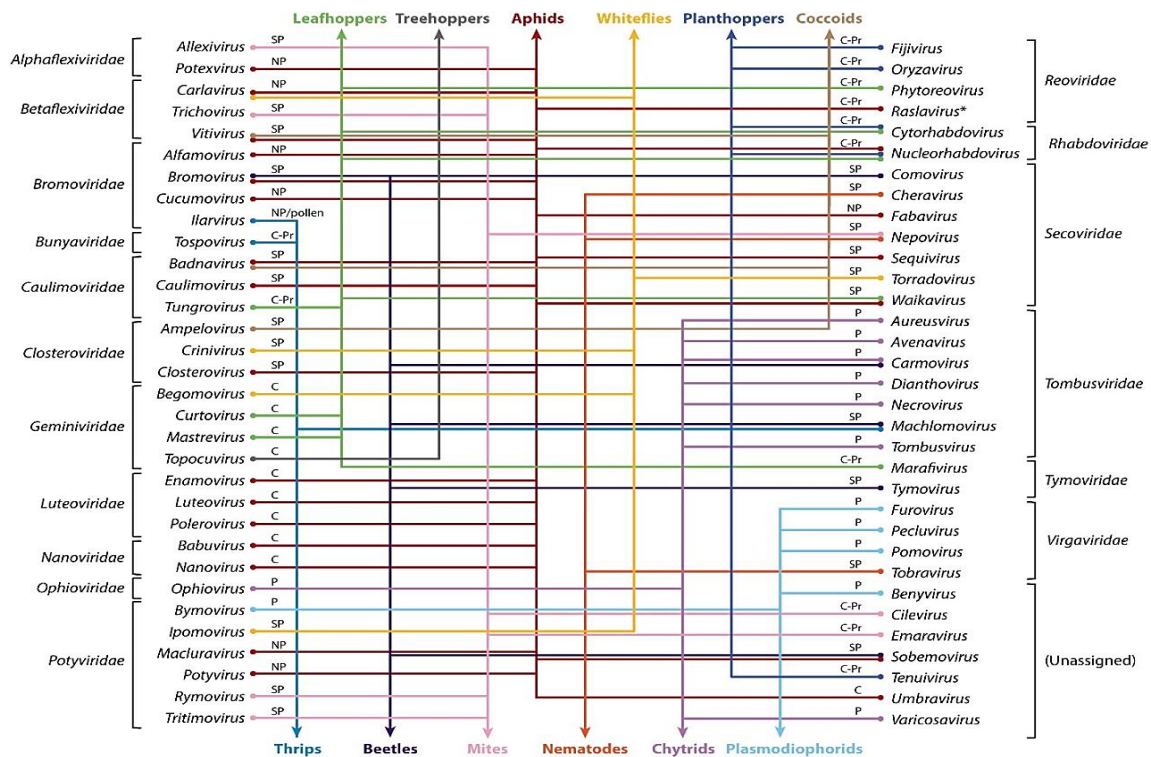


Figure 1.1 Diagram summarizing knowledge of plant virus-vectors relationships. Genera of viruses belonging to different families are connected through colored lines and arrows with their different vectors (common names). Abbreviations: C, circulative (non-propagative); C-Pr, circulative-propagative; NP, non-persistent; P, persistent; SP, semi-persistent. Figure from Bragard et al., (2013).

1.2 Mite pests of agricultural importance

Mites (phylum Arthropoda; class Arachnida; subclass Acari) are numerous species of minute arachnids that are predators, parasites, or saprophytes. They have a body size of usually less than a millimeter and live in a wide range of specialized habitats (Fitzgerald et al., 2007; Bensoussan et al., 2016). Their correct

identification is not an easy task as many species look very similar by the naked eye or under hand-lens (Krants, Lindquist 1979). For their correct identification and description, acaralogists have been using the depth of field and magnification of scanning electron microscope (SEM) for more than 40 years. The sample preparation for SEM, however, requires a series of steps that may cause artifacts in the specimens when compared to light microscopy specimen descriptions. To overcome this, one of the most used approaches that has been developed is the use of a low-temperature field emission SEM (Wergin et al., 2000).

Plant-associated mites can be either beneficial as they predate onto plant pests or can be detrimental as they feed on the plant, although not all are serious plant pests. Phytophagous mites feed by piercing the mesophyll plant cells and ingesting the cellular components (Fitzgerald et al., 2007). They have a short developmental time, typically a female-biased offspring ratio, and a high fecundity that allow them to accumulate large populations and completely infest crops in a few days or weeks (Blaazer et al., 2018). Additionally, some mites can not only transmit plant viruses (Bragard et al., 2013; Dhooria 2016), but also suppress the natural plant defense system which in turn may lead to increased susceptibility to other pests and pathogens. Because of these features, several are important pests and one of the major limiting factors of indoor and outdoor agricultural systems (Dhooria 2016; Blaazer et al., 2018).

Most of the plant-feeding mites belong to five families grouped into two superfamilies: Tetranychidae and Tenuipalpidae families both belonging to the superfamily Tetranychoidae, and Eriophyidae, Phytoptidae and Diptilomiopidae families belonging to the Eriophyoidea superfamily (Gulati 2014). Additionally, there are some members in the order Oribatida, superfamily Eupodoidea and families Tarsonemidae and Tuckerellidae (Gulati 2014; Smith Meyer et al., 2014). They can cause a variety of symptoms: chlorosis, foliage bronzing, stunting, severe defoliation, yield reduction, gall formation, and indirectly by transmitting plant viruses (Gulati 2014). Their members can be both highly specialized and extremely polyphagous (Rioja et al., 2017). According to Dhooria (2016), Tetranychidae (spider mites), Tenuipalpidae (false spider or flat mites) and Eriophyoidea (eriphyid or worm mites) members can transmit plant viruses to different crops. However, other authors only recognize flat mites and worm mites as plant virus vectors (Hull 2014b; Bragard et al., 2013). Virus members belonging to the genera *Allexivirus*, *Trichovirus*, *Rymovirus*, *Tritimovirus*, *Poacevirus*, *Nepovirus*, *Cilevirus*, and *Emaravirus* are transmitted by mites (Figure 1.1) (Bragard et al., 2013; Stenger et al., 2016).

1.3 Plant viruses transmitted by mites

The trend of increasing discovery and characterization of new plant viruses infecting economically important crops due to HTS has also applied to those transmitted (or believed to be transmitted) by mites (Maliogka et al., 2018; Villamor et al., 2019). Mites that transmit plant viruses belong to the families Tetranychidae and Tenuipalpidae, and the superfamily Eriophyoidea (Bragard et al., 2013; Hull 2014b; Dhooria 2016). The ability of Tetranychidae members to transmit plant viruses currently has only limited support in the literature.

1.4 Spider mites (Tetranychidae)

The Tetranychidae family consists of medium sized (0.3-0.8mm) plant-feeding mites that are polyphagous. There are about 1200 species and they have round to oval-shaped bodies. They present a variety of colors: green, brown, red, black, orange, or combinations of these colors depending on the life stage and species (Saito 2010). Generally, they live on the underside of the leaves and make protective silk webs to protect the colony from predators, giving them their name. (Saito 2010; Hull 2014b). These polyphagous mites have a wide variety of hosts at the genus level, however, at the species level almost all species inhabit a very narrow range of hosts (Saito 2010). The genus *Tetranychus* is probably the most economically important as it contains 135 species, and because the cosmopolitan two-spotted spider mite (*T. urticae*) is one of the most infamous plant pests (Figure 1.2) (Saito 2010; Rioja et al., 2017; Bensoussan et al., 2016).



Figure 1.2 Two-spotted spider mite (*Tetranychus urticae*, body length ~0.5mm) on common bean leaf. From [https://commons.wikimedia.org/wiki/File:Tetranychus_urticae_\(4883560779\).jpg](https://commons.wikimedia.org/wiki/File:Tetranychus_urticae_(4883560779).jpg)

1.4.1 Plant viruses transmitted by spider mites (Tetranychidae)

Barley yellow streak mosaic disease was initially identified and closely associated with recurring drought and infestations by the brown wheat mite (*Petrobia latens* Müller) in Montana, USA and Alberta, Canada (Robertson and Carroll 1988). It was demonstrated that the brown wheat mite could transmit the disease by performing a set of experiments using the mite. Long filamentous viral-like particles were observed only in symptomatic barley plants, and the virus was tentatively named barley yellow streak virus. The putative virus was also mechanically transmitted to *Nicotiana benthamiana* and *Chenopodium quinoa*. The same disease was later reported in dryland barley in Idaho, Utah, and Alaska in similar dry conditions and was accompanied by infestations of the brown wheat mite (Skaf 1992; Robertson and Brumfield 2000). Nevertheless, no additional studies were performed to further characterize the disease, the putative virus, or its potential spider mite vector (Dhooria 2016).

1.5 Eriophyid mites (Eriophyoidea)

The Eriophyoidea members are very small sized (less than 0.3 mm) plant-feeding mites. Their host range is generally restricted to one or few closely related plant hosts, as they are highly specialized with dominant monophagy, forming intimate relationships with their hosts. They only have two pairs of legs and their body is elongated like a worm, giving them their common name (Figure 1.3) (Zhang 2017). There are about 5000 species and their numbers keep increasing as they have received tremendous attention by acarologists in recent years. In recent years, more new members of this superfamily have been described than any other mite superfamily (Smith Meyer et al., 2014; Zhang 2017). However, it is also estimated that only ~15-20% and ~5% of eriophyid mite species occurring in temperate and (sub)-tropical regions, respectively, have been described so far (Stenger et al., 2016). According to the symptoms a particular species causes, they may also be called gall mites, witches' broom mites, rust mites, bud mites, blister mites, etc. However, not all eriophyid mites cause visible damage on their hosts (Smith Meyer et al. 2014). Some of the symptoms eriophyid mites cause may be often confused with symptoms caused by plant viruses. There are some eriophyid mite-vectored diseases that have been long studied as they affect economically important crops, although some of them were recently linked to plant viruses vectored by eriophyid mites (Dhooria 2016; Bragard et al., 2013).



Figure 1.3 Wheat curl mites (*Aceria tosichella*) feeding on wheat leaves. From Navia et al., (2013).

1.5.1 Plant viruses transmitted by eriophyid mites (Eriophyoidea)

Eriophyid mite-transmitted viruses are members of the genera *Allexivirus*, *Trichovirus*, *Rymovirus*, *Tritimovirus*, *Poacevirus*, and *Emaravirus* (Stenger et al., 2016). Additionally, blueberry necrotic ring blotch virus (BNRBV) is a *Blunervirus* (family: *Kitaviridae*) member (Quito-Avila et al., 2013; Melzer et al., 2018) that may be vectored by eriophyid mites (Burkle et al., 2012; Robinson et al., 2012). Among all the eriophyid mite-transmitted viruses, *Emaravirus* (family: *Fimoviridae*) members are the ones that have gained the most attention throughout the last few years as the number of described species numbers has increased considerably. Many of these emaraviruses and have been associated with long-studied diseases of unknown or controversial etiology, as well as new, emerging diseases (Kubota 2017).

1.5.1.1 *Fimoviridae*-*Emaravirus*

Emaraviruses (order: *Bunyavirales*, family: *Fimoviridae*) are eriophyid mite-borne negative-sense ssRNA viruses that have a multiple segmented genome with up to ten genomic segments (Elbeaino et al., 2018; Kubota et al., 2020). *European mountain ash ringspot-associated virus* is the former type species of the genus that was created in 2011. Including this virus, there are ten members recognized by the International Committee on Taxonomy of Viruses (ICTV) that belong to the genus. Several putative members, which have not been officially recognized by the ICTV, have been partially and fully characterized in the literature (Mielke-Ehret and Mühlbach 2012; Elbeaino et al., 2018; Kubota et al., 2020). Each genomic segment codes for a single protein. RNA segments 1-4 are considered the core segments coding for RNA-dependent RNA polymerase (RdRp), glycoprotein precursor (GP), nucleocapsid protein (NC) and movement protein (MP), respectively (Figure 1.4A) (Elbeaino et al., 2018; Mielke-Ehret and Mühlbach 2012). RNA segments 5-8 from different members show no clear homology

and their functions are yet to be determined (Zheng et al., 2017) which may lead to hypothesize the plasticity of their genome and perhaps existence of more than ten genomic segments for some species (Stewart 2016). For most of the emaraviruses, it has been demonstrated that they cause similar cytopathic effects in their host plants namely the presence of double membrane bounded bodies (DMBs) with average size of 80-100 nm in the cytoplasm of infected host cells (Figure 1.4B). Both 5' and 3' termini of all the genomic segments have 13-20 nt (depending on the segment) that are conserved and complementary to each other (5'-AGUAGUGUUCUCC-3' at the 5'-end, 5'-GGAGUUCACUACU-3' at the 3'-end). These conserved termini are predicted to be involved in the formation of a 'panhandle structure' typical of negative-sense ssRNA viruses, which may be involved in their replication (Elbeaino et al., 2018).

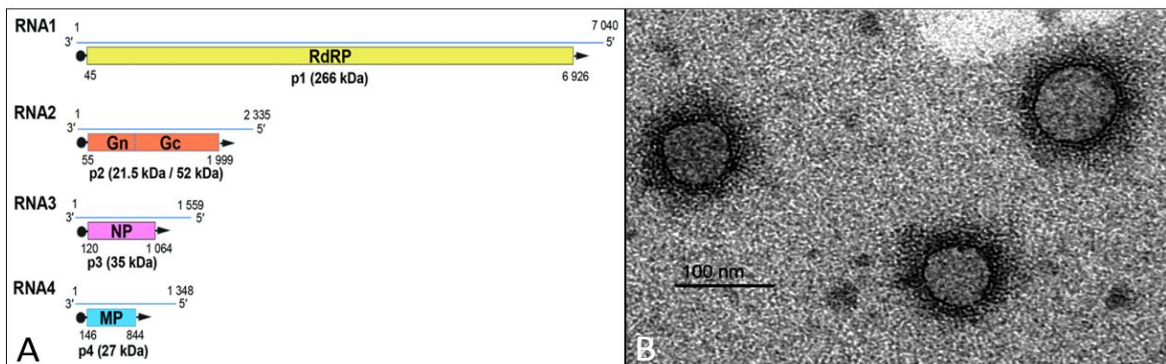


Figure 1.4 Genomic organization and virion of emaraviruses. A) Genomic organization of European mountain ash ringspot-associated virus (EMARaV). All the genes are represented in the virion-complementary sense RNA, from which the proteins are translated. RNA-dependent RNA polymerase (RdRp), glycoprotein (G), nucleocapsid (NC) and movement protein (MP) genes are coded by RNA 1, 2, 3 and 4, respectively. B) Double membrane bounded bodies (DMBs) of EMARaV virions revealed by immunosorbent electron microscope (ISEM). Both figures are from Elbeaino et al., (2018).

After European mountain ash ringspot associated virus (EMARaV) was characterized (Mielke and Muehlbach 2007) and with the use of HTS, additional emaraviruses have been characterized and demonstrated to be the causal agents of long recognized and studied diseases, as well as new and emergent diseases. Pigeonpea sterility mosaic virus 1 (PPSMV 1) and PPSMV 2, rose rosette virus (RRV), high plains wheat mosaic virus (HPWMoV), and fig mosaic virus (FMV) are the causal agents of pigeon pea sterility mosaic disease in pigeonpea (Elbeaino et al., 2015), rose rosette disease in roses (Laney et al., 2011), high plains disease in maize and wheat (Tatineni et al., 2014), and fig mosaic disease

in fig (Elbeaino et al., 2009a; Elbeaino et al., 2009b), which, respectively are examples of long studied diseases of debated etiology whose viral causal agents were only recently characterized.

The symptoms associated with emaraviruses infection are variable and may depend on the host. However, normally blotching, leaf mottling, chlorotic ringspots, vein clearing, sterility of flowers, witches' broom and general mosaic are symptoms associated with emaravirus infection (Elbeaino et al., 2018). Likely, *Emaravirus* members are semi-persistently transmitted by their specific eriophyid mite vector due to the short retention period of the virus in its vector, absence of a latent period, and no report of transovarial transmission (Bragard et al., 2013).

1.6 Flat mites (Tenuipalpidae)

Tenuipalpidae members are known as false spider mites due to their physiological resemblance to spider mites. These mites, however, do not make silk webs, are slow-moving and are dorsoventrally flattened as another common name, flat mite, suggests (Figure 1.5A) (Gerson 2008; Fathipour and Maleknia 2016). They are smaller than spider mites with an average size of 0.25-0.4 mm in length making them very difficult to see by naked eye. Their body shape is variable from elongate, ovoid, round, triangular, pyriform to paper-thin (Figure 1.5B) (Beard et al., 2012; Smith Meyer et al., 2014; Fathipour and Maleknia 2016). Their body presents variations on red color, however, some other color variations from yellow, green, orange to brown are also seen (Figure 1.5B) (Beard et al., 2012). Normally, they feed near the midribs, veins and underside of the leaves, at protected sites in the fruits, and on plant bark and galls. Most of the flat mites have a narrow host range, but some such as the *Brevipalpus phoenicis* species complex, may be polyphagous. They are best adapted to subtropical to tropical regions, not tolerating arid conditions (Gerson 2008; Fathipour and Maleknia 2016; Smith Meyer et al., 2014). Their life cycle comprises five stages: egg, larva, protonymph, deutonymph, and adult. Depending on the temperature, the host plant, and possibly population density, the whole life cycle may take 3-4 weeks and their adult longevity may range from 8-47 days. They reproduce predominantly by thelytoky parthenogenesis, meaning that they can produce offspring without fertilization and females only are produced from unfertilized eggs. Therefore, males are rarely seen for some species and their identification is entirely based on female specimens (Gerson 2008). The scarcity of male tenuipalps may be also attributed as an effect of the bacterial endosymbiont in the *Cardinium* genus that has been found to "feminize" its symbiont (Kitajima et al., 2007).

There are about 1100 described species in the family classified into 38 genera (Beard et al., 2012). *Brevipalpus* and *Tenuipalpus* harbor more than 600 species and are the most economically important genera, however, only some species are major pests causing discernible direct and/or indirect injury and crop yield affection by toxin injection and/or plant virus transmission, respectively (Gerson 2008). The most important species in the family are *B. californicus*, *B. obovatus* and *B. phoenicis* species complexes which are the most intercepted tenuipalpid mites and also vector important quarantine plant viruses. The red palm mite (*Raoiella indica*) which has been spreading to new tropical and subtropical areas in the Western hemisphere is also of regulatory importance in the USA (Beard et al., 2012; Gerson 2008). So far, only *Brevipalpus* mites have been found to transmit plant viruses and some are associated with well known and long studied diseases (Freitas-Astúa et al., 2018; Rodrigues and Childers 2013).

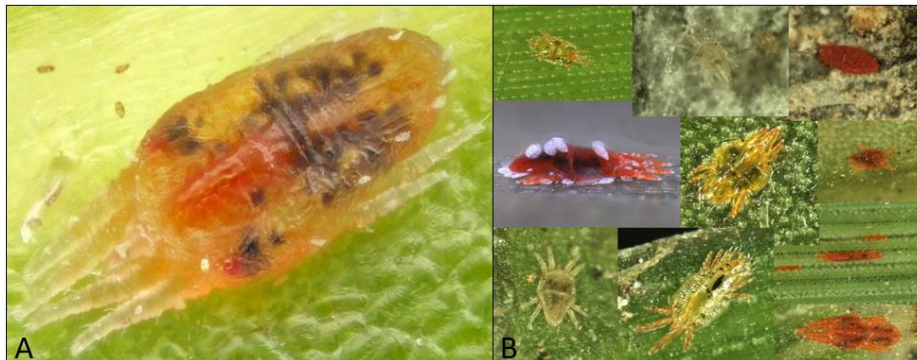


Figure 1.5 Flat mites shapes and colors. A) Tenuipalpidae member feeding on *Ilex verticillata*. From <https://twitter.com/Bertonemyia/status/794561817733431296?s=20>. B) Different flat mites in a range of shapes and colors. From http://idtools.org/id/mites/flatmites/about_id.php

1.6.1 Plant viruses transmitted by flat mites (Tenuipalpidae)

Brevipalpus-transmitted viruses (BTVs), different from most plant viruses, cannot establish systemic infection in their host naturally, but rather are confined to localized lesions (Freitas-Astúa et al., 2018; Rodrigues and Childers 2013). Based on the cytopathological features such as viroplasm observed in infected tissue using transmission electron microscope (TEM), they can be classified into the cytoplasmic type (BTV-C) and the nuclear type (BTV-N) (Kitajima et al., 2003a). BTVs have been found affecting economically important crops such as citrus, coffee, passion fruit, orchids and other ornamentals. The localized symptoms caused by these viruses are very similar and characterized by chlorotic or green spots and ringspots that may present in leaves, fruits and stem (Figure 1.6) (Freitas-Astúa et al., 2018; Kitajima

et al., 2003a). Both BTV-C and BTV-N have been found infecting citrus in single and mixed infections (Roy et al., 2015a; Ramos-González et al., 2018a) and causing one of the most important and studied diseases on citrus, citrus leprosis (Roy et al., 2015a; Freitas-Astúa et al., 2018). Citrus leprosis is a non-systemic multi-etiological disease that is characterized by chlorotic and/or necrotic oval- or circular-shaped lesions in leaves, stems and fruits (Figure 1.6) that severely affects fruit yield. Citrus leprosis affects a large spectrum of commercial citrus species and hybrids. It can cause branch dieback and occasionally death in young trees (Roy et al., 2015a; Ramos-González et al., 2018a). The symptoms of this disease have been characterized since the early 20th century in the Americas, but it was in the late 20th century and the 21st century that BTV-C or BTV-N were associated with the disease and characterized, respectively (Roy et al., 2015a; Ramos-González et al., 2018a; Freitas-Astúa et al., 2018). Citrus leprosis was restricted to South and Central America with BTV-C being prevalently linked to the disease (Ramos-González et al., 2018a). However, citrus leprosis was recently reported in South Africa and caused by a BTV-N (Cook et al., 2019). Furthermore, citrus leprosis epidemics that severely affected citrus orchards in Florida, US through the early to middle 1900s disappeared due to sulfur applications and several freezes that killed mite populations vectoring the disease. Since then, citrus leprosis has not been reported in the US. A BTV-N resembling orchid fleck virus (OFV) and sharing only 80% nucleotide sequence identity was partially characterized from an herbarium citrus leprosis sample from Florida which further suggested that citrus leprosis in Florida may have been caused predominantly by BTV-N (Hartung et al., 2015; Kitajima et al., 2011).

While in other hosts, only single BTV-C or BTV-N infections have been reported. Orchid fleck disease in orchids, coffee ringspot disease in coffee and passion fruit green spot disease in passion fruit are caused by two BTV-N and one BTV-C, respectively. BTV-N causing orchid fleck is considered cosmopolitan, while coffee ringspot disease has been reported in Brazil and Costa Rica, and passion fruit green spot disease has been reported in Brazil only (Dietzgen et al., 2018b; Freitas-Astúa et al., 2018). BTV-C belong to the family *Kitaviridae* (Freitas-Astúa et al., 2018; Melzer et al., 2018; ICTV, 2019) while BTV-N belong to the genus *Dichorhavirus* (family: *Rhabdoviridae*) (Dietzgen et al., 2018).

1.7 *Rhabdoviridae*-Plant rhabdoviruses

Rhabdoviridae (order: *Mononegavirales*) members are classified into 40 genera and infect animals and plants (Walker et al., 2021). Plant rhabdoviruses (*Betarhabdovirinae* subfamily) are negative-sense ssRNA viruses that belong to six genera including *Cytorhabdovirus*, *Alphanucleorhabdovirus*, *Betanucleorhabdovirus*, *Gammanucleorhabdovirus*, *Dichorhavirus* and *Varicosavirus* and infect

monocots and dicots (Walker et al., 2021). These viruses are transmitted in a persistent, circulative and propagative manner by their vector (Dietzgen et al., 2020).

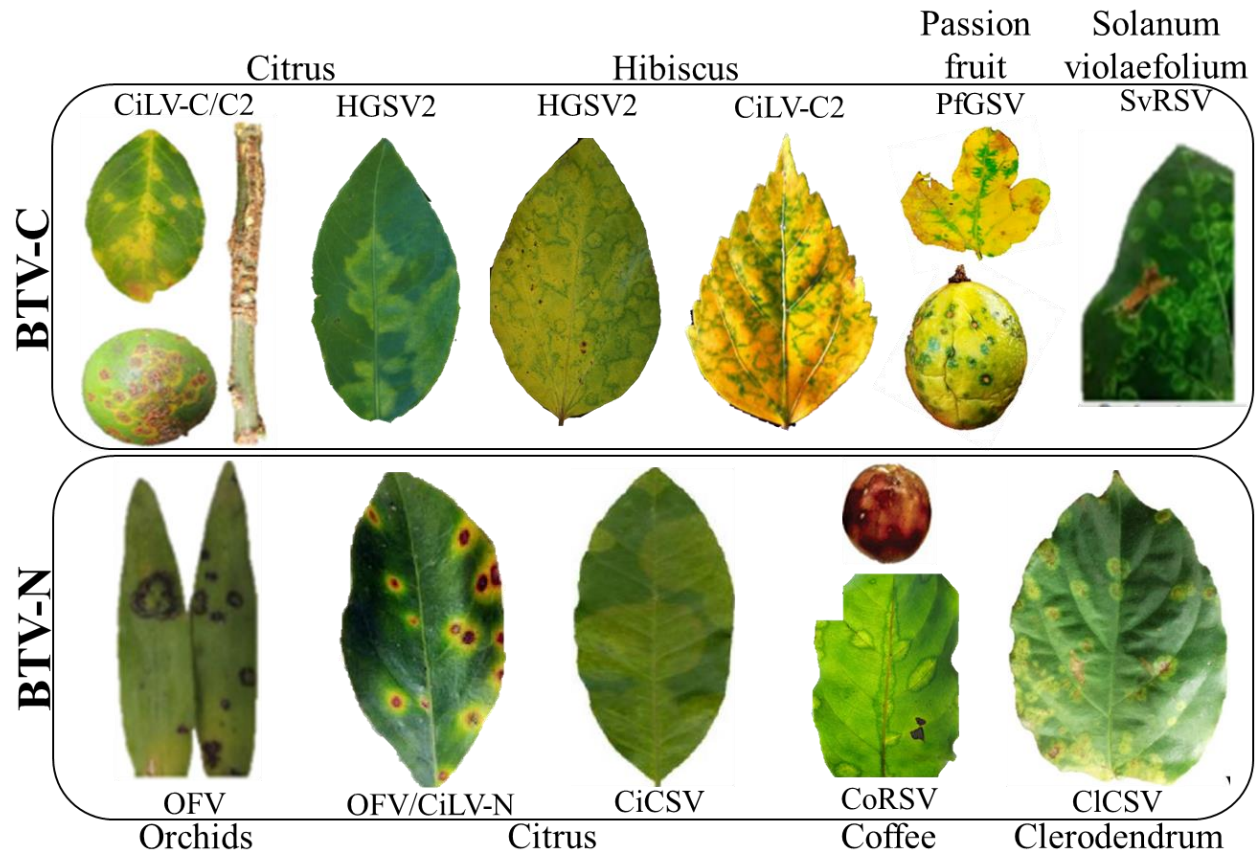


Figure 1.6 Symptoms caused by *Brevipalpus*-transmitted viruses (BTV) in citrus, hibiscus, orchids, coffee, passionfruit, *Solanum violaeifolium* and *Clerodendrum* spp. BTV-C and BTV-N cause a cytopathological effect in cytoplasm and nucleus, respectively. Abbreviations: citrus leprosis virus C (CiLV-C), CiLV-C2, CiLV-N, hibiscus green spot virus 2 (HGSV-2), passionfruit green spot virus (PfGSV), *Solanum violaeifolium* ringspot virus (SvRSV), orchid fleck virus (OFV), citrus chlorotic spot virus (CiCSV), coffee ringspot virus (CoRSV) and *Clerodendrum* chlorotic spot virus (CiCSV). Figure created with images adapted from Freitas Astúa et al., (2018), Roy et al., (2015a), Ramos-González et al., (2018), Ramos-González et al., (2020), Chabi-Jesus et al., (2018) and Ramos González et al., (2017).

Alpha-, beta- and gammanucleorhabdoviruses, and cytorhabdoviruses have an unsegmented genome like the majority of rhabdoviruses, and are transmitted by hemipteran insects: aphids, leafhoppers, or aphids. While dichorha- and varicosaviruses have a bi-segmented genome and are transmitted by *Brevipalpus* mites and chytrid fungi, respectively (Dietzgen et al., 2020). Plant rhabdovirus genomic organization

consists of five conserved canonical genes in the order 3' - nucleocapsid protein (N), phosphoprotein (P), matrix protein (M), glycoprotein (G) and polymerase (L) - 5'. Additionally, some species may have one or several extra genes that are overlapping with the five canonical genes or are interspersed throughout the whole genome making a complete genomic organization of 6-10 gene products (Figure 1.7).

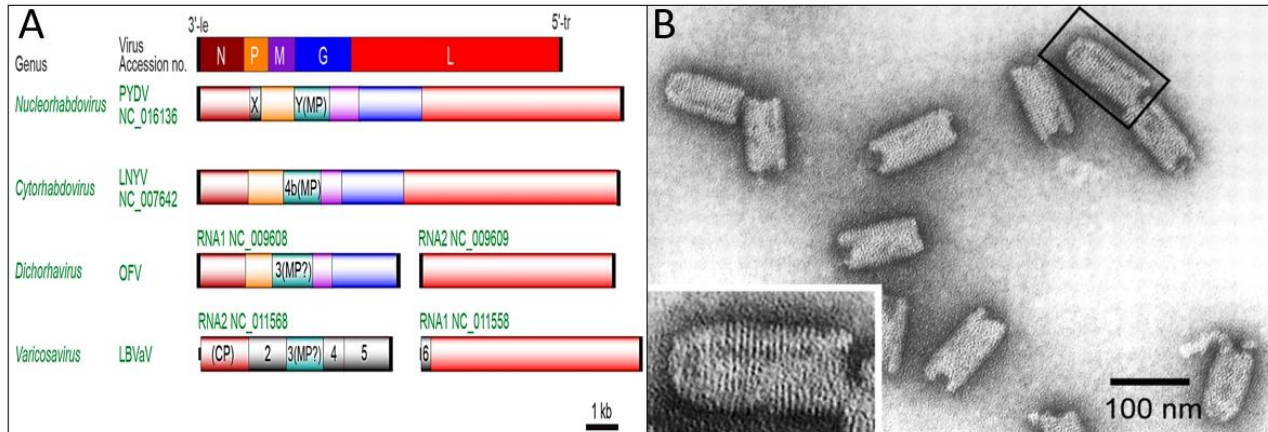


Figure 1.7 Comparative genome organization of plant rhabdoviruses and dichorhavirus virion.

A) Comparative genome organization of plant rhabdoviruses. The five canonical conserved and structural genes (N, P, M, G and L) are shaded in wine, golden, purple, blue and red, respectively. Additional genes including confirmed or putative movement protein (MP) and with unknown functions are included and shaded in different colors. The 3'-leader and 5'-trailer regions are not drawn to scale. Virus type species of each genera: potato yellow dwarf virus (PYDV), lettuce necrotic yellows virus (LNYV), orchid fleck virus (OFV) and lettuce big vein-associated virus (LBVaV). Figure adapted from Dietzgen et al., (2017).
 B) Transmission electron micrograph of pure OFV virion preparations. Figure from Kondo et al., (2006).

1.7.1 Rhabdoviridae-Dichorhavirus

So far, five *Dichorhavirus* members have been characterized. *Orchid fleck dichorhavirus* was fully characterized in 2006 and is the type species of this genus that was created in 2014 (Kondo et al., 2006; Dietzgen et al., 2014). Orchid fleck virus (OFV) is the causal agent of a cosmopolitan disease, orchid fleck disease, in several species of orchids (Kondo et al., 2006). Later, coffee ringspot virus (CoRSV) was characterized as the causal agent of coffee ringspot disease in Brazil and Costa Rica (Ramalho et al., 2014; Dietzgen et al., 2018a; Freitas-Astúa et al., 2018). Initially, BTV-Ns causing citrus leprosis in Mexico were characterized and referred to as “citrus leprosis virus nuclear type” and “citrus necrotic spot virus” (Roy et al., 2015b; Cruz-Jaramillo et al., 2014). However, based on a >90% nucleotide identity of

these viruses to the OFV orchid strain genome, these viruses were referred to as citrus infecting strains of OFV (Amarasinghe et al., 2017). From Brazil only, three additional dichorhviruses were recently characterized, citrus leprosis virus N (CiLV-N) and citrus chlorotic spot virus (CiCSV) infecting sweet orange (*Citrus sinensis* L.) causing citrus leprosis in non-commercial citrus areas (Ramos-González et al., 2017; Chabi-Jesus et al., 2018), and Clerodendrum chlorotic spot virus (ClCSV) infecting *Clerodendrum* spp. (Ramos-González et al., 2018b). Some putative dichorhviruses that still require characterization have been reported in several hosts in Australia, USA, Argentina, and Brazil (Dietzgen et al., 2018).

Dichorhviruses genomic RNA 1 (~6.5 kb) codes for N, P, P3 (putative MP), M and G genes, while genomic RNA 2 (~6 kb) codes for L gene (Figure 1.7A). Their virions are bacilliform but shorter (40x~100-110nm, Figure 1.7B) than nucleo- and cytorhabdoviruses virions (~75x180nm) (Dietzgen et al., 2020; Dietzgen et al., 2017). Additionally, their virions do not appear to be enveloped (Figure 1.7B), but they might be found associated with host membranes (Dietzgen et al., 2014). Rhabdovirus virion length is determined by the length of the genomic RNA they possess (Jaykar et al., 2004), therefore the reduced size of *Dichorhavirus* virions and their bi-segmented genome suggests that RNA 1 and 2 are separately packaged into different virions (Kondo et al., 2006; Dietzgen et al., 2018a). Both termini of each genomic RNA are complementary to each other, and all genes are separated by conserved gene junctions whose entire open reading frame (ORF) is defined by partially complementary 3' leader and 5' trailer sequences that have regulatory functions. Additionally, each ORF is individually expressed as a sub genomic RNA (sgRNA) (Dietzgen et al., 2017). Except for having a bi-segmented genome, dichorhviruses resemble nucleorhabdoviruses in several features including nuclear cytopathological effects, phylogenetic evolution and significant sequence identity, gene order, structural protein composition and transcriptional mechanisms (Dietzgen et al., 2014; Dietzgen et al., 2017).

Classical plant rhabdoviruses, namely alpha-, beta- and gammanucleorhabdoviruses, and cytorhabdoviruses, may have evolved from arthropod viruses based on phylogenetic analyses in the family *Rhabdoviridae* (Whitfield et al., 2018) This hypothesis comes from the fact that groups of related plant rhabdoviruses cluster according to the vector type. Leafhoppers transmit plant rhabdoviruses from both monocots and dicots, planthoppers from monocots, and aphids from dicots (Figure 1.8) (Whitfield et al., 2018). Considering the persistent, circulative and probable propagative transmission of dichorhviruses by *Brevipalpus* (Knorr 1968; Kitajima and Alberti 2014), dichorhviruses likely evolved from mite viruses and during the evolution, they gained the ability to replicate in plant cells as well, but with a limited vascular movement as they are found naturally causing local infections delimited by local lesions at the mite feeding sites (Dietzgen et al., 2020; Freitas-Astúa et al., 2018; Dietzgen et al., 2018a).

However, in experimental hosts (*Chenopodium quinoa* and *C. amaranticolor*) and at higher temperatures (~28°-30°C), OFV, CoRSV and CICSV were shown to become systemic (Dietzgen et al., 2018a) while OFV has been observed to cause spontaneous systemic infections (Kondo et al., 2006).

1.8 *Kitaviridae*

The family *Kitaviridae* is a recently created family of plant viruses that has been ratified by the ICTV (Walker et al., 2019; ICTV 2019). *Kitaviridae* members are most closely related to the family *Virgaviridae*, but also show some phylogenetic resemblance to *Bromoviridae* and *Closteroviridae* family members (Figure 1.9). This family groups three previously unassigned genera of positive-sense ssRNA plant viruses that cause local lesions only in their hosts: *Cilevirus*, *Higrevirus* and *Blunervirus* (Melzer et al., 2018). These three genera possess a bacilliform virion and are likely transmitted by mites. Although vector transmission assays are still to be performed for higre- and blunerviruses, kitavirus infection is generally associated with mite presence (Melzer et al., 2018; Freitas-Astúa et al., 2018; Burkle et al., 2012). They have significant characteristics that differentiate one another. First, cile-, higre- and blunerviruses have bi-, tri- and tetrapartite genomes, respectively. Second, although the virion size for blunerviruses have not been determined, cileviruses seem to have a larger virion (50x120nm) than that of higreviruses (30x50nm). Third, each genus possesses a different type of MP: cileviruses have the 30K superfamily of viral MP, higreviruses possess a triple gene block (TGB) group of MP, while blunerviruses have the 3A family of viral MP (Melzer et al., 2018). Finally, the replication-associated polyproteins are in a single genomic RNA for cile- and higreviruses, but in two genomic RNAs for blunerviruses (Melzer et al., 2018; Quito-Avila et al., 2013). Both cileviruses and higreviruses possess a poly-A tail in the 3'-end of their genomes (Roy et al., 2015a; Ramos-González et al., 2020; Melzer et al., 2012). Although the first isolate of the type species of blunervirus, BNRBV, was not reported to possess a poly-A tail at the 3'-end, the characterization of a variant of BNRBV and a new species of *Blunervirus*, tea plant necrotic ring blotch virus, reported the presence of a poly-A tail in their genomes (Cantu-Iris et al., 2013; Hao et al., 2018) showing congruence in the evolutionary and transcriptional mechanisms employed by kitaviruses. Higreviruses and cileviruses are more phylogenetically related between each other when either the RdRp (Figure 1.9) or p23 protein are analyzed which are the two genes shared by kitaviruses (Melzer et al., 2018; Roy et al., 2015a).

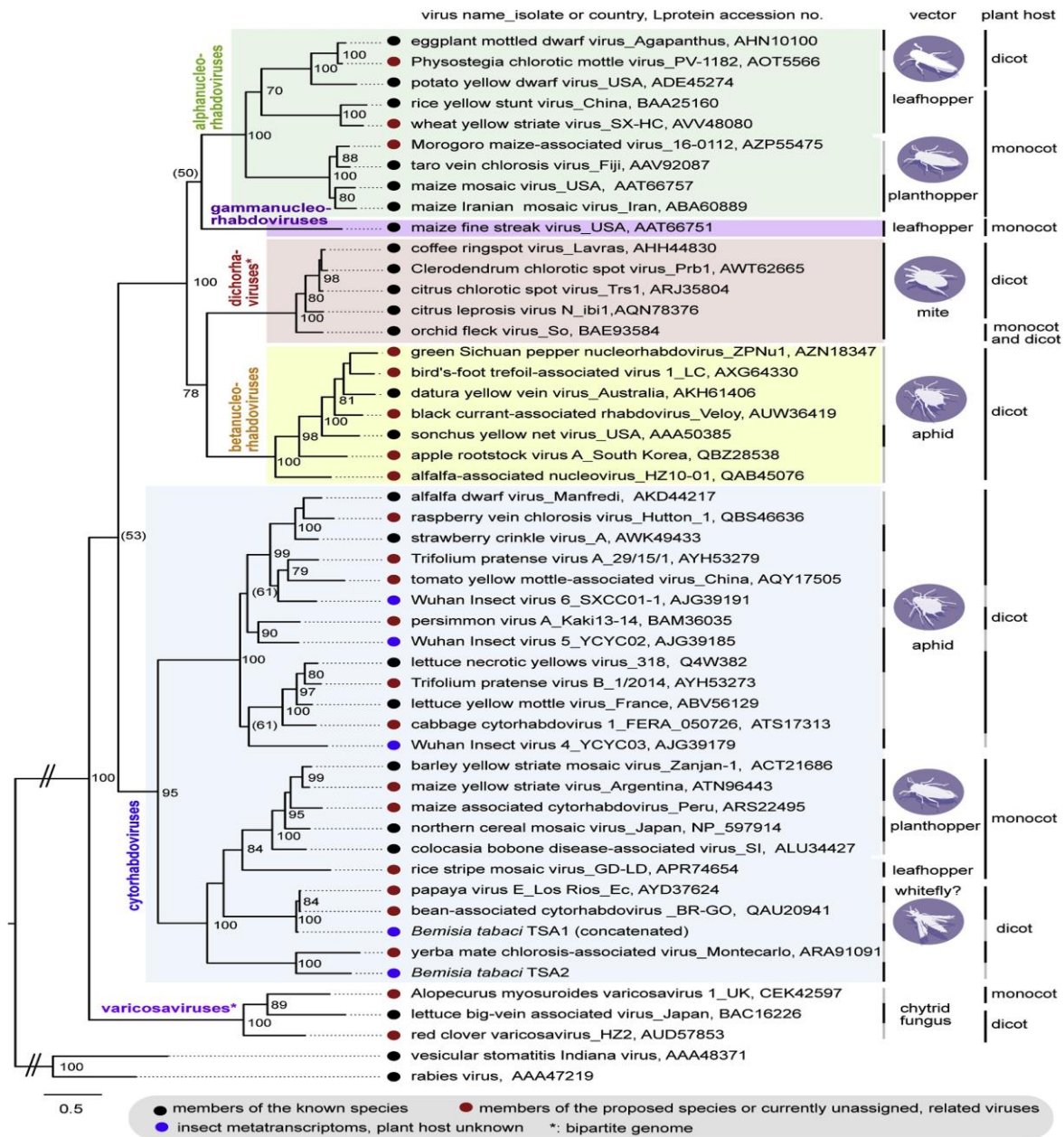


Figure 1.8 Maximum Likelihood phylogenetic tree of the full-length L protein sequences of plant rhabdoviruses. Nucleorhabdoviruses are highlighted by pale green, purple and yellow colored rectangles that correspond to the genera Alpha-, Gamma- and Betanucleorhabdovirus, respectively. Cytorhabdoviruses and dichorviruses are highlighted by light blue and brown colored rectangles, respectively. Plant rhabdovirus transmission for which vector has been demonstrated has a solid black line on the right side of the rectangle. Figure from Dietzgen et al., (2020).

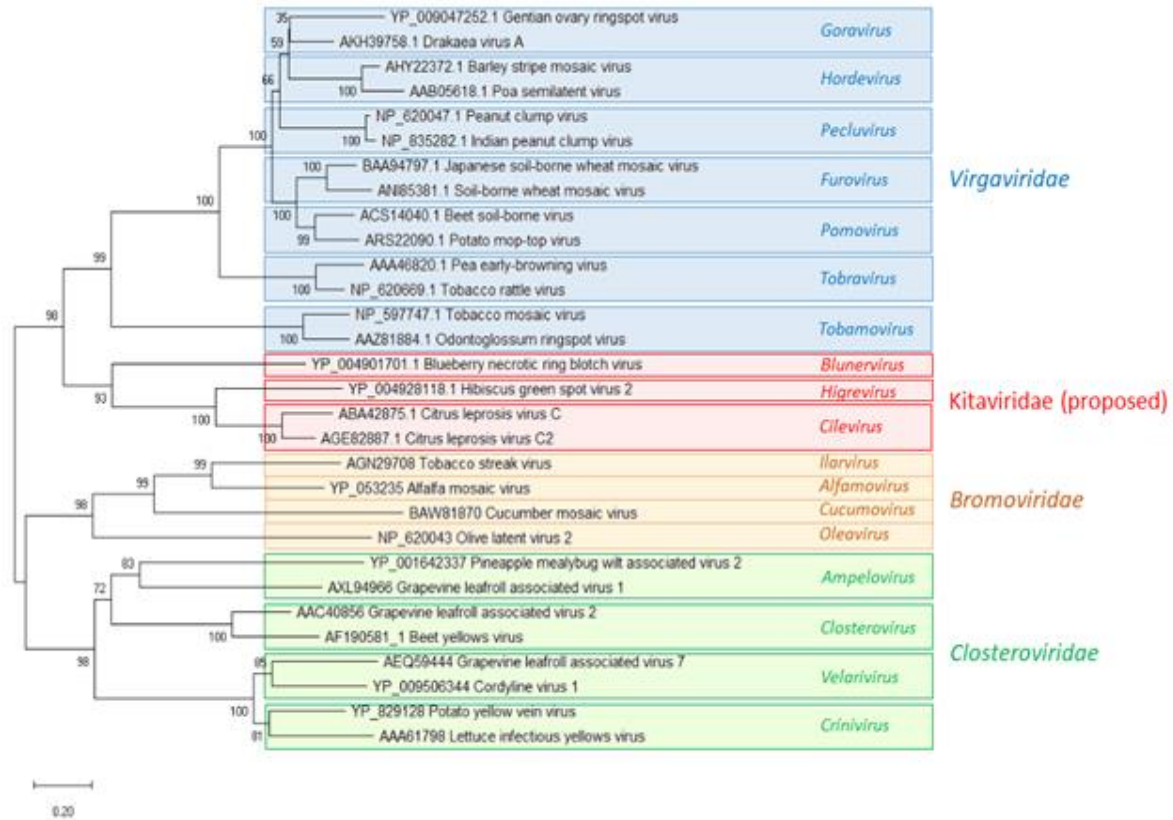


Figure 1.9 Phylogenetic relationships of *Kitaviridae* members (red): cile-, higre- and blunerviruses with *Virgaviridae* (blue), *Bromoviridae* (Golden) and *Closteroviridae* (light green) families members. Figure from Melzer et al., (2018).

Considering the high number of insect-specific viruses, namely nelorpi- and sandewaviruses, (Nunes et al., 2017) and arthropod viruses (Shi et al., 2016) that have been characterized and resemble kitaviruses, it has been suggested that kitaviruses and arthropod viruses share a common ancestor and highlights the possibility that kitaviruses evolved from mite viruses (Nunes et al., 2017; Ramos-González et al., 2020). This hypothesis is further supported by the fact that similar to dichorhavirus, kitaviruses are transmitted by mites in a persistent circulative and likely propagative manner (Roy et al., 2015a; Freitas-Astúa et al., 2018).

1.8.1 Higrevirus

Hibiscus green spot virus-2 (HGSV-2) is the type species and the sole member of the genus *Higrevirus*. HGSV-2 genome is segmented into three genomic RNAs with ~8.3 kbp, ~3.2 kbp and ~3.1 kbp sizes, excluding the poly-A tail (Figure 1.10) (Melzer et al., 2012).

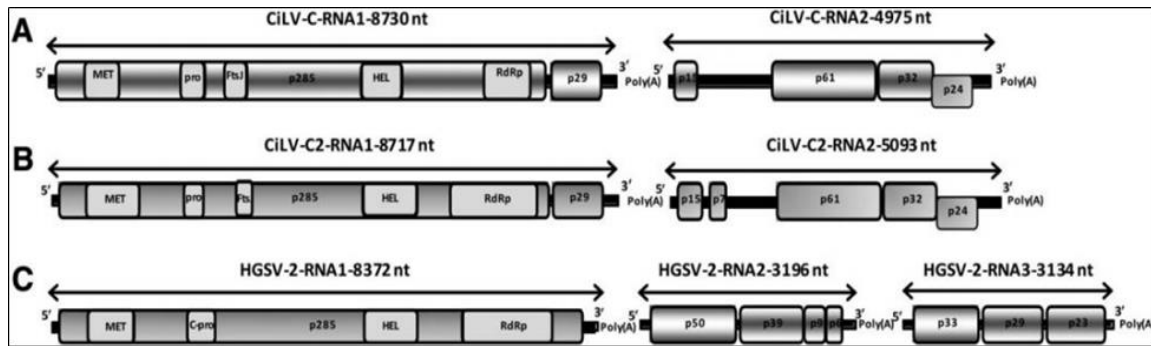


Figure 1.10 Genomic organization of cile- and higreviruses. A) Genomic organization of RNA 1 and 2 of citrus leprosis virus C (CiLV-C). B) Genomic organization of RNA 1 and 2 of CiLV-C2. C) Genomic organization of RNA 1, 2 and 3 of hibiscus green spot virus 2 (HGSV-2). Figure from Roy et al., (2015a).

RNA 1 codes for a polyprotein (ORF 1) containing replication-associated domains and a putative protein (p10) whose ORF overlaps with ORF 1 and shows no homology to any known plant virus gene. RNA 2 codes for p50, p39, p9 and p6 proteins. Proteins p50, p9 and p6 show no homology to any known viral protein, while p39 shows some similarity to *Tobamovirus* (family *Virgaviridae*) helicase proteins. p39, p9 and p6 proteins have characteristics of TGB genes (Melzer et al., 2012). RNA 3 codes for p33, p29 and p23 with the two former proteins being unrelated to any viral protein and the latter protein shows homology with p24 protein of CiLV-C, other kitaviruses (Melzer et al., 2012) and negeviruses, a taxon of insect-specific viruses (Vasilakis et al., 2013; Nunes et al., 2017).

This virus has been found infecting *Hibiscus arnottianus*, volkamer lemon (*Citrus volkameriana*) (Melzer et al., 2012), hau tree (*H. tiliaceus*), mandarin, and navel sweet orange, and has been found in Hawaii only (Roy et al., 2015a). Symptoms caused on all the hosts resemble and are characterized by the presence of green spots surrounded by chlorotic halos. In the case of citrus, citrus leprosis-like are caused by this virus, rather than citrus leprosis, due to the absence of necrosis in symptomatic leaves and fruits different from citrus leprosis symptoms (Figure 1.6). In the case of *Hibiscus* spp., HGSV-2 symptoms are more obvious when leaves are often senescent (Melzer et al., 2012; Roy et al., 2015a). Like *Cilevirus* members, HGSV-2 virions are bacilliform, although smaller and also viroplasm are observed in the cytoplasm of infected host cells (Figure 1.11b) (Roy et al., 2015a; Melzer et al., 2018). Although transmissions assays have not been performed for HGSV-2, Tenuipalpid mites likely represent a putative vector of this virus (Melzer et al., 2012).

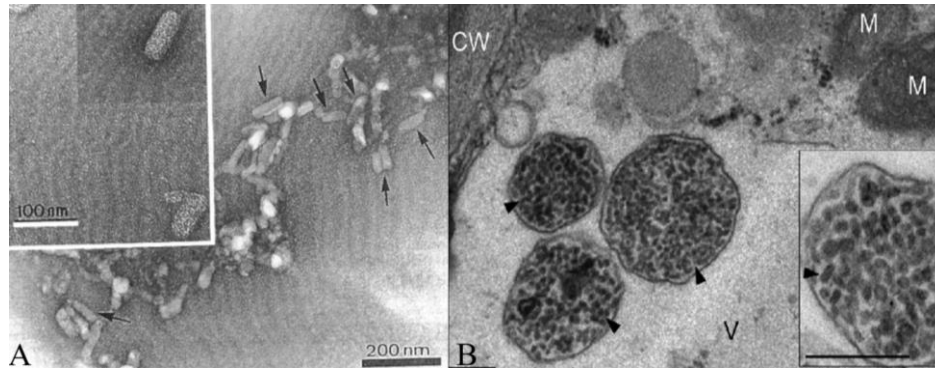


Figure 1.11 Cilevirus virion and hibrevirus viroplasm. A) Transmission electron micrograph of pure citrus leprosis virus C (CiLV-C) virion preparations. Figure from Locali-Fabris et al., (2012). B) Viroplasm caused by hibiscus green spot virus 2 (HGSV-2) in the cytoplasm of infected host cells observed using transmission electron microscopy. Figure from Melzer et al., (2012).

1.8.2 *Cilevirus*

The first two *Cilevirus* members officially recognized by the ICTV were originally characterized from citrus and causing CL, CiLV-C and CiLV-C2 (Locali-Fabris et al., 2006; Roy et al., 2013). Cileviruses possess a bacilliform virion (Figure 1.11a) and form viroplasm associated to the nucleus (Freitas-Astúa et al., 2018). *Cilevirus* bi-partite genome has a size of ~8.7 kbp ~5-5.1 kbp for RNA 1 and 2, respectively. Akin to HGSV-2, RNA 1 codes for a polyprotein (ORF 1) containing replication-associated domains (Roy et al., 2013) and additionally codes for p29 (Figure 1.10), a putative viral coat protein of cileviruses (Leastro et al., 2018). RNA 2 codes for p15, p61, p32 and p24 (Figure 1.10). Proteins p15, p61 and p24 have unknown functions (Roy et al., 2013) although p61 and p24 do share similarities with the putative glycoprotein and the putative virion membrane protein (Pfam: 16504) of negevirus, respectively (Ramos-González et al., 2020; Nunes et al., 2017). Whereas p32 is the movement protein of cileviruses (Melzer et al., 2018). In the RNA 2, there is a non-coding genomic region of ~1000 nucleotides that separates p15 and p61 (Figure 1.10) and is known as intergenic region (Leastro et al., 2018).

Both CiLV-C and CiLV-C2 are persistently circulative transmitted by *Brevipalpus yothersi* mites (Roy et al., 2015a; Ramos-González et al., 2016), although there is neither clear consensus nor sufficient evidence to claim that cileviruses can replicate in their vectors (Roy et al., 2015a; Alberti and Kitajima 2014). Transcriptional strategies of cileviruses involves likely the production of 3' co-terminal sgRNAs (Freitas-Astúa et al., 2018; Roy et al., 2013; Ramos-González et al., 2020).

CiLV-C is the prevalent virus causing citrus leprosis and has been found from Argentina to Mexico (Roy et al., 2015a; Ramos-González et al., 2018). CiLV-C genomic variability (CRD isolate) is low, however, recently a new isolate of CiLV-C (SJP) was found in Brazil that shares ~85% nucleotide sequence identity with the CRD isolate (Ramos-González et al., 2016). CiLV-C infects mostly citrus, however, it has been found infecting other hosts naturally not exceeding 10 plant species (Roy et al., 2015a; Ramos-González et al., 2018). Additionally, CiLV-C has been transmitted experimentally to additional hosts belonging to 28 families (Garita et al., 2014).

CiLV-C2 shares ~55% nucleotide identity with CiLV-C and was initially characterized from sweet orange in Colombia (Roy et al., 2013). In parallel, a hibiscus strain of this virus (CiLV-C2) was characterized from *Hibiscus* sp. showing green ringspots on senescent leaves (Figure 1.6) in Hawaii, US and sharing ~86% and ~83% nucleotide identity to the RNA 1 and 2, respectively, of CiLV-C2 from citrus (Melzer et al., 2013b). The hibiscus strain of CiLV-C2 was then found in Colombia and Florida, US infecting *Hibiscus rosa-sinensis* and causing identical symptoms to those observed in Hawaii (Roy et al., 2015a; Roy et al., 2018a; Roy et al., 2018b). Interestingly, CiLV-C2 (hibiscus strain) has not been found infecting citrus in Hawaii or Florida in the US (Melzer et al., 2013b; Roy et al., 2018a). These hibiscus isolates of CiLV-C2 have greater variability in the RNA 2, ~83% nucleotide identity and ~92% overall amino acid identity to CiLV-C2 (Melzer et al., 2013b). Possibly the protein variation in the RNA 2-coded proteins may give the hibiscus strain of CiLV-C2 its specificity for hibiscus and/or inability to infect citrus.

In Brazil, passion fruit green spot and passion fruit sudden death diseases are two diseases that show similar symptoms with the latter sometimes resulting in death of the plants. Passion fruit green spot disease has been associated with a putative *Cilevirus*, passion fruit green spot virus (PfGSV) (Kitajima et al., 2003b). Symptoms are characterized by brilliant green spots on yellow mature fruits (Figure 1.6) and necrotic lesions on stems. Green spots may be visualized in senescent leaves as well (Figure 1.6) (Kitajima et al., 2003b; Antonioli-Luizon et al., 2009). Both diseases are transmitted by *Brevipalpus phoenicis* mites (Kitajima et al., 2003b). Recently, five isolates of PfGSV were characterized and associated with passion fruit green spot and passion fruit sudden death diseases in Brazil (Ramos-González et al., 2020). PfGSV shows identical genomic organization in RNA 1 and 2 to those of cileviruses. PfGSV RNA 1 and 2 shares ~72% and 64% nucleotide identity to RNA 1 and 2 of CiLV-C2, respectively. Additionally, PfGSV harbors a new orphan ORF located in the RNA 2 intergenic region coding for a protein with unknown function, and presents a shorter intergenic region (~835 nucleotides) than CiLV-C and CiLV-C2 (~1000-1100 nucleotides) (Ramos-González et al., 2020).

1.9 Reverse genetics

With the advent of the genomics era and the generation of the whole genomic sequences of a good range of organisms, researchers have now the option to go from genotype (sequence) to determine the gene(s) function and observe the phenotype, a process termed reverse genetics. To be able to infer the gene function, the sequence (genotype) needs to be altered by specific nucleic acid changes by genetic engineering (Tierney and Lamour 2005). Plant viruses code for a plethora of genes whose function is unknown, and the study of their genes functions has been challenging due to their dependence on a plant host to replicate (Pasin et al., 2019). Virus infectious clones were produced as a creative and sharp reverse genetics system to characterize the function of viral genes and features. Virus infectious clones are produced by delivering a DNA copy of the DNA/RNA viral genome into its cell host. For delivery of the viral genome, different approaches are employed, but normally the viral genome is inserted into a plasmid vector for future transcription, transfection, etc. (Bridgen 2012). Virus infectious clones are indispensable for the functional characterization of viral components such as genes, proteins, transcripts and non-translated elements. Additionally, they provide a more robust, standardized, and simple inoculation method that facilitates virus-host, virus-vector and virus-virus studies as well as crop breeding. This is especially useful for plant viruses whose mechanical transmission is not feasible or easy (Pasin et al., 2019).

The production of the first virus infectious clone in the history of virology was developed for a bacterial DNA phage, T2 bacteriophage. This breakthrough was achieved by simply delivering DNA extracted from pure T2 bacteriophage into protoplasts of *Escherichia coli* (Fraser et al., 1957). Since then, the development of DNA virus infectious clones has been generally considered straightforward to perform because it only requires the delivery of the viral DNA into host cells (Bridgen 2012). The first plant DNA virus infectious clone was developed for cauliflower mosaic virus (CaMV) (Family: *Caulimoviridae*, Genus: *Caulimovirus*) (Howell et al., 1980). Development of RNA virus infectious clones soon followed, and this process involved the rescue of the virus from viral transcripts delivered into the cell host. The first RNA virus infectious clone was achieved for a bacterial RNA phage, Qbeta phage (Taniguchi et al., 1978). Whereas, brome mosaic virus (BMV) and potato spindle tuber viroid were the first RNA plant virus and viroid, respectively, for which an infectious clone system was developed (Ahlquist et al., 1984; Cress et al., 1983).

As part of a breakthrough to develop infectious clones of plant viruses, an inoculation method using *Agrobacterium tumefaciens* harboring a tumor inducing (Ti) plasmid with the viral genome inserted in the

T-DNA was developed to efficiently deliver the cDNA copy of plant viruses into the host (Grimsley et al., 1986). Since this breakthrough, most of plant virus infectious clone genetic systems rely upon this system. It is also possible to inoculate plants by using a biolistic device to directly insert plasmids harboring the viral genome driven by plant promoter sequences (Nagyová and Subr 2007). This approach, however, has been applied successfully for few plant viruses.

1.10 Infectious clones of RNA viruses

The development of RNA virus infectious clones has faced several difficulties that may be specific for the type of RNA genome the virus has, namely positive-sense ssRNA, negative-sense ssRNA or double-stranded RNA (dsRNA). Additional unique genomic features some viruses possess are fundamental considerations for development of infectious clones (Figure 1.12) (Bridgen 2012).

(a)	DNA 5' ————— 3' 3' ————— 5'	Infectious when introduced into cells. Transcribed into mRNA which in turn is translated into protein. Rescue from 1957.
(b)	+ RNA 5' ————— 3'	Infectious when introduced into cells. Translated directly into protein. Rescue from 1978.
(c)	- RNA 3' ————— 5'	NOT infectious when introduced into cells. Needs to be encapsidated in replication proteins. Replicated via + RNA intermediate. Transcribed into + mRNA which is translated. Rescue from 1994.
(d)	- RNA, segmented genome 3' — 5' 3' — 5' 3' — 5'	NOT infectious when introduced into cells. Needs to be encapsidated in replication proteins. Replicated via + RNA intermediates. Transcribed into + mRNA which is translated. Rescue procedures hindered by multiple (up to 8) segments. Rescue from 1996.
(e)	dsRNA, segmented genome 5' ——— ——— ——— 3' 3' ——— ——— ——— 5'	Infectious when introduced into cells. Rescue procedures hindered by multiple segments and difficulties in artificially generating dsRNAs. Rescue from 2007.

Figure 1.12 Requirements for the development of virus infectious clones. a) DNA viruses, b) positive-sense single-stranded RNA (ssRNA) viruses, c) negative-stranded ssRNA viruses, d) negative-stranded ssRNA viruses with a multisegmented genome and e) double-stranded RNA (dsRNA) viruses having a segmented genome. Figure from Bridgen (2012).

Theoretically the insertion of cDNA copies or transcripts of a positive-sense ssRNA virus into the cell host should be enough to produce infectious viruses, however, additional difficulties have been encountered for some plant viruses due to their genome size and/or the host (Satyanarayana et al., 1999). Infectious clone for citrus tristeza virus (CTV) (Family: *Closteroviridae*, Genus: *Closterovirus*) was of

great interest to further study the biological effects of the different divergent genotypes of CTV, a phloem-limited virus. A multi-step cloning strategy and frameshift mutations had to be adopted to overcome the cloning of long genome size of CTV (~20 kb) (Satyanarayana et al., 1999) and minimize the toxicity of viral sequences in *E. coli* (Satyanarayana et al., 2003), respectively. Still CTV cDNA viral genome copies were difficult to produce, and the first attempts to inoculate/infect citrus were in vain. cDNA transcripts from the CTV infectious clone developed were capable to infect *N. benthamiana* protoplasts only and produce CTV virions, but incapable of infecting citrus. To overcome this obstacle, virions obtained from infected *N. benthamiana* protoplasts were used as sap inoculum to inoculate citrus using a 'slash inoculation' technique (Satyanarayana et al., 2001). Later, it was further designed and realized that when the CTV infectious clone was co-agroinoculated with p19 from tomato bushy stunt virus (TBSV), a potent gene silencing suppressor, CTV was capable of establishing successful systemic infection on *N. benthamiana* plants which were later used as inoculum for slash inoculation onto citrus (Ambrós et al., 2011).

Negative-sense ssRNA virus infectious clone studies proved more challenging due to the more complex viral assembly and infection processes (Figure 1.12) (Bridgen 2012). For plant viruses with negative-sense RNA genome, a ribonucleoprotein (RNP) complex is necessary to start infection and is considered the minimal infection unit. The RNP complex is composed of the RNA genome encapsidated by the viral nucleoprotein (N) and associated with the replication proteins (L) whose association is dependent on a viral phosphoprotein (P) cofactor or genomic panhandle structures for non-segmented or segmented viruses, respectively (Ruigrok et al., 2011). For segmented negative-sense ssRNA viruses, infectious clone development complexity is increased due to the requirement of the presence of the constructs for each genomic segment in the same cell (Bridgen 2012; Pasin et al., 2019). In this context, the development of the first infectious clone for negative-sense ssRNA plant virus (Wang et al., 2015) was achieved 21 years later than its homologue infectious clone for rabies virus (Schnell et al., 1994). The first infectious clone for Sonchus yellow net virus (SYNV) (Family: *Rhabdoviridae*, Genus: *Nucleorhabdovirus*) was achieved by co-agroinoculation of antigenomic RNA of SYNV, viral suppressors of RNA silencing, and N+P+L core proteins (Wang et al., 2015).

1.11 Second and third generation sequencing

Sanger sequencing developed by Frederick Sanger and colleagues in 1977 is referred to as the first generation sequencing. Sanger sequencing allows to obtain a DNA sequence of no more than 1200-1500 nucleotides of a single molecule whose partial sequence is known (Sanger et al., 1977). The development

of HTS technologies in 2005 allowed researchers to obtain thousands to millions of DNA molecules per run and included molecules with unknown sequences. Between 2005 and 2012, different HTS technologies were developed by different companies and the read length was between 100 to no more than 1000 nucleotides. These HTS technologies were known as short read HTS or also known as second generation sequencing, deep sequencing, or next-generation sequencing, however, the two latter terms have not been broadly used as the first former term due to possible ambiguous meaning (Grada & Weinbrecht 2013). Although various short read HTS technologies coexisted in the market during several years, nowadays, the market is dominated by Illumina platforms (previously called Solexa). Between 2010 to 2014, the third generation sequencing technologies emerged and were developed by Pacific Biosciences and Oxford Nanopore companies. Both technologies can produce long reads with an average size of 10,000-100,000 nucleotides reads. Therefore, these HTS technologies are also referred to as long read HTS technologies (Lee et al., 2016).

Each short and long reads HTS technology has advantages and drawbacks. Due to the cost per run, throughput per run, and low raw error rate, Illumina platforms currently dominate the HTS market. However, long reads HTS technologies have been gaining popularity because the long reads better facilitate the assembly of more complex repetitive regions that are commonly present in eukaryotic organisms (van Dijk et al., 2018; De Bustos et al., 2016). To curate the likely errors introduced by long reads HTS technologies, Illumina short read HTS technology is employed in parallel and this is also called a hybrid genome assembly. Oxford Nanopore with its MinION instrument are revolutionizing the sequencing field by allowing researchers to perform sequencing *in situ* of environmental samples due to its low cost of equipment and field deployability. This instrument has been used in very remote locations including Antarctica, Africa, and even outer space (Castro-Wallace et al., 2017).

1.12 LITERATURE CITED

Ahlquist, P., French, R., Janda, M., Loesch-Fries, L.S. (1984). Multicomponent RNA plant virus infection derived from cloned viral cDNA. *Proc. Natl. Acad. Sci. USA*, 81, 7066–7070.

Alberti, G., Kitajima, E.W. (2014). Anatomy and fine structure of *Brevipalpus* mites (Tenuipalpidae) – Economically important plant-virus vectors. *Zoologica* 160: 1-192.

Amarasinghe, G.K., Ayllon, M.A., Bao, Y., Basler, C.F., Blasdell, K.R., Briese, T., et al., (2019). Taxonomy of the order Mononegavirales: update 2019. *Arch Virol* 164(7): 1967-1980.

Amarasinghe, G.K., Bao, Y., Basler, C.F., Bavari, S., Beer, M., Bejerman, N. et al., (2017). Taxonomy of the order Mononegavirales: update 2017. *Arch Virol* 162: 2493-2504. <https://doi.org/10.1007/s00705-017-3311-7>

Ambrós, S., El-Mohtar, C., Ruiz-Ruiz, S., Pena, L., Guerri, J., Dawson, W.O., Moreno, P. (2011). Agroinoculation of Citrus tristeza virus causes systemic infection and symptoms in the presumed nonhost *Nicotiana benthamiana*. *Mol Plant-Microbe Interact* 24: 1119-1131

Anderson, P.K., Cunningham, A.A., Patel, N.G., Morales, F.J., Epstein, P.R., Daszak, P. (2004). Emerging infectious diseases of plants: pathogen pollution, climate change and agrotechnology drivers. *Trends Ecol. Evol.* 19(10): 535-544.

Antonioli-Luizon, R., Jesus-Brabosa, C., Ferraz-Laranjeira, F., Kitajima, E. W., and Freitas-Astúa, J. (2009). Diagnóstico da Pinta Verde: Definhamento Precoce do Maracujazeiro. Available at: <https://www.embrapa.br/busca-de-publicacoes/-/publicacao/711786/diagnostico-da-pinta-verde-definhamento-precoce-do-maracujazeiro> (accessed April 19, 2020).

Arena, G.D., Ramos-González, P.L., Nunes, M.A., Chabi-Jesus, C., Calegario, R.F., Kitajima, E.W., ... Freitas-Astúa, J. (2017). *Arabidopsis thaliana* as a model host for *Brevipalpus* mite-transmitted viruses. *Sci Agric* 74(1): 85–89. <https://doi.org/10.1590/1678-992x-2015-0380>

Beard, J.J., Ochoa, R., Bauchan, G.R., Trice, M.D., Redford, A.J., Walters, T.W. and Mitter, C. (2012). Flat Mites of the World Edition 2. Identification Technology Program, CPHST, PPQ, APHIS, USDA; Fort Collins, CO. Retrieved from <http://idtools.org/id/mites/flatmites/> on 2020-04-02

Bensoussan, N., Santamaria, M.E., Zhurov, V., Diaz, I., Grbic, M., and Grbic, V. (2016). Plant-herbivore interaction: dissection of the cellular pattern of *Tetranychus urticae* feeding on the host plant. *Front Plant Sci* 7:1105. doi: 10.3389/fpls.2016.01105

Blaazer, C.J.H., Villacis-Perez, E.A., Chafi, R., Van Leeuwen, T., Kant, M.R., Schimmel, B.C.J. (2018). Why do herbivorous mites suppress plant defenses?. *Front Plant Sci* 9: 1057.

Bragard, C., Caciagli, P., Lemaire, O., Lopez-Moya, J.J., MacFarlane, S., Peters, D., Susi, P., Torrance, L. (2013). Status and Prospects of Plant Virus Control Through Interference with Vector Transmission. *Annu Rev Phytopathol* 51: 177-201.

Bridgen, A. (2012). Introduction. In Bridgen, A (editor). *Reverse genetics of RNA viruses, Applications and Perspectives*. Oxford, UK: Wiley-Blackwell. pp 1-15.

Burkle, C., Olmstead, J.W., Harmon, P.F. (2012). A potential vector of Blueberry necrotic ring blotch virus and symptoms on various host genotypes. *Phytopathology* 102:S4.17.

Cantu-Iris, M., Harmon, P.F., Londono, A., Polston, J.E. (2013). A variant of blueberry necrotic ring blotch virus associated with red lesions in blueberry. *Arch Virol* 158(10): 2197-2200. doi: 10.1007/s00705-013-1653-3.

Castro-Wallace, S.L., Chiu, C.Y., John, K.K. Stahl, S.E. Rubins, K.H., McIntyre, A.B.R., ... Burton, A.S. (2017). Nanopore DNA Sequencing and Genome Assembly on the International Space Station. *Sci Rep* 7, 18022. doi: 10.1038/s41598-017-18364-0

Chabi-Jesus, C., Ramos-Gonzalez, P.L., Tassi, A.D., Guerra-Peraza, O., Kitajima, E.W., Harakava, R., Beserra Jr., J.E.A., Salaroli, R.B., Freitas-Astúa, J. (2018). Identification and characterization of citrus chlorotic spot virus, a new Dichorhavirus associated with citrus leprosis-like symptoms. *Plant Dis* 102: 1588-1598.

Cook, G., Kirkman, W., Clase, R., Steyn, C., Basson, E., Fourie, P. H., Moore, S. D., Grout, T.G., Carstens, E., Hattingh, V. (2019). Orchid fleck virus associated with the first case of citrus leprosis-N in South Africa. *Eur J Pl Pathol* 155, 1373-1379. doi:10.1007/s10658-019-01854-4

Cress, D.E., Kiefer, M.C., Owens, R.A. (1983) Construction of infectious potato spindle tuber viroid cDNA clones. *Nucleic Acids Res.* 11, 6821–6835.

Cruz-Jaramillo, J.L., Ruiz-Medrano, R., Rojas-Morales, L., Lopez-Buenfill, J.A., Morales-Galvan, O., Chavarin-Palacio, C., Ramirez-Pool, J.A., Xoconostle-Cazares, B. (2014). Characterization of a proposed dichorhavirus associated with the citrus leprosis disease and analysis of the host response. *Viruses* 6(7): 2602-2622. doi: 10.3390/v6072602

De Bustos, A., Cuadrado, A. & Jouve, N. (2016). Sequencing of long stretches of repetitive DNA. *Sci Rep* 6, 36665. doi: 10.1038/srep36665

Dhooria, M.S. (2016). Mite transmission of plant diseases. *Fundam Appl Acarol*: 327-339. Elsevier Inc.

Dietzgen, R.G., Bejerman, N.E., Goodin, M.M., Higgins, C.M., Huot, O.B., Kondo, H., Martin, K.M., Whitfield, A.E. (2020). Diversity and epidemiology of plant rhabdoviruses. *Virus Res* 281: 197942. <https://doi.org/10.1016/j.virusres.2020.197942>.

Dietzgen, R.G., Freitas-Astúa, J., Chabi-Jesus, C., Ramos-González, P.L., Goodin, M.M., Kondo, H., ... Kitajima, E.W. (2018a). Dichorhavirus in their Host Plants and Mite Vectors. *Adv Virus Res* 102(1): 119-148. <https://doi.org/10.1016/bs.aivir.2018.06.001>

Dietzgen, R.G., Kondo, H., Goodin, M.M., Kurath, G., Vasilakis, N. (2017). The family Rhabdoviridae: mono- and bipartite negative-sense RNA viruses with diverse genome organization and common evolutionary origins. *Virus Res* 227: 158-170.

Dietzgen, R.G., Kuhn, J.H., Clawson, A.N., Freitas-Astúa, J., Goodin, M.M., Kitajima, E.W., Kondo, H., Wetzel, T., Whitfield, A.E. (2014). Dichorhavirus: a proposed new genus for *Brevipalpus* mite-transmitted, nuclear, bacilliform, bipartite, negative-strand RNA plant viruses. *Arch Virol* 159(3): 607-619. doi: 10.1007/s00705-013-1834-0.

Dietzgen, R.G., Mann, K.S., Johnson, K.N. (2016). Plant Virus-Insect Vector Interactions: Current and Potential Future Research Directions. *Viruses* 8(11): 303.

Dietzgen, R. G., Tassi, A. D., Freitas-Astúa, J., & Kitajima, E. W. (2018b). First report of orchid fleck virus and its mite vector on green cordyline. *Australas Plant Dis Notes* 13: 11. <https://doi.org/10.1007/s13314-018-0295-4>

Druciarek, T., Lewandowski, M. and Tzanetakis, I. (2019). A new, sensitive and efficient method for taxonomic placement in the Eriophyoidea and virus detection in individual eriophyoids. *Exp. Appl. Acarol.* 78, 247-261. Doi:10.1007/s10493-019-00382-4

Elbeaino, T., Digiario, M., Alabdullah, A., de Stradis, A., Minafra, A., Mielke, N., Castellano, M.A., Martelli, G.P. (2009a). A multipartite single-stranded negative-sense RNA virus is the putative agent of fig mosaic disease. *J Gen Virol* 90:1281–1288. <https://doi.org/10.1099/vir.0.008649-0>

Elbeaino, T., Digiario, M., Martelli, G.P. (2009b). Complete nucleotide sequence of four RNA segments of fig mosaic virus. *Arch Virol* 154:1719–1727.

Elbeaino, T., Digiario, M., Mielke-Ehret, N., Muehlbach, H.P., Martelli, G.P. (2018). ICTV Virus Taxonomy Profile: Fimoviridae. *J Gen Virol* 99(11):

Elbeaino, T., Digiario, M., Uppala, M., Sudini, H. (2015). Deep sequencing of dsRNAs recovered from mosaic-diseased pigeonpea reveals the presence of a novel emaravirus: pigeonpea sterility mosaic virus 2. *Arch Virol* 160: 2019-2029. <https://doi.org/10.1007/s00705-015-2479-y>

Elbeaino, T., Whitfield, A., Sharma, M., Digiario, M. (2013). Emaravirus-specific degenerate PCR primers allowed the identification of partial RNA-dependent RNA polymerase sequences of Maize red stripe virus and Pigeonpea sterility mosaic virus. *Journal of Virological Methods* 188(1-2): 37-40. doi: 10.1016/j.jviromet.2012.11.037

Fathipour, Y., Maleknia, B. (2016). Mite predators. In: Omkar, editor. *Ecofriendly Pest Management for Food Security*. Academic Press, USA. pp. 329-366.

Fitzgerald, J., N. Pepper, M. Easterbrook, T. Pope, and M. Solomon. 2007. Interactions among phytophagous mites, and introduced and naturally occurring predatory mites, on strawberry in the UK. *Exp Appl Acarol* 43: 33-47.

Fraser, D., Mahler, H. R., Shug, A. L. and Thomas, C.A. (1957). The infection of sub-cellular *Escherichia coli*, strain B, with a DNA preparation from T2 bacteriophage. *Proceedings of the National Academy of Sciences of the United States of America* 43(11): 939-947.

Freitas-Astúa, J., Ramos-González, P.L., Arena, G.D., Tassi, A.D., & Kitajima, E.W. (2018). Brevipalpus-transmitted viruses: parallelism beyond a common vector or convergent evolution of distantly related pathogens? *Curr Opin Virol* 33: 66-73. <https://doi.org/10.1016/j.coviro.2018.07.010>

Garita, L.C., Tassi, A.D., Calegario, R.F., Carbonell, S.A.M., Freitas-Astúa, J., Kitajima, E.W. (2013). Common bean (*Phaseolus vulgaris* L.): experimental local lesion host for Citrus leprosis virus C (CiLV-C) and some other cytoplasmic-type *Brevipalpus*-transmitted viruses. *Plant Dis* 97:1346-1351.

Garita, L.C., Tassi, A.D., Calegario, R.F., Freitas-Astúa, J., Salaroli, R.B., Romão, G.O., & Kitajima, E.W. (2014). Experimental host range of Citrus leprosis virus C (CiLV-C). *Trop Plant Pathol* 39(1): 43-55. <https://doi.org/10.1590/S1982-56762014005000004>

Gonsalves, D., Tripathi, S., Carr, J.B., and Suzuki, J.Y. (2010). Papaya Ringspot virus. *The Plant Health Instructor*. DOI: 10.1094/PHI-I-2010-1004-01

Grada, A. & Weinbrecht, K. (2013). Next-Generation Sequencing: Methodology and Application. *Journal of Investigative Dermatology* 133, e11. doi:10.1038/jid.2013.248

Greninger, A.L. (2018). A decade of RNA virus metagenomics is (not) enough. *Virus Res* 244(15): 218-299. <https://doi.org/10.1016/j.virusres.2017.10.014>

- Grimsley, N., Hohn, B., Hohn, T., Walden, R. (1986). “Agroinfection”, an alternative route for viral infection of plants by using the Ti plasmid. *Proc. Natl Acad. Sci. USA*, 83, 3282–3286.
- Gulati, R. (2014) Eco-friendly management of phytophagous mites. In: Abrol DP (ed) *Integrated pest management: current concepts and ecological perspective*. Elsevier Inc, New York, pp 461–491
- Hawaii Department of Agriculture. (2020). Top 20 Agricultural Commodities Produced. State of Hawaii, 2018. Retrieved from https://hdoa.Hawaii.gov/add/files/2020/02/Top-20-Ag-Commodities_SOH_R_02.14.pdf (July 3, 2020)
- Hao, X., Zhang, W., Zhao, F., Liu, Y., Qian, W., Wang, Y., Wang, L., Zeng, J., Yang, Y., Wang, X. (2018). Discovery of plant viruses from tea plant (*Camelia sinensis* (L.) O. Kuntze) by metagenomic sequencing. *Front Microbiol* 9: 2175. doi: 10.3389/fmicb.2018.02175
- Hartung, J.S., Roy, A., Fu, S., Shao, J., Schneider, W.L., Brlansky, R.H. (2015). History and diversity of citrus leprosis virus recorded in herbarium specimens. *Phytopatol* 105: 1277-1284.
- Howell, S.H., Walker, L.L., Dudley, R.K. (1980). Cloned cauliflower mosaic virus DNA infects turnips (*Brassica rapa*). *Science* 208: 1265–1267.
- Hull, R. (2014a). Plant virology: Introduction. In: *Matthew’s Plant Virology*. Academic Press, USA, pp 7-10
- Hull, R. (2014b). Plant virology: Plant to plant movement. In: *Matthew’s Plant Virology*. Academic Press, USA, pp 684-6846
- International Committee on Taxonomy of Viruses (2019). ICTV Master Species List 2019 v2. Checklist dataset <https://doi.org/10.15468/i4jnfv> accessed via GBIF.org on 2020-03-27.
- Jaykar, H.R., Jeetendra, E., Whitt, M.A. (2004). Rhabdovirus assembly and budding. *Virus Res* 106: 117-132.
- Kitajima, E.W., Alberti, G. (2014). Anatomy and fine structure of *Brevipalpus* mites (Tenuipalpidae)—economically important plant–virus vectors. Part 7. Ultrastructural detection of cytoplasmic and nuclear types of *Brevipalpus*-transmitted viruses. *Fortschr. Zool.*, 160: 173-192.
- Kitajima, E.W., Chagas, C.M., Harakava, R., Calegario, R.F., Freitas-Astúa, J., Rodrigues, J.C.V., & Childers, C.C. (2011). Citrus leprosis in Florida, USA, appears to have been caused by the nuclear type of citrus leprosis virus (CiLV-N). *Virus Reviews & Research* 16(1–2). <https://doi.org/10.17525/vrr.v16i1-2.51>

- Kitajima, E.W., Chagas, C.M., Rodrigues, J.C.V. (2003a). *Brevipalpus*-transmitted plant virus and virus-like diseases: cytopathology and some recent cases. *Exp Appl Acarol* 30: 135-160.
- Kitajima, E.W., Groot, T.V.M., Novelli, V.M., Freitas-Astúa, J., Alberti, G. & de Moraes, G.J. (2007). In situ observation of the *Cardinium* symbionts of *Brevipalpus* (Acari: Tenuipalpidae) by electron microscopy. *Exp Appl Acarol* 42: 263–271.
- Kitajima, E.W., Rezende, J.A.M., Rodrigues, J.C.V. (2003b). Passion fruit green spot virus vectored by *Brevipalpus phoenicis* (Acari: Tenuipalpidae) on passion fruit in Brazil. *Exp Appl Acarol* 30, 225–231. doi: 10.1023/B:APPA.0000006551.74604.84
- Kitajima, E.W., Rodrigues, J.C.V., & Freitas-Astúa, J. (2010). An annotated list of ornamentals naturally found infected by *Brevipalpus* mite-transmitted viruses. *Sci Agri* 67(3): 348–371. <https://doi.org/10.1590/S0103-90162010000300014>
- Knorr, L.C. (1968). Studies on the etiology of leprosis in citrus. Proceedings of 4th Conference International Organization Citrus Virologists: 332-341
- Kondo, H., Maeda, T., Shirako, Y., Tamada, T. (2006). Orchid fleck virus is a rhabdovirus with an unusual bipartite genome. *J. Gen. Virol* 87(8): 2413-2421.
- Krants, G. W. and E. E. Lindquist. 1979. Evolution of phytophagous mites (Acari). *Ann Rev Entomol* 24: 121-158.
- Kubo, K.S., Novelli, V.M., Bastianel, M., Locali-Fabris, E.C., Antonioli-Luizon, R., Machado, M.A., & Freitas-Astúa, J. (2011). Detection of *Brevipalpus*-transmitted viruses in their mite vectors by RT-PCR. *Exp App Acarol* 54(1): 33–39. <https://doi.org/10.1007/s10493-011-9425-9>
- Kubota, K. (2017). Emergence of emaraviruses, the eriophyid mite-transmitted viruses in plants. *Uirusu* 67(1): 37-48.
- Kubota, K., Usugi, T., Tomitak, Y., Shimomoto, Y., Takeuchi, S., Kadono, F., Yanagisawa, H., Chiaki, Y, Tsuda, S. (2020). *Perilla* mosaic virus is a highly divergent emaravirus transmitted by *Shevtchenkella* sp. *Phytopathol* (in press). doi: 10.1094/PHYTO-01-20-0013-R.
- Laney, A.G., Keller, K.E., Martin, R.R., Tzanetakis, I.E. (2011). A discovery 70 years in the making: characterization of the Rose rosette virus. *J Gen Virol* 92:1727–1732

Leastro, M.O., Kitajima, E.W., Silva, M.S., Resende, R.O., & Freitas-Astúa, J. (2018). Dissecting the subcellular localization, intracellular trafficking, interactions, membrane association, and topology of citrus leprosis virus C proteins. *Front Plant Sci* 9: 1299. <https://doi.org/10.3389/fpls.2018.01299>

Lee, H., Gurtowski, J., Yoo, S., Nattestad, M., Marcus, S., Goodwin, S., McCombie, W.R., Schatz, M.C. (2016). Third-generation sequencing and the future of genomics. *bioRxiv (Pre-Print)* 048603; doi: <https://doi.org/10.1101/048603>

Lindbo, J.A. (2007). TRBO: A high-efficiency tobacco mosaic virus RNA-based overexpression vector. *Plant Physiol.* 145(4): 1232-1240. doi: 10.1104/pp.107.106377.

Locali-Fabris, E. C., Freitas-Astúa, J., Souza, A. A., Takita, M. A., AstúaMonge, G., Antonioli-Luizon, R., Rodrigues, V., Targon, M. L. P. N., and Machado, M. A. 2006. Complete nucleotide sequence, genomic organization, and phylogenetic analysis of Citrus leprosis virus cytoplasmic type (CiLV-C). *J. Gen. Virol.* 87:2721-2729.

Locali-Fabris, E.C., Freitas-Astúa, J., Machado, M.A. (2012) Genus: Cilevirus. Part II – The positive sense single stranded RNA viruses. In: King, A.M.Q., Adams, M.J., Carstens, E.B., Lefkowitz, E.J., editors. *Virus Taxonomy, Classification and Nomenclature of Viruses. Ninth Report of the International Committee on Taxonomy of Viruses.* Elsevier, Academic Press. pp. 1169-1172.

Maliogka, V.I., Minafra, A., Saldarelli, P., Ruiz-Garcia, A.B., Glasa, M., Katis, N., Olmos, A. (2018) Recent advances on detection and characterization of fruit tree viruses using high-throughput sequencing technologies. *Viruses* 10(8): E436. doi: 10.3390/v10080436.

Melzer, M., Ayin, C., Sugano, J., Uchida, J., Kawate, M., Borth, W., and Hu, J. (2013a). Differentiation and Distribution of Cordyline Viruses 1–4 in Hawaiian ti Plants (*Cordyline fruticosa* L.). *Viruses* 5:1655–1663.

Melzer, M.J., Borth, W.B., Sether, D.M., Ferreira, S., Gonsalves, D., Hu, J.S. (2010). Genetic diversity and evidence for recent modular recombination in Hawaiian Citrus tristeza virus. *Virus Genes* 40, 111-118. doi:10.1007/s11262-009-0409-3

Melzer, M.J., Freitas-Astúa, J., Rodriguez, J.C.V., Roy, A., Wei, G. (2018). Create one new family *Kitaviridae* comprising three previously unassigned genera, *Cilevirus*, *Blunervirus* and *Higrevirus* 2018.002P. <https://talk.ictvonline.org/ictv/proposals/2018.002P.A.Kitaviridae.zip>. Accessed 13 Apr 2020

- Melzer, M.J., Sether, D.M., Borth, W.B., Hu, J.S. (2012). Characterization of a virus infecting *Citrus volkameriana* with citrus leprosis-like symptoms. *Phytopathol* 102(1): 122-127. doi: 10.1094/PHYTO-01-11-0013.
- Melzer, M.J., Sether, D.M., Borth, W.B., Mersino, E.F., and Hu, J.S. (2011). An assemblage of closteroviruses infects Hawaiian ti (*Cordyline fruticosa* L.). *Virus Genes* 42:254–260.
- Melzer, M.J., Simbajon, N., Carrillo, J., Borth, W.B., Freitas-Astúa, J., Kitajima, E.W. et al., (2013b). A cilevirus infects ornamental hibiscus in Hawaii. *Arch Virol* 158(11): 2421-2424. doi: 10.1007/s00705-013-1745-0
- Melzer, M.J., Sugano, J.S., Uchida, J.Y., Borth, W.B., Kawate, M.K., and Hu, J.S. (2013c). Molecular characterization of closteroviruses infecting *Cordyline fruticosa* L. in Hawaii. *Front. Microbiol.* 4:39 (doi:10.3389/fmicb.2013.00039).
- Melzer, M.J., Sugano, J., Uchida, J., Kawate, M., Borth, W., Hu, J. (2014). Partial characterization of a novel emara-like virus from *Cordyline fruticosa* (L.) with ti ringspot disease. *Phytopathol* 104(S3): S3.79
- Mielke, N., Muehlbach, H.P. (2007). A novel, multipartite, negative-strand RNA virus is associated with the ringspot disease of European mountain ash (*Sorbus aucuparia* L.). *J Gen Virol* 88:1337–1346
- Mielke-Ehret, N., Mühlbach, H.P. (2012). Emaravirus: a novel genus of multipartite, negative strand RNA plant viruses. *Viruses* 4(9): 1515-1536. doi: 10.3390/v4091515
- Nagyová, A., Subr, Z. (2007). Infectious full-length clones of plant viruses and their use for construction of viral vectors. *Acta Virol.* 51, 223–237.
- Navia, D., de Mendonça, R.S., Skoracka, A., Szydło, W., Knihinicki, D., Hein, G.L., da Silva Pereira, P.R., Truol, G., Lau, D. (2013) Wheat curl mite, *Aceria tosichella*, and transmitted viruses: an expanding pest complex affecting cereal crops. *Exp Appl Acarol* 59(1-2): 95-143.
- Nunes, M.R.T., Contreras-Gutierrez, M.A., Guzman, H., Martins, L.C., Feitoza Barbirato, M., Savit, C. et al., (2017). Genetic characterization, molecular epidemiology and phylogenetic relationships of insect-specific viruses in the taxon Negevirus. *Virology* 504: 152-167. doi: 10.1016/j.virol.2017.01.022
- Pasin, F., Menzel, W., Daros, J.A. (2019). Harnessed viruses in the age of metagenomics and synthetic biology: an update on infectious clone assembly and biotechnologies of plant viruses. *Plant Biotechnol* 17(6): 1010-1026. doi: 10.1111/pbi.13084

- Quito-Avila, D.F., Brannen, P.M., Cline, W.O., Harmon, P.F., Martin, R.R. (2013). Genetic characterization of blueberry necrotic ring blotch virus, a novel RNA virus with unique genetic features. *J Gen Virol* 94(6): 1426-1434. doi: 10.1099/vir.0.050393-0.
- Ramalho, T.O., Figueira, A.R., Sotero, A.J., Wang, R., Geraldino, D.P.S., Farman, M., Goodin, M.M. (2014). Characterization of coffee ringspot virus-Lavras: a model for an emerging threat to coffee production and quality. *Virology* 464-465: 385-396. doi: 10.1016/j.virol.2014.07.031.
- Ramos-González, P.L., Chabi-Jesus, C., Arena, G.D., Tassi, A.D., Kitajima, E.W., & Freitas-Astúa, J. (2018a). Leprosis de los cítricos: una enfermedad multietiológica singular. *Citrus leprosis: a unique multietiological disease. Citrus in the Americas* 1(1): 4–19.
- Ramos-González, P.L., Chabi-Jesus, C., Banguela-Castillo, A., Tassi, A.D., Rodrigues, M. da C., Kitajima, E.W., ... Freitas-Astúa, J. (2018b). Unveiling the complete genome sequence of clerodendrum chlorotic spot virus, a putative dichorhavirus infecting ornamental plants. *Arch Virol* 163(9): 2519–2524.
- Ramos-González, P.L., Chabi-Jesus, C., Guerra-Peraza, O., Breton, M.C., Arena, G.D., Nunes, M.A., ... Freitas-Astúa, J. (2016). Phylogenetic and molecular variability studies reveal a new genetic clade of *Citrus leprosis virus C*. *Viruses* 8(6): 153. <https://doi.org/10.3390/v8060153>
- Ramos-González, P.L., Chabi-Jesus, C., Guerra-Peraza, O., Tassi, A.D., Kitajima, E.W., Harakava, R., Salaroli, R.B., Freitas-Astúa, J. (2017). *Citrus leprosis virus N*: A new dichorhavirus causing citrus leprosis disease. *Phytopathol* 107: 963-976.
- Ramos-González, P.L. Dos Santos, G.F., Chabi-Jesus, C., Harakava, R., Kitajima, E.W., Freitas-Astúa, J. (2020). Passion Fruit Green Spot Virus Genome Harbors a New Orphan ORF and Highlights the Flexibility of the 5'-End of the RNA2 Segment Across Cileviruses. *Front. Microbiol.* 11:206. doi: 10.3389/fmicb.2020.00206.
- Rioja, C., Zhurov, V., Bruinsma, K., Grbic, M., and Grbic, V. (2017). Plant-herbivore interactions: a case of an extreme generalist, the Two-Spotted Spider Mite *Tetranychus urticae*. *Mol. Plant Microbe Interact.* 30, 935–945. doi: 10.1094/MPMI-07-17-0168-CR
- Robertson, N.L., Brumfield, S.K. (2000). First report of barley yellow streak mosaic virus-infected barley in Alaska. *Plant Dis* 84(5): 595.
- Robertson, N.L., Carroll, T.W. (1988). Virus-like particles and a spider mite intimately associated with a new disease in of Barley. *Science* 240(4856): 1188-1190. doi: 10.1126/science.240.4856.1188.

- Robinson, T.S., Brannen, P.M., Deom, C.M. (2012). Blueberry necrotic ring blotch: A new disorder of southern highbush blueberries. *Phytopathology* 102:S4.101.
- Rodrigues, J.C.V., Childers, C.C. (2013). *Brevipalpus* mites (Acari: Tenuipalpidae): vectors of invasive, non-systemic cytoplasmic and nuclear viruses in plants. *Exp Appl Acarol* 59: 165-175.
- Roy, A., Choudhary, Leon, M.G., Shao, J., Govindarajulu, A., Achor, D., et al., (2013). A novel virus of the genus *Cilevirus* causing symptoms similar to citrus leprosis. *Phytopathol* 103(5): 488-500. doi: 10.1094/PHYTO-07-12-0177-R
- Roy, A., Hartung, J.S., Schneider, W.L., Shao, J., Leon, G., Melzer, M.J., Beard, J.J., Otero-Colina, G., Bauchan, G.R., Ochoa, R., Brlansky, R.H. (2015a). Role bending: Complex relationships between viruses, hosts, and vectors related to citrus leprosis, an emerging disease. *Phytopathology* 105(7): 1013-1025. doi: 10.1094/PHYTO-12-14-0375-FI.
- Roy, A., Stone, A.L., Melzer, M.J., Hartung, J.S., Mavrodieva, V.A., Nakhla, M.K. et al., (2018a). First report of a cilevirus associated with green ring spot on senescent hibiscus leaves in Tampa, Florida. *Plant Dis* 102(6): 1181. doi: 10.1094/PDIS-11-17-1699-PDN
- Roy, A., Stone, A.L., Melzer, M.J., Shao, J., Hartung, J.S., Mavrodieva, V.A. et al., (2018b). Complete Nucleotide Sequence of a Novel Hibiscus-Infecting Cilevirus from Florida and Its Relationship with Closely Associated Cileviruses. *Genome Announcements* 6(4): e01521-17
- Roy, A., Stone, A.L., Shao, J., Otero-Colina, G., Wei, G., Choudhary, N., Achor, D., Levy, L., Nakhla, M.K., Hartung, J.S., Schneider, W.L., Brlansky, R.H. (2015b). Identification and molecular characterization of nuclear citrus leprosis virus, a member of the proposed dichorhavirus genus infecting multiple citrus species in Mexico. *Phytopathol* 105(4): 564-575. doi: 10.1094/PHYTO-09-14-0245-R.
- Ruigrok, R.W., Crepin, T., Kolakofsky, D. (2011). Nucleoproteins and nucleocapsids of negative-strand RNA viruses. *Curr Opin Microbiol* 14: 504–510.
- Sanger, F., Nicklen, S., Coulson, A.R. (1977). DNA sequencing with chain-terminating inhibitors. *Proc. Natl. Acad. Sci. U.S.A.* 74 (12): 5463–7
- Satyanarayana, T., Bar-Joseph, M., Mawassi, M., Albiach-Martí, M.R., Ayllón, M.A., Gowda, S. et al., (2001). Amplification of Citrus tristeza virus from a cDNA clone and infection of Citrus trees. *Virology* 280: 87-96.

Satyanarayana, T., Gowda, S., Ayllon, M.A., Dawson, W.O. (2003). Frameshift mutations in infectious cDNA clones of Citrus tristeza virus: a strategy to minimize the toxicity of viral sequences to *Escherichia coli*. *Virology* 313: 481-491.

Satyanarayana, T., Gowda, S., Boyko, V.P., Albiach-Martí, M.R., Mawassi, M., Navas-Castillo, J. et al., (1999). An engineered closterovirus RNA replicon and analysis of heterologous terminal sequences for replication. *Proc. Natl. Acad. Sci. USA*, 96 (1999), pp. 7433-7438

Schnell, M.J., Mebatsion, T., Conzelmann, K.K. (1994). Infectious rabies viruses from cloned cDNA. *The EMBO Journal* 13(18): 4195–4203.

Smith Meyer, M.K.P., Craemer, C., Naser, S. (2014). Plant feeding mites. Retrieved from: <https://www.arc.agric.za/arc-ppri/Pages/Biosystematics/Plant-Feeding-Mites.aspx> on 2020-03-27

Stenger, D.C., Hein, G.L., Tatineni, S., French, R.C. (2016). Eriophyid mite vectors of plant viruses. In: J.K. Brown, editor. *Vector-Mediated Transmission of Plant Pathogens*. St. Paul, MN: APS Press. pp. 263-274.

Stewart, L.R. (2016). Sequence diversity of wheat mosaic virus isolates. *Virus Res* 213: 299-303. doi: 10.1016/j.virusres.2015.11.013.

Taniguchi, T., Palmieri, M. and Weissmann, C. (1978). A Qbeta DNA-containing hybrid plasmid giving rise to Qbeta phage formation in the bacterial host (proceedings). *Annales de Microbiologie* 129: B(4): 535–536.

Tassi, A.D., Garita-Salazar, L.C., Amorim, L., Novelli, V.M., Freitas-Astúa, J., Childers, C.C., & Kitajima, E.W. (2017). Virus-vector relationship in the Citrus leprosis pathosystem. *Exp App Acarol* 71(3): 227–241. <https://doi.org/10.1007/s10493-017-0123-0>

Tatineni, S., McMechan, A.J., Wosula, E.N., Wegulo, S.N., Graybosch, R.A., French, R., Hein, G.L. (2014). An eriophyid mite-transmitted plant virus contains eight genomic RNA segments with unusual heterogeneity in the nucleocapsid protein. *J Virol* 88:11834–11845.

Tierney, M.B., Lamour, K.H. (2005). *An Introduction to Reverse Genetic Tools for Investigating Gene Function*. The Plant Health Instructor. DOI: 10.1094/PHI-A-2005-1025-01.

van Dijk, E.L., Jaszczyszyn, Y., Naquin, D., Thermes, C. (2018). The third revolution in Sequencing Technology. *Trends in Genetics* 34(9): 666-681. doi: 10.1016/j.tig.2018.05.008

Vasilakis, N., Forrester, N.L., Palacios, G., Nasar, F., Savji, N., Rossi, S.L. et al., (2013). Negevirus: a proposed new taxon of insect-specific viruses with wide geographic distribution. *J Virol* 87(5): 2475-2488. doi: 10.1128/JVI.00776-12.

Villamor, D.E.V., Ho, T., Al Rwahnih, M., Martin, R.R., Tzanetakis, I.E. (2019). High Throughput Sequencing for plant virus detection and Discovery. *Phytopathology* 109(5): 716-725. doi: 10.1094/PHYTO-07-18-0257-RVW.

Wang, Q., Ma, X., Qian, S., Zhou, X., Sun, K., Chen, X. et al., (2015). Rescue of a plant negative-strand RNA virus from cloned cDNA: Insights into enveloped plant virus movement and morphogenesis. *PLoS Pathog* 11(10): e1005223. doi: 10.1371/journal.ppat.1005223

Walker, P.J., Freitas-Astúa, J., Bejerman, N., Blasdell, K.R., Breyta, R., et al., (2021). ICTV Virus Taxonomy Profile: *Rhabdoviridae*. *J. Gen. Virol* (in press)

Walker, P.J., Siddell, S.G., Lefkowitz, E.J., Mushegian, A.R., Dempsey, D.M., Dutilh, B.E., Harrach, B. et al., (2019). Changes to virus taxonomy and the International Code of Virus Classification and Nomenclature ratified by the International Committee on Taxonomy of Viruses (2019). *Arch Virol* 164: 2417-2429. <https://doi.org/10.1007/s00705-019-04306-w>

Wergin, W.P., Ochoa, R., Erbe, E.F., Craemer, C., Raina, A.K. (2000). Use of low-temperature field emission scanning electron microscopy to examine mites. *Scanning* 22: 145-155.

Whitfield, A.E., Falk, B.W., Rotenberg, D. (2015). Insect vector-mediated transmission of plant viruses. *Virology* 479-480: 278-289.

Whitfield, A.E., Huot, O.B., Martin, K.M., Kondo, H., Dietzgen, R.G. (2018). Plant rhabdoviruses—their origins and vector interactions. *Current Opinion in Virology* 33: 198-207.

Zhang, Z. (2017). Eriophyoidea and allies: where do they belong? *Syst Appl Acarol* 22(8): 1091-1095.

Zheng, Y., Navarro, B., Wang, G., Wang, Y., Yang, Z., Xu, W., Zhu, C., Wang, L., Di Serio, F., Hong, N. (2017). Actinidia chlorotic ringspot-associated virus: a novel emaravirus infecting kiwifruit plants. *Mol Plant Pathol* 18(4): 569–581. <https://doi.org/10.1111/mpp.12421>

Zhu, B., Cai, G., Hall, E.O., Freeman, G.J. (2007). In-Fusion assembly: seamless engineering of multidomain fusion proteins, modular vectors, and mutations. *BiotTechniques* 43(3): 354-359. doi: 10.2144/000112536

OBJECTIVES

The overall goal of this study is to expand our knowledge on mite-associated viruses that are present in Hawaiian agroecosystems by characterizing these viruses at the molecular and biological level.

Considering the federal actionable pest status for some of these viruses, and the emergent nature of others present, this knowledge will be relevant for crop production in Hawaii and other tropical and sub-tropical US commodities.

Specific objectives:

1. Identification and natural host range of citrus leprosis viruses in Hawaii.
2. Characterization of a new kitavirid infecting hibiscus in Hawaii .
3. Perform a further molecular and biological characterization of hibiscus green spot virus 2.
4. Characterize the virome of tenuipalpid mites in Hawaii, with an emphasis on Kita- and Kita-like viruses.
5. Characterize a new emaravirus infecting ti plants (*Cordyline fruticosa*) in Hawaii.

CHAPTER II

IDENTIFICATION AND NATURAL HOST RANGE OF CITRUS LEPROSIS VIRUSES IN HAWAII

2.1 INTRODUCTION

Citrus leprosis (CL) is considered the most important quarantine and emerging disease in citrus producing countries where the disease is not present (Hartung et al., 2013; Robinson 2021). CL is a multi-etiological disease caused by viruses belonging to two distinct genera transmitted by *Brevipalpus* spp. mites. These brevipalpus-transmitted viruses (BTVs) accumulate in two different parts of plant cells (Ramos-González et al., 2018). Three dichorhavirus (Family *Rhabdoviridae*, BTV-N) causing CL replicate in the nucleus: citrus leprosis virus N (CiLV-N, Ramos-González et al., 2017), citrus chlorotic spot virus (CiCSV, Chabi-Jesus et al., 2017), and the citrus strains (Cruz-Jaramillo et al., 2014; Roy et al., 2015a; Roy et al., 2015b) and one orchid strain (Cook et al., 2019) of orchid fleck virus (OFV). Two cileviruses (Family *Kitaviridae*, BTV-C) causing CL replicate in the cytoplasm: citrus leprosis virus C (CiLV-C, Locali-Fabris et al., 2006; Pascon et al., 2006) and CiLV-C2 (Roy et al., 2013). Hibiscus green spot virus 2 (HGSV-2) is a *Kitaviridae* member in the genus *Higrevirus* which is likely transmitted by *Brevipalpus* mites (Melzer et al., 2012). HGSV-2 infects citrus causing chlorotic blotches on leaves and fruits, but occasionally may cause necrotic damage on twigs. These symptoms on citrus are referred to as CL-like symptoms, rather than CL symptoms, due to the general absence of necrosis in symptomatic leaves and fruits, which differs from CL. HGSV-2 is the only *Kitaviridae* member found infecting citrus, namely volkameriana lemon, mandarin, and sweet orange in Hawaii (Melzer et al., 2012; Roy et al., 2015a). To date, CL disease has mainly been restricted to South and Central American countries where it is caused by both BTV-C and BTV-N (Ramos-González et al., 2018), while it was recently reported in South Africa being caused by an orchid strain of the OFV, a BTV-N (Cook et al., 2019). Interestingly, a hibiscus strain of CiLV-C2 was characterized infecting hibiscus in Hawaii (Melzer et al., 2013); however, this and other viruses responsible for CL have not been found infecting citrus in Hawaii with the most recent survey performed in 2018.

In February and March 2020, CL symptoms were observed on the island of Hawaii on outgrown rough lemon rootstocks and mandarin scions growing in a semi-abandoned citrus orchard. Typical symptoms of leprosis were observed on leaves as well as on twigs. Infestations of *Brevipalpus* spp. mites were also observed on collected plant samples. Identification of the pathogen causing these symptoms is needed to

take appropriate action and implement a response plan to eradicate or at least prevent the further spread of the disease.

In addition to citrus, symptoms typical of those caused by BTV infection were observed in passion fruit vines (*Passiflora edulis*) in three locations in Honolulu in 2019. Passion fruit green spot virus (PfGSV), which has not been reported in Hawaii, is the only BTV officially reported to infect this host in Brazil. The presence of symptoms consistent with BTV infection in Hawaiian passion fruit suggests either a new BTV is present in Hawaii, or a BTV present in Hawaii has an expanded host range.

The goal of this chapter is to characterize the BTVs present in the citrus and passion fruit samples from Hawaii and Oahu Islands, respectively. BTV-C- and BTV-N-specific primers were designed to facilitate diagnostic procedures for the identification of BTVs. For BTV-C-specific primers, RT-PCR assays were validated and optimized using positive controls of CiLV-C2 and HGSV-2. These primers were then used in RT-PCR assays to provide initial BTV identity in the citrus and passion fruit samples. Finally, high-throughput sequencing (HTS) was used to validate the results obtained by RT-PCR and characterize near complete genomes of the BTVs.

2.2 MATERIALS AND METHODS

2.2.1 BTV-C- and BTV-N-specific primer design

In September 2019, all the accession sequences available at GenBank for *Kitaviridae* members: cileviruses, higrevirus and blunerviruses, namely CiLV-C, CiLV-C2, HGSV-2, blueberry necrotic ring blotch virus (BNRBV) and tea plant necrotic ring blotch virus (TPNRBV), were downloaded in fasta format. Similarly, all the accession sequences available at GenBank for dichorhavirus, namely OFV, CiLV-N, CiCSV and Clerodendrum chlorotic spot virus (ClCSV), were downloaded in fasta format. For BTV-C, cileviruses and HGSV-2, the coding sequences for the RNA-dependent RNA polymerase (RdRp) and virion membrane protein (SP24 gene homolog) were identified using the NCBI conserved domain search tool (www.ncbi.nlm.nih.gov/Structure/cdd/wrpsb.cgi) and underwent multiple alignment. For dichorhavirus (BTV-N), the coding sequences for the nucleoprotein (N) and polymerase (L) genes were identified using the NCBI conserved domain search tool and were similarly aligned. Finally, the coding sequences for the RdRp of cileviruses and HGSV-2 were aligned with the nucleotide coding sequences for the RdRp of blunerviruses, which were inferred using the NCBI conserved domain search tool. The multiple nucleotide sequence alignments were performed using the ClustalW algorithm (Thompson et al., 1994) implemented in Geneious 10.1.3 (Kearse et al., 2012).

Primaclade (Gadberry et al., 2005) was used for screening conserved domains and designing degenerate primers. The primer thermodynamic parameters, such as GC content and melting temperature ($^{\circ}\text{T}_m$), were analyzed with the assistance of Oligoanalyzer v3.1 (Owczarzy et al., 2008). The values of the thermodynamic parameters used were as described by Arif & Ochoa-Corona (2013).

2.2.2 PCR Annealing Temperature Optimization

All RT-PCR assays were performed in 15 μL reaction volumes using positive controls corresponding to a ten-fold dilution of cDNA obtained from *Hibiscus* spp. tissue infected with CiLV-C2 or HGSV-2. See below for RNA extraction and cDNA synthesis procedures. A gradient PCR experiment with annealing temperature ($^{\circ}\text{T}_a$) ranging from 45 $^{\circ}\text{C}$ to 55 $^{\circ}\text{C}$ was performed to determine the optimum $^{\circ}\text{T}_a$ of the primer sets. PCR conditions were as follow: 94C for 3 min, 30 cycles of 94C for 30s, $^{\circ}\text{T}_a$ for 30s and 72C for 30s. A final extension at 72C for 3 min was performed.

2.2.3 Tissue collection

In February and March 2020, leaf and stem tissues from mandarin and rough lemon displaying CL symptoms were collected from a semi-abandoned orchard in Waiakea on the island of Hawaii. The symptoms were characterized by circular- and oval-shaped chlorotic and necrotic lesions on leaves as well as chlorotic lesions on the stem of twigs (Figure 2.1).

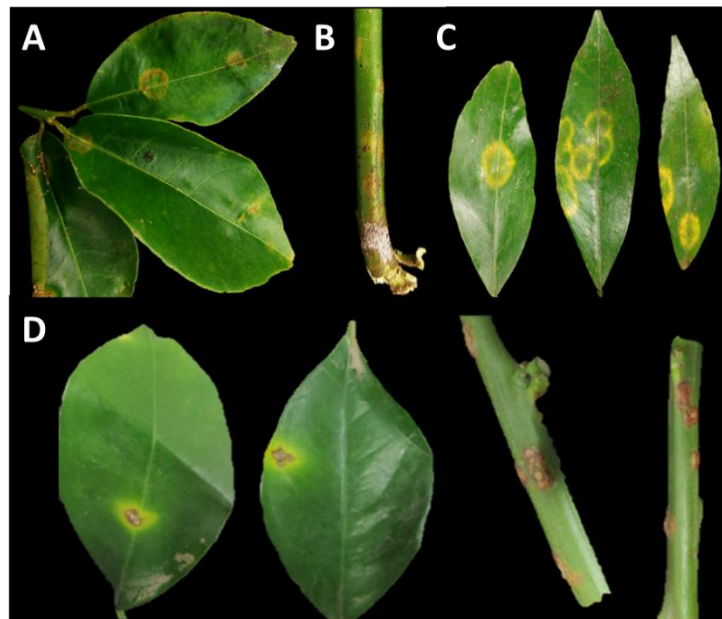


Figure 2.1 (A-C) Citrus leprosis (CL) symptoms observed in the leaves (A) and twigs (B) of an outgrown rough lemon rootstock (*C. jambhiri*) and mandarin leaves (*C. reticulata*) (C). The symptomatic trees were found in a semi-abandoned orchard located on Hawaii Island. D) CL symptoms

observed in the leaves and twigs of Valencia sweet orange (*C. sinensis*) in South Africa and caused by an orchid strain of OFV. Adapted from Cook et al. (2019).

In July 2019, passion fruit plants displaying varied viral-like symptoms were observed in three community gardens located in Honolulu: Ala Wai Community Garden, Makiki Community Garden and Manoa Community Garden. The symptoms observed in symptomatic passion fruit plants from the Ala Wai Community Garden were characterized by distortion, and green chlorotic spots were only observed on senescing leaves (Figure 2.2A and 2.2B). At the same time, the symptoms observed in plants collected from the Makiki and Manoa Community Gardens were similar and corresponded to distortion and chlorotic mottling (Figure 2.2C).

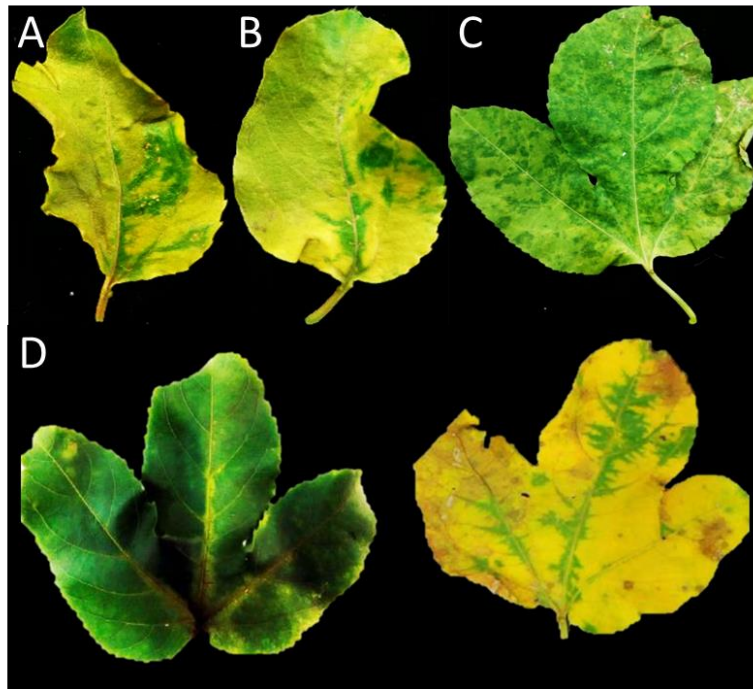


Figure 2.2 (A-C) Viral-like symptoms of passion fruit samples collected from three Community Gardens located in Honolulu, Oahu. A) and B) Ala Wai Community Garden. Leaves presented green chlorotic spots and distortion on senescing leaves. C) Makiki and Manoa Community Gardens. Leaves presented distortion (not shown) and chlorotic mottling. D) Green chlorotic spots caused by the cilevirus passion fruit green spot virus (PfGSV) on normal (left) and senescent (right) passion fruit leaves. Adapted from Ramos-Gonzalez et al. (2020).

2.2.4 Virus Detection

Total RNA was extracted from 50-150 mg of symptomatic tissue. Individual RNA extracts were obtained from three rough lemon and three mandarin samples and 40 symptomatic passion fruit leaves from the three community gardens. RNA extractions were performed using NucleoSpin RNA Plus kit (Macherey-Nagel, Düren, Germany) or Spectrum Plant Total RNA kit (Sigma-Aldrich, St. Louis, MO) following the manufacturer's instructions. Individual RNA extracts were pooled to obtain two CL pools of RNA, one for rough lemon and one for mandarin samples, and three passion fruit pools of RNA, one per community garden. These pool of RNAs were reverse transcribed into cDNA using random primers and M-MLV reverse transcriptase (Promega) using the manufacturer's protocol. Two microliters of cDNAs were tested by endpoint PCR using GoTaq Green Master Mix (Promega) using BTV-specific primers (Table 2.1) to evaluate BTV presence. Also, the presence of the two BTVs already reported in Hawaii, namely CiLV-C2 and HGSV-2, was assessed using virus-specific primers, CiLV-C2-RdRP-F/R and HGSV-2-RdRp-F/R (Olmedo-Velarde et al. 2021), in the CL sample. 0.5 μ M was used as the final primer concentration for all the endpoint RT-PCR assays. The annealing temperature for CiLV-C2- and HGSV-2-specific primers was 55 °C, whereas the optimum annealing temperature determined using gradient PCR was used for BTV-specific primers. Non-template controls (DEPC-treated water) were used in all the assays. Amplicons were either gel extracted, purified and bi-directionally sequenced or cloned into pGEM-T Easy (Promega, Madison, WI) and three clones were sequenced.

2.2.5 Genome sequencing

Total RNA was extracted from 150 mg of symptomatic citrus tissue (Figure 2.1) from the Hawaii Island using the NucleoSpin RNA Plus kit (Macherey-Nagel, Düren, Germany). Total RNA was ribodepleted using the Plant Ribo-Zero rRNA removal kit (Illumina, San Diego). Illumina libraries were prepared using TruSeq Stranded Total RNA Library Prep kit (Illumina, San Diego). HTS was performed on an Illumina MiSeq 2x300 bp (V2) platform at the USDA-APHIS-PPQ-CPHST laboratory in Beltsville, Maryland.

Double-stranded RNAs (dsRNAs) were extracted from ~20 g of a pool of symptomatic passion fruit leaf tissue collected from the three Community Gardens in Honolulu (Oahu Island) and using either CF-11 (Whatman, Maidstone, UK) or C6288 (Sigma, St. Louis, MO) cellulose chromatography (Morris and Dodds, 1979) and resolved by 1X TBE-1% agarose gel electrophoresis. Randomly amplified cDNAs were generated (Melzer et al., 2010) and prepared for high-throughput sequencing (HTS) using a Nextera

XT DNA Library Prep kit (Illumina, San Diego, CA). HTS was performed on an Illumina MiSeq 2 x 300 bp (V2) platform at the University of Hawaii Advanced Studies in Genomics, Proteomics, and Bioinformatics (ASGPB) Laboratory.

Genome assembly and bioinformatic analyses were performed as described (Olmedo-Velarde et al., 2019). Briefly, after paired-end reads were trimmed and quality filtered using Trimmomatic 0.35.3 (Bolger et al., 2014), they were mapped to the *Citrus reticulata* genome (https://ftp.ncbi.nih.gov/genomes/genbank/plant/Citrus_reticulata/) and *Passiflora edulis* (https://ftp.ncbi.nih.gov/genomes/genbank/plant/Passiflora_edulis/) draft genomes for the CL and passion fruit samples, respectively. Using the non-host reads, Trinity 2.2.0 (Grabherr et al., 2011) produced *de novo* assembled contigs that were annotated using BLASTX search (Altschul et al., 1997) against the viral genome database (<ftp://ftp.ncbi.nih.gov/genomes/Viruses/all.fna.tar.gz>). Contiguous sequences (contigs) with similarity to BTV sequences were then used as reference for an iterative mapping approach (Dey et al., 2019) using Geneious mapper plug-in implemented in Geneious v. 10.1.3 (Kearse et al., 2012) and raw reads. The NCBI ORFfinder program (www.ncbi.nlm.nih.gov/orffinder) was used to identify putative open reading frames (ORFs) *in silico* and examine the genomic organization of the sequenced BTVs.

2.2.6 Phylogenetic Analyses

Phylogenetic relationships between the BTVs found in the symptomatic citrus and passion fruit samples were inferred using the nucleotide sequences of multiple RdRp domain sequences and multiple concatenated genomic sequences for the BTVs found in the passion fruit and citrus samples, respectively. Multiple nucleotide sequence alignments were performed with ClustalW (Thompson et al., 1994) implemented in MEGA 7.0.25 (Kumar et al., 2016). Ambiguous positions for each alignment were curated using Gblocks 0.91b (<https://ngphylogeny.fr>) (Talavera and Castresana, 2007). The best model of nucleotide evolution for each alignment was used to generate a Maximum Likelihood tree with 1,000 bootstrap repetitions.

2.2.7 Barcoding and virus detection in flat mites

Five individual flat mites feeding on the citrus samples presenting leprosis symptoms were collected. Eight individual flat mites (*Brevipalpus* spp.) feeding on the symptomatic passion fruit leaves collected in Ala Wai Community Garden were also collected. These mites were used for direct reverse transcriptase

(DRT)-PCR assays (Druciarek et al., 2019). Briefly, individual *Brevipalpus* mites were introduced into a PCR tube containing 10 µl of water and random hexamer primers and crushed using a needle under a dissecting microscope. Then, cDNA was synthesized using random primers and SuperScript III reverse transcription kit (ThermoFisher Scientific, Waltham, MA) using the manufacturer's instructions. Two microliters of ten-fold diluted cDNA reactions were used in endpoint PCR for DNA barcoding and internal PCR control using the 28S rRNA primers, D1D2w2: 5'-ACAAGTACCDTRAGGGAAAGTTG-3', 28Sr0990: 5'-CCTTGGTCCGTGTTTCAAGAC-3' (Druciarek et al., 2019; Sonnenberg et al. 2007; Mironov et al. 2012) that produce a ~700 bp expected amplicon. All DNA barcoding PCR assays were performed using Q5 High Fidelity DNA Polymerase (New England Biolabs, Ipswich, MA). Furthermore, endpoint RT-PCR assays using virus-specific primers were performed as detailed above to detect the presence of BTVs in the mite specimens. All amplicons were gel extracted, purified and bi-directionally sequenced.

2.3 RESULTS

2.3.1 BTV-specific primers and PCR assay optimization

Using multiple nucleotide sequence alignments and Primalclade (Gadberry et al., 2005), two BTV-C specific primer sets (Cile-Higre-R1-F/R and Cile-Higre-R2-F/R) were designed to target the RdRp (RNA 1) and p24 (RNA 2 and 3) genes, respectively (Figure 2.3A and 2.3B, and Table 2.1). Similarly, two BTV-N specific primer sets (Dichorha-R1-F/R and Dichorha-R2-F/R) were designed to target the N (RNA 1) and L (RNA 2) genes, respectively (Figure 2.4 and Table 2.1). Also, the primer set Kitavirid-F/R was designed to target conserved RdRp domains present in the RdRp gene (RNA 1 and 2) of kitavirids (Figure 2.3C and Table 2.1). All primer pairs possessed similar °Tm values which differed less than 2 °C between each primer in a pair. Although not all the designed primers presented ideal thermodynamic features, i.e., self-dimer and hetero-dimer values higher than -9 kcal/mole, all primer sets proved useful in RT-PCR assays producing the expected sized amplicons with few or none non-specific products (described below). A gradient PCR was performed to evaluate the best °Ta within a range of six temperatures (ranging between 45 to 55 °C) and demonstrate primers' ability to amplify the target gene sequence. The two primer sets specific for BTV-C RNA 1 and 2, and the primer set specific for kitavirids were evaluated using positive control cDNA for CiLV-C2 and HGSV-2 (Figure 2.5). Due to the lack of a positive control cDNA for any BTV-N, a gradient PCR for determining the best °Ta of BTV-N specific primers was not performed.

Table 2.1 Cilevirus/Higrevirus-specific, dichorhavirus-specific, and kitavirid-specific primer sets designed using multiple nucleotide sequence alignments and Primaclade (Gadberry et al., 2005). Thermodynamic features are provided including GC%, mean °Tm, and both self-dimer and hetero-dimer formation expressed as -kcal/mole.

Primer Name	Target	RNA	Gene	Expected Size (bp)	Sequence (5'-3')	Length	GC%	°Tm (mean)	Self-dimer (-kcal / mole)	Hetero-dimer (-kcal / mole)
Cile-Higre-R1-F	Cilevirus-	1	RdRp	280-310	GCTKAARAATWSTGAACCBKIGT	24	38.2	62.5°C	-11.49	-8.94
Cile-Higre-R1-R	Higrevirus				AANKTSGTCTTYCCWGCACC	20	52.5	62.5°C	-7.25	
Cile-Higre-R2-F	Cilevirus-	2/3	SP24	198	AAYMCRDTTMTTRAGTGGGC	20	44.2	58.8°C	-8.3	-15.05
Cile-Higre-R2-R	Higrevirus				CTTAGCRTAMACRTGSAAWGA	21	40.5	58.3°C	-9.44	
Dichorha-R1-F	Dicho-	1	N	~350	CAYCACTGYGCBRTNGCWGATGA	23	55.1	66.9°C	-21.36	-17.15
Dichorha-R1-R	rhavirus				AGKATRTSWGCCATCCKGGCTATBAG	26	50.6	66.4°C	-10.68	
Dichorha-R2-F	Dicho-	2	L	~500	CAGTGTGAGAAGACNTTYGARATHCC	26	45.5	63.6°C	-13.18	-6.58
Dichorha-R2-R	rhavirus				CTCATYTGYTGRITCCAYTTYCTGAA	26	40.4	63.4°C	-5.02	
Kitavirid-F	<i>Kita-</i>	1/2	RdRp	~411	CCGACATNAANAARTAYGAYAAGTCWC	28	37.5	63.1°C	-8.23	-6.73
Kitavirid-R	<i>viridae</i>				A	28	39.3	64.7°C	-10.48	

R = A or G, Y = C or T, S = G or C, W = A or T, K = G or T, M = A or C, B = C or G or T, D = A or G or T, H = A or C or T, N = A or C or G or T. RdRp = RNA-dependent RNA polymerase. SP24 = transmembrane protein likely coding for a virion membrane protein. N gene = nucleoprotein. L gene = Polymerase gene.

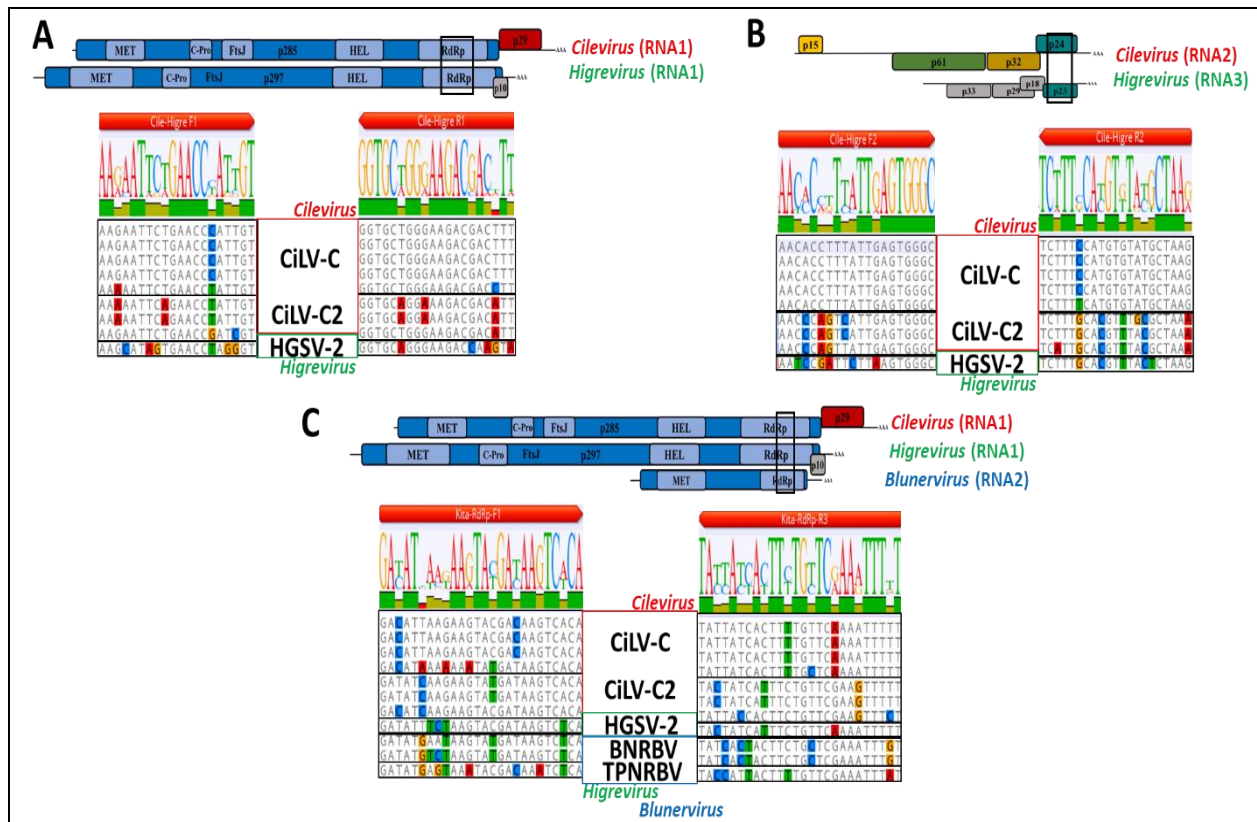


Figure 2.3 Representation of multiple nucleotide sequence alignments for the RNA-dependent RNA polymerase (RdRp) (A) and SP24 (B) genes of BTV-C (cileviruses and higrevirus), and for the RdRp gene (C) of kitavirids (cileviruses, higrevirus and blunerviruses). CiLV-C, citrus leprosis virus C; CiLV-C2; HGSV-2, hibiscus green spot virus 2; BNRBV, blueberry necrotic ring blotch virus; TPNRBV, tea plant necrotic ring blotch virus.

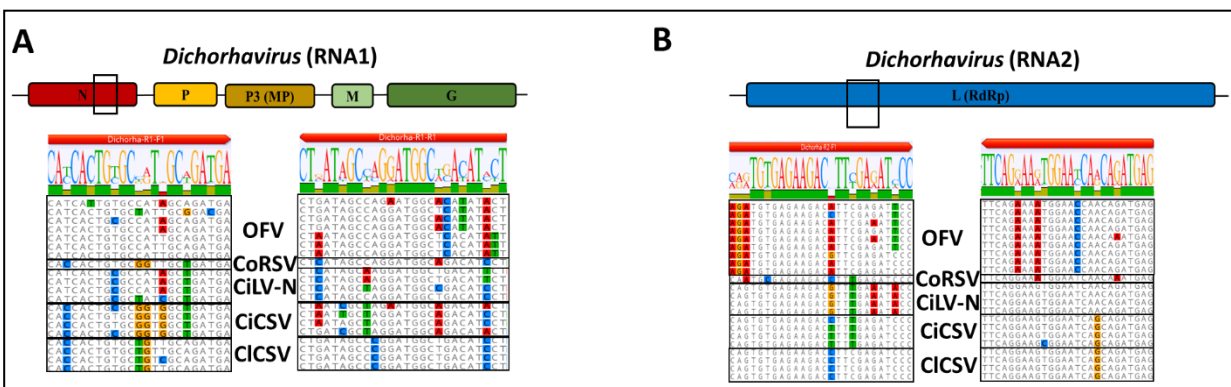


Figure 2.4 Representation of multiple sequence alignments for the nucleoprotein (N) gene (A) and polymerase (L) gene (B) of dichorhviruses. OFV, orchid fleck virus; CoRSV, coffee ringspot virus; CiLV-N, citrus leprosis virus N; CiCSV, citrus chlorotic spot virus; CICSV, Clerodendrum chlorotic spot virus.

Gradient PCR showed that for both cilevirus positive controls (CiLV-C2 and HGSV-2), the three primer sets; Cile/Higre-R1-F/R, Cile/Higre-R2-F/R and Kitavirids-F/R; amplified the expected products of the RdRp (280-310 bp), SP24 (198 bp) and RdRp (411 bp) genes, respectively, within the evaluated temperature range. However, the best performance was observed between 45 – 49 °C for the three primer sets (Figure 2.5). A °Ta of 45 °C was selected as the best annealing temperature for subsequent RT-PCR assays.

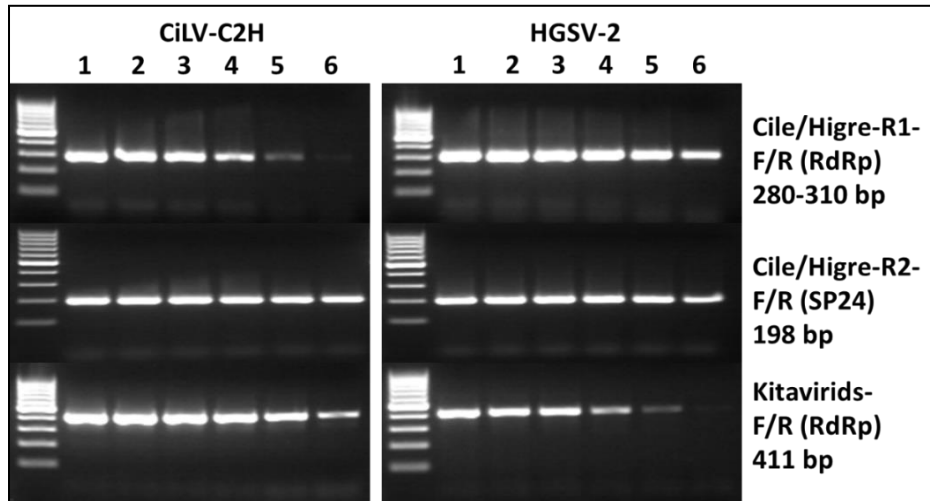


Figure 2.5 Gradient PCR for Cile/Higre-R1-F/R, Cile/Higre-R2-F/R and Kitavirids-F/R within six temperatures ranging from 45°C to 55°C (1 = 45 °C, 2 = 47 °C, 3 = 49 °C, 4 = 51 °C, 5 = 53 °C, 6 = 55 °C). Positive control cDNA preparations for the hibiscus strain of citrus leprosis virus C2 (CiLV-C2) and hibiscus green spot virus (HGSV-2) were used for the assays. A 100 bp ladder (ThermoFisher Scientific, Waltham, MA) was used in all the assays.

2.3.2 Detection of BTVs in citrus and passion fruit samples

RT-PCR assays using Cile/Higre-R1-F/R, Cile/Higre-R2-F/R, Kitavirids-F/R, Dichorha-R1-F/R and Dichorha-R2-F/R suggested the presence of a BTV-N and a BTV-C in the citrus and the passion fruit samples coming from Hawaii and Oahu Islands, respectively (Figure 2.6 and 2.7). RT-PCR assays using CiLV-C2-specific, HGSV-2-specific, BTV-C-specific, and kitavirids-specific primers tested negative on the citrus samples, whereas a positive control for these assays tested positive. Similarly, RT-PCR assays using BTV-N-specific primers tested negative on all the passion fruit samples (data not shown).

Sequencing of the BTV-N amplicon (RNA 1 and 2) obtained from the pool of RNAs of the rough lemon samples suggested the presence of OFV. A BLASTn search revealed the BTV-N amplicon sequences share >99% nucleotide identity to an orchid strain of OFV (AF321775 and AB516441). Whereas sequencing of the BTV-C (RNA 1 and 2) and kitavirid amplicons (RNA 1) obtained from the pool of RNAs of the passion fruit leaf samples, and a BLASTn search revealed the amplicon sequences shared >97% nucleotide identity to CiLV-C2 previously characterized infecting hibiscus plants in Hawaii (KC626783 and KC626784). RT-PCR positive results were obtained only from the pool of RNAs corresponding to passion fruit samples collected from the Ala Wai community garden. In contrast, the pool of RNAs corresponding to passion fruit samples from the other two community gardens tested negative (Figure 2.7).

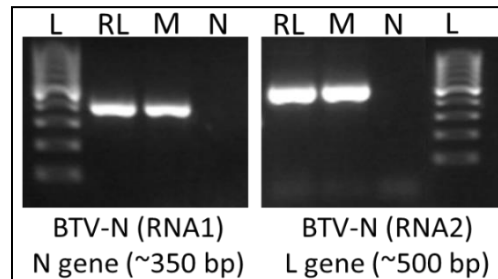


Figure 2.6 RT-PCR assay for detection of BTV-N RNA 1 (N gene, ~350 bp) and RNA 2 (L gene, ~500 bp) on the pool of RNAs of the citrus samples from Hawaii Island. L= 100 bp ladder (ThermoFisher Scientific, Waltham, MA), N = non-template control (NTC), RL = pool of RNAs extracted from symptomatic rough lemon leaf samples, M = pool of RNAs extracted from symptomatic mandarin leaf samples.

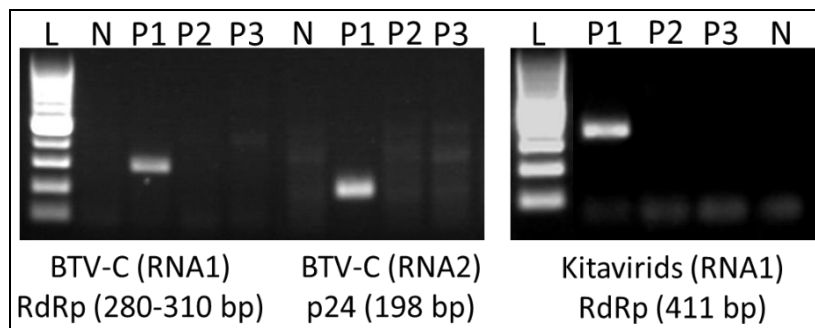


Figure 2.7 RT-PCR assays for detection of BTV-C RNA 1 (RdRp, 280-310 bp) and RNA 2 (p24 gene, 198 bp), and kitavirids RNA 1/2 (RdRp, 411 bp) on the passion fruit leaf samples from Oahu. L = 100 bp ladder (ThermoFisher Scientific, Waltham, MA), N = non-template control (NTC), P1 = pool of RNAs extracted from symptomatic passion fruit leaf samples from Ala Wai community garden, P2 = pool of RNAs extracted from symptomatic passion fruit leaf samples from Makiki community garden and

P3 = pool of RNAs extracted from symptomatic passion fruit leaf samples from Manoa community garden.

The presence of OFV causing CL in mandarin and rough lemon samples was further confirmed using RT-PCR assays and the OFV-specific primer sets OFV-Orc-GPF (5'-AGCGATAACGACCTTGATATGACACC-3') / OFV-Orc-GPR, (5'-TGAGTGGTAGTCAATGCTCCATCAT-3'); and OFV-R2-GF1 (5'-CARTGTCAGGAGGATGCATGGAA-3') / OFV-R2-GR (5'-GACCTGCTTGATGTAATTGCTTCCTTC-3') (Roy et al., 2020). The RNA extracted from two rough lemon and three mandarin symptomatic leaf samples were tested. The RNA extracted from one asymptomatic rough lemon leaf sample was also included in the RT-PCR assays. The symptomatic samples tested positive for OFV using OFV-Orc-GPF/GPR and OFV-R2-GF1/GR whereas the asymptomatic sample and the NTC control tested negative for both primer sets (Figure 2.8). Direct Sanger sequencing of the amplicons obtained from one mandarin sample and BLASTn searches revealed the amplicon sequences shared 97-98% identity with published OFV sequences (AB244417 and AB516441).

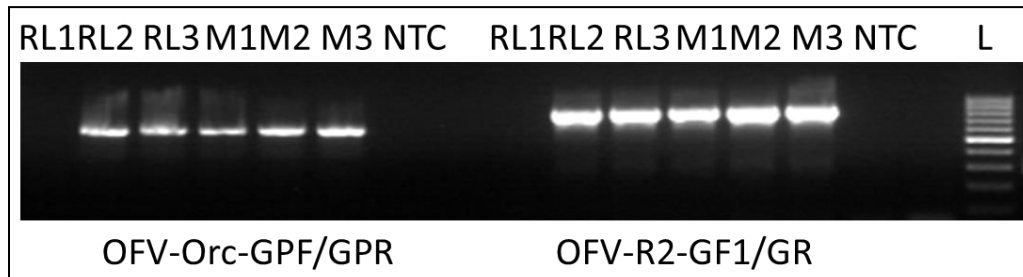


Figure 2.8 RT-PCR assays for detection of OFV using OFV-specific primer sets (OFV-Orc-GPF/GPR and OFV-R2-GF1/GR; Roy et al., 2020) on the citrus leprosis samples from the Hawaii Island. L = 100 bp ladder (ThermoFisher Scientific, Waltham, MA), RL1-3 = rough lemon leaf samples (RL1 did not have leprosis symptoms), M1-3 = mandarin samples, NTC = non-template control.

The presence of CiLV-C2 infecting passion fruit was confirmed using RT-PCR assays and a CiLV-C2-specific primer set CiLV-C2-RdRp-F (5'-ACAAGATGGCGGACGAACTG-3') / CiLV-C2-RdRp-R (5'-AGCCATGTCATCGGGATCCA-3') (Olmedo-Velarde et al., 2021). Similar to the results obtained by RT-PCR assays using BTV-C-specific and kitavirid-specific primer sets (Figure 2.7), only the pool of RNAs prepared from RNAs extracts obtained from passion fruit leaf samples coming from the Ala Wai community garden tested positive for CiLV-C2. RNA pools composed of RNA extracts obtained from

passion fruit leaf samples from Makiki and Manoa community gardens tested negative for CiLV-C2 (data not shown). To further examine the presence of CiLV-C2 at the Ala Wai community garden, 19 individual RNA extracts from symptomatic and asymptomatic passion fruit leaf samples collected at this location underwent RT-PCR assays. Of the 19 samples tested, 16 were positive for the virus (Figure 2.9). Of these, 13 presented apparent symptoms of BTV infection (Figure 2.2 A and B). Direct Sanger sequencing of one amplicon and a BLASTn search revealed that the amplicon sequence shared 99.0% nucleotide identity to the RNA 1 of CiLV-C2 previously reported infecting hibiscus plants in Hawaii (KC626783).

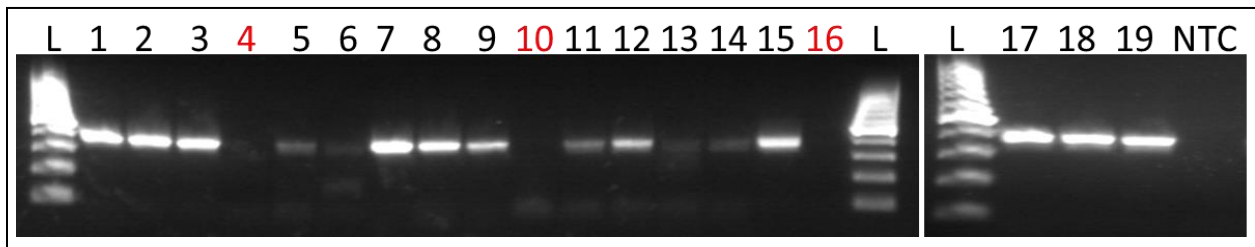


Figure 2.9 RT-PCR assays for detection of CiLV-C2 on 19 passion fruit leaf samples from the Ala Wai community garden. L = 100 bp ladder (ThermoFisher Scientific, Waltham, MA). 1, 2, 5-8, 11-14 and 17-19 = passion fruit leaves presenting symptoms caused by BTVs (Figure 2.2 A and B). 3,4, 9,10, 15 and 16 = passion fruit leaves not presenting obvious viral-like symptoms. NTC = non-template control. Numbers for samples that tested negative for CiLV-C2 are highlighted in red.

2.3.3 Molecular characterization of OFV in citrus and CiLV-C2 in passion fruit in Hawaii

Illumina HTS generated 19.6 M (75 bp) and 6.5 M (100 bp) of paired-end reads for the CL and passion fruit samples, respectively. *De novo* assembly of the non-host reads of both datasets using Trinity produced 6,677 and 2,215 contigs, respectively. BLASTx searches revealed that two contigs of 6,438 bp (MW021482) and 5,986 bp (MW021483) were found in the CL sample to have 98.7% nucleotide identity to RNA1 (AB244417) and RNA2 (AB244418), respectively, of the isolate So of OFV infecting orchids in Japan. Whereas two contigs of 8,536 bp (MW413437) and 4,878 bp (MW413438) were found in the passion fruit sample to have 99.2% and 97% nucleotide identity to RNA 1 (KC626783) and RNA2 (KC626784), respectively, of CiLV-C2 previously reported infecting hibiscus plants in Hawaii. The genomic organization of both BTVs, OFV and CiLV-C2, infecting citrus and passion fruit, respectively, were identical for both RNA 1 and 2 to previously characterized isolates of these viruses (data not shown).

2.3.4 BTVs are present as mixed virus infections

BLASTx searches revealed the presence of contig sequences corresponding to other viruses additional to the contig sequences of OFV and CiLV-C2. OFV was found in mixed infections with citrus vein enation virus (CVEV) and at least two genotypes (VT and RB) of citrus tristeza virus (CTV) in the CL samples. CiLV-C2 was found in mixed infections with bean common mosaic virus (BCMV), cucumber mosaic virus (CMV) and its satellite, dasheen mosaic virus (DsMV), and watermelon mosaic virus (WMV) in the passion fruit sample. These latter results were congruent with multiple dsRNA bands that were resolved on a 1X-TBE agarose electrophoresis gel (Figure 2.10).

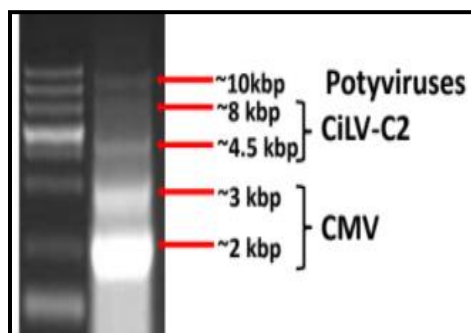


Figure 2.10 Multiple dsRNA bands observed following resolution by 1X TBE agarose gel electrophoresis. Right lane: Bands of ~2 and ~3 kbp were observed and congruent with the three genomic RNA sizes of cucumber mosaic virus (CMV). Bands of ~4.5 and ~8 kbp were observed and congruent with the two genomic RNA segment sizes of citrus leprosis virus C2 (CiLV-C2). Also, a single band of ~10 kbp was observed and congruent with the potyviruses' genomic RNA size. Left lane: 1 kb plus ladder (ThermoFisher Scientific, Waltham, MA).

2.3.5 Phylogenetic relationships of OFV and CiLV-C2

An unrooted phylogenetic tree was inferred from multiple nucleotide sequence alignments using concatenated full genomic sequences of RNA 1 and 2 of different OFV isolates infecting citrus and orchids. A Maximum Likelihood (ML) algorithm based on the Tamura-Nei (TN93) model was used with 1,000 bootstrap repetitions as branch support. The OFV isolate from Hawaii infecting citrus clustered together with OFV isolates infecting orchids (Orc2) in China (AB516442/3) and Japan (AB244417/8) (Figure 2.11).

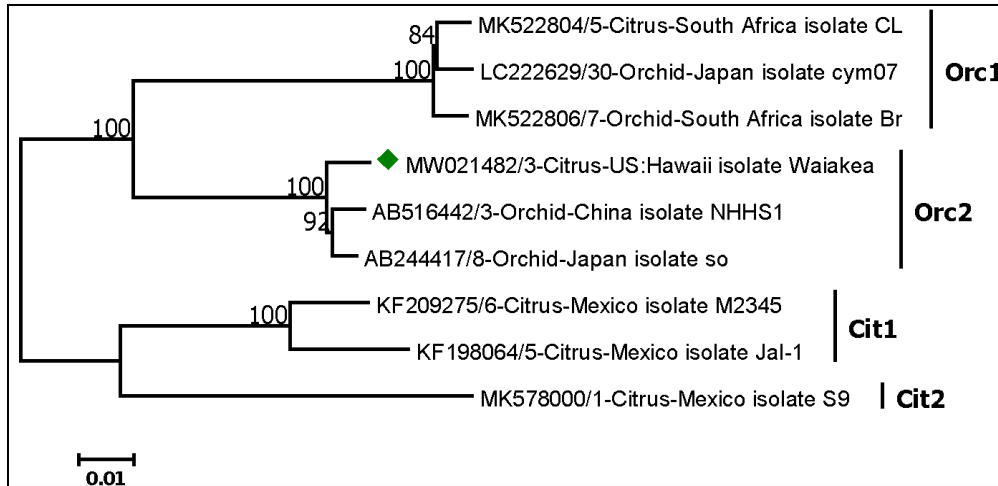


Figure 2.11 Phylogenetic relationship of orchid fleck virus (OFV) isolated from Hawaiian citrus with other OFV isolates infecting citrus (Cit1 and Cit2) and orchids (Orc1 and Orc2) based on the concatenated full genomic sequences of RNA 1 and 2. The tree was constructed using the Maximum Likelihood method using the Tamura-Nei (TN93) model, with 1,000 bootstrap pseudo-replicates as percentage values for branch support. GenBank accession numbers are provided before each OFV isolate and host. The scale represents the number of substitutions per unit branch length. The green diamond indicates the OFV isolate from Waiakea, Hawaii.

Similarly, a phylogenetic tree was inferred from multiple nucleotide sequence alignments using the RdRp domain sequences of cileviruses. The tree was generated using the Maximum Likelihood algorithm based on the TN93 model with 1,000 bootstrap repetitions as branch support. CiLV-C2 infecting passion fruit clustered together with two hibiscus isolates of CiLV-C2 infecting hibiscus plants in Hawaii (KC626783) and Florida (MG253805) (Figure 2.12).

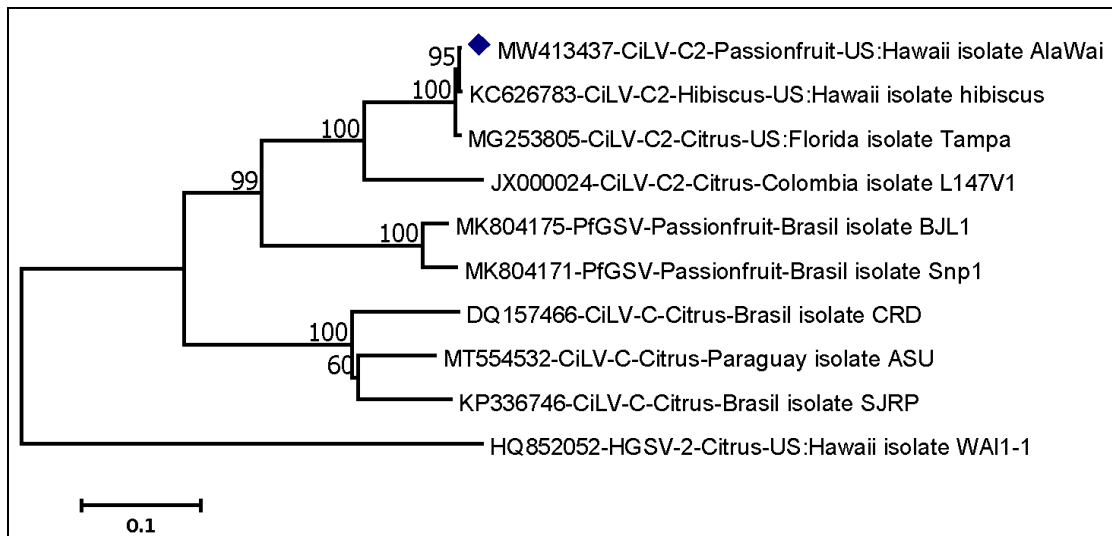


Figure 2.12 Phylogenetic relationship of CiLV-C2 (hibiscus isolate of CiLV-C2) infecting passion fruit in Hawaii with other cileviruses based on the RdRp domain nucleotide sequences. The tree was constructed using the Maximum Likelihood method and the Tamura-Nei (TN93) model, with 1,000 bootstrap pseudo-replicates as percentage values for branch support. The RdRp domain nucleotide sequence of hibiscus green spot virus (HGSV-2) was used as an outgroup. The GenBank accession numbers are provided before each cilevirus isolate and host. The scale represents the number of substitutions per unit branch length. The dark blue diamond indicates the CiLV-C2 isolate infecting passion fruit in Hawaii.

2.3.6 Flat mites barcoding and CiLV-C2 detection

The sequences of the 28S amplicons that were obtained from the five individual flat mites feeding on the citrus samples presenting leprosis symptoms and obtained using DRT-PCR assays (Druciarek et al., 2019) presented 100% nucleotide identity among one another. A BLASTn search of a consensus of the five sequences showed that it shares 100% nucleotide identity to *B. yothersi* (MK293678) with 86% query coverage. Similarly, the sequences of the 28S amplicons from the eight individual flat mites feeding on the symptomatic passion fruit leaf samples presented 100% nucleotide identity among one another. A BLASTn search using the consensus sequence showed that it shares 100% nucleotide identity to *B. yothersi* (MZ478051) with 86% query coverage. A pairwise alignment of the consensus sequences of mites from both hosts revealed they share 99.8% nucleotide identity between each other.

DRT-PCR assays using OFV-specific primers (OFV-Orc-GPF/GPR and OFV-R2-GF1/GR) did not detect the presence of the virus in the five putative *B. yothersi* specimens feeding on symptomatic citrus samples

(data not shown). In contrast, DRT-PCR assays using CiLV-C2-specific primers (CiLV-C2-RdRp-F/R) detected the presence of the virus in 6 out of the 8 putative *B. yothersi* specimens feeding on symptomatic passion fruit leaf samples (Figure 2.13).

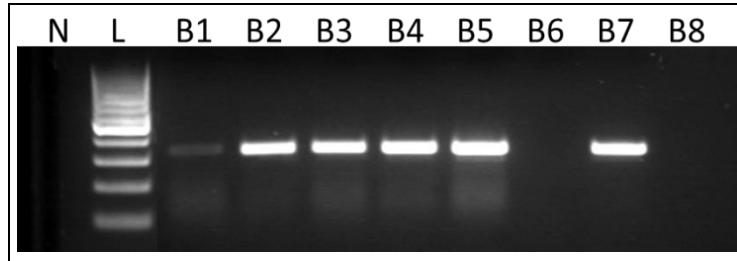


Figure 2.13 DRT-PCR assays for detection of CiLV-C2 on single brevipalpus (B1-B8) mite specimens. Mites were feeding on passion fruit leaf samples presenting symptoms consistent with BTV infection (Figure 2.2 A and B) collected from the Ala Wai community garden. L = 100 bp ladder (ThermoFisher Scientific, Waltham, MA); N = non-template control (DEPC water).

2.4 DISCUSSION

Multiple nucleotide sequence alignments and Primalade (Gadberry et al., 2005) allowed the design of degenerate primers that have the potential for universal detection of BTV-C and BTV-N as well as kitavirids (Table 4.1). The BTV-C- and kitavirids-specific primers were validated using CiLV-C2 and HGSV-2 (Figure 2.5), representing viruses from two distinct genera. The best annealing temperature (45 °C) that was selected from the gradient PCR assays was helpful in the optimal detection of both BTV-C (Figures 2.5 and 2.6) and BTV-N (Figure 2.6). The symptoms observed in the passion fruit leaf samples collected from the Ala Wai community garden (Oahu Island) and the citrus samples collected from Waiakea (Hawaii Island) were characterized by chlorotic and/or necrotic lesions that are congruent with the symptoms caused by BTVs (Kitajima et al., 2003). These symptoms on citrus and passion fruit resembled those caused by an orchid strain of OFV in *C. sinensis* (Cook et al., 2019) and passion fruit green spot virus (PfGSV) (Ramos-Gonzalez et al., 2020), respectively (Figures 2.1 and 2.2). The symptoms caused by CiLV-C2 on passion fruit in Hawaii were more obvious on senescent leaves than on normal ones (Figure 2.2). This same observation has been previously recorded for other BTVs, namely PfGSV infecting passion fruit (Ramos-Gonzalez et al., 2020), CiLV-C2 infecting hibiscus plants (Melzer et al., 2013; Roy et al., 2015), and HGSV-2 infecting *H. arnottianus* and *H. tiliaceus* (Melzer et al., 2012; Roy et al., 2015a). The BTV-C- and BTV-N-specific diagnostic assays developed in this study were robust and specific. They allowed the detection of OFV causing CL in rough lemon and mandarin on the

Island of Hawaii and CiLV-C2 infecting a new host, passion fruit on the Island of Oahu. Sanger sequencing of amplicons obtained by the BTV-N and BTV-C-specific diagnostic assays confirmed the identity of the BTVs in the samples from both Hawaiian Islands. The presence of both BTVs was further confirmed using virus-specific primer sets, and Sanger sequencing corroborated the identity of OFV and CiLV-C2 infecting citrus and passion fruit, respectively.

Illumina HTS on ribodepleted total RNA and dsRNA corroborated the results obtained by RT-PCR assays and allowed the characterization of near-complete genomes of the orchid strain of OFV infecting citrus (MW021482 and MW021483) and CiLV-C2 infecting passion fruit (MW413437 and MW413438), respectively. The genomic nucleotide sequences of both BTVs presented nucleotide identities >97% to the sequence of an orchid strain (Orc2) of OFV infecting orchids (Kondo et al., 2006) and the hibiscus strain of CiLV-C2 infecting hibiscus plants in Hawaii (Melzer et al., 2013; Roy et al., 2015a). Phylogenetic analyses corroborated the placement of the BTVs characterized in this study within the OFV and CiLV-C2 evolutionary clades (Figures 2.11 and 2.12).

OFV can naturally infect orchids and citrus. Two citrus (Cit1 and Cit2) and two orchid strains (Orc1 and Orc2) of OFV were characterized and classified based on the genetic variability and their host (Kondo et al., 2017; Roy et al., 2019). Recently, an orchid strain of OFV (Orc1) was found causing CL in Navel and Valencia sweet orange (*C. sinensis*) in South Africa. It was suggested that a likely host jump of OFV (Orc1) occurred through mite transmission in South Africa. This speculation was presented based on the almost identical (99%) nucleotide genomic OFV sequences obtained from both citrus and orchids found in the same provinces in that country (Cook et al., 2019). OFV characterized in this study clustered with two orchid isolates (Orc2) characterized from orchids in China and Japan (Figure 2.11). Although it is plausible to speculate that a likely host jump occurred in Hawaii from orchids to citrus, OFV has not been reported to be infecting orchids in the Hawaiian Islands. Also, orchid samples collected nearby from the same semi-abandoned citrus orchard in Waiakea, where OFV was found causing CL, were collected and tested for OFV using RT-PCR assays detailed above. Among the orchids surveyed, very few plants presented symptoms that OFV may cause. However, all the surveyed symptomatic orchid samples tested negative for OFV (data not shown).

CiLV-C2 clustered with two other hibiscus isolates of CiLV-C2 (Figure 2.12) previously found infecting hibiscus plants in Hawaii (Melzer et al., 2013; Roy et al., 2015a) and Florida (Roy et al., 2018a; Roy et al., 2018b). Therefore, it can be speculated that this host jump found in Hawaii for CiLV-C2 may have

been mediated through the migration of viruliferous *Brevipalpus* mites from hibiscus to passion fruit plants.

HTS and bioinformatic analyses also revealed that both BTVs were infecting their plant hosts in mixed infections with other plant viruses. OFV was found co-infecting the rough lemon and mandarin samples presenting CL symptoms with CVEV and two genotypes of CTV. CTV is a citrus virus considered an ‘omnipresent’ pathogen in Hawaiian citrus trees (Melzer et al., 2010). While although the presence of CVEV was already suspected in the Hawaiian Islands several years ago (Melzer et al., 2012), it was recently confirmed that CVEV is indeed present in the Hawaiian Islands after a recent citrus survey (Olmedo-Velarde et al., unpublished results). CiLV-C2 was found in mixed infections on passion fruit with the potyviruses BCMV, DsMV, WMV, and CMV and its satellite. WMV and CMV were previously reported infecting passion fruit in Hawaii (Watanabe et al., 2016; Dragich et al., 2014). Although BCMV has been previously found infecting passion fruit (Tsatsia and Jackson, 2019), this is the first time the virus has been found infecting this plant in the Islands. Furthermore, this would be the first report of DsMV infecting a plant host outside the *Araceae* family. For both cases, it is unknown if any of the two BTVs, OFV and CiLV-C2, may interact synergistically when present in mixed infections with any of the previously detailed viruses.

DRT-PCR assays detailed by Druciarek et al. (2019) allowed to provide an initial and putative *Brevipalpus* mite species identification on five and eight individual mite specimens feeding on the CL and passion fruit samples, respectively. Sequencing of the amplicons of the partial 28S rRNA gene and BLASTn searches revealed that the identity for the flat mite specimens was *B. yothersi* for both plant hosts. Also, DRT-PCR assays demonstrated that the five *B. yothersi* feeding on the CL samples were not viruliferous and tested negative for OFV. *B. californicus*, not *B. yothersi*, has been recorded as the mite vector for the natural transmission of citrus and orchid strains of OFV (Kondo et al., 2003; Garcia-Escamilla et al., 2017; Roy et al., 2019). Thus, it is not surprising that OFV was not detected in the *B. yothersi* mites feeding on the CL samples. Interestingly, dichorhavirus associated with citrus groves in Brazil and Mexico have been recorded at relatively high elevations (>400 meters over the sea level) and low humidity, which seems to be associated with the specific presence of their mite vectors (Freitas-Astúa et al. 2018; Roy et al. 2015a). The semi-abandoned citrus orchard, where OFV was found causing CL in Hawaii, is in Waiakea on the Hawaii Island. Waiakea is at a low elevation (~4 meters over the sea level), and the average humidity is relatively high (> 60%). Then, the presence of OFV causing CL on the Hawaii Island is rather an exception to what has been reported before. Previously, it has been found that although both *B. yothersi* and *B. californicus* are present in citrus groves, *B. yothersi* is more prevalent

(Beltran-Beltran et al., 2020; Salinas-Vargas et al., 2016). It is possible that the reported mite vector of OFV, *B. californicus*, is not abundant in the citrus groves in Waiakea. Therefore, the low incidence of leprosis symptoms in the semi-abandoned citrus orchard in Waiakea may be proportional to the low presence of *B. californicus* mite specimens. However, proper studies to examine the incidence of the different *Brevipalpus* mite populations present in this citrus grove with a recent history of CL on the Hawaii Island are required.

Furthermore, DRT-PCR assays using virus-specific primers allowed to confirm that 6 out of the 8 *B. yothersi* mites feeding on passion fruit were viruliferous and tested positive for CiLV-C2. It has been demonstrated that *B. yothersi* effectively transmits the citrus isolate of CiLV-C2 in Colombia (Roy et al., 2013; Roy et al., 2015a). However, proper transmission assays are required to confirm the mite transmission of CiLV-C2 by *B. yothersi*.

In 2013, a recovery plan for preparation and possible arrival to the U.S. of viruses causing CL was released as part of the “National Plant Disease Recovery System (NPDRS) called for in Homeland Security Presidential Directive Number 9” (Hartung et al., 2013). Among the strategies and recommendations to manage and avoid the entry of CL are: “Studies should be considered to identify additional hosts and the specific mite species that are vectors”, “Develop and deploy molecular and serological tests that distinguish among the various forms of CL viruses”, “Monitor citrus groves and commercial nurseries, including distributors that market to homeowners, for plants with symptoms of leprosis” and “Active pursuit of methods to manage this disease upon introduction is essential in order to avoid the economic consequences experienced by other countries”.

This study provides the first report of OFV in Hawaii and the first time CL has been observed in the United States since it was eradicated from Florida in the 1960s, although that outbreak was attributed to infection by citrus leprosis virus-N0, a distant relative of OFV (Hartung et al. 2015). The recent detection of CL associated with OFV infection in South Africa (Cook et al. 2019) and now Hawaii, underscores the threat this pathogen poses to the global citrus industry.

Moreover, this study reports passion fruit as an additional host for CiLV-C2. This virus is likely being transmitted from host to host by *B. yothersi* mites in Hawaii, but more studies are needed to conclude this. Importantly, studies are required in order to assess if *B. yothersi* feeding on passion fruit plants infected with CiLV-C2 can efficiently transmit the virus to citrus plants.

Finally, robust and BTV-specific diagnostic molecular assays were developed. These BTV diagnostic assays can be helpful for the initial assessment of BTV presence in citrus samples presenting symptoms of leprosis or any plant hosts presenting viral symptoms caused by BTVs. Considering several BTVs may cause CL, these diagnostic assays are currently being used for a state-wide survey looking for symptomatic citrus leaf, twigs, and fruit samples. Additional hosts of dichorhviruses are also being surveyed, including orchids, ti plants *Cordyline fruticosa* (Dietzgen et al., 2018), coffee, and *Clerodendrum* plants (Freitas-Astúa et al., 2018).

2.5 REFERENCES

- Arif, M. & Ochoa-Corona, F.M. (2013) Comparative assessment of 5' A/T-rich overhang sequences with optimal and sub-optimal primers to increase PCR yields and sensitivity. *Mol Biotechnol* 55(1), 17–26. doi: 10.1007/s12033-012-9617-5.
- Beltran-Beltran, A. K., Santillán-Galicia, M. T., Guzmán-Franco, A. W., Teliz-Ortiz, D., Gutiérrez-Espinoza, M. A., Romero-Rosales, F., & Robles-García, P. L. (2020) Incidence of Citrus leprosis virus C and Orchid fleck dichorhavirus Citrus Strain in Mites of the Genus *Brevipalpus* in Mexico. *Journal of Economic Entomology*. doi:10.1093/jee/toaa007
- Cook, G., Kirkman, W., Clase, R., Steyn, C., Basson, E., Fourie, P. H., Moore, S. D., Grout, T.G., Carstens, E., Hattingh, V. (2019). Orchid fleck virus associated with the first case of citrus leprosis-N in South Africa. *Eur J Pl Pathol* 155, 1373-1379. doi:10.1007/s10658-019-01854-4
- Chabi-Jesus, C., Ramos-González, P.L., Tassi, A.D., Guerra-Peraza, O., Kitajima, E.W., Harakava, R., Beserra Jr., J.E.A., Salaroli, R.B., Freitas-Astúa, J. (2018). Identification and characterization of citrus chlorotic spot virus, a new Dichorhavirus associated with citrus leprosis-like symptoms. *Plant Dis* 102: 1588-1598.
- Cruz-Jaramillo, J.L., Ruiz-Medrano, R., Rojas-Morales, L., Lopez-Buenfill, J.A., Morales-Galvan, O., Chavarin-Palacio, C., Ramirez-Pool, J.A., Xoconostle-Cazares, B. (2014). Characterization of a proposed dichorhavirus associated with the citrus leprosis disease and analysis of the host response. *Viruses* 6(7): 2602-2622. doi: 10.3390/v6072602
- Dragich, M., Melzer, M., Nelson, S. (2014) Cucumber mosaic virus in Hawaii. Retrieved on October 6, 2021 from <https://www.ctahr.hawaii.edu/oc/freepubs/pdf/PD-101.pdf>
- Freitas-Astúa, J., Ramos-González, P.L., Arena, G.D., Tassi, A.D., & Kitajima, E.W. (2018). *Brevipalpus*-transmitted viruses: parallelism beyond a common vector or convergent evolution of distantly related pathogens? *Curr Opin Virol* 33: 66–73. <https://doi.org/10.1016/j.coviro.2018.07.010>
- Gadberry, M.D, Malcomber, S.T, Doust, A.N. & Kellogg, E.A. (2005) Prismaclade - a flexible tool to find primers across multiple species. *Bioinformatics* 21(7), 1263-1264. doi: 10.1093/bioinformatics/bti134.
- Garcia-Escamilla, P., Duran-Trujillo, Y., Otero-Colina, G., Valdovinos-Ponce, G., Santillan-Galicia, M. T., Ortiz-Garcia, C. F., Velazquez-Monreal, J. J., and Sanchez-Soto, S. (2017) Transmission of viruses associated with cytoplasmic and nuclear leprosis symptoms by *Brevipalpus yothersi* and *B. californicus*. *Trop. Plant Pathol.* 43:69-77.

Hartung, J.S., Roy, A., Fu, S., Shao, J., Schneider, W.L., Bransky, R.H. (2015) History and Diversity of Citrus leprosis virus Recorded in Herbarium Specimens. *Phytopathology* 105(9): 1277-1284.

<https://doi.org/10.1094/PHYTO-03-15-0064-R>

Kearse, M., Moir, R., Wilson, A., Stones-Havas, S., Cheung, M., Sturrock, S., Buxton, S., Cooper, A., Markowitz, S., Duran, C., Thierer, T., Ashton, B., Meintjes, P., and Drummond, A. 2012. Geneious Basic: An integrated and extendable desktop software platform for the organization and analysis of sequence data. *Bioinformatics* 28:1647–1649.

Kitajima, E.W., Chagas, C.M., & Rodrigues, J.C.V. (2003) Brevipalpus-transmitted plant virus and virus-like diseases: cytopathology and some recent cases. *Exp. Appl. Acarol.* 30, 135-160.

Kondo, H., Hirota, K., Maruyama, K., Andika, I. B., and Suzuki, N. (2017) A possible occurrence of genome reassortment among bipartite rhabdoviruses. *Virology* 508:18-25

Kondo, H., Maeda, T., Shirako, Y., Tamada, T. (2006) Orchid fleck virus is a rhabdovirus with an unusual bipartite genome. *Journal of General Virology*, 87(8), 2413–2421. doi:10.1099/vir.0.81811-0

Kondo, H., Maeda, T., and Tamada, T. (2003) Orchid fleck virus: Brevipalpus californicus mite transmission, biological properties and genome structure. *Exp. Appl. Acarol.* 30:215-223.

Locali-Fabris, E. C., Freitas-Astúa, J., Souza, A. A., Takita, M. A., Astúa Monge, G., Antonioli-Luizon, R., Rodrigues, V., Targon, M. L. P. N., and Machado, M. A. 2006. Complete nucleotide sequence, genomic organization, and phylogenetic analysis of Citrus leprosis virus cytoplasmic type (CiLV-C). *J. Gen. Virol.* 87:2721-2729.

Melzer, M. J., Borth, W. B., Sether, D. M., Ferreira, S., Gonsalves, D., & Hu, J. S. (2009). Genetic diversity and evidence for recent modular recombination in Hawaiian Citrus tristeza virus. *Virus Genes*, 40(1), 111–118. doi:10.1007/s11262-009-0409-3

Melzer, M.J., Sether, D.M., Borth, W.B., Hu, J.S. (2012). Characterization of a virus infecting Citrus volkameriana with citrus leprosis-like symptoms. *Phytopathol* 102(1): 122-127. doi: 10.1094/PHYTO-01-11-0013.

Melzer, M.J., Simbajon, N., Carrillo, J., Borth, W.B., Freitas-Astúa, J., Kitajima, E.W. et al., (2013). A cilevirus infects ornamental hibiscus in Hawaii. *Arch Virol* 158(11): 2421-2424. doi: 10.1007/s00705-013-1745-0

Olmedo-Velarde A, Hu J and Melzer MJ (2021) A Virus Infecting *Hibiscus rosa-sinensis* Represents an Evolutionary Link Between Cileviruses and Higreviruses. *Front. Microbiol.* 12:660237. doi: 10.3389/fmicb.2021.660237

Owczarzy R, Tataurov AV, Wu Y, Manthey JA, Mcquisten KA, Almabrazi HG, Pedersen KF, Lin Y, Garretson J, McEntaggart NO, Sailor CA, Dawson RB & Peek AS (2008) IDT SciTools: a suite for analysis and design of nucleic acid oligomers. *Nucleic Acids Res* 36, 163–169. doi: 10.1093/nar/gkn198.

Pascon, R. C., Kitajima, J. P., Breton, M. C., Assumpção, L., Greggio, C., Zanca, A. S., Silva, J. M. F., ... Rasera da Silva, A. C. R. (2006). The Complete Nucleotide Sequence and Genomic Organization of Citrus Leprosis Associated Virus, Cytoplasmatic type (CiLV-C). *Virus Genes*, 32(3), 289–298. doi:10.1007/s11262-005-6913-1

Ramos-González, P.L., Chabi-Jesus, C., Arena, G.D., Tassi, A.D., Kitajima, E.W., & Freitas-Astúa, J. (2018). Leprosis de los cítricos: una enfermedad multietiológica singular. *Citrus leprosis: a unique multietiological disease. Citrus in the Americas* 1(1): 4–19.

Ramos-González, P.L., Chabi-Jesus, C., Guerra-Peraza, O., Tassi, A.D., Kitajima, E.W., Harakava, R., Salaroli, R.B., Freitas-Astúa, J. (2017). Citrus leprosis virus N: A new dichorhavirus causing citrus leprosis disease. *Phytopathol* 107: 963-976.

Ramos-Gonzalez, P.L., Santos, G.F., Chabi-Jesus, C., Harakava, R., Kitajima, E.W. & Freitas-Astúa, J. (2020) Passion Fruit Green Spot Virus Genome Harbors a New Orphan ORF and Highlights the Flexibility of the 5'-End of the RNA2 Segment Across Cileviruses. *Front. Microbiol.* 11:206. doi: 10.3389/fmicb.2020.00206.

Robinson, A. (2021). Citrus Diseases to Pay Attention to. Retrieved on November 11, 2021, from <https://citrusindustry.net/2021/01/22/citrus-diseases-to-pay-attention-to/>

Roy, A., Choudhary, Leon, M.G., Shao, J., Govindarajulu, A., Achor, D., et al., (2013). A novel virus of the genus Cilevirus causing symptoms similar to citrus leprosis. *Phytopathol* 103(5): 488-500. doi: 10.1094/PHYTO-07-12-0177-R

Roy, A., Hartung, J.S., Schneider, W.L., Shao, J., Leon, G., Melzer, M.J., Beard, J.J., Otero-Colina, G., Bauchan, G.R., Ochoa, R., Brlansky, R.H. (2015a). Role bending: Complex relationships between viruses, hosts, and vectors related to citrus leprosis, an emerging disease. *Phytopathology* 105(7): 1013-1025. doi: 10.1094/PHYTO-12-14-0375-FI.

Roy, A., Stone, A. L., Otero-Colina, G., Wei, G., Brlansky, R. H., Ochoa, R., Bauchan, G., Schneider, W.L., Nakhla, M.K., Hartung, J. S. (2019). Reassortment of RNA2 genome segments creates stable lineages among strains of Orchid fleck virus infecting citrus in Mexico. *Phytopathology*.

doi:10.1094/phyto-07-19-0253-fi

Roy, A., Stone, A.L., Shao, J., Otero-Colina, G., Wei, G., Choudhary, N., Achor, D., Levy, L., Nakhla, M.K., Hartung, J.S., Schneider, W.L., Brlansky, R.H. (2015b). Identification and molecular characterization of nuclear citrus leprosis virus, a member of the proposed dichorhavirus genus infecting multiple citrus species in Mexico. *Phytopathol* 105(4): 564-575. doi: 10.1094/PHYTO-09-14-0245-R.

Salinas-Vargas, D., M. T. Santillán-Galicia, A. W. Guzmán-Franco, A. Hernández-López, L. D. Ortega-Arenas, and G. Mora-Aguilera. (2016) Analysis of genetic variation in *Brevipalpus yothersi* (Acari: Tenuipalpidae) populations from four species of citrus host plants. *PLoS One* 11: e0164552.

Thompson, J.D., Higgins, D.G., and Gibson, T.J. 1994. CLUSTAL W: improving the sensitivity of progressive multiple sequence alignment through sequence weighting, position-specific gap penalties and weight matrix choice. *Nucleic Acids Res.* 22:4673–4680.

Tsatsia, H., Jackson, G. (2019) Bean common mosaic virus. Retrieved on October 6, 2021 from https://apps.lucidcentral.org/pppw_v10/text/web_full/entities/bean_common_mosaic_043.htm

Watanabe, S., Ruschel, R., Marrero, G., Sether, D., Borth, W., Hu, J., Melzer, M. (2016) A distinct lineage of Watermelon mosaic virus naturally infects honohono orchid (*Dendrobium anosmum*) and passion fruit (*Passiflora edulis*) in Hawaii. *New Disease Reports* 34, 13. <http://dx.doi.org/10.5197/j.2044-0588.2016.034.013>

Ye, J., Coulouris, G., Zaretskaya, I., Cutcutache, I., Rozen, S. & Madden, T. (2012) Primer-BLAST: A tool to design target-specific primers for polymerase chain reaction. *BMC Bioinformatics* 13, 134. doi: 10.1186/1471-2105-13-134.

CHAPTER III

MOLECULAR CHARACTERIZATION OF A NEW KITAVIRID INFECTING HIBISCUS IN HAWAII

3.1 INTRODUCTION

The family *Kitaviridae* encompasses three genera of positive-sense ssRNA plant viruses: *Blunervirus*, *Cilevirus*, and *Higrevirus* (Melzer et al. 2018). Although related, there are considerable physical and genetic distinctions between members of the different genera. First, cile- and higreviruses are associated with a bacilliform virion, whereas a spherical virion has been observed for the lone blunervirus for which microscopy has been reported (Kitajima et al. 1974; Melzer et al. 2012; Hao et al. 2018). Second, cile-, higre- and blunerviruses have bi-, tri- and tetrapartite genomes, respectively (Quito-Avila et al., 2020). Third, different lineages of movement protein (MP) are present in the family: blunerviruses and cileviruses have a 3A/30K superfamily MP, whereas the lone higrevirus member possesses a triple gene block-like MP module (Quito-Avila et al., 2020). Finally, the replication-associated polyproteins are encoded by a single genomic RNA for cile- and higreviruses, but are split between two genomic RNAs for blunerviruses (Quito-Avila et al. 2013; Quito-Avila et al., 2020). As such, higreviruses and cileviruses share a closer phylogenetic relationship when conserved protein sequences are analyzed.

In recent years, several unclassified insect-infecting viruses, namely nelorpi- and sandewaviruses, (Nunes et al., 2017) and arthropod viruses (Shi et al., 2016) have been characterized that resemble kitaviruses and appear to reside within the kitavirus clade. The RNA-dependent RNA polymerase (RdRp) of kitaviruses and that of the unsegmented negeviruses (nelorpi- and sandewaviruses) have a common phylogenetic origin and homologs of p24, a predicted virion membrane protein, are currently found only in these plant- and arthropod-infecting viruses (Kuchibhatla et al., 2014). The evidence of a common ancestry between these viruses has led to the hypothesis that plant-infecting kitaviruses arose from these arthropod-infecting viruses, with the arthropod vector being a potential origin (Nunes et al., 2017; Ramos-González et al., 2020). The arthropod vector has only been confirmed for cileviruses, with *Brevipalpus* spp. (Acari: Tenuipalpidae) mites responsible for transmission in a persistent circulative, and likely propagative manner (Roy et al., 2015; Freitas-Astúa et al., 2018).

The family *Kitaviridae* is currently composed of seven recognized species among the three genera: *Blueberry necrotic ring blotch virus*, *Tea plant necrotic ring blotch virus*, and *Tomato fruit blotch virus* (genus *Blunervirus*); *Citrus leprosis virus C*, *Citrus leprosis virus C2*, and *Passion fruit green spot virus* (genus *Cilevirus*); and *Hibiscus green spot virus 2* (genus *Higrevirus*). To better understand the diversity and evolutionary history of this family, it is imperative that additional members be described. In this chapter, HTS was used to identify and characterize a new kita-like virus in Hawaii that infects *Hibiscus rosa-sinensis* in a non-systemic manner. This virus has distinctive genomic characteristics and phylogenetic analyses indicate it is an intermediate of cileviruses and higreviruses. Its bipartite genome suggests a tentative and temporary placement in the genus *Cilevirus*, and the name hibiscus yellow blotch virus (HYBV) is proposed.

3.2 MATERIALS AND METHODS

3.2.1 Tissue collection and virus indexing

In July 2019, *Hibiscus rosa-sinensis* (L.) leaves displaying viral-like symptoms consistent with those caused by a brevipalpus-transmitted virus (BTV) (Kitajima et al., 2003) were collected from a single tree in Pearl City, Hawaii. Symptoms were characterized by yellow blotches surrounded by a green halo on both green and senescing leaves (Figure 3.1). Additional samples from the same tree were collected in November 2019 and March 2020. Leaf samples displaying green ringspot symptoms consistent with BTV infection in Hawaii (Melzer et al., 2013) were subsequently collected from six *Hibiscus* spp. trees growing within 1.6 km of the original *H. rosa-sinensis* tree.

To determine if the *H. rosa-sinensis* tree was infected with hibiscus green spot virus 2 (HGSV-2) and the hibiscus strain of citrus leprosis virus C2 (CiLV-C2H), which have been associated with similar, yet distinct, symptoms in Hawaii's hibiscus plants, virus-specific RT-PCR assays were performed using existing protocols (Melzer et al., 2012; Melzer et al., 2013).

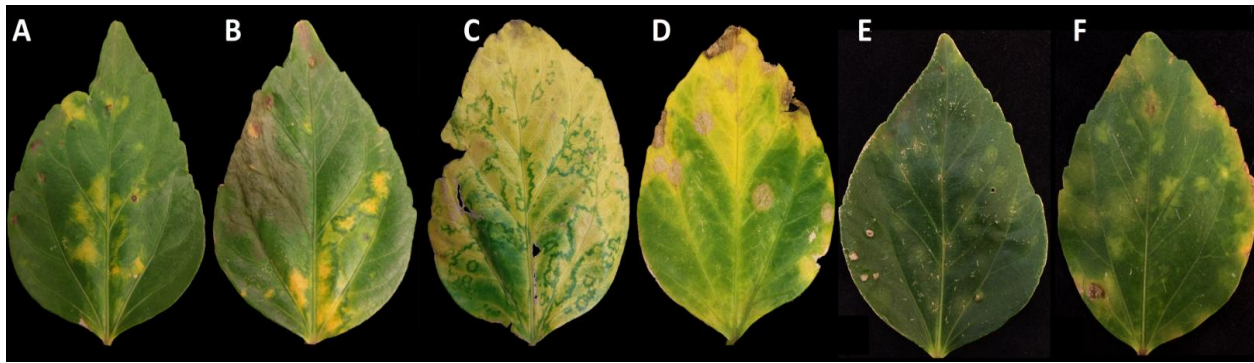


Figure 3.1 Variation in lesion symptoms displayed by *Hibiscus rosa-sinensis* leaves infected by hibiscus yellow blotch virus. Yellow blotches developed on mature leaves, and a dark green perimeter became visible as the leaves senesced. Lesions observed in A-B were predominant in July 2019; lesions observed in C-D were predominant in November 2019; lesions in E-F were predominant in March 2020. The lesions observed in D present a necrotic center that was sometimes observed in senescent leaves.

3.2.2 Genome sequencing

Double-stranded RNAs (dsRNAs) were extracted from ~5 g of symptomatic leaf tissue collected from the *H. rosa-sinensis* tree in Pearl City using either CF-11 (Whatman, Maidstone, UK) or C6288 (Sigma, St. Louis, MO) cellulose chromatography (Morris and Dodds, 1979) and resolved by 1X TBE-1% agarose gel electrophoresis. Using dsRNAs as template, randomly amplified cDNAs were generated (Melzer et al., 2010) and prepared for HTS using a Nextera XT DNA Library Prep kit (Illumina, San Diego, CA). HTS was performed on an Illumina MiSeq 2 x 300 bp (V2) platform at the University of Hawaii Advanced Studies in Genomics, Proteomics, and Bioinformatics (ASGPB) Laboratory. Genome assembly and bioinformatic analyses were performed as described (Olmedo-Velarde et al., 2019). Briefly, paired-end reads were trimmed, and quality filtered using Trimmomatic 0.35.3 (Bolger et al., 2014). Trinity 2.2.0 (Grabherr et al., 2011) produced de novo assembled contigs that were annotated using BLASTX search (Altschul et al., 1997) against the viral genome database (<ftp://ftp.ncbi.nih.gov/genomes/Viruses/all.fna.tar.gz>). Contiguous sequences (contigs) with similarity to cilevirus sequences were then used as reference for an iterative mapping approach (Dey et al., 2019) using Geneious mapper plug-in implemented in Geneious v. 10.1.3 (Kearse et al., 2012) and raw reads. A group of overlapping primer sets (Table 3.1) that were designed as detailed below and based on the contigs of HYBV were used to validate the HTS output and bridge gaps by RT-PCR. Termini were characterized by 5' RACE as detailed by (Navarro et al., 2018) on poly-A tailed dsRNAs and poly-dG-tailed cDNAs that were generated using *E. coli* Poly(A) Polymerase (New England Biolabs, Ipswich, MA) and Terminal

Deoxynucleotidyl Transferase (ThermoFisher Scientific, Waltham, MA), respectively. 3' RACE was performed by RT-PCR using an oligo-dT primer to target the poly-A tracts at the 3'-end of both RNA 1 and 2. Primers employed for genome validation and RACE experiments are detailed in Table 3.1. Amplicons were cloned into pGEM-T Easy (Promega, Madison, WI) and three to five clones were sequenced.

Table 3.1 Primers used in this study for 5' and 3' RACE, genomic sequence validation, and detection of hibiscus yellow blotch virus (HYBV). Primers used for the detection of citrus leprosis virus C2 (CiLV-C2) and hibiscus green spot virus 2 (HGSV-2) in one-step RT-qPCR assays are also provided.

Name	Sequence (5' - 3')	Target	Purpose
744	GACCACGCGACGTGTCGAVTTTTTTTTTTTTTTT	poly-A tail	5' and 3' RACE
743	TTACTAATATCCCCCCCCCCCC	poly dC tail	5' RACE
880	CGCTTGCATCTGGAGGAGTT	RNA 1	5' RACE
881	GGTTGTGTGTCTCCTGGCA	RNA 1	Genome validation
882	GCTCTGGCCGATATCATAGAATC	RNA 1	Genome validation
883	GTCTCAAGTCTGTCACGTTACC	RNA 1	Genome validation
884	TCGCAGTCTTCCACGAAGTT	RNA 1	Genome validation
885	ATACTCTGACTGGTCTAAACGAGATG	RNA 1	Genome validation
886	CAGCAATCGATCTATAGAAACCCATAC	RNA 1	Genome validation
887	GAGGCTTTTGAGGAGTTTGT	RNA 1	Genome validation
888	CGCTTAAAGACGACAGTATCAGC	RNA 1	Genome validation
889	TCTTTGGTTACTGGTATCGG	RNA 1	Genome validation
890	TGCTGTATTGACCTCTCGGA	RNA 1	Genome validation
891	GGAGCACCTACAGATGTTG	RNA 1	Genome validation
892	CCTTCAGGTAAATACGGAGC	RNA 1	Genome validation
893	TGAGTTGCCACCCCTAGCTA	RNA 1	Genome validation
894	CACTCCTGTATAACTCGTTCCGG	RNA 1	Genome validation
895	AAACTGGTACCCTGATCTGG	RNA 1	Genome validation
896	TGAGCTTCATACCATAGATCGATCAG	RNA 1	Genome validation
897	CTGGTAAGCGTTCTCTCGAG	RNA 1	Genome validation
898	TACCCAGTACGCCACACCA	RNA 1	Genome validation
899	TGTGACCGACCCTTGGAGTA	RNA1	3' RACE
900	AGAACAACCTGAACACGAGA	RNA 2	5' RACE
901	TTCCGGGTACACGTATGGC	RNA 2	Genome validation
902	AAACAATGGGTGCCGTGACA	RNA 2	Genome validation
903	TGTCCAATTGTGTATAGATGAGGT	RNA 2	Genome validation
904	ACCTAGGTCCGTCAACAGATG	RNA 2	Genome validation
905	CGCTTGCTGACTCCGCTTT	RNA 2	Genome validation
906	TGGTCTTTACGGATTTAGCATTGG	RNA 2	Genome validation
909	CTATTACTCCTACCGCAGAG	RNA 2	Genome validation

HYBV-p33-R	GCCGAACCAGGGAACATGAT	RNA 2	Genome validation and RT-PCR assays
HYBV-p33-F	ACCGGTGGCTAATTCTTCTG	RNA 2	3' RACE and RT-PCR assays
HYBV-p10-F	ACACTATTCGAGCAGTTGTATTGGA	RNA 1	RT-PCR assays
HYBV-p10-R	CACCCTCCCAACCGTTTCA	RNA 1	
HYBV-RdRp-F	TGTATGCGTCCTGTGCTGTC	RNA 1	Detection of HYBV
HYBV-RdRp-R	ATTCTTTGAGCTCGGCAGGT	RNA1 1	
Cile-p15F	CCCTTWCAYGADWTATCVTGTRAWTG	Cilevirus-p15	p15 amplification
CiLV-C2-RdRp-F	ACAAGATGGCGGACGAACTG	CiLV-C2	Detection of CiLV-C2 on one-step RT-qPCR
CiLV-C2-RdRp-R	AGCCATGTCATCGGGATCCA	RNA 1 (RdRp)	
HGSV-2-RdRp-F	GGTGCCCGTGTGTCTCATT	HGSV-2	Detection of HGSV-2 on one-step RT-qPCR
HGSV-2-RdRp-R	CGTCACACCACTCAGCAACA	RNA1 (RdRp)	

3.2.3 Genomic and Proteomic Analyses

The NCBI ORFfinder program (www.ncbi.nlm.nih.gov/orffinder) was used to identify putative open reading frames (ORFs) *in silico*. Conserved domains were predicted using either the NCBI conserved domain search tool (www.ncbi.nlm.nih.gov/Structure/cdd/wrpsb.cgi) or HMMSCAN (www.ebi.ac.uk/Tools/hmmer/search/hmmscan) implemented in HMMER (Potter et al., 2018). HMMSCAN was also used for the prediction of transmembrane helices, signal peptides, coiled coils and protein disorders. Protein transmembrane helices were also predicted and visualized using TMHMM (Krogh et al., 2001) implemented in Geneious 10.1.3. Signal peptides for protein cleavage were predicted using SignalP-5.0 (www.cbs.dtu.dk/services/SignalP-5.0/).

BLASTP searches were used to retrieve protein homologs and infer putative function. Furthermore, putative orphan proteins showing no homology to any protein in any database were aligned using their structural information and the Espresso algorithm (Armougom et al., 2006) implemented in T-Coffee (<http://tcoffee.crg.cat/apps/tcoffee/do:espresso>) (Di Tommaso et al., 2011). Protein sequence alignment was evaluated using TCS (Chang et al., 2014) implemented in T-Coffee.

Pairwise protein sequence comparisons using orthologous sequences retrieved from GenBank were performed using LALIGN (www.ebi.ac.uk/Tools/psa/lalign) (Huang and Miller, 1991). In addition, the percentage pairwise protein identities of multiple alignments of the replication-associated polyproteins,

putative MPs, and the putative structural p23 orthologs were determined using sequence demarcation tool (SDT) 1.2 (Muhire et al., 2014) and the MUSCLE algorithm implemented in SDT 1.2.

The 5' and 3' untranslated regions (UTR) of all isolates of recognized and putative/newly described kitaviruses, including HYBV, were analyzed. Intra-species UTR sequences underwent multiple alignment using the ClustalW algorithm (Thompson et al., 1994) implemented in Geneious 10.1.3 (Kearse et al., 2012). Nucleotide composition such as A/T% and their length were determined for all the 5' and 3' UTR. Conserved 5' and 3' termini were identified, and their length, nucleotide identity as well as the best consensus sequence were manually determined based on these alignments.

3.2.4 Phylogenetic Analyses

Phylogenetic relationships between HYBV and members of the family *Kitaviridae*, *Virgaviridae*, *Bromoviridae*, *Closteroviridae*, and negeviruses were inferred using the amino acid sequences of multiple proteins/domains conserved among some or all these viruses. Multiple protein alignment was performed with ClustalW (Thompson et al., 1994) implemented in MEGA 7.0.25 (Kumar et al., 2016). Ambiguous positions for each alignment were curated using Gblocks 0.91b (<https://ngphylogeny.fr>) (Lemoine et al., 2019). The best model of protein evolution for each alignment was used to generate a Maximum Likelihood tree with 1,000 bootstrap repetitions. Bayesian phylogeny was inferred using BEAST 2.6.2 (Bouckaert et al., 2019) and the best model of protein evolution with three Markov chain Monte Carlo runs of 10,000,000 generations with sampling every 1,000 trees. The runs were combined using LogCombiner in BEAST and 10% of the sample trees were discarded as “burn-in”. Tracer 1.7.1 (Rambaut et al., 2018) was used to confirm sample sizes were above 200 for all the parameters. Maximum clade credibility and posterior probabilities were annotated using TreeAnnotator in BEAST 2.6.2. The output trees were visualized in FigTree 1.4.4.

3.2.5 Transmission Electron Microscopy

Using leaf samples collected in March 2020 from the Pearl City *H. rosa-sinensis* tree, ultra-thin sections for transmission electron microscopy were prepared and observed as described (Melzer et al., 2012; Olmedo-Velarde et al., 2019). Briefly, 1x2 mm pieces excised from asymptomatic tissue and the margin of lesions from symptomatic leaves were fixed using 2% glutaraldehyde and 2% paraformaldehyde, and post-fixed using a 0.1 M sodium cacodylate solution containing 1% osmium tetroxide. Ultra-thin sections were embedded, stained with uranyl acetate and lead citrate.

Partially purified virion preparations were obtained as described by Colariccio et al. (2000). Briefly, ~5 g of symptomatic *H. rosa-sinensis* leaf tissue was powdered with liquid nitrogen and mixed with 20 mL of extraction buffer (0.05 M phosphate buffer pH 7.0 containing sodium DIECA, 0.1% (w/v) ascorbic acid and 0.02 M sodium sulphite) for 30 minutes. After clarification, 0.5% (w/v) sodium chloride and 6% (w/v) 6000 polyethylene glycol were added to the suspension, and partially purified virions were pelleted by centrifugation at 8,000 x G for 10 minutes. The pellet was resuspended with 1 mL of extraction buffer overnight. All steps were performed at ~4°C. A ten-fold dilution of the partially purified virion preparations was negatively-stained on formvar/carbon-coated grids using 1% uranyl acetate (UA) or 1% phosphotungstic acid (PTA). A density plot based on the diameter of observed particles was created with ggplot2 (Wickham, 2016).

Ultra-thin sections and negatively-stained partially purified virion preparations were viewed with a HT7700 120kV transmission electron microscope (Hitachi High Technologies America Inc., Dallas, TX) at the University of Hawaii Biological Electron Microscope Facility.

3.2.6 Virus Detection

Total RNA was extracted from 100-200 mg of plant samples collected in July 2019 using NucleoSpin RNA Plus kit (Macherey-Nagel, Düren, Germany) or Spectrum Plant Total RNA kit (Sigma-Aldrich, St. Louis, MO). These RNA extracts were reverse transcribed into cDNA using random primers and M-MLV reverse transcriptase (Promega) using the manufacturer's protocol. Two microliters of cDNAs were tested by endpoint PCR using GoTaq Green Master Mix (Promega). Virus-specific primer sets for HYBV were designed to target the RNA-dependent RNA polymerase (RdRp) domain and p10 in RNA 1, and p33 in RNA 2, respectively. Primer3 (Untergasser et al., 2012) was used for the primer design with consideration of thermodynamic primer features (Arif and Ochoa-Corona et al., 2013). HYBV-RdRp-F/R, HYBV-p10-F/R, and HYBV-p33-F/R (Table 3.1) were used for specific detection of HYBV in endpoint RT-PCR assays using 0.5 µM as final primer concentration and 55 °C as the annealing temperature. Furthermore, one-step quantitative reverse transcription (RT-qPCR) assays were implemented using HYBV-RdRp-F/R, and CiLV-C2-RdRp-F/R and HGSV-2-RdRp-F/R (Table 3.1). The two latter primer sets were designed as described above and based on a consensus sequence of an alignment of the RdRp sequences of CiLV-C2 and HGSV-2 available in GenBank as well as sequences from additional isolates of CiLV-C2 and HGSV-2. One-step RT-qPCR assays were implemented using iScript One-Step RT-PCR Kit with SYBR Green (Bio-Rad, Hercules, CA) and 0.25 µM of each primer. Each reaction was performed in three replicates. Cycling parameters for all RT-qPCR assays consisted of cDNA synthesis at 50 °C for 40 min.

Later, an initial denaturation was performed at 95 °C for 1 min, followed by 35 cycles of denaturation at 95 °C for 10 s and an annealing-extension step at 60 °C for 1 min during which time data was collected. Melt curve analysis was performed as follows: 95 °C for 1 min, pre-melting conditioning at 60 °C for 1 min followed by a melting temperature cycle range from 60 °C to 95 °C. Positive cDNA controls, specific for each virus, and non-template controls (DEPC-treated water) were used in all the assays.

3.2.7 Mite barcoding and virus detection in flat mites

Four individual flat mites (*Brevipalpus* spp.), collected in 2020 from the symptomatic *H. rosa-sinensis* tree in Pearl City were used for direct reverse transcriptase (DRT)-PCR assays (Druciarek et al., 2019). Briefly, individual *Brevipalpus* mites were introduced into a PCR tube containing 10 µl of water and random hexamer primers and crushed using a needle under a dissecting microscope. Then, cDNA was synthesized using random primers and SuperScript III reverse transcription kit (ThermoFisher Scientific, Waltham, MA) using the manufacturer's instructions. Two microliters of ten-fold diluted cDNA reactions were used in endpoint PCR for DNA barcoding and internal PCR control using the 28S rRNA primers, D1D2w2: 5'-ACAAGTACCDTRAGGGAAAGTTG-3', 28Sr0990: 5'-CCTTGGTCCGTGTTTCAAGAC-3' (Druciarek et al., 2019; Sonnenberg et al. 2007; Mironov et al. 2012) that produce a ~700 bp expected amplicon. The cytochrome oxidase unit I (COI) gene was additionally amplified using the COI primers, DNF: 5'-TACAGCTCCTATAGATAAAAAC-3', DNR: 5'-TGATTTTTTGGTCACCCAGAAG-3' (Navajas et al. 1996) that produce a ~450bp expected amplicon. All DNA barcoding PCR assays were performed using Q5 High Fidelity DNA Polymerase (New England Biolabs, Ipswich, MA). Furthermore, endpoint RT-PCR assays using primers HYBV-RdRp-F/R, HYBV-p10-F/R and HYBV-p33-F/R were performed as detailed above to detect the presence of HYBV in the mite specimens. All amplicons were gel extracted, purified and bi-directionally sequenced or cloned into pGEM-T Easy with three clones sequenced per amplicon.

3.3 RESULTS

3.3.1 Symptom monitoring and virus indexing

The expression of symptoms in a *H. rosa-sinensis* plant consistent with BTV infection was periodically observed from July 2019 to March 2020. The predominant symptomology varied over this nine-month period, ranging from faint, circular chlorotic blotches (March 2020), chlorotic blotches with a green perimeter (July 2019), to circular necrotic lesions (November 2019) that may represent an advanced stage

of the faint, circular chlorotic blotches (Figure 3.1). Symptoms were often most dramatic in senescing leaves. Total RNA extracted from symptomatic leaf tissue (Figure 3.1) tested negative for CiLV-C2 and HGSV-2 in two-step RT-PCR assays. Positive and non-template (water) controls performed as expected (data not shown). Subsequent testing using the two-step RT-PCR assay and primers HYBV-RdRp-F/R revealed that all symptomatic tissues were positive for HYBV (data not shown).

3.3.2 Molecular characterization of hibiscus yellow blotch virus

Agarose gel electrophoresis revealed the presence of two dsRNA bands of ~8 and ~4.5 kbp isolated from symptomatic *H. rosa-sinensis* tissue (Figure 3.2).

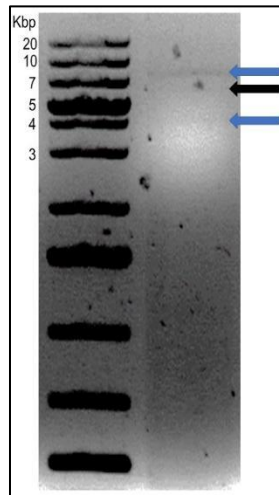


Figure 3.2 Agarose gel electrophoresis of dsRNAs extracted from hibiscus yellow blotch virus (HYBV)-infected *Hibiscus rosa-sinensis* leaves (right lane). Blue arrows at ~8 Kbp and ~4.5 Kbp indicate the observed dsRNAs that likely represent RNA 1 and RNA 2 of HYBV, respectively. The black arrow at ~6 kbp likely represents the genome of hibiscus latent Fort Pierce virus. Numbers on left give size in kilobase pairs (Kbp) for select fragments of the ThermoFisher 1 kb Plus ladder (left lane).

HTS of a library generated from these dsRNAs produced ~24 M paired-end reads that were *de novo* assembled into 2,178 contiguous sequences (contigs). Of these, 27 showed similarity to cileviruses and higreviruses. Iterative mapping of raw reads and reassembling of these contigs led to the generation of three larger contigs of 8,127, 3,676, and 507 bp in length. BLASTX searches showed the three contigs putatively coded proteins showing low to moderate identity to the replication-associated polyprotein coded by RNA 1 of cileviruses and HGSV-2, p61 through p24 coded by RNA 2 of cileviruses, and to p29

coded by RNA 1 of cileviruses, respectively. Using the sequence of the 8,127 bp contig, 5' and 3' RACE was performed to complete the RNA 1. Using the sequence of the 3,676 bp contig, 5' RACE was used to determine the 5' terminal sequence, and 3' RACE using primer 909 (Table 3.1) resulted in a ~1,620 bp amplicon which included the sequence of the 507 bp contig. RT-PCR using primer 909 and HYBV-p33-R (Table 3.1) validated the 3' RACE result by bridging the ~307 nt sequence gap between the 3,676 and 507 bp contigs.

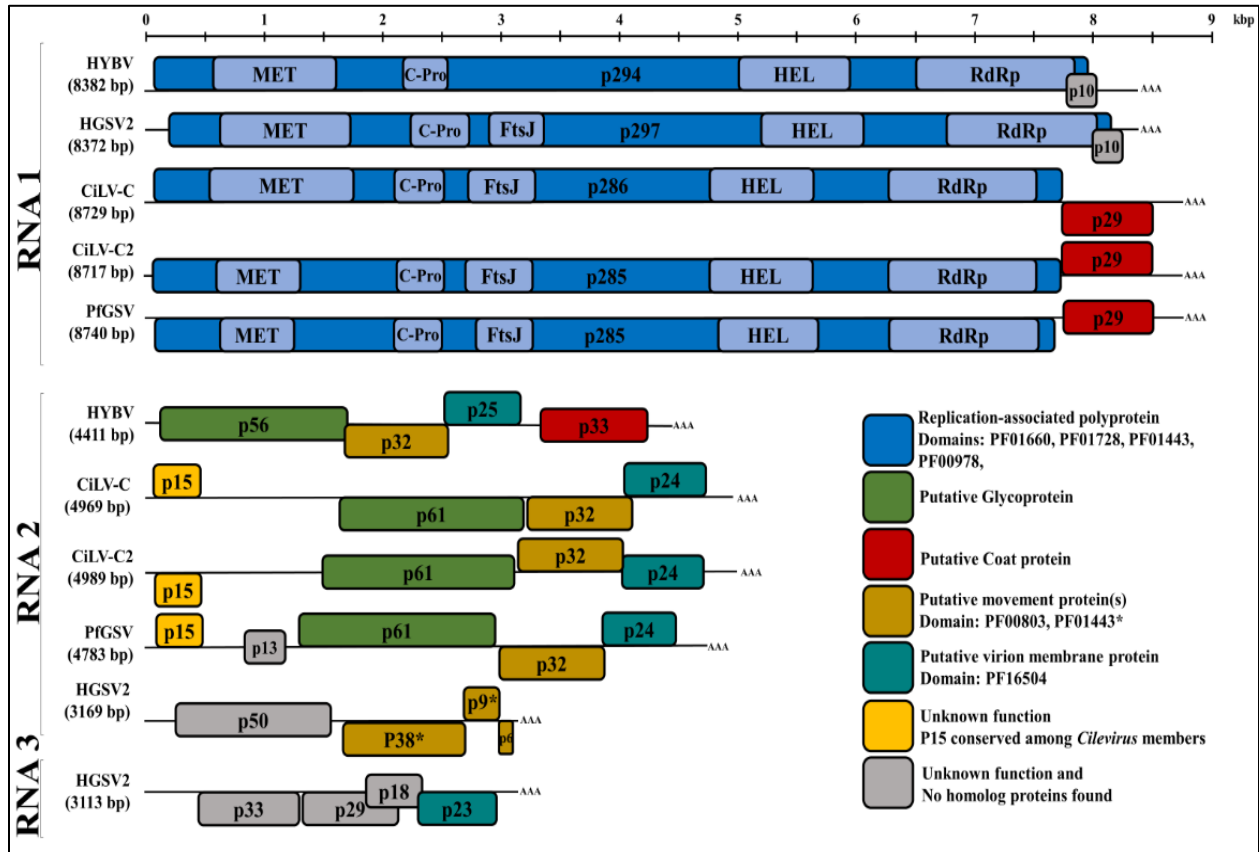


Figure 3.3 Genome organization comparison between hibiscus yellow blotch virus (HYBV) and *Cilevirus* and *Higrevirus* members. Boxes represent open reading frames (ORFs), and similarly colored ORFs encode proteins of similar function as indicated. RNA 1 (8382 bp) contains two ORFs coding for the replication-associated polyprotein (p294) and a protein with unknown function (p10). RNA 2 (4411 bp) contains four ORFs coding for the putative glycoprotein (p56), putative movement protein (p32), putative virion membrane protein (p25) and putative coat protein (p33). Cileviruses represented: citrus leprosis virus C (CiLV-C) and CiLV-C2, and passion fruit green spot virus (PFGSV). Higreviruses represented: hibiscus green spot virus 2 (HGSV-2). MET, methyltransferase; C-Pro, cysteine like protease; FtsJ, methyltransferase; HEL, helicase; RdRp, RNA-dependent RNA polymerase; AAA, poly(A) tail. Scale at top of figure indicates approximate size in kilobase pairs.

Excluding the poly-A tails at their 3' end, RNA 1 and RNA 2 of HYBV were 8,382 and 4,411 nt, respectively (Figure 3.3). The 8,382 bp RNA 1 molecule (GenBank accession MT472637) had a large ORF that putatively encoded a 294 kDa replication-associated polyprotein of 2,645 amino acids (aa). This putative polyprotein possessed viral methyltransferase (MET; PF01660, aa residues 144-495), cysteine protease (C-Pro; PF02338, aa residues 681-816), viral helicase 1 (HEL; PF01443, aa residues 1,640-1,932) and RdRp 2 (PF00978, aa residues 2,148-2,587) domains (Figure 3.3). This polyprotein was most similar to that of CiLV-C2H, with an identity of 37% (Table 3.2, Figure 3.4). The individual MET, C-Pro, HEL and RdRp 2 domains were 49%, 39%, 44% and 61% identical to those of CiLV-C2H, respectively. No transmembrane helices were found in this protein; however, coiled coil and disorder regions were identified at aa residues 1620-1640 and 1461-1468, respectively. In the 3'-terminal region of RNA 1, an 85 aa ORF was identified that putatively encoded a 10 kDa protein harboring two transmembrane helices. This protein of unknown function, designated p10, showed no similarity to any protein in the current databases as determined by a BLASTP search. However, it did resemble the size, genomic location, and secondary structure of a previously undescribed ORF of HGSV-2 (Figure 3.3 and Figure 3.5A). A structural alignment of the two putative proteins obtained using Expresso implemented in T-Coffee revealed an identity of ~20% (Table 3.2 and Figure 3.5B and 3.5C).

Table 3.2 Percent amino acid identities between orthologous proteins of hibiscus yellow blotch virus (HYBV) and *Kitaviridae* members: higreviruses include: hibiscus green spot virus 2 (HGSV-2); cileviruses include: citrus leprosis virus C (CiLV-C), CiLV-C2 (with isolates indicated), and passion fruit green spot virus (PfGSV); blunerviruses include: blueberry necrotic ring blotch virus (BNRBV), tea plant necrotic ring blotch virus (TPNRBV), and tomato fruit blotch virus (TFBV).

Protein	HGSV-2 ²	CiLV-C (CRD)	CiLV-C (SJP)	CiLV-C2 (Citrus-Co)	CiLV-C2 (Hibiscus-HI)	PfGSV (Snp1)	BNRBV	TPNRBV	TFBV
RNA1-Polyprotein	33.9	35.9	36.1	36.3	36.6	36.4	32.1	26.3	26.0
RNA1-p10	19.7	-	-	-	-	-	-	-	-
RNA2-p56¹	-	20.8	22.3	20.7	19.5	19.1	-	-	-
RNA2-p32	- ²	40.6	39.6	45.9	44.4	45.3	36.6	32.7	34.1
RNA2-p25¹	27.7	40.0	39.4	38.2	37.3	39.8	23.2	26.9	22.4
RNA2-p33¹	-	20.3	23.1	25.6	32.8	28.1	-	-	-

Orthologous proteins showing the highest identity to the HYBV proteins are bold.

¹ p56, p25 and p33 of HYBC shows resemblance to p61, p24 and p29 of cileviruses, respectively

² HGSV-2 codes for a triple gene block-like movement proteins rather than 3A or 30K movement proteins (Melzer et al. 2018).

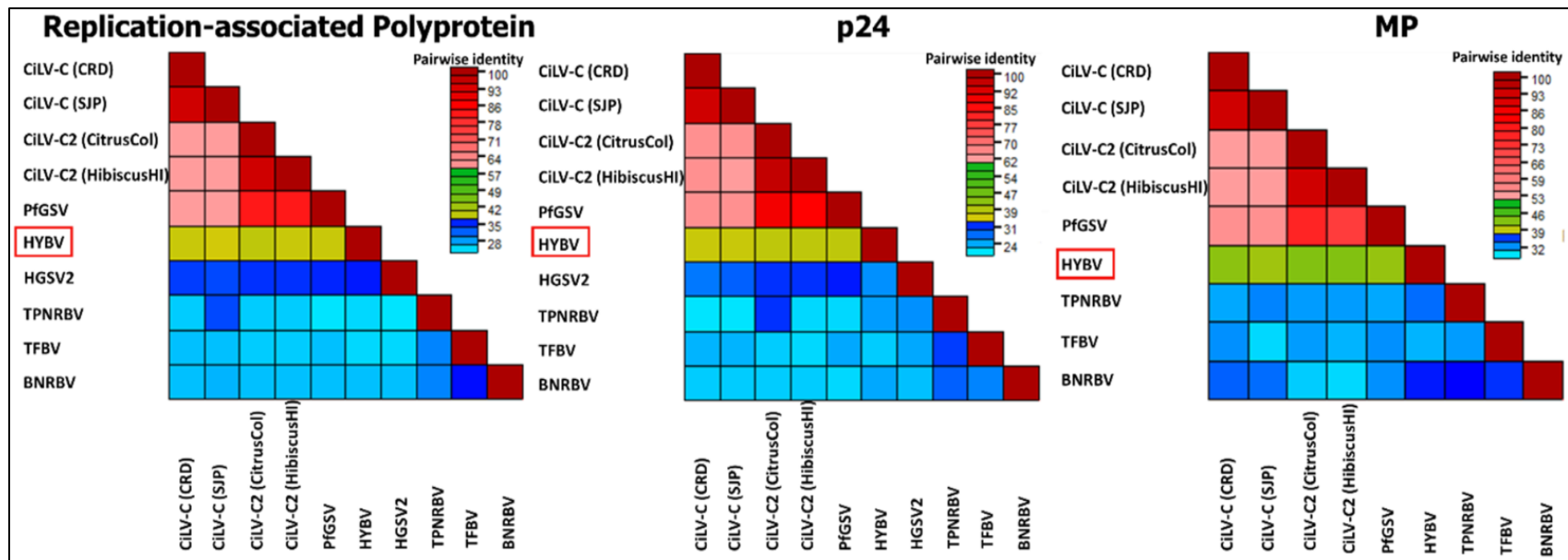


Figure 3.4 Pairwise protein sequence similarity matrix of the replication-associated polyprotein, p24 and putative movement protein of hibiscus yellow blotch virus (HYBV) with their homologs of *Cilevirus*, *Higrevirus* and *Blunervirus* members using sequence demarcation tool (SDT) 1.2. *Cilevirus* species and isolates include: citrus leprosis virus C (CiLV-C) and CiLV-C2 (Citrus isolate from Colombia: CitrusCol. Hibiscus isolate from Hawaii: HibiscusHI), and passion fruit green spot virus (PFGSV). *Higrevirus* member: hibiscus green spot virus 2 (HGSV-2). Blunerviruses include: blueberry necrotic ring blotch virus (BNRBV), tea plant necrotic ring blotch virus (TPNRBV), and tomato fruit blotch virus (TFBV).

(32 kDa) in which several disorder regions were identified with the largest located in the C-terminus, at aa residues 270-301. This protein has a conserved domain (PF00803, aa residues 6-227) of viral movement proteins (MP) and likely represents the MP of HYBV (Figure 3.3). It shared moderate (33-46%) identity with orthologs of kitaviruses (Table 3.2). The third ORF putatively encoded a 230 aa protein, p25, and harbors an SP24 conserved domain (PF16504, aa residues 33-156) which possesses four transmembrane helices (Figure 3.3). SP24 is present in kitavirids, negeviruses and chroparaviruses, with the latter two being taxons of insect-specific viruses (Kuchibhatla et al., 2014). Two disorder regions were found in the C-terminus of the HYBV p25, and the protein shared moderate (23-40%) identity with orthologs of recognized kitaviruses (Table 3.2). The 3'-terminal ORF putatively encoded a 312 aa protein orthologous (20-33% aa identity) to p29 encoded on RNA1 of cileviruses (Table 3.2), which is a predicted coat protein (Leastro et al., 2018). A long disorder region was identified in aa 52-163 of the p33.

3.3.3 Transmission electron microscopy

Ultra-thin sections prepared from foliar lesions revealed the presence of small congregations of spherical structures approximately 50-60nm in diameter (Figure 3.6). These spherical structures, contained in cytosolic vesicles, were typically near the endoplasmic reticulum. Although not common in cells from symptomatic tissue, these structures were not observed in ultra-thin sections obtained from asymptomatic leaves. Despite extensive examination of six thin sections from both symptomatic and asymptomatic leaves, neither electron-dense viroplasm or bacilliform virus-like particles were observed.

Abundant rod-shaped and spherical particles were observed in the partially purified, negatively-stained virus preparations. Rod-shaped virions were approximately 20 nm in width and up to 370 nm in length and were consistent with tobamovirus virion morphology (Figure 3.6). Spherical particles encompassing a wide range of diameters were observed. A density plot based on the measurement of 156 particles indicated diameters of 33 and 66nm were most prevalent, and these particle sizes were most readily observed with phosphotungstic acid (PTA) and uranyl acetate (UA) staining, respectively (Figure 3.6).

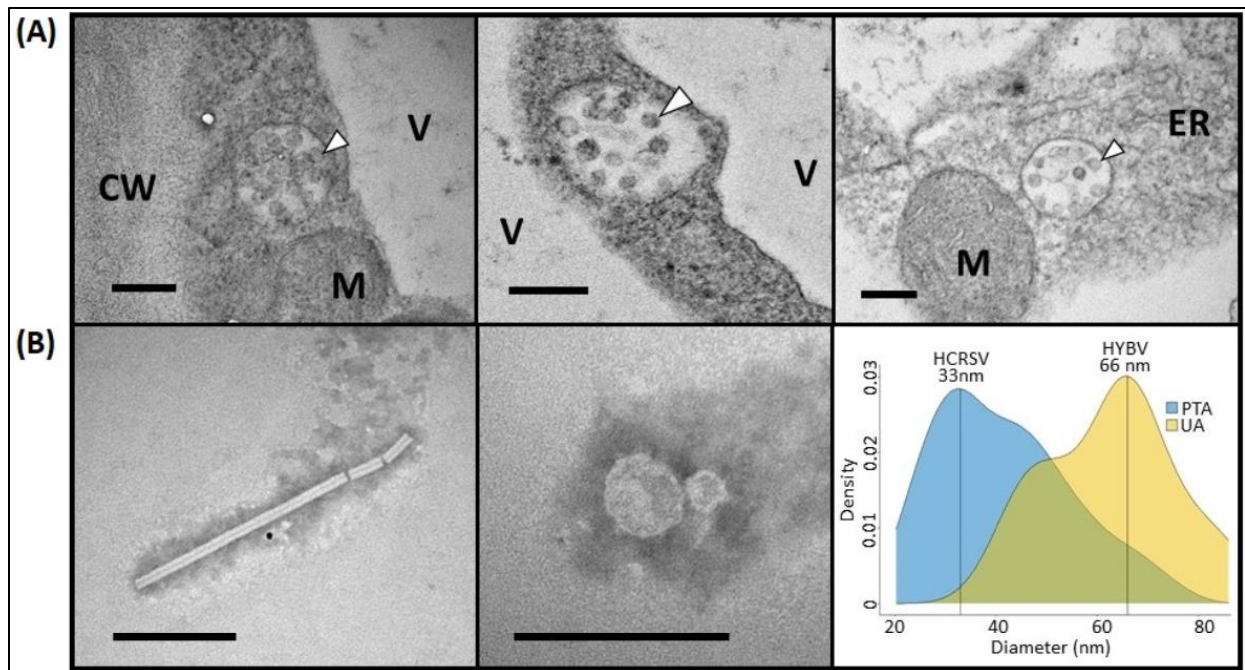


Figure 3.6 Panel (A): Electron micrographs of hibiscus yellow blotch virus-infected *Hibiscus rosa-sinensis* leaves containing aggregates of electron dense spherical structures (arrowheads) typically between 50-60nm in diameter. Similar structures were not observed in healthy tissue. CW, cell wall; ER, endoplasmic reticulum; M, mitochondrion; V, vacuole. Panel (B): Electron micrographs of a rod-shaped virion (left) and spherical particles (center) partially purified from *H. rosa-sinensis* leaves co-infected with hibiscus latent Fort Pierce virus (HLFPV), hibiscus chlorotic ringspot virus (HCRSV), and hibiscus yellow blotch virus (HYBV). The rod-shaped virion is consistent with the HLFPV virion, whereas the spherical particles could represent HCRSV and HYBV virions. A density plot was generated to determine the frequency of spherical particles stained with either phosphotungstic acid (PTA) or uranyl acetate (UA) based on their diameter (right). Particle diameters of 33 and 66 nm were most frequently recorded, which may correspond to HCRSV and HYBV virions, respectively. Bar = 200nm for all micrographs.

3.3.4 Phylogenetic placement of hibiscus yellow blotch virus

Phylogenies of HYBV were inferred with two character-based algorithms: Maximum Likelihood and Bayesian inference. Both algorithms predicted a similar relationship between HYBV and other viruses for each protein sequence analyzed. For the RdRp and p24 proteins, HYBV formed a monotypic lineage between the cilevirus and higrevirus clades (Figures 3.7 and 3.8). For the p61 and p29 proteins, which only have homologs in cileviruses, HYBV consistently formed a basal branch (Figure 3.8). For the MP,

which has homologs in cileviruses, blunerviruses, and other plant-infecting viruses, HYBV was placed between the cilevirus and blunervirus clades (Figure 3.8). Furthermore, in the RdRp and p24 phylogenies, *Kitaviridae* members and negeviruses formed a monophyletic group sharing a common ancestor (Figures 3.7 and 3.8).

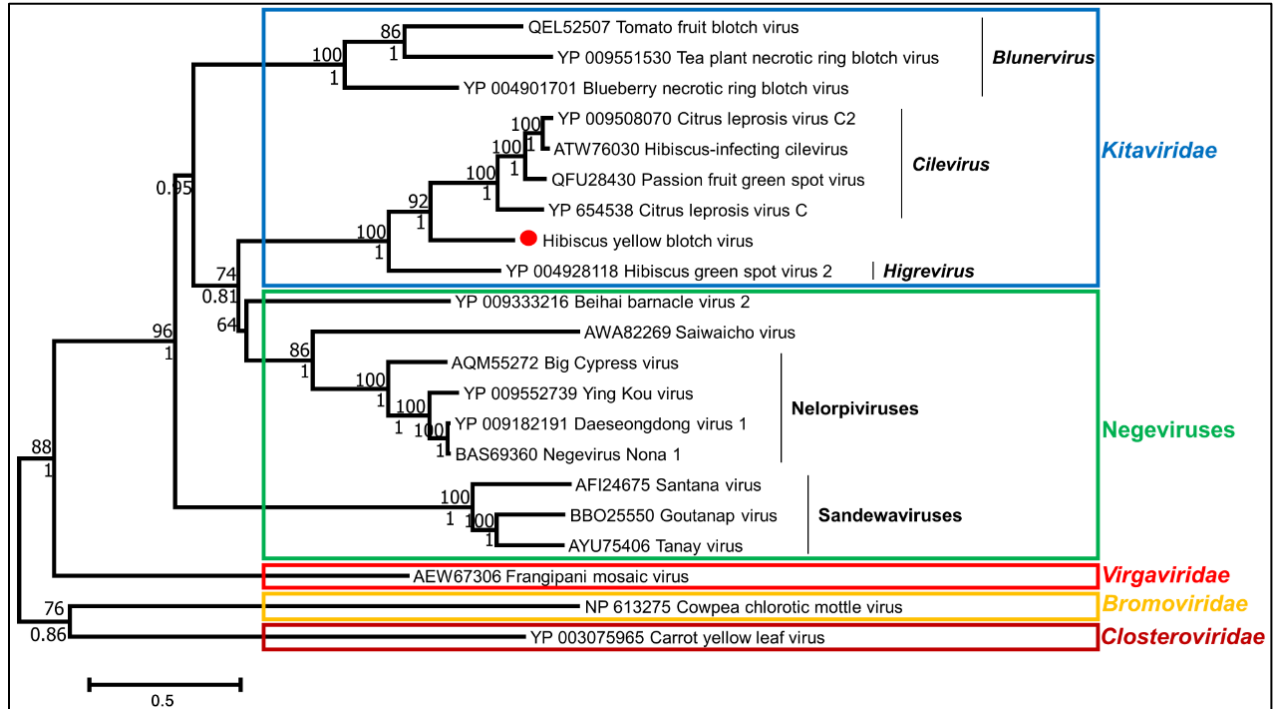


Figure 3.7 Phylogenetic relationships among members of the families *Kitaviridae*, *Virgaviridae*, *Bromoviridae*, *Closteroviridae* and negeviruses based on an RNA-dependent RNA polymerase (RdRp) multiple protein alignment using CLUSTAL and inferred using Maximum Likelihood algorithm implemented in MEGA 7.0.25. Bootstrap values generated by Maximum Likelihood are shown above the branches after 1000 repetitions. Posterior probabilities that were calculated using Bayesian inference with three Markov Chain Monte Carlo runs of 10,000,000 generations and implemented in BEAST 2 are shown under the branches. Missing values indicate values below 50 (bootstrap) or 0.7 (posterior probability). GenBank accession numbers are provided prior to each virus name. Scale at bottom indicates the number of substitutions per given branch length.

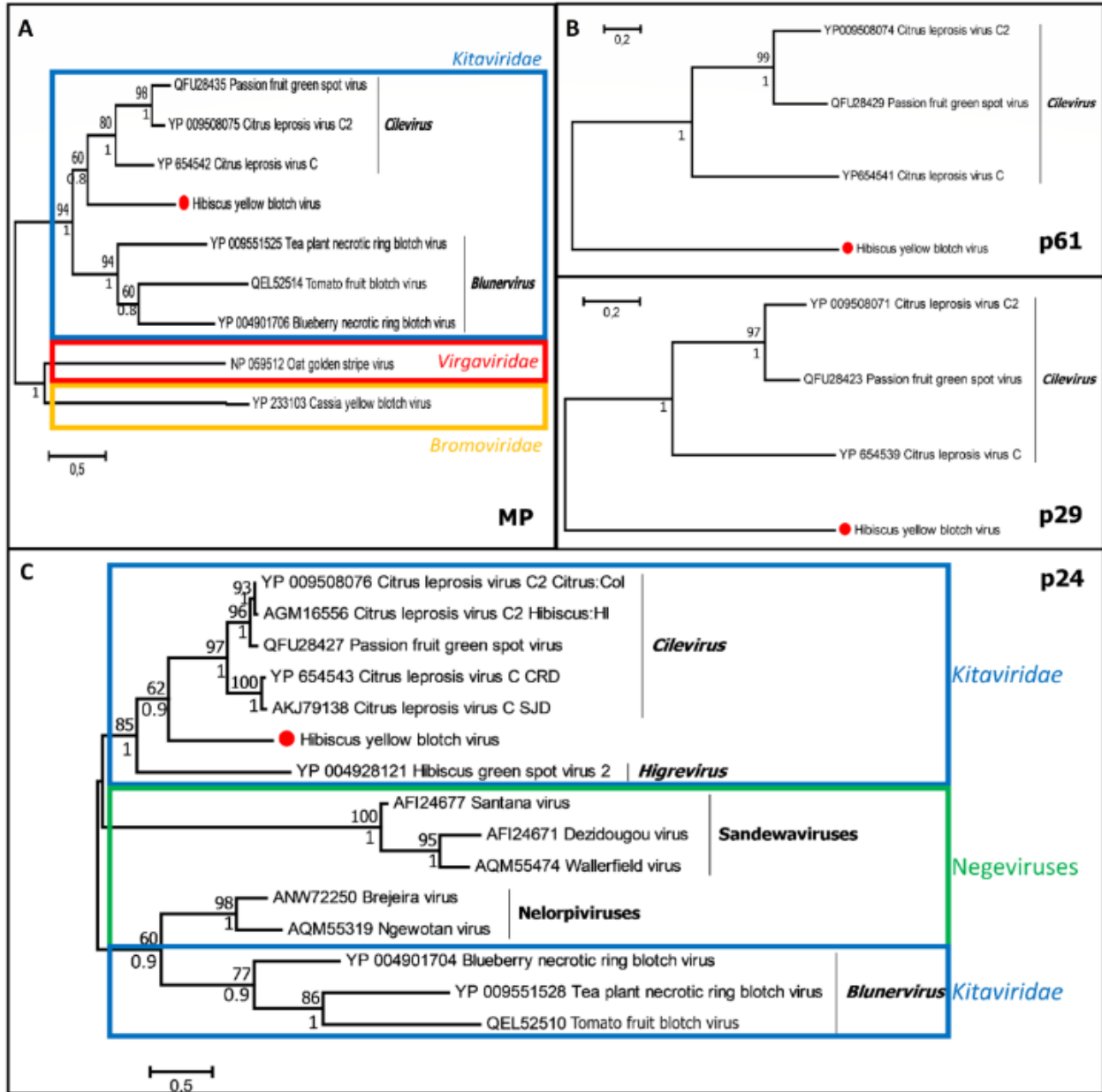


Figure 3.8 Phylogenetic placement of hibiscus yellow blotch virus (HYBV) with other viruses possessing conserved proteins. Clockwise from upper left: MP, putative movement protein (p32 of HYBV); p61, putative glycoprotein (p56 of HYBV); p29, putative coat protein (p33 of HYBV); and p24, putative virion membrane protein (p25 of HYBV). All phylogenies were inferred by a multiple protein alignment using CLUSTAL and the Maximum Likelihood algorithm implemented in MEGA 7.0.25. Bootstrap values generated by Maximum Likelihood are shown above the branches after 1000 repetitions. Posterior probabilities that were calculated using Bayesian inference with three Markov chain Monte Carlo runs of 10,000,000 generations and implemented in BEAST 2 are shown under the branches. Missing values indicate values below 50 (bootstrap) or 0.7 (posterior probability).

3.3.5 Protein comparisons between genera in the Kitaviridae family

To evaluate genetic divergence between HYBV and cileviruses in the context of inter-genera divergence within the family *Kitaviridae*, protein sequence identity matrices of the replication-associated polyprotein, p24, and putative MP of kitavirids were obtained using SDT 1.2. The matrices show overall low to moderate protein identity levels, from 21-45%, for the three proteins of HYBV with their kitavirid homologs (Table 3.2 and Figure 3.4). Cileviruses, including the recently characterized passion fruit green spot virus (PfGSV), present high protein intra-genus identities ranging from 59-81, 62-89, and 51-75% for the replication-associated polyprotein, p24 and MP, respectively. However, cileviruses present a low protein identity, not surpassing 45%, with their homologs of HYBV, HGSV-2 and blunerviruses. The sole higrevirus, HGSV-2, has low protein identity ranges of 24-36 and 22-33% with other kitavirids for the replication-associated polyprotein and p24, respectively. Blunerviruses also show low protein identity ranges of 24-36, 20-31, and 29-38% with other kitavirids, including other blunerviruses, for the replication-associated polyprotein, p24 and MP, respectively. In general, kitavirids present broad protein identity ranges of 24-81%, 20-89% and 29-75% for the replication-associated polyprotein, p24 and MP.

3.3.6 Analyses of untranslated regions of kitavirids

Multiple nucleotide sequence alignments revealed that cileviruses, HGSV-2, and HYBV share common features in their UTR, including AT richness. They possess conserved 5' and 3' termini, and conserved long 3' UTRs in all of their genomic segments (Table 3.3).

All their 5' termini start with a G or C, while most of their 3' termini end with a C. Most of their UTR length are uniform among intra-species genomic segments. Furthermore, cileviruses present a long conserved 3' termini of ~122 nucleotides and the last three conserved nucleotides are GAC. Similar to cileviruses, HYBV possesses a long conserved 3' terminus of 171 nucleotides and the last three conserved nucleotides for each RNA segment are GCC. HGSV-2 possesses a shorter conserved 3' terminus of 78 nucleotides with the last three not clearly conserved. Whereas blunerviruses also presented AT-rich 5' and 3' UTRs, but shorter semi-conserved termini in their genomic segments. Their UTR lengths are variable among intra-species genomic segments.

Table 3.3 Kitavirus intra-species nucleotide composition analysis of the 5' and 3' untranslated regions (UTR), and 5' and 3' conserved termini among the genomic segments of each virus species.

Kitavirus species ¹	Genbank Accession	5' UTR		Conserved 5' termini			3' UTR		Conserved 3' termini		
		AT %	Length (bp)	Length (bp)	Nucleotide identity (%)	Best consensus sequence in the last nucleotides ⁴	AT %	Length (bp)	Length (bp)	Nucleotide identity (%)	Best consensus sequence in the last nucleotides ⁴
HYBV	MT472637-8	55.5	267-297	65	69.2	CATAAACKAAGAGTAGACTYRCKGGT TG	63.2	198-341	171	91.4	AACMTCYTTTAGCTTTTGTKTTT-AAAAGCC
CiLV-C	DQ157465-6 DQ352194-5	69.9	65-108	108	61.1	GATAAAWCT(A)RTCAA	61.5	228-254	126	92.9	TTWRWTTTTCTTTCTTTTGCTT-ATA(T)GAC
CiLV-C2 ² (Citrus)	JX000024-5	67.2	92-118	10	70.0	ATARAAWSAA	64.9	223-349	127	90.6	(C)ITYCTTTCTTTT(TC)TTGT-CATTWTGAC
CiLV-C2 ² (Hibiscus)	MG253804- 5 KC626783-4	63.7	56-119	32	81.1	CATAGAATC(AA)CRATASTRCTAT	64.5	222-346	126	97.9	TTCTTCTTTTCTTTTTTGTCAT-TTTGAC
PfGSV	MK804171- 2	66.5	108-149	19	57.9	SATRTRRR(A)TACAAAAYWT	68.3	240-307	119	86.6	TYTTMTTTTCTTTCTTTTGTC-TMTA(T)GAC
<i>Cilevirus</i> ³		67.5	56-149	6	77.2	(S)ATRTRR	63.6	222-349	122	78.9	TYW(V)(N)YTTYTYTTYTYTTG-TCWHTW(T)GAC
HGSV-2	HQ852052-4	55.8	214-464	13	79.5	CATAAAWTD(M)AAA	63.9	114-196	78	69.4	(T)TTSTHTWTCYTTTCT(TC)(C)TWKTC(C)S(T)G(C)
BNRBV	JN651148- 51 KC433316-9	60.2	48-412	7	91.8	SACAAAT	65.1	146-429	9	70.8	WTTATWMYCG
TPNRBV	MG781152- 5	54.6	96-383	12	70	(TGGGGAA)TTR(C)S	59.3	128-941	85	70.9	TTADTAAGAT(AAC)
TFBV	MK517477- 80	58.5	77-426	20	78.8	RWTTAA(CA)(T)CWTMAATCMAC	55.6	76-333	13	80	CKTTY(ACTCAGCT)

¹ Hibiscus yellow blotch virus (HYBV), citrus leprosis virus C (CiLV-C) and C2 (CiLV-C2), passionfruit green spot virus (PfGSV), hibiscus green spot virus 2 (HGSV-2), blueberry necrotic ring blotch virus (BNRBV), tea plant necrotic ring blotch virus (TPNRBV) and tomato fruit blotch virus (TFBV).

² CiLV-C2 possesses notable differences in the RNA 2 for strains infecting citrus and hibiscus. Differences in the untranslated regions as well as conserved termini were identified.

³ *Cilevirus* was the only genus in the family *Kitaviridae* whose members possessed conserved termini. *Higrevirus* was not considered in the analysis as a genus because it currently contains only a single species. No clear conserved termini were found among *Blunervirus* members.

⁴ Nucleotides between parentheses are not present in either all genomic segments or all virus isolates. HYBV, cileviruses and HGSV-2 presented long conserved 3' termini and longer consensus sequences than 30 nucleotides were obtained, however, only 30 nucleotides in the conserved termini sequences are presented. D= A, G, or T; K=G or T; M= A or C; R=A or G; S=C or G; W=A or T; Y=C or T.

3.3.7 Hibiscus yellow blotch virus detection in flat mites

Four individual flat mites (*Brevipalpus* spp.) were collected from a symptomatic *H. rosa-sinensis* tree infected with HYBV. HYBV RNA 1 and RNA 2 were amplified by DRT-PCR in two of these four mites using three different HYBV-specific primer sets (Figure 3.9).

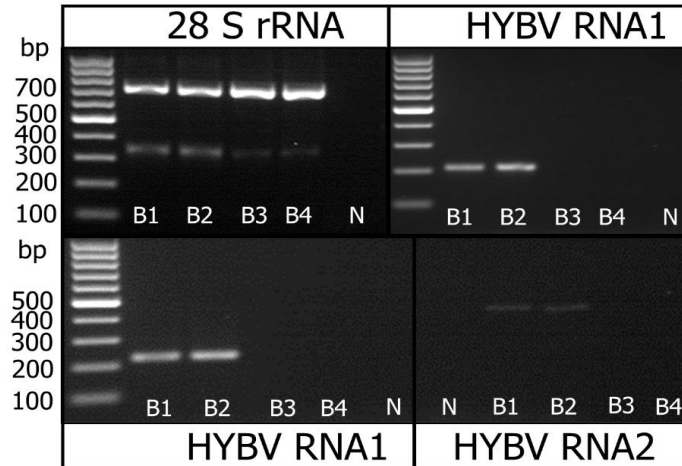


Figure 3.9 Agarose gel electrophoresis of 28S rRNA, hibiscus yellow blotch (HYBV) RNA 1 and RNA 2 amplicons using direct RT-PCR (DRT-PCR) assays described by Druciarek et al. (2019). dRT-PCR assays were performed on four individual brevipalpus mites (B1-B4) collected from a HYBV-infected *Hibiscus rosa-sinensis* plant. Upper panel: 28S rRNA and HYBV-RNA 1 amplicons were amplified using primer sets D1D2w2/28Sr0990 and HYBV-RdRp-F/R with expected amplicon sizes of ~700 and 223 bp, respectively. Bottom panel: HYBV-RNA 1 and RNA2 amplicons were amplified using primer sets HYBV-p10-F/R and HYBV-p33-F/R with expected amplicons of 210 and 438 bp, respectively. A non-template control (N) was included in all the assays. Sanger sequencing of the 28S rRNA amplicon later suggested mites B1 and B2 were *B. yothersi*, while the identity of mites B3 and B4 was ambiguous. DNA ladder is 100 bp (ThermoFisher Scientific, Waltham, MA), and sizes of select fragments are provided in base pairs (bp).

Direct sequencing showed the three sequences share 100% nucleotide identity to the RdRp and p10 regions in RNA 1 and p33 in RNA 2 of HYBV isolate present in the from the symptomatic *H. rosa-sinensis* tree. Using 28s rRNA primers, a prominent ~700bp amplicon of expected size was produced from each of the four individual mites using DRT-PCR, as well as a faint ~340bp amplicon which was sequenced and found to be non-specific (Figure 3.9). Direct sequencing of the ~700 bp 28S rRNA amplicon for those two individual mites, and a pairwise alignment showed that both sequences shared

100% nucleotide identity. A BLASTN search using the consensus sequence (MT812697) showed that it shares 99.7% nucleotide identity to *B. yothersi* (MK293649) with 87% query coverage. Direct sequencing of the 28S rRNA region was performed for the other two mites in which HYBV was not detected. A pairwise alignment revealed that both sequences shared 100% nucleotide identity. A BLASTN search of a consensus of both sequences (MT812698) showed that it shares 99.4% nucleotide identity to *B. papayensis* (MT664800) with 87% query coverage. Furthermore, direct sequencing of the ~450 bp amplicons generated using the COI primers (data not shown) further corroborated the identity of *B. yothersi* after a BLASTN search showed the consensus sequence (MT796740) shares 99.6% nucleotide identity to *B. yothersi* (MW587269) with 100% query coverage. A consensus sequence (MT796741) for the COI gene of the two other mites, in which HYBV was not detected, showed 100% identity to *B. obovatus* (DQ450495) after a BLASTN search with a 90% query coverage.

3.3.8 Natural mixed infections in hibiscus

In addition to HYBV, HTS data from the dsRNA library also identified the complete genomic sequences of hibiscus chlorotic ringspot virus (HCRSV, *Betacarmovirus*) and hibiscus latent Fort Pierce virus (HLFPV, *Tobamovirus*) in the Pearl City sample using *de novo* assembly and an iterative mapping approach. The genome of HCRSV from the sample was 3,969 nt in length (MT512573) and assembled from 1,386,006 reads with an average depth of 33,785. The genome shared 95.4% nucleotide identity to an HCRSV isolate from Singapore (X86448). No dsRNAs associated with this virus were observed following agarose gel electrophoresis, however, any dsRNAs of this size would have been obscured by the loading dye (Figure 3.2). The RdRp, p2, p3, and CP of HCRSV shared 95%, 95.7% and 92.3% protein identity, respectively, to those of the HCRSV isolate from Singapore, while the CP shared 99.4% protein identity to that of HCRSV isolate SB01 from Brazil (AZL87708). The genome of HLFPV was 6,408 nt in length (MT512572) assembled from 1,667,706 reads with an average depth of 35,941. The genome shared 99.4% nucleotide identity to HLFPV isolate J from Japan (AB917427). This genome size was consistent in size with a faint dsRNA observed following agarose gel electrophoresis (Figure 3.2). Replication-associated polyprotein, MP and CP of HLFPV show 98.5%, 99.7% and 97.5% protein identity, respectively, to those of HLFPV isolate J (AB917427).

Samples from six *Hibiscus* spp. plants designated A-F displaying symptoms typical of BTV infection (Kitajima et al., 2003) were collected within 1.6 km of the original HYBV-infected tree (Figure 3.10). The presence of CiLV-C2, HGSV-2 and HYBV, was assessed by one-step RT-qPCR and two-step RT-PCR assays. Three out of six of the samples (A, B and D) tested positive for HYBV in both PCR assays. Only one sample (A), which also tested positive for HYBV, tested positive for CiLV-C2 in both PCR assays. None of the samples tested positive for HGSV-2. In all the assays, positive and non-template

controls tested as expected (Figure 3.11). The genetic diversity of HYBV in these samples was assessed for RNA1 and RNA2 by sequencing amplicons generated using primer sets HYBV-RdRp-F/HYBV-p10-R and 909/HYBV-p33-R, respectively (Table 3.1). These amplicons were 100% identical for RNA1 and >99.6% identical for RNA2.

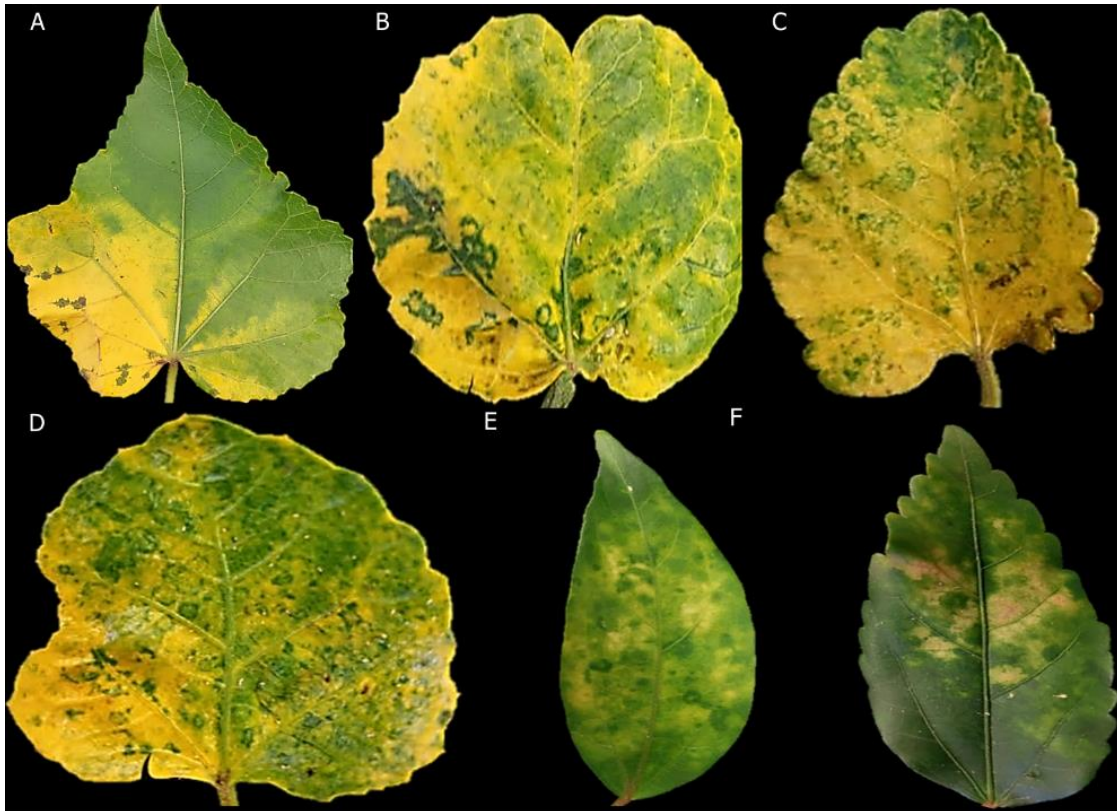


Figure 3.10 Leaves collected from symptomatic *Hibiscus* spp. plants growing within 1.6 kilometers of the hibiscus yellow blotch virus (HYBV)-infected *H. rosa-sinensis* plant. Samples A, B, and D tested positive for HYBV using RT-PCR. Sample A also tested positive for citrus leprosis virus C2 by RT-PCR. None of the samples tested positive for hibiscus green spot virus 2 by RT-PCR.

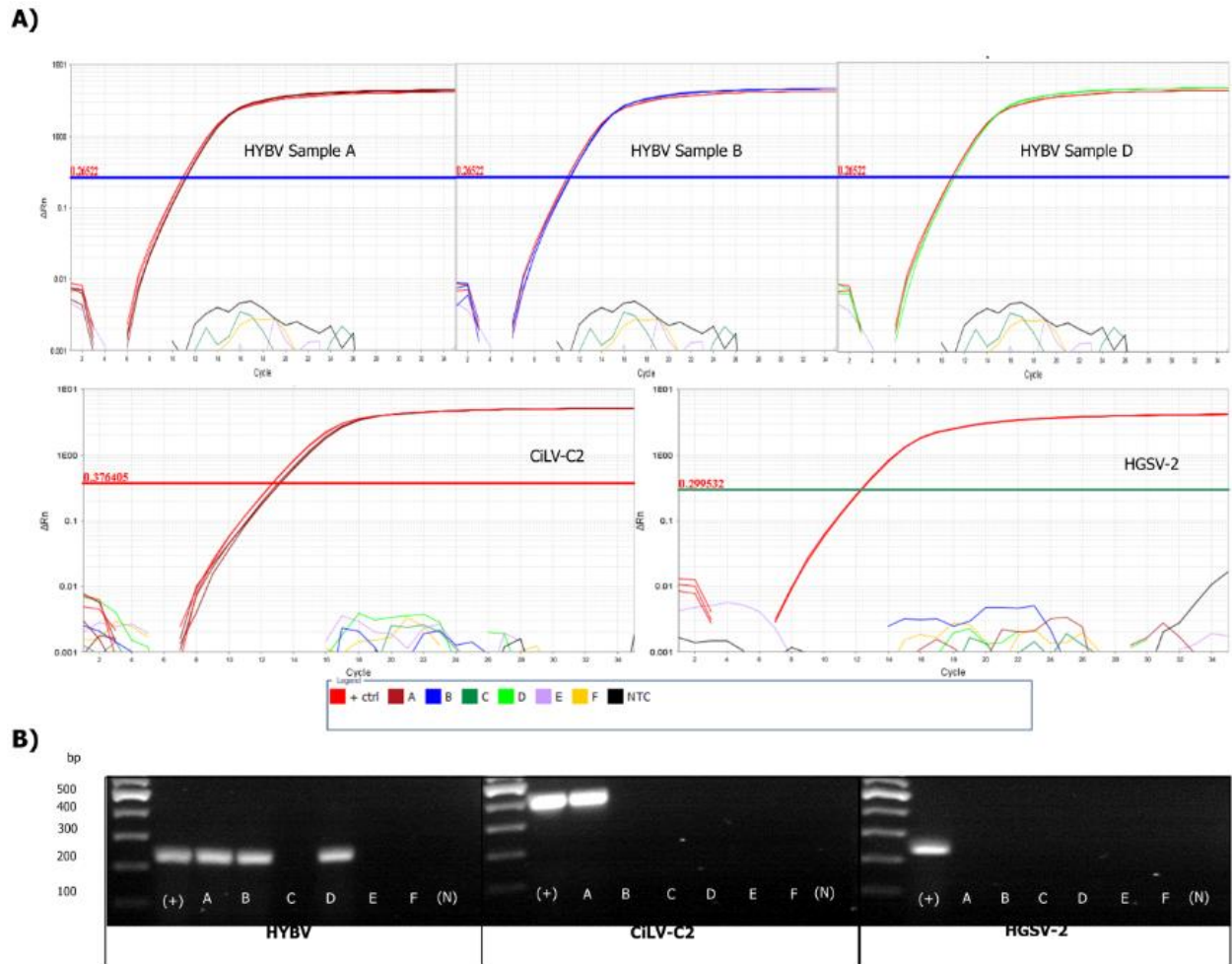


Figure 3.11 Detection of hibiscus yellow blotch virus (HYBV), citrus leprosis virus C2 (CiLV-C2), and hibiscus green spot virus 2 (HGSV-2) in *Hibiscus* spp. samples by RT-qPCR (A) and RT-PCR (B) assays. Six samples (A-F) of *Hibiscus* spp. (Figure 3.10) collected within 1.6 km of the HYBV-infected *H. rosa-sinensis* underwent both assays using HYBV-RdRp-F/R, CiLV-C2-RdRp-F/R and HGSV-2-RdRp-F/R (Table 3.1) for virus detection. Samples A, B and D tested positive for HYBV in both one-step RT-qPCR (A) and two-step RT-PCR (B) assays. Due to similar amplification curve of samples A (dark red), B (blue) and D (light green), individual amplification curves are provided for each sample and compared with a positive control (red). Sample A was the only CiLV-C2-positive sample in both one-step RT-qPCR (A) and two-step RT-PCR (B) assays. No samples tested positive for HGSV-2. Expected size of amplicons for HYBV, CiLV-C2 and HGSV-2 are 223 bp, 386 bp and 227 bp, respectively. NTC and (N) represent non-template controls for A) and B) respectively. the DNA ladder in B) is the 100bp Ladder from ThermoFisher, and fragment sizes are provided at left in base pairs (bp).

3.4 DISCUSSION

The *Kitaviridae* family is a recently created taxon currently comprised of three genera of plant pathogenic viruses: *Blunervirus*, *Cilevirus*, and *Higrevirus* (Quito-Avila et al., 2020; Melzer et al., 2018). Kitavirids share an evolutionary history based on the three proteins they commonly possess: replication-associated polyprotein, p24 protein, and in the case of blunerviruses and cileviruses, the MP. Additionally, mites (eriophyid and flat or false spider) have been reported as the putative or confirmed vectors of these viruses (Burkle et al., 2012; Rodrigues et al., 2016). Interestingly, systemic infection of their plant host is rare; most kitavirid infections of plants are restricted to localized lesions (Quito-Avila et al., 2020). Several *Kitaviridae* members have been characterized through the use of HTS (Quito-Avila et al., 2013; Roy et al., 2013; Hao et al., 2018; Ramos-Gonzalez et al., 2020) which is an increasingly important and efficient technique for virus discovery and characterization, including in numerous studies in different agricultural systems (Villamor et al., 2019).

In this study, we have characterized a new kitavirid infecting *H. rosa-sinensis* in Hawaii using HTS of a dsRNA library. The symptoms displayed on leaves infected with this virus resemble those associated with infection by cileviruses and other kitavirids (Figure 3.1) (Melzer et al., 2013; Rodrigues et al., 2016). RT-PCR assays specific for CiLV-C2 and HGSV-2 indicated these two kitavirids, which commonly infect hibiscus in Hawaii, were absent, suggesting the presence of another pathogen. HTS and bioinformatic analyses allowed the complete bipartite genome of this new kitavirid to be characterized. The genomic RNAs, determined to be 8.3 and 4.4 kb in size, were consistent with the dsRNAs observed by agarose gel electrophoresis (Figure 3.2). RNA 1 codes for a RdRp and a putative p10 protein with unknown function. RNA 2 codes for p56, p32, p25 and p33 proteins that likely represent the putative glycoprotein, putative movement protein, putative virion membrane protein and putative coat protein, respectively. This genomic organization resembles that of cileviruses, but with some key differences (Figure 3.3). First, p33 is located in the 3' region of RNA 2, but the homolog of this protein in cileviruses (p29) is located in the 3' region of RNA 1. These represent the putative viral coat proteins (Leastro et al., 2018), and this observation suggests a gene rearrangement event in an ancestor of these viruses. Second, p15 is the most variable conserved orphan protein present in the 5' region of RNA 2 of the three classified and putative *Cilevirus* species (Ramos-Gonzalez et al., 2020). This new kitavirid lacks a p15 homolog in the 5' region of its RNA 2. The absence of a p15 homolog was supported by an inability to identify this putative protein *in silico*, using 5' RACE, and through degenerate RT-PCR assays targeting conserved amino acid sequences identified following the alignment of cilevirus p15 sequences. Based on sequence comparisons and recombination analyses of the 5' end of the cilevirus RNA 2, it has been previously suggested that the high nucleotide variability present in that region is the result of continuous illegitimate (non-homologous)

recombination processes that may occur at the inter-species level (Ramos-Gonzalez et al., 2016). Therefore, recombination processes may have contributed to the loss of a p15 homolog in an ancestor of HYBV. Finally, a 3'-terminal ORF encoding a putative 10 kDa protein is present in HYBV RNA 1. Although the predicted p10 protein shares no homology to viral proteins in GenBank, a pairwise protein structural alignment of the HYBV p10 and the product of a similarly sized and positioned ORF encoded by HGSV-2 using EXPRESSO T-Coffee revealed they share statistically significant structural similarities. A global pairwise alignment showed they share 19.7 % protein identity. Furthermore, both p10 proteins of HYBV and HGSV-2 possess two transmembrane domains (Figure 3.5). This suggests these putative orphan proteins of HYBV and HGSV-2 are either distant orthologs or represent structural convergence of two unrelated proteins. It has been suggested that some orphan proteins may help plant viruses to infect and colonize its arthropod host/vector (Kuchibhatla et al., 2014; Solovyev and Morozov, 2017). Based on this same hypothesis, it has been speculated that kitaviruses have two sets of movement genes, and specifically cileviruses have the MP gene in conjunction with the p24 (putative virion membrane protein) and p61 (putative glycoprotein) proteins involved in virus movement within the mite host (Solovyev and Morozov, 2017). Based on the genomic organization of HYBV, this new kitavirid represents a distinct member within the family *Kitaviridae* that shares genomic similarities with members of both *Cilevirus* and *Higrevirus* genera.

Phylogenetic analyses of all conserved protein products support the placement of HYBV within the *Kitaviridae* family, specifically in an intermediate position between the cilevirus and higrevirus clades (Figures 3.7 and 3.8). The sequence identities of the three conserved kitavirid proteins, namely RdRp, p24 and MP, of HYBV with kitavirid homologs was found to be low to moderate (<45%). A similar scenario is observed for HGSV-2, the sole *Higrevirus* member and members of the genus *Blunervirus* (<38%). Conversely, the *Cilevirus* proteins have high identities (>54%) (Table 3.2 and Figure 3.4). The relatively high protein identity levels among the *Cilevirus* protein homologs and the phylogenetic relatedness may suggest a more recent divergence within the genus, whereas blunerviruses diverged much earlier or might have undergone a more rapid evolution due to host or vector selective pressures. Considering the low protein identity level in the genus *Blunervirus*, it is plausible that in the future when more viruses belonging to the blunervirus clade are characterized, the genus may be divided into additional genera. The phylogenetic placement of HYBV, coupled with its distinctive genome organization, suggests this virus represents a distinct lineage intermediate of cileviruses and higreviruses. However, until more kitavirids are characterized which will allow greater resolution of the family's taxonomy, it seems appropriate to consider HYBV a basal member of the genus *Cilevirus*, as it shares the most features with members of this taxon.

Multiple nucleotide sequence alignments of the 5' and 3' UTR revealed that HYBV possesses long conserved 5' and 3' UTRs rich in AT among its genomic segments (Table 3.3), a feature shared by other cileviruses, most notably CiLV-C. Both 5' and 3' termini of HYBV RNA 1 and 2 were also highly conserved, with the latter being longer and sharing a higher nucleotide identity. Previously, it was found that the blunervirus BNRBV contains AT-rich UTRs and conserved termini (Quito-Avila et al., 2013). Also, the formation of stem-loop secondary structures in the 3' UTR of the four RNAs was predicted and may be associated to the regulation of virus genome replication as well as protein synthesis (Quito-Avila et al., 2013). Interestingly, most of the cileviruses, HYBV, HGSV-2 and BNRBV have a G/C, and C as their first and last nucleotide, respectively (Table 3.3). While sequencing clones for the 5' RACE experiments for HYBV RNA 1 and 2, some indicated G (rather than the more common C) as the first nucleotide (data not shown). Considering the multiple plant hosts, limited *Brevipalpus* species associated to kitavirids, and conserved UTRs in some kitavirids, it is plausible that these regions may play a role in regulation of different virus infectious cycle processes within their hosts.

Flat mites are polyphagous and the presence of several *Brevipalpus* species on the same host plant has been reported previously (Salinas-Vargas et al., 2016). DNA barcoding using dRT-PCR (Druciarek et al., 2019) targeting the 28S rRNA and COI indicated mites tentatively identified as *B. yothersi* and an unidentified *Brevipalpus* sp., were present on the HYBV-infected *H. rosa-sinensis* plant. For this latter specimen, the COI sequence suggested its identity to be *B. obovatus*, however, the 28S rRNA sequence provided its identity to be *B. papayensis*. *B. yothersi* and *B. papayensis* are two of the seven recently created *Brevipalpus* species that were derived from the *B. phoenicis* species complex (Beard et al., 2015). Therefore, the identity of this *Brevipalpus* specimen needs further identification based on morphological keys using scanning electron microscopy (Beard et al., 2013). *B. yothersi* has been reported as the main vector of CiLV-C and CiLV-C2 (Ferreira et al., 2020; García-Escamilla et al., 2018; Roy et al., 2013). In this study we demonstrated the ingestion and potential acquisition of HYBV by *B. yothersi* using dRT-PCR assays targeting both RNA 1 and 2 of the virus. Considering the low number of individual *Brevipalpus* used in this study, the non-systemic nature of infection, and the ability of several *Brevipalpus* species to vector CiLV-C (Nunes et al., 2018), it is plausible that the other *Brevipalpus* sp. that could not be identified by DNA barcoding in this study may play a role in the transmission of HYBV. Additional transmission experiments are required to validate the transmission of HYBV by *B. yothersi* and other *Brevipalpus* species, and include confirmation of the mite species.

TS data indicated that HCRSV and HLFPV were co-infecting the *H. rosa-sinensis* plant harboring HYBV. HCRSV infection has been associated with distinct mild ringspot symptoms and HLFPV with a latent infection (Zhou et al., 2006; Kamenova et al., 2004). Neither of these are consistent with the

observed symptoms of yellow chlorotic blotches with a dark green perimeter that are typical of a BTV infection (Figures 3.1 and 3.10), making HYBV the most likely causal agent of the observed symptoms. However, the presence of HCRSV and HLFPV, as well as the presence of CiLV-C2, as co-infections with HYBV may impact host symptoms and other aspects of this pathosystem. The development of an infectious clone of HYBV would greatly help elucidate its role as a causal agent of the observed disease. Until such a clone is available, the conventional and quantitative RT-PCR assays developed in this study for the detection of HYBV will help to further determine any relationship between HYBV infection, co-infection with other pathogens, and symptom expression. Although the presence of non-viral pathogens or physiological disorders cannot be excluded, the observed symptoms were absent from other hibiscus plants in the immediate area that would presumably be exposed to the same pathogen inoculum and growing conditions as the symptomatic plant. Additional symptomatic plants were observed up to 1.6 km away, some of which tested negative for HYBV, CiLV-C2, and HGSV-2 (Figure 3.10). This suggests additional related viruses may be present in Hawaii's hibiscus, adding to the complexity of this pathosystem.

3.5 LITERATURE CITED

- Altschul, S.F., Madden, T.L., Scha ffer, A.A., Zhang, J., Zhang, Z., Miller, W. et al. (1997). Gapped BLAST and PSI-BLAST: A new generation of protein database search programs. *Nucleic Acids Res.* 25, 3389-3402.
- Arif, M. & Ochoa-Corona, F. (2013). Comparative assessment of 5' A/T-rich overhang sequences with optimal and sub-optimal primers to increase PCR yields and sensitivity. *Mol. Biotechnol.* 55, 17-26. doi: 10.1007/s12033-012-9617-5
- Armougom, F., Moretti, S., Poirot, O., Audic, S., Dumas, P., Schaeli, B., et al. (2006). Espresso: automatic incorporation of structural information in multiple sequence alignments using 3D-Coffee. *Nucleic Acids Res.* 34(Web Server issue), W604-W608. doi:10.1093/nar/gkl092
- Beard, J.J., Ochoa, R., Bauchan, G.R., Trice, M.D., Redford, A.J., Walters, T.W. et al. (2013). Flat Mites of the World – EDITION 2 Fort Collins, Colorado, CPHST, PPQ, APHIS, USDA.
- Beard, J.J., Ochoa, R., Braswell, W.E. & Bauchan, G.R. (2015). *Brevipalpus phoenicis* (Geijskes) species complex (Acari: Tenuipalpidae) - a closer look. *Zootaxa* 3944(1): 1-67.
- Bolger, A.M., Lohse, M. & Usadel, B. (2014). Trimmomatic: A flexible trimmer for Illumina sequence data. *Bioinformatics* 30, 2114-2120.
- Bouckaert, R., Vaughan, T.G., Barido-Sottani, J., Duchêne, S., Fourment M., Gavryushkina A., et al. (2019). BEAST 2.5: An advanced software platform for Bayesian evolutionary analysis. *PLoS computational biology*, 15(4), e1006650.
- Chang, J.M., Di Tommaso, P. & Notredame, C. (2014). TCS: a new multiple sequence alignment reliability measure to estimate alignment accuracy and improve phylogenetic tree reconstruction. *Mol. Biol. Evol.* 31(6), 1625-1637. doi:10.1093/molbev/msu117
- Colariccio, A., Lovisolo, O., Boccardo, G., Chagas, C.M., d'Aquilio, M. & Rossetti, V. (2000). Preliminary purification and double stranded RNA analysis of citrus leprosis virus. *Proceedings Conference International Organization of Citrus Virologists*, 14, 159-163.
- Dey, K.K., Sugikawa, J., Kerr, C. & Melzer, M.J. (2019). Air potato (*Dioscorea bulbifera*) plants displaying virus-like symptoms are co-infected with a novel potyvirus and a novel ampelovirus. *Virus Genes* 55(1), 117-121. doi: 10.1007/s11262-018-1616-6.

Di Tommaso, P., Moretti, S., Xenarios, I., Orobitg, M., Montanyola, A., Chang, J.M., et al. (2011) T-Coffee: a web server for the multiple sequence alignment of protein and RNA sequences using structural information and homology extension. *Nucleic Acids Res.* 39(Web Server issue), W13-W17.

doi:10.1093/nar/gkr245

Druciarek, T., Lewandowski, M. & Tzanetakis, I. (2019). A new, sensitive and efficient method for taxonomic placement in the Eriophyoidea and virus detection in individual eriophyoids. *Exp. Appl. Acarol.* 78, 247-261. Doi:10.1007/s10493-019-00382-4

Ferreira, L.M., Nunes, M.A, Sinico, T.E., Soares, A.J., & Novelli, V.M. (2020). *Brevipalpus* species vectoring citrus leprosis virus (Cilevirus and Dichorhavirus). *J. Econ. Entomol.* 113, 1628-1634.

Freitas-Astúa, J., Ramos-González, P.L., Arena, G.D., Tassi, A.D., & Kitajima, E.W. (2018). *Brevipalpus*-transmitted viruses: parallelism beyond a common vector or convergent evolution of distantly related pathogens? *Curr Opin Virol* 33: 66–73. <https://doi.org/10.1016/j.coviro.2018.07.010>

García-Escamilla, P., Duran-Trujillo, Y., Otero-Colina, G., Valdovinos-Ponce, G., Santillán-Galicia, M.T., Ortiz-García, C.F., et al. (2018). Transmission of viruses associated with cytoplasmic and nuclear leprosis symptoms by *Brevipalpus yothersi* and *B. californicus*. *Trop. Plant Pathol.* 43:69-77.

Grabherr, M.G., Haas, B.J., Yassour, M., Levin, J.Z., Thompson, D.A., Amit, I et al. (2011). Full-length transcriptome assembly from RNA-Seq data without a reference genome. *Nat. Biotechnol.* 29, 644-652.

Hao, X., Zhang, W., Zhao, F., Liu, Y., Qian, W., Wang, Y., et al. (2018). Discovery of plant viruses from tea plant (*Camellia sinensis* (L.) O. Kuntze) by metagenomic sequencing. *Front. Microbiol.* 9: 2175. doi: 10.3389/fmicb.2018.02175.

Huang, X. & Miller, W. (1991). A time-efficient, linear-space local similarity algorithm. *Adv. Appl. Math.* 12, 337-357.

International Committee on Taxonomy of Viruses (2019). ICTV Master Species List 2019 v2. Checklist dataset <https://doi.org/10.15468/i4jnfv> accessed via GBIF.org on 2020-03-27.

Kamenova, I. & Adkins, S. (2004) Transmission, In Planta Distribution, and Management of Hibiscus latent Fort Pierce virus, a Novel Tobamovirus Isolated from Florida Hibiscus. *Plant Dis.* 88(6), 674-679.

Kitajima, E.W., Chagas, C.M., & Rodrigues, J.C.V. (2003) *Brevipalpus*-transmitted plant virus and virus-like diseases: cytopathology and some recent cases. *Exp. Appl. Acarol.* 30, 135-160.

- Kitajima, E.W., Rosillo, M.A., Portillo, M.M., Müller, G.W., & Costa, A.S. (1974). Microscopia electronica de tecidos foliares de laranjeiras infectadas pela lepra explosiva da Argentina. *Fitopatologia (Lima)* 9, 254-258.
- Kearse, M., Moir, R., Wilson, A., Stones-Havas, S., Cheung, M., Sturrock, S. et al. (2012). Geneious Basic: An integrated and extendable desktop software platform for the organization and analysis of sequence data. *Bioinformatics* 28, 1647-1649.
- Krogh, A., Larsson, B., von Heijne, G., & Sonnhammer, E.L.L. (2001). Predicting transmembrane protein topology with a hidden Markov model: Application to complete genomes. *J. Mol. Biol.* 305(3), 567-580.
- Kuchibhatla, D.B., Sherman, W.A., Chung, B.Y., et al. (2014) Powerful sequence similarity search methods and in-depth manual analyses can identify remote homologs in many apparently "orphan" viral proteins. *J Virol.* 88(1),10-20. doi:10.1128/JVI.02595-13
- Kumar, S., Stecher, G. & Tamura, K. (2016). MEGA 7: Molecular Evolutionary Genetics Analysis version 7.0 for bigger datasets. *Mol. Biol. Evol.* 33, 1870-1874.
- Leastro, M.O., Kitajima, E.W., Silva, M.S., Resende, R.O. & Freitas-Astúa, J. (2018). Dissecting the subcellular localization, intracellular trafficking, interactions, membrane association, and topology of Citrus leprosis virus C protein. *Front. Plant Sci.* 9:1299. doi: 10.3389/fpls.2018.01299
- Melzer, M.J., Borth, W.B., Sether, D.M., Ferreira, S., Gonsalves, D. & Hu, J.S. (2010). Genetic diversity and evidence for recent modular recombination in Hawaiian Citrus tristeza virus. *Virus Genes* 40, 111-118. doi:10.1007/s11262-009-0409-3
- Melzer, M.J., Freitas-Astúa, J., Rodriguez, J.C.V., Roy, A. & Wei, G. (2018). Create one new family Kitaviridae comprising three previously unassigned genera, Cilevirus, Blunervirus and Higreivirus 2018.002P. melzer@hawaii.edu. <https://talk.ictvonline.org/ictv/proposals/2018.002P.A.Kitaviridae.zip>. Accessed 08 Aug 2020
- Melzer, M.J., Sether, D.M., Borth, W.B. & Hu, J.S. (2012). Characterization of a virus infecting Citrus volkameriana with citrus leprosis-like symptoms. *Phytopathol.* 102(1), 122-127. doi: 10.1094/PHYTO-01-11-0013
- Melzer, M.J., Simbajon, N., Carillo, J., Borth, W.B., Freitas-Astúa, J., Kitajima, E.W., et al., (2013). A cilevirus infects ornamental hibiscus in Hawaii. *Arch. Virol.* 158, 2421–2424. doi: 10.1007/s00705-013-1745-0

Mironov, S.V., Dabert, J. & Dabert, M. (2012). A new feather mite species of the genus *Proctophyllodes* Robin, 1877 (Astigmata: Proctophyllodidae) from the long-tailed tit *Aegithalos caudatus* (Passeriformes Aegithalidae)-morphological description with DNA barcode data. *Zootaxa* 3253: 54-61.

Morris, T.J. & Dodds, J.A. (1979). Isolation and analysis of doubled-stranded RNA from virus-infected plant and fungal tissue. *Phytopathol.* 69, 854-858.

Muhire, B.M., Varsani, A. & Martin, D.P. (2014). SDT: A Virus Classification Tool Based on Pairwise Sequence Alignment and Identity Calculation. *PLoS ONE* 9(9): e108277. doi: 10.1371/journal.pone.0108277

Navarro, B., Minutolo, M., De Stradis, A., Palmisano, F., Alioto, D. & Di Serio, F. (2018). The first phlebo-like virus infecting plants: a case study on the adaptation of negative-stranded RNA viruses to new hosts. *Mol. Plant Pathol.* 19(5), 1075-1089. doi: 10.1111/mpp.12587.

Nunes, M.R.T., Contreras-Gutierrez, M.A., Guzman, H., Martins, L.C., Feitoza Barbirato, M., Savit, C. et al., (2017). Genetic characterization, molecular epidemiology and phylogenetic relationships of insect-specific viruses in the taxon Negevirus. *Virology* 504: 152-167. doi: 10.1016/j.virol.2017.01.022

Nunes, M.A., de Carvalho Mineiro, J.L., Rogerio, L.A., Ferreira, L.M., Tassi, A., Novelli, V.M., et al. (2018). First report of *Brevipalpus papayensis* as vector of coffee ringspot virus and citrus leprosis virus C. *Plant Dis.* 102(5): 1046. doi: 10.1094/PDIS-07-17-1000-PDN

Olmedo-Velarde, A., Park, A.C., Sugano, J., Uchida, J.Y., Kawate, M., Borth, W.B. et al., (2019). Characterization of Ti Ringspot-Associated Virus, a Novel Emaravirus Associated with an Emerging Ringspot Disease of *Cordyline fruticosa*. *Plant Dis.* 103(9), 2345-2352.

Potter, S.C., Luciani, A., Eddy, S.R., Park, Y., Lopez, R. & Finn, R.D. (2018). HMMER web server: 2018 update. *Nucleic Acids Res.* 46(W1), W200-W204. doi: 10.1093/nar/gky448

Quito-Avila, D.F., Freitas-Astúa, J., & Melzer, M.J. (2020). “Bluner-, Cile-, and higreviruses (kitaviridae),” in Reference Module in Life Sciences, ed. B. D. Roitberg (Amsterdam: Elsevier), 1–5.

Quito-Avila, D.F., Brannen, P.M., Cline, O.W., Harmon, P.F. & Martin, R.R. (2013). Genetic characterization of Blueberry necrotic ring blotch virus, a novel RNA virus with unique genetic features. *J. Gen. Virol.* 94(6): 1426-1434. doi: 10.1099/vir.0.050393-0

Rambaut, A., Drummond, A.J., Xie, D., Baele, G. & Suchard, M.A. (2018). Posterior summarisation in Bayesian phylogenetics using Tracer 1.7. *Syst. Biol.* 67(5), 901-904. doi:10.1093/sysbio/syy032

- Ramos-Gonzalez, P.L., Chabi-Jesus, C., Guerra-Peraza, O., Breton, M.C., Arena, G.D., Nunes, M.A. et al. (2016). Phylogenetic and molecular variability studies reveal a new genetic clade of Citrus leprosis virus C. *Viruses* 8(6): 153. doi: 10.3390/v8060153
- Ramos-Gonzalez, P.L., Santos, G.F., Chabi-Jesus, C., Harakava, R., Kitajima, E.W. & Freitas-Astúa, J. (2020) Passion Fruit Green Spot Virus Genome Harbors a New Orphan ORF and Highlights the Flexibility of the 5'-End of the RNA2 Segment Across Cileviruses. *Front. Microbiol.* 11:206. doi: 10.3389/fmicb.2020.00206.
- Rodrigues, J.C.V., Childers, C.C. & Kitajima, E.W. (2016). *Brevipalpus* spp. (Acari: Tenuipalpidae): Vectors of Cytoplasmic and Nuclear Viruses in Plants. In: J.K. Brown, editor. *Vector-Mediated Transmission of Plant Pathogens*. St. Paul, MN: APS Press. pp. 309-318.
- Roy, A., Choudhary, N., Leon, G.M., Shao, J., Govindarajulu, A., Achor, D. et al. (2013). A novel virus of the genus Cilevirus causing symptoms similar to citrus leprosis. *Phytopathol.* 103(5): 488-500. doi: 10.1094/PHYTO-07-12-0177-R.
- Roy, A., Hartung, J.S., Schneider, W.L., Shao, J., Leon, G., Melzer, M.J., et al. (2015). Role bending: Complex relationships between viruses, hosts, and vectors related to citrus leprosis, an emerging disease. *Phytopathology* 105(7): 1013-1025. doi: 10.1094/PHYTO-12-14-0375-FI.
- Salinas-Vargas, D., Santillan-Galicia, M.T., Guzman-Franco, A.W., Hernandez-Lopez, A., Ortega-Arenas, L.D. & Mora-Aguilera, G. (2016). Analysis of genetic variation in *Brevipalpus yothersi* (Acari: Tenuipalpidae) populations from four species of citrus host plants. *PLoS One* 11(10): e0164552. DOI: 10.1371/journal.pone.0164552
- Solovyev, A.G. & Morozov, S.Y. (2017). Non-replicative Integral Membrane Proteins Encoded by Plant Alpha-Like Viruses: Emergence of Diverse Orphan ORFs and Movement Protein Genes. *Front. Plant Sci.* 8:1820. doi: 10.3389/fpls.2017.01820
- Sonnenberg, R., Wolte, A.W. & Tautz, D. (2007). An evaluation of LSU rDNA D1-D2 sequences for their use in species identification. *Front. Zool.* 4, 6.
- Untergasser, A., Cutcutache, I., Koressaar, T., Ye, J., Faircloth, B.C., Remm, M., et al. (2012). Primer3 - new capabilities and interfaces. *Nucleic Acids Res.* 40(15): e115
- Villamor, D.E.V., Ho, T., Al Rwahnih, M., Martin, R.R. & Tzanetakis, I.E. (2019). High throughput sequencing for plant virus detection and Discovery. *Phytopathol* 109(5): 716-725. doi: 10.1094/PHYTO-07-18-0257-RVW.

Wickham, H. (2016). *ggplot2: Elegant Graphics for Data Analysis*. Springer-Verlag New York. Retrieved from <https://ggplot2.tidyverse.org>

Zhou, T., Fan, Z.F., Li, H.F. & Wong, S.M. (2006) Hibiscus chlorotic ringspot virus p27 and Its Isoforms Affect Symptom Expression and Potentiate Virus Movement in Kenaf (*Hibiscus cannabinus* L.). *Mol. Plant Microbe In.* 19(9), 948-957.

CHAPTER IV

FURTHER MOLECULAR AND BIOLOGICAL CHARACTERIZATION OF HIBISCUS GREEN SPOT VIRUS 2

4.1 INTRODUCTION

Hibiscus green spot virus 2 is a positive-stranded RNA virus with a tripartite genome, and the sole member of the plant virus genus *Higrevirus* (family *Kitaviridae*). *Hibiscus green spot virus 2* (HGSV-2) was originally characterized from infections of *Citrus volkameriana* and *Hibiscus arnottianus* in Hawaii (Melzer et al., 2012), and was later found to infect *C. reticulata*, *C. sinensis* and *H. tiliaceus* (Roy et al., 2015a). In citrus, HGSV-2 is associated with citrus leprosis-like symptoms that include chlorotic blotches on leaves and fruits, and occasional necrotic lesions on twigs. In hibiscus, HGSV-2 is associated with green spots on leaves that are more obvious when leaves are senescent (Melzer et al., 2012; Roy et al., 2015a). HGSV-2 transmission by *Brevipalpus* sp. mites has been speculated, however, proper transmission assays are required (Melzer et al., 2012). Although partial nucleotide sequences of the genome of HGSV-2 infecting *C. volkameriana*, *C. sinensis*, *C. reticulata*, *H. arnottianus* and *H. tiliaceus* presented >97% nucleotide identity (Roy et al., 2015a), the full genome of HGSV-2 was sequenced from a volkamer lemon tree (Melzer et al., 2012). RNA 1 (8,354 bp) codes for a 273 kDa replication-associated polyprotein containing methyl-transferase, cysteine protease, helicase and RNA-dependent RNA polymerase domains. RNA 2 (3,169 bp) codes for putative proteins with no clear function with molecular masses of 50, 13, 39, 9 and 6 kDa. Although p39, p9 and p6 present some typical characteristics of triple gene block (TGB) genes, i.e. helicase presence in one of the protein-coded genes and transmembrane regions presence in the others (Melzer et al., 2012); a study performed by Lazareva et al (2016) suggested that p39 and p9 represent a new and specialized transport module called binary movement block (BMB) of genes. Indeed, p39 and p9, BMB1 and BMB2, respectively, were necessary and sufficient to mediate cell-to-cell movement of a transport-deficient infectious clone of potato virus X in *Nicotiana benthamiana*. RNA 3 (3,113 bp) codes for three putative proteins with molecular masses of 33, 29 and 23 kDa. Of these three putative proteins, only p23 shares similarity with other viral proteins, and represents a member of the SP24 (PF16504) protein family which is encoded by other kitavirids (Quito-Avila et al., 2020) and a large group of related insect- and other arthropod-infecting viruses which are awaiting classification (Kuchibhatla et al., 2014).

The aim of this present chapter is to further characterize HGSV-2 at the molecular and biological levels. This chapter describes the further molecular characterization of HGSV-2 by sequencing two additional isolates of HGSV-2 infecting hibiscus and citrus from Oahu and Maui Islands, respectively. Additionally, the development of a reverse-genetic system of HGSV-2 is detailed. An infectious clone of HGSV-2 may help to further characterize and corroborate the gene functions and proteins putatively coded by HGSV-2. Finally, the transmission of HGSV-2 by *Brevipalpus* sp. mites is described.

4.2 MATERIALS AND METHODS

4.2.1 Virus source and nucleic acid extraction

H. arnottianus, *C. sinensis*, and *C. reticulata* leaf samples showing typical symptoms caused by HGSV-2 characterized by green blotches surrounded by a chlorotic halo (Figure 4.1) were collected from Honolulu (Oahu Island) in 2019 and Pukalani (Maui Island) in 2021, respectively. Total RNA was extracted from these symptomatic tissues using Spectrum Plant Total RNA kit (Sigma-Aldrich, St. Louis, MO) according to the manufacturer's instructions. Additionally, double-stranded RNA (dsRNA) was isolated from ~5 g of *H. arnottianus* symptomatic tissues using Sigmacell Type 101 (Sigma, St. Louis, MO) cellulose chromatography following the procedure of Morris and Dodds (1979).



Figure 4.1 Symptoms of hibiscus green spot virus 2 infection on *Hibiscus arnottianus* (left) and *Citrus sinensis* (right) characterized by the presence of green blotches surrounded by a chlorotic halo. *H. arnottianus* and *C. sinensis* samples were collected from the islands of Oahu and Maui, respectively.

4.2.2 Genome sequencing

To obtain the complete and near complete genomic sequence of a hibiscus and a citrus isolates of HGSV-2, respectively, cDNA synthesis was performed using total RNA extracts from each HGSV-2 isolate, oligo dT primers and SuperScript III reverse transcription kit (ThermoFisher Scientific, Waltham, MA) using the manufacturer's instructions. A group of overlapping primer sets based on the previous complete genomic sequence of HGSV-2 (HQ852052-HQ852054; Melzer et al., 2012) were designed using Primer3 (Untergasser et al. 2012). Thermodynamic primer features detailed by Arif and Ochoa-Corona (2013) were considered during the design process. RT-PCR assays were used to amplify overlapping regions spanning the nearly complete genome of the RNA 1, 2, and 3 of HGSV-2. The 5' termini of the hibiscus isolate of HGSV-2 were characterized by 5' RACE as detailed by (Navarro et al., 2018) on poly-A tailed dsRNAs and poly-dG-tailed cDNAs that were generated using *E. coli* Poly(A) Polymerase (New England Biolabs, Ipswich, MA) and Terminal Deoxynucleotidyl Transferase (ThermoFisher Scientific, Waltham, MA), respectively. The 3' termini were characterized by 3' RACE using an oligo-dT primer to target the poly-A tracts at the 3'-end of RNA 1, 2 and 3 of HGSV-2. Primers employed for genome sequencing and RACE experiments are detailed in Table 4.1. All amplicons were gel extracted, purified and bi-directionally sequenced or cloned into pGEM-T Easy (Promega, Madison, WI) with three to five clones sequenced per amplicon. For amplicons obtained by RACE, 7 to 13 clones were sequenced. The NCBI ORFfinder program (www.ncbi.nlm.nih.gov/orffinder) was used to identify putative open reading frames (ORFs) *in silico* and examine the genomic organization of the newly sequenced HGSV-2 isolates. Conserved domains were predicted using either the NCBI conserved domain search tool (www.ncbi.nlm.nih.gov/Structure/cdd/wrpsb.cgi) or HMMSCAN (www.ebi.ac.uk/Tools/hmmer/search/hmmscan) implemented in HMMER (Potter et al., 2018).

Table 4.1 PCR primers used for the sequencing and detection of citrus and hibiscus isolates of hibiscus green spot virus 2 (HGSV-2), and construction of 35SRbz-HGSV-2-RNA1/2/3 as part of a reverse genetics system for HGSV-2.

#	Primer Name	Sequence (5'-3')	T _m (°C)	Use
1	HGSV-2-RNA1-RdRp-F	GGTGCCCGTGTGTCTCATT	62	Diagnostic RT-PCR assays for detection of HGSV-2 RNA 1/2/3
2	HGSV-2-RNA1-RdRp-R	CGTCACACCACTCAGCAACA	62	
3	HGSV-2-RNA2-BM1-F	GCTGAACGGTGTTCCTGGTG	64	
4	HGSV-2-RNA2-BM1-R	CCCGTGCATGAACAAGTCGA	62	
5	HGSV-2-RNA3-p39F	CTCGGTGCTCTTGTGTTGC	62	
6	HGSV-2-RNA3-p39R	GCAAAGACACGAACCCAAGC	62	
7	744	GACCACGCGACGTGTCTG AVTTTTTTTTTTTTTTTTT		Primers used for RACE experiments for determination of 5'-end and 3'-end using poly-A tailing of dsRNA and oligo-dT anchored primer
8	HGSV2-RNA1-261R	TTGCCACGGAGCTTGTTAGA	60	
9	HGSV2-RNA1-8235F	TGGTGAACGCGTGAATTTGG	60	
10	HGSV2-RNA2-311R	CGCCTTCTAGACCAGCCAAA	62	
11	HGSV2-RNA2-2859F	GTACGCGGTTTCATGCTAGGT	62	
12	HGSV2-RNA3-187R	ACCAGCTCTCGGATGCGATAG	59.7	
13	HGSV2-RNA3-2878F	TTCGGTCGGTTGAGGAAAAGG	62	
14	743	TTACTAATATCCCCCCCCCCCC		Primers used for RACE experiments for determination of 5'-end using terminal deamino transferase (TdT) method
15	HGSV2-R2-outer	CGCCTTCTAGACCAGCCAAAAGACGTA	63.9	
16	HGSV2-R2-inner238	CAAGCGAGGAAACAAAACCT	58	
17	HGSV2-R1-outer	TTGCCACGGAGCTTGTTAGAATCCTTG	62.4	
18	HGSV2-R1-inner228	ACAAAAGATTCCATCGCTGA	56	
19	HGSV2-R3-outer	CAGCTCTCGGATGCGATAGCACTATC	63.9	
20	HGSV2-R3-inner149	ACCGAGCATGGCAACGTG	58	
21	pJL89-seqF	TGGATTGATGTGATA TCTCCACTGAC	59.1	Primers used for amplification and sequencing of the hibiscus and citrus isolates of HGSV-2 as well as sequencing of 35SRbz-HGSV2-RNA1, 35SRbz-HGSV2-RNA2 and 35SRbz-HGSV2-RNA3
22	pJL89-seqR	GCCAAATGTTTGAACGATCG	58	
23	HGSV2-RNA1-F1	TTCATTTGGAGAGGCATAA ATTAAAACAGGTGACTGG	64.1	
24	HGSV2-RNA1-R1	TCCTACCACCTTCAAACAG	60	
25	HGSV2-RNA1-F2	TTACTACGAAGGCAGTGTTG	58	
26	HGSV2-RNA1-R2	TCTCCATCCACAGTCGGGTCGA	61.8	
27	HGSV2-RNA1-F3	AAGAGCTAGTGCTTCACGAAAAGTCC	60.8	
28	HGSV2-RNA1-R3	GGATGACTAGTACCAACCAC	60	
29	HGSV2-RNA1-F4	CGGTTTTGTGTGATAAAGGG	58	
30	HGSV2-RNA1-R4	GGTACATATTAGCCTCGTCCG	60	
31	HGSV2-RNA1-F5	GATAGATTACGGATCCAAGC	58	
32	HGSV2-RNA1-R5	CGTCACACCACTCAGCAACA	62	

33	HGSV2-RNA1-F6	GGTGCCCGTGTGTCTCATT	62	
34	HGSV2-RNA1-R6	GCCATGCCGACCCTTTTTTT TTTTTTTTGCGGAAAAGAAG AAAAGAAAAGACAAACGAGG	70.6	
35	HGSV2-RNA2-F1	<u>TTGGAGAGGCATAAAATTACAAA</u> TAACGTTACTGTGACAGG	65.2	
36	HGSV2-RNA2-R1	CTTGATATCATAGCCACGGGTCA	58.4	
37	HGSV2-RNA2-F2	TCGTTGGGAACAATGAGGAG	60	
38	HGSV2-RNA2-R2	<u>ATGCCATGCCGACCCTTTTTTT</u> TTTTTTTTCACGACTAGG	66.3	
39	HGSV2-RNA3-F1	<u>TTGGAGAGGCATAAAATTACAAA</u> CAATTCTACTGAGGTGATCCC	67.1	
40	HGSV2-RNA3-R1	CCAACCTTTCTACACAAACGG	58	
41	HGSV2-RNA3-F2	TGGATACTGGAAGAAGGGTA	58	
42	HGSV2-RNA3-R2	<u>ATGCCATGCCGACCCTTTTTTTTTT</u> TTTTTGCAGGGAAAAGAGAAAGGGG	68.6	
43	pJL89-35S-R	TTTATGCCTCTCCAAAT GAAATGAACTTCC	59.9	pJL89 and pJL89-Fragment1 linearization
44	pJL89-Rbz-F	GGGTCGGCATGGCATCTC	60	
45	35s-HGSV-2- RNA2-F	<u>TTGGAGAGGCATAAAATTACAAA</u> TAACGTTACTGTGACAGG	65.2	Amplification of RNA2 of HGSV-2 with 9 and 15 bp of 35S and Rbz from pJL89, respectively
46	Rbz-HGSV-2- RNA2-R	<u>ATGCCATGCCGACCCTTTTTTT</u> TTTTTTTTCACGACTAGG	66.3	
47	35s-HGSV-2- RNA3-F	<u>TTGGAGAGGCATAAAATTACAAA</u> CAATTCTACTGAGGTGATCCC	67.1	Amplification of RNA3 of HGSV-2 with 9 and 15 bp of 35S and Rbz from pJL89, respectively
48	Rbz-HGSV-2- RNA3-R	<u>ATGCCATGCCGACCCTTTTTTTTTT</u> TTTTTGCAGGGAAAAGAGAAAGGGG	68.6	
49	35s-HGSV-2- RNA1-F	<u>TTCATTTGGAGAGGCATAAATTA</u> AAACAGGTGACTGGTTTTGCAAG	67	Amplification of Fragment1 spanning 1-2766 bp of HGSV-2-RNA1, and 14 bp of 35S
50	Rbz-HGSV-2- RNA1-2766R	<u>ATGCCATGCCGACCCTCTC</u> CATCCACAGTCGGGTCTGA	74.1	
51	HGSV-2-R1-2766R	TCTCCATCCACAGTCGGGTCTGA	61.9	pJL89-Fragment1 linearization
52	HGSV-2-R1-2766F	CCGACTGTGGATGGAGAGT ATTTTGGAGAGAAGGAGCT	69.6	Fragment2 amplification spanning 2,750-8369 bp of HGSV2-RNA1, and 20bp of Rbz
53	Rbz-HGSV-2- RNA1-R	<u>TGGAGATGCCATGCCGACC</u> TTTTTTTTTTTTTTGCGGAAAAG AAGAAAAGAAAAGACAAACGAGG	71.9	

Underlined nucleotide sequences represent non-complementary HGSV-2 genomic regions that correspond to the pJL89 vector sequence

4.2.3 Construction of a full-length cDNA clone of HGSV-2

The full-length cDNA clone of HGSV-2 was constructed using the In-Fusion HD cloning kit (Takara Bio, Mountain View, CA). For preparing a cDNA clone of a hibiscus isolate of HGSV-2 RNA1 (8,369 bp, including a 15 bp poly-A tail), a similar strategy detailed by Matsumura et al. (2019) to construct a cDNA clone of citrus sudden death-associated virus (35SRbz-CSDaV) was adopted. Briefly, a set of primers (Table 4.1) was designed to insert two fragments, spanning the full HGSV-2 RNA 1, into the binary vector pJL89 (Lindbo, 2007). HGSV-2 RNAs 2 and 3 were inserted into pJL89 as single, full-length

fragments (Figure 4.2). The fragments spanning the full HGSV-2 RNA1, 2 and 3 were inserted immediately downstream of the double-enhanced cauliflower mosaic virus (CaMV) 35S promoter (2 x 35S) and upstream of the hepatitis delta virus ribozyme (HDV-Rbz) by 15 to 20-base complementary overlapping ends following the In-Fusion HD cloning kit manufacturer's instructions. The cDNA was synthesized using 100 ng of dsRNA extracted from the HGSV-2-*H. arnottianus* infected tissues, oligo dT primers, and SuperScript III reverse transcription kit (ThermoFisher Scientific, Waltham, MA) using the manufacturer's instructions. The pJL89 was linearized using inverse PCR and pJL89-specific primers (Table 4.1). The linearized pJL89 vector (4,675 bp) and the HGSV-2 RNA 1, 2 and 3 fragments were obtained using PCR assays and the CloneAmp HiFi PCR premix (Takara Bio, Mountain View, CA) using the PCR conditions detailed in Table 4.2. All the amplicons were gel purified using NucleoSpin Gel and PCR Clean-up Mini kit (Macherey-Nagel, Duren, Germany). The In-Fusion reactions were performed using 60-80 ng of the linearized pJL89 vector, 70-100 ng of the corresponding purified HGSV-2 fragments and 1X In-Fusion HD Enzyme Premix (Takara Bio, Mountain View, CA) following the manufacturer's instructions. After incubating the reactions at 50 °C for 15 min and then on ice for 2 min, they were used for heat-shock transformation at 42 °C for 60 s using *Escherichia coli* Stellar competent cells (Takara Bio, Mountain View, CA). Transformed colonies were plated onto LB agar medium amended with kanamycin (100 µg / mL) and grown overnight at 37 °C. Individual colonies were screened by colony-PCR using HGSV-2 RNA 1, 2 and 3 -specific primers (Table 4.1) and the RT-PCR conditions described below. PCR-positive colonies were grown overnight at 37 °C in 2 mL of LB media amended with Kanamycin (100 µg / mL) shaking at 200 rpm. Plasmid purification was performed using Plasmid Mini Kit (Qiagen, Valencia, CA, USA). The full-length cDNA clones of HGSV-2 were confirmed by restriction digestion using *Hind*III restriction enzyme (New England Biolabs, Ipswich, MA, USA) and Sanger sequencing using overlapping primers designed along the HGSV-2 RNA 1, 2 and 3 genomic sequences detailed above (Table 4.1). Sequences were analyzed using Geneious v10.1.3 (Kearse et al. 2012) and the ORFs were confirmed using the ORF finder function of the Geneious software. Clones containing sequences presenting >99% nucleotide identity and the correct genomic organization were named 35SRbz-HGSV-2-RNA1/2/3, for cDNA clones of the hibiscus isolate of HGSV-2 RNA 1, 2 and 3, respectively. The proteins putatively coded by 35SRbz-HGSV-2-RNA1/2/3 and the hibiscus isolate of HGSV-2 were aligned using their structural information and the Expresso algorithm (Armougom et al., 2006) implemented in T-Coffee (<http://tcoffee.org.cat/apps/tcoffee/do:expresso>) (Di Tommaso et al., 2011).

Table 4.2 PCR conditions for linearization of vector pJL89 and pJL89-Fragment1 as well as amplification of Fragments 1 and 2 of HGSV-2-RNA1 and HGSV-2-RNA2 and 3.

Target	Primers	PCR conditions			
		Initial denaturation	Cycling 1	Cycling 2	Final extension
pJL89 linearization	43	98 °C	(98 °C -10s		72 °C
	44	1 min	54 °C - 15s 72 °C - 60s) x 35		7 min
HGSV-2 RNA 2	45	98 °C	(98 °C -10s	(98 °C -10s	72 °C
	46	1 min	50 °C - 30s 72 °C - 210s) x 8	60 °C - 30s 72 °C - 210s) x 30	7 min
HGSV-2 RNA 3	47	98 °C	(98 °C -10s	(98 °C -10s	72 °C
	48	1 min	55 °C - 30s 72 °C - 210s) x 8	55 °C - 30s 72 °C - 210s) x 30	7 min
HGSV-2 RNA 1 Fragment 1	49	98 °C	(98°C -10s	(98°C -10s	72 °C
	50	1 min	52° C - 30 s 72 °C - 210 s) x 5	60° C - 30 s 72 °C - 210 s) x 33	7 min
pJL89-Fragment1 linearization	51	98 °C	(98 °C -10s		72 °C
	44	1 min	54 °C - 30s 72 °C - 60s) x 35		7 min
HGSV-2 RNA 1 Fragment 2	52	98 °C	(98 °C -10s	(98 °C -10s	72 °C
	53	1 min	60 °C - 30s 72 °C - 300s) x 8	65 °C - 30s 72 °C - 300s) x 30	7 min

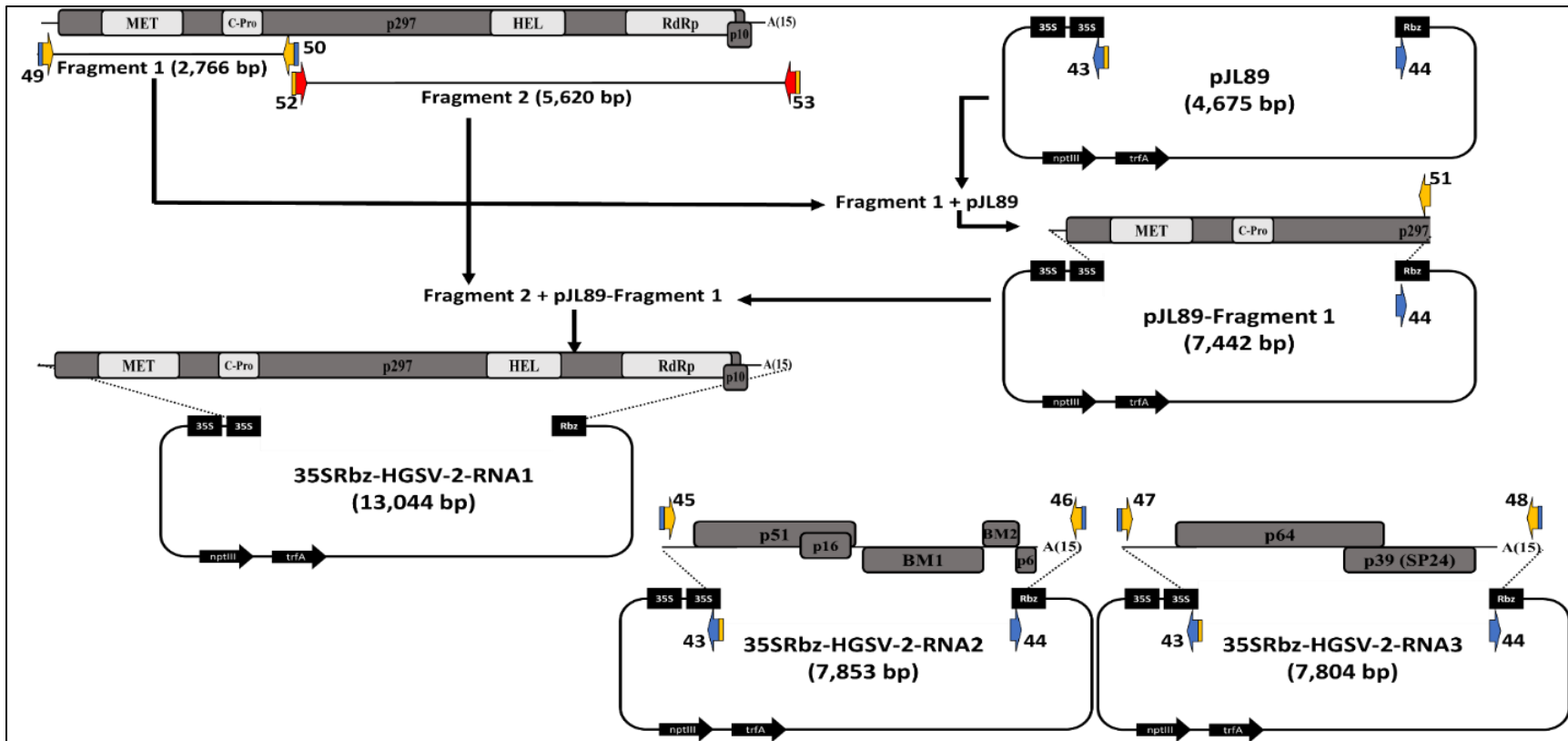


Figure 4.2 Schematic diagram of the strategy adapted from Matsumura et al. (2019) to clone the HGSV-2-RNA 1 (8,369 bp) into pJL89. First, Fragment 1 spanning nucleotides 1-2,766 of HGSV-2-RNA1 was inserted into pJL89 using In-Fusion cloning to obtain pJL89-Fragment 1 (7,442 bp). Then, Fragment 2 spanning nucleotides 2,750-8,369 of HGSV-2-RNA1 was inserted into pJL89-Fragment1 using In-Fusion cloning to obtain 35SRbz-HGSV-2-RNA1 (12,567 bp). HGSV-2-RNA2 and HGSV-2-RNA3 were individually inserted into pJL89 using In-Fusion cloning to generate 35SRbz-HGSV-2-RNA2 (7,853 bp) and 35SRbz-HGSV-2-RNA3 (7,804 bp), respectively. For the three RNAs, a 15 bp poly-A tail was present in the 3' termini. Fragment 1 of HGSV-2-RNA1, HGSV-2-RNA2, and RNA3 had a 15 bp-overlap with the pJL89 vector, whereas the fragment 2 of HGSV-2-RNA1 had a 17-20 bp overlap with the pJL89-Fragment 1 and the Rbz-pJL89 vector. Primer sequences used for these experiments are detailed in Table 4.1 (primer numbers 43-53).

4.2.4 Preparation and transformation of competent cells

A single colony of *Agrobacterium tumefaciens* EHA105 was grown overnight in 5 mL of LB media containing rifampicin (25 µg / mL) at 29 °C and shaking at 150 rpm. After the culture was incubated on ice for 30 min, three 1.5 mL aliquots of the culture were transferred to pre-chilled 1.5 mL tubes. The cultures were centrifuged at 4,000 rpm for 10 min at 4 °C. After the supernatant was removed, the pelleted cells were resuspended in 1 mL of ice cold 20 mM CaCl₂, and the tubes were incubated on ice for 10 min. The cells were centrifuged at 4,000 rpm for 5 min at 4 °C. After the supernatant was removed, the pelleted cells were resuspended in 0.2 mL of ice cold 20 mM CaCl₂. The tubes were incubated on ice until transformation or flash-frozen in liquid nitrogen for 5 min and stored at -80 °C.

35SRbz-HGSV-2-RNA1/2/3 clones were individually introduced into chemically competent *A. tumefaciens* EHA105 cells by the freeze-thaw method. Briefly, 10 µL of plasmid (concentration 8-30 ng / µL) was mixed with 0.2 mL of competent *A. tumefaciens* EHA105 cells by tapping gently with one finger. After the cells were incubated on ice for 5 min, they were flash-frozen in liquid nitrogen for 5 min. The cells were then incubated in a dry bath at 37 °C for 5 min, followed by incubation on ice for 2-5 min. After 1 mL of S.O.C media was added to the cells, the culture was transferred to 15 mL snap-cap tubes and incubated for 4 – 5 hours at 30 °C and shaking at 150 rpm. The culture was then transferred to 1.5 mL tubes and centrifuged at 4,000 rpm for 5 min at room temperature. After the supernatant was removed, the pelleted cells were resuspended in 0.1 mL of LB media. Cells were plated on LB plates amended with kanamycin (100 µg / mL) and rifampicin (25 µg / mL) and grown for two to four days at 29 °C. Individual colonies were screened by colony-PCR using HGSV-2 RNA1, 2, and 3 – specific primers (Table 4.1). PCR-positive colonies were grown overnight at 29C for two days in 10 mL of YEP media containing kanamycin (100 µg / mL) and rifampicin (25 µg / mL). Then, 500 µL of each culture was mixed with 50% glycerol and stored at -80 °C. The culture (9.5 mL) was centrifuged at 2,000xg for 15 min. Pelleted cells were resuspended in 0.25 mL of buffer P1 containing 0.1 mg / mL of RNase A and plasmid extraction was continued using Plasmid Mini Kit (Qiagen, Valencia, CA, USA) according to the manufacturer's instructions. Plasmids were digested with *EcoRI*, *EcoRV*, or *HindIII* (Genewiz, South Plainfield, NJ) to confirm vector and insert sizes.

4.2.5 Agroinfiltration assays

A. tumefaciens EHA105 cell lines individually containing 35SRbz-HGSV-2-RNA1/2/3 clones were streaked on LB plates which were amended with kanamycin (100 µg / mL) and rifampicin (25 µg / mL) and grown at 29 °C for 1-2 days. Cells were then scraped from the plates and resuspended in filter-sterilized buffer containing 10 mM MgCl₂ and 10 mM 2 (N-morpholino)-ethanesulfonic acid (MES), pH

5.6. After the optical density (OD) at an absorbance wavelength of 600 nm (A₆₀₀) of the suspended cells were adjusted to 0.2, the cells were incubated for 2 to 4 h in the dark at room temperature in the presence of 100 µM acetosyringone. Immediately before infiltration, the 35SRbz-HGSV-2-RNA1, 35SRbz-HGSV-2-RNA2, and 35SRbz-HGSV-2-RNA3 cultures were mixed using equal amounts. Bacterial mixtures were then infiltrated into the abaxial sides of leaves of two week old black common bean (*Phaseolus vulgaris*) plants, two-month-old *H. arnottianus* seedlings, and five to six leaf-stage *N. benthamiana* and *N. tabacum* plants using a 1-mL needle-less syringe. For the agroinfiltration, the cotyledonary leaves of the common bean plants and *H. arnottianus* seedlings were used whereas the true leaves of *N. benthamiana*, *N. tabacum* and *H. arnottianus* seedlings were used. The experiments were repeated three times using common bean as indicator host, whereas the other hosts were infiltrated only once. A negative control, *A. tumefaciens* EHA105 harboring empty pJL89 vector, was included in most of the experiments that were performed. Plants were grown in a room with a 16h / 8h light/dark photoperiod at a temperature of 24 ± 1 °C. The plants were observed for a period of up to 4 months.

4.2.6 Partial purification, observation and mechanical transmission of the recombinant HGSV-2

Partially purified virion preparations were obtained as described by Colariccio et al. (2000). Briefly, ~10 g of symptomatic cotyledonary *P. vulgaris* leaf tissue agroinfiltrated with 35SRbz-HGSV-2-RNA-1/2/3, as detailed above and showing symptoms potentially caused by the HGSV-2 infectious clone, was powdered with liquid nitrogen and mixed with 40 mL of extraction buffer [0.05 M phosphate buffer pH 7.0 containing sodium DIECA, 0.1% (w/v) ascorbic acid and 0.02 M sodium sulphite] for 30 minutes. After clarification, 0.5% (w/v) sodium chloride and 6% (w/v) 6000 polyethylene glycol were added to the suspension, and partially purified virions were pelleted by centrifugation at 8,000 x G for 10 minutes. The pellet was resuspended with 1 mL of extraction buffer overnight. All steps were performed at ~4°C. A ten-fold dilution of the partially purified virion preparations was negatively-stained on formvar/carbon-coated grids using 1% phosphotungstic acid. Negatively-stained partially purified virion preparations were viewed with a HT7700 120kV transmission electron microscope (Hitachi High Technologies America Inc., Dallas, TX) at the University of Hawai'i Biological Electron Microscope Facility. Also, RNA was extracted from 0.2 mL of the partially purified virion prep using the PureLink RNA mini kit (ThermoFisher Scientific, Waltham, MA), according to the manufacturer's instructions for liquid samples. The presence of the genomic RNA of HGSV-2 was determined using the DNase-RT-PCR assays specific for HGSV-2 and detailed below. Furthermore, cotyledonary *P. vulgaris* leaf tissue agroinfiltrated with 35SRbz-HGSV-2-RNA1/2/3, as detailed above and showing symptoms caused by the HGSV-2 infectious clone was macerated using cold, freshly prepared TACM buffer (0.05 M Tris, 0.1%

ascorbic acid, 0.1% L-cysteine and 0.5% 2-mercaptoethanol pH 8.0) (Colariccio et al., 1995) in a ratio of 1 g of tissue per 5 mL of buffer. Three leaves per plant of four *N. benthamiana* plants were inoculated by gently rubbing the inoculum on the leaves previously dusted with carborundum. Three leaves of one *N. benthamiana* plant were mock-inoculated and served as a control. Plants were provided a 16 / 8 h light / dark photoperiod in a growth room with a temperature of 24 ± 1 °C. Inoculated leaves of the plants were examined every day for one week.

4.2.7 Establishment of an isoline colony of *Brevipalpus* sp. mites

An isoline of *Brevipalpus* sp. mites was established by placing single females collected from a mandarin tree with no history of HGSV-2 symptoms growing at the University of Hawaii at Manoa campus onto detached mandarin (*C. reticulata*) stems with leaves or onto mandarin or lime (*C. latifolia*) fruits. Before colony establishment, the stems with tender fully expanded leaves were removed from a mandarin tree with a razor blade. The cut was made in a way to keep a 5 cm-long segment of the stem attached to the leaf petiole. The stem bases were placed into 15 mL conical tubes containing distilled water and sealed with parafilm. The mandarin and lime fruits were washed with water and soap, dried for 2 hours and the distal end of the fruits were covered with a fine layer of paraffin wax to prevent desiccation. For both the detached stems with leaves and the fruit, petroleum jelly was used to limit the movement of the mites.

4.2.8 Transmission assays using *Brevipalpus* sp. mites

Mite transmission assays conditions were similar to those reported by Roy et al (2013) with some modifications. Three detached *C. sinensis* leaves presenting HGSV-2 symptoms were placed in 1.5 mL tubes containing distilled water and sealed with parafilm. Virus lesions were delimited with petroleum jelly to restrict mite movement to the symptomatic area only. Fifteen non-viruliferous mites from the colony were transferred to each of the three detached *C. sinensis* leaves presenting HGSV-2 symptoms. An acquisition access period (AAP) of three days was used for virus acquisition. After AAP, five mites per leaf were transferred to *C. sinensis* and *C. reticulata* trees grafted onto C35 rootstock acquired at a local nursery. A total of four leaves per tree were infested with these putatively viruliferous mites. Five mites from the colony were also directly transferred to one leaf of the same citrus trees, serving as a non-viruliferous control. To keep mites confined to the leaves, petroleum jelly was applied to the petiole of the infested leaves. An inoculation access period (IAP) of three days was used. After the IAP, all the surviving mites were removed and stored in 95% ethanol for further analysis.

A symptomatic *C. reticulata* leaf that tested positive for HGSV-2 in the previous assay, was used to assess the ability of the citrus isolate of HGSV-2 to establish infection on hibiscus plants. For this assay, 30 non-viruliferous mites were transferred to the single citrus leaf presenting HGSV-2 symptoms.

Additional petroleum jelly was added to the petiole of the leaf to make sure the mites were confined to the symptomatic leaf. An AAP period of three days was used. Groups of five mites were then transferred to six leaves of three *H. arnottianus* seedlings. Groups of five non-viruliferous mites were also transferred to two leaves of an additional *H. arnottianus* seedling that was used as a transmission control.

All mite transfers and manipulations were performed using a number 01 fine Sable brush and a stereoscopic microscope (Figure 4.3). For AAP and IAP of both assays, a temperature of 24 ± 1 °C with $60 \pm 5\%$ relative humidity was recorded in the experimental room. A 16 / 8 h light / dark photoperiod was provided to the recipient plants, and the plants were observed for a period of 4 months.



Figure 4.3 Set up for the transfer of *Brevipalpus* sp. mites from an isoline colony to a detached *C. sinensis* leaf presenting HGSV-2 symptoms and maintained in a 1.5 mL tube containing distilled water. Mite transfers and manipulations were performed using a number 01 fine Sable brush under a stereoscopic microscope.

4.2.9 (DNase)-RT-PCR and (DNase)-RT-qPCR assays

Total RNA was extracted from 100-150 mg of tissue of the assayed leaves for the experiments detailed above using either NucleoSpin RNA Plus kit (Macherey-Nagel, Düren, Germany) or Spectrum Plant Total RNA kit (Sigma-Aldrich, St. Louis, MO). These RNA extracts were digested with RQ1 RNase-free DNase (Promega, Madison, WI) and then reverse transcribed into cDNA using random primers and M-MLV reverse transcriptase (Promega, Madison, WI) or a Maxima-H minus reverse transcription kit (ThermoFisher Scientific, Waltham, MA) using the manufacturer's protocol. Two microliters of two-fold dilutions of cDNAs were tested by endpoint PCR using GoTaq Green Master Mix (Promega). Virus-specific primer sets for RNA 1, 2 and 3 of HGSV-2 were designed based on a consensus sequence of an alignment of the RNA 1, 2 and 3 sequences of the hibiscus and citrus isolate generated in this study as well as the original citrus isolate sequenced by Melzer et al. (2012). Primer3 (Untergasser et al., 2012) was used for the primer design with consideration of thermodynamic primer features (Arif and Ochoa-Corona, 2013). Primers were designed to target conserved regions in the RNA-dependent RNA polymerase (RdRp) domain in RNA 1, p33 (BMB1) in RNA 2, and p39 (SP24 protein) in RNA 3 (Table 4.1). These primers were used for specific detection of HGSV-2 in endpoint RT-PCR assays using 0.5 μ M as final primer concentration and 55 °C as the annealing temperature. A non-template control (NTC) of DEPC-treated water was used in all the assays. Furthermore, conventional RT-PCR assays were also performed on leaves used in the mite transmission assays and they were performed as detailed above, except for the DNase digestion step which was omitted.

4.2.10 Mite identification using molecular barcoding and scanning electron microscopy, and virus acquisition status

Three mites that were previously used in the transmission studies of HGSV-2 were used for DRT-PCR assays as detailed by Druciarek et al. (2019). Briefly, individual *Brevipalpus* mites were introduced into a PCR tube containing 10 μ l of water and random hexamer primers and crushed using a needle under a dissecting microscope. Then, cDNA was synthesized using random primers and SuperScript III reverse transcription kit (ThermoFisher Scientific, Waltham, MA) using the manufacturer's instructions. Two microliters of ten-fold diluted cDNA reactions were used in endpoint PCR for DNA barcoding and internal PCR control using the 28S rRNA primers, D1D2w2: 5'-ACAAGTACCDTRAGGGAAAGTTG-3', 28Sr0990: 5'-CCTTGGTCCGTGTTTCAAGAC-3' (Druciarek et al., 2019; Sonnenberg et al. 2007; Mironov et al. 2012) that produce a ~700 bp expected amplicon. All DNA barcoding PCR assays were performed using Q5 High Fidelity DNA Polymerase (New England Biolabs, Ipswich, MA). To verify the viruliferous status of mites used in the transmission assays, two-step RT-qPCR assays were implemented using iTaq Universal SYBR Green Supermix (Bio-Rad, Hercules, CA, United States), 0.25 μ M primers

targeting the RdRp and BMB1 regions and the mite cDNA. Primers targeting the *Ubiq* gene in *Brevipalpus* spp. were used as an internal control (Rogerio et al., 2019). Each reaction was performed in three replicates. Cycling parameters for the RT-qPCR assays consisted of an initial denaturation at 95°C for 1 min, followed by 35 cycles of denaturation at 94°C for 10 s and an annealing-extension step at 60°C for 1 min during which time data was collected. Melt curve analysis was performed as follows: 95°C for 1 min, pre-melting conditioning at 60°C for 1 min followed by a melting temperature cycle range from 60°C to 95°C. Positive cDNA control specific for HGSV-2 and NTCs were used in all the RT-qPCR assays. Additionally, endpoint RT-PCR assays using primers specific for HGSV-2 RNA3 were performed as detailed above using the mite cDNA. An NTC was used in all the RT-PCR assays. All amplicons were gel extracted, purified and bi-directionally sequenced.

Furthermore, five additional mites were fixed with 2% paraformaldehyde + 2.5% glutaraldehyde in 0.1 M sodium cacodylate buffer pH 7.4 for 1 – 2 hours at room temperature. Then the mites were washed three times with 0.1 M cacodylate buffer pH 7.4 for 20 – 30 minutes and postfixed with 1% osmium tetroxide in 0.1 M sodium cacodylate buffer pH 7.4 for 1 hour. Then the specimens were dehydrated through graded ethanol series (30 – 95 %) and dried in a Tousimis Samdri-795 critical point dryer. Specimens were mounted on aluminum stubs with conductive carbon tape followed by coating with gold/palladium in a Hummer 6.2 sputter coater and viewed with a Hitachi S-4800 Field Emission Scanning Electron Microscope at an accelerating voltage of 5.0 kV.

4.3 RESULTS

4.3.1 HGSV-2 presents distinct genome organization within isolates that have low overall genomic sequence diversity

Complete and near complete genomic sequences of HGSV-2 isolates were obtained from hibiscus and citrus hosts, respectively, using a group of overlapping amplicons (Table 4.1) and Sanger sequencing. HGSV-2 RNA 1 presented the same genomic organization and ORF length of the replication-associated polyprotein to what was previously detailed for the 2009 citrus isolate of HGSV-2 (HQ852051). However, a small ORF (273 bp) putatively coding for a 10 kDa protein in the 3' region of RNA 1 was identified in all three HGSV-2 isolates analyzed. This putative protein designated p10, also contains two small transmembrane regions (data not shown). In contrast, RNA 2 and 3 of the HGSV-2 isolates analyzed in this study presented some key differences from the previously characterized isolate (Figure 4.4A). For RNA 2, two key differences were identified: first, an additional nucleotide (thymine) was found at position 1,220 in both HGSV-2 isolates sequenced in this study (Figure 4.5A), resulting in changes to the putative ORF lengths being coded in the 5' region. The 5' region of RNA 2 of the original

2009 citrus isolate (HQ852053) putatively encodes for p50 (ORF length: 1,308 bp) and p13 (ORF length: 360 bp). In contrast, the 5' region of RNA 2 of both newly sequenced HGSV-2 isolates putatively encodes for p51 (ORF length 1,341 bp) and p16 (ORF length: 414 bp) (Figure 4.4A). Second, an additional six nucleotides (5'-GAAAAT-3') were found in the 5'-untranslated region of RNA 2 of the newly sequenced hibiscus isolate of HGSV-2 (Figure 4.5B).

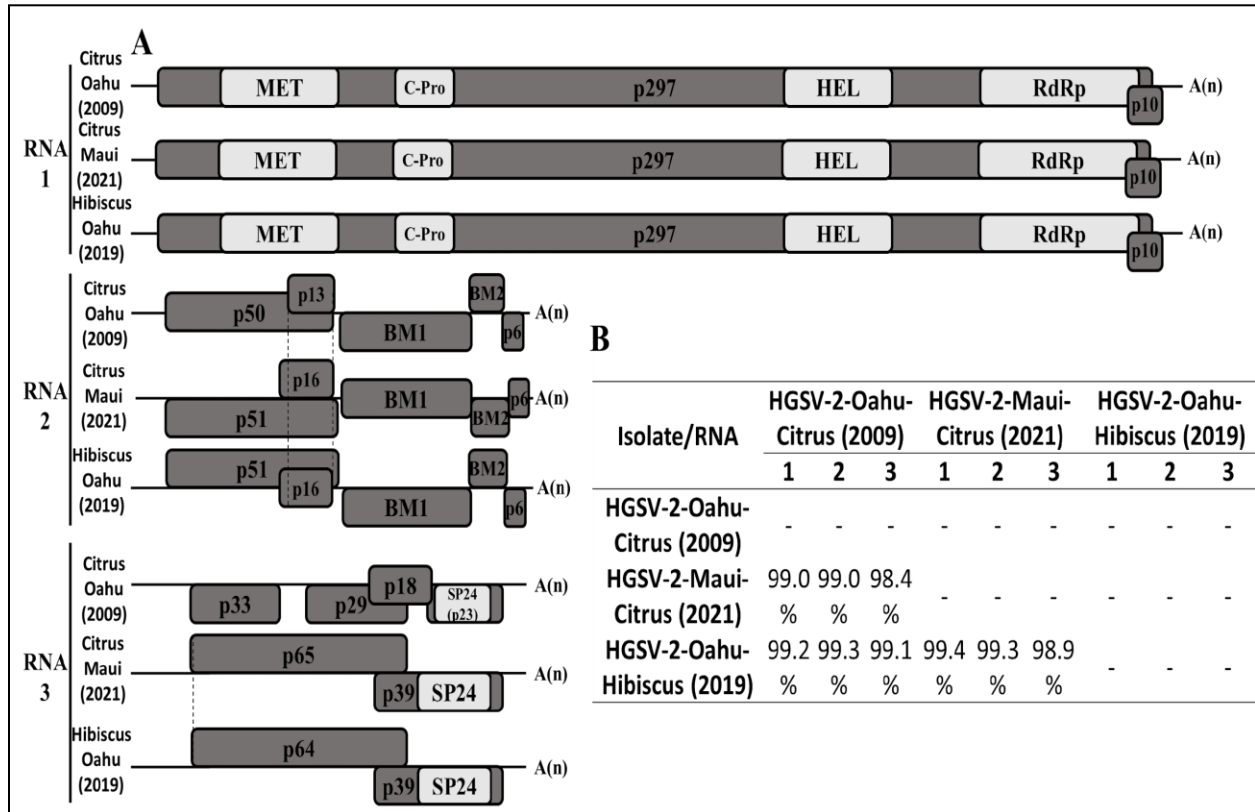


Figure 4.4 Genomic organization (A) and diversity (B) of the HGSV-2 isolates sequenced in this study and compared to the original citrus isolate of HGSV-2 (HQ852052-4, Melzer et al., 2012). A) ORFs are represented by gray-colored boxes while conserved domains are represented by silver-colored boxes. No differences were found in the RNA 1 of the three HGSV-2 isolates. For RNA 2, differences in the p50/51 and p13/16 ORF lengths were observed in the 5' region of the RNA 2 of the isolates. In contrast to the four ORFs encoded by RNA 3 that were reported in the original citrus isolate of HGSV-2, only two overlapping open reading frames (encoding p64/65 and p39) were identified the newly sequenced hibiscus and citrus isolates of the virus, as a result of ORF merging. Conserved domains: methyltransferase (MET), cysteine protease (C-Pro), helicase (HEL), RNA-dependent RNA polymerase (RdRp) and putative virion membrane (SP24). B). Overall, low genetic diversity, 0.6 – 1.6%, was found in the three HGSV-2 isolates.

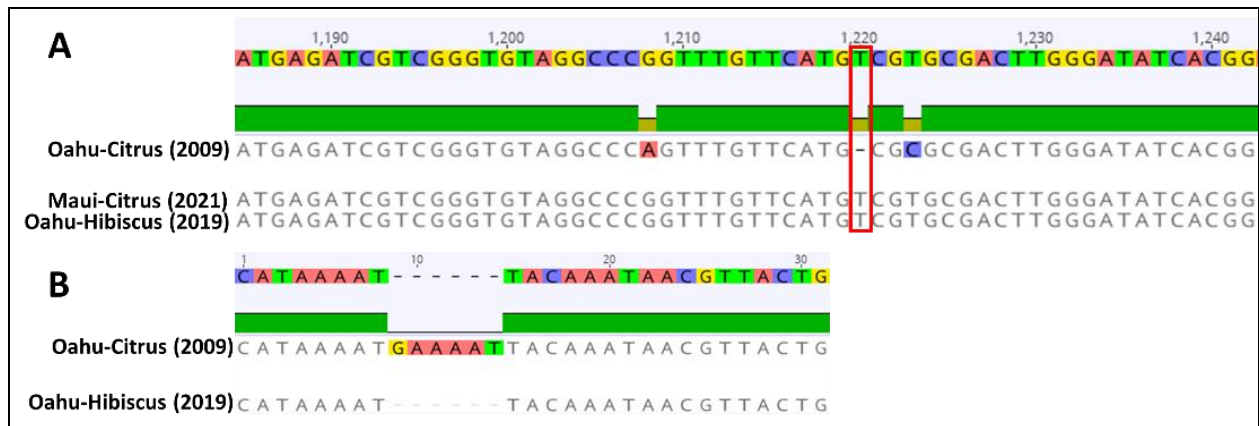


Figure 4.5 Important sequence differences found in RNA 2 between the original citrus isolate of HGSV-2 (HQ852053) and the HGSV-2 isolates from this study. A) Thymine (T) insertion at position 1,220 of RNA 2 of the newly sequenced isolates. This insertion modified the ORF lengths putatively encoded in the 5' end of RNA 2 (Figure 4.4A). B) 5'-terminus pairwise comparison of the newly sequenced hibiscus isolate of HGSV-2 indicates a six residue deletion in the untranslated region when compared to the original citrus isolate.

For RNA 3, the HGSV-2 isolates sequenced in this study contained two putative overlapping ORFs rather than four putative ORFs as previously reported (Figure 4.4A). Both HGSV-2 isolates from this study possessed a non-synonymous change at nucleotide position 1,362 (A → C) (Figure 4.6A) which merged the ORFs putatively encoding p33 and p29 of the 2009 citrus isolate of HGSV-2 (HQ852054) into a single ORF putatively encoding a protein of 64 kDa (Figure 4.4A). Also, the absence of a guanine (G) residue at nucleotide position 2,333 was discovered in the HGSV-2 isolates from this study (Figure 4.6B), which merged the ORFs putatively coding for p18 and p23 previously reported for HGSV-2 (HQ852054) into a single ORF putatively coding for a protein of 39 kDa (Figure 4.4A). Finally, a two-nucleotide deletion (5'-TT-3') was found in the 5' region of the coding region of p64 that was present only in the hibiscus isolate but absent in the citrus isolates from Oahu (previous study; HQ852054) and from Maui (this study) (Figure 4.6C). This two-nucleotide deletion resulted in the N-terminal region of p64 being eight amino acids shorter in the hibiscus isolate of HGSV-2.

Despite the differences found in the genomic organization of the three HGSV-2 isolates, the genetic variability was low overall. Using pairwise nucleotide comparisons between the three isolates, RNA 1 presented nucleotide identities of 99 – 99.4%, RNA 2 of 99 – 99.3%, and RNA 3 of 98.4 – 99.1 % (Figure 4.4B). The methyltransferase (MET, PF01660), cysteine protease (C-Pro, PF02338), helicase (HEL, PF01443) and RNA-dependent RNA polymerase (RdRp, PF00978) conserved domains that were found

by Melzer et al. (2012) in the replication-associated polyprotein encoded by RNA 1, were found in both the citrus and hibiscus isolates of HGSV-2 from this study. Similarly, the putative virion membrane protein domain (SP24, PF16504) that was found in p23 of RNA 3 of the original citrus isolate of HGSV-2 (HQ852054) was also present in the p39 of RNA 3 of the HGSV-2 isolates from this study (Figure 4.4A).

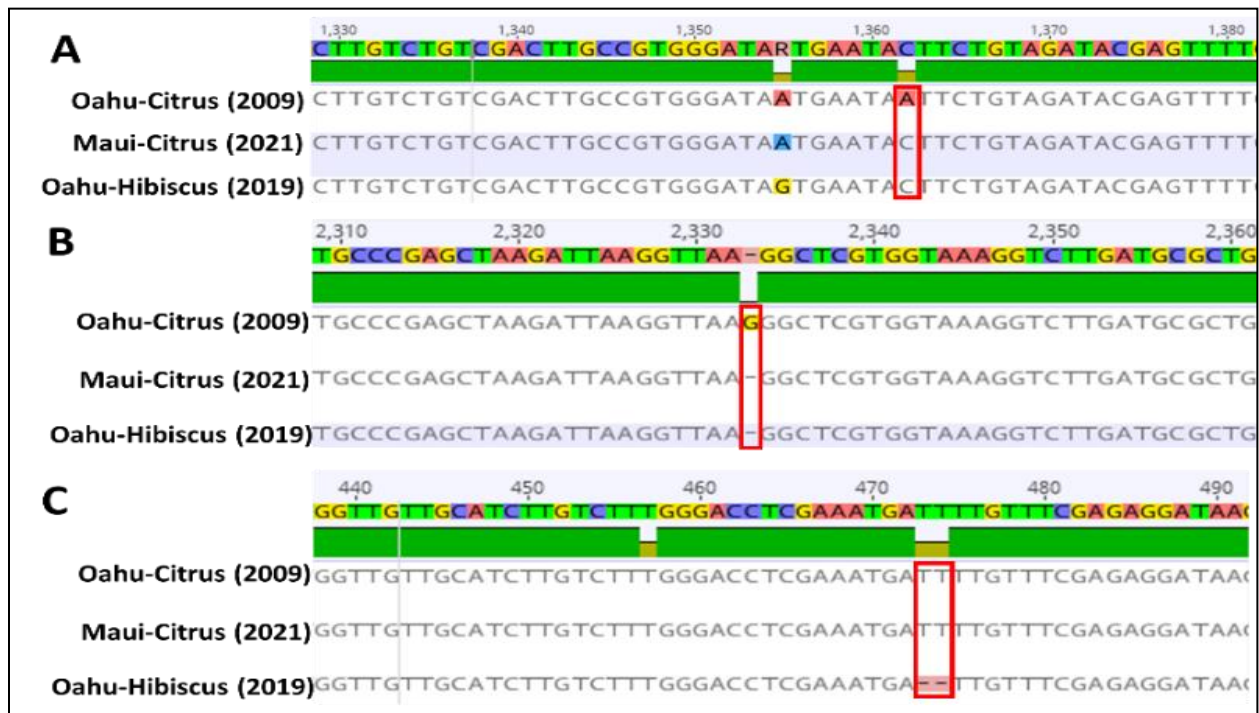


Figure 4.6 Important sequence differences in RNA 3 between the original citrus isolate of HGSV-2 (HQ852054) and the HGSV-2 isolates from this study. A) Transversion (A→C) at position 1,362 that fuses previously reported ORFs encoding p33 and p29 into a single ORF encoding p64 in the HGSV-2 isolates from this study (Figure 4.4A). B) Absence of a guanine (G) residue at position 2,333 that fuses previously reported ORFs encoding p18 and p23 into a single ORF encoding p39 present in the HGSV-2 isolates from this study (Figure 4.4A). C) Two nucleotide deletion (TT) present in the 5' region of the ORF putatively coding for p64 and present only in the hibiscus, but not the two citrus isolates.

4.3.2 Construction of a full-length cDNA clone of HGSV-2

Full length cDNA clones of the RNA 1, 2 and 3 of HGSV-2 (35SRbz-HGSV-2-RNA1/2/3) were obtained using In-fusion cloning following the procedure detailed in Figure 4.2. The full-length HGSV-2 RNA1, 2 and 3 cDNA clones were inserted immediately downstream of the cauliflower mosaic virus (CaMV) 35S promoter and followed immediately by the hepatitis delta virus ribozyme in the binary vector pJL89. A

poly-T tail of 15 nucleotides was added at the end of the cDNA clones of each genomic segment. The 35SRbz-HGSV-2-RNA1/2/3 cDNA clones were sequenced using overlapping primers spanning the full-length genome. Sequence analysis showed differences between the hibiscus isolate of HGSV-2 and the full-length cDNA clones. RNA 1 had 84 nucleotide differences that resulted in 28 non-synonymous substitutions with respect to the sequence of the hibiscus isolate of HGSV-2. RNA 2 had 3 nucleotide differences with respect to the sequence of the hibiscus isolate of HGSV-2 and 1 resulted in a non-synonymous substitution. RNA 3 had 29 nucleotide differences resulting in 11 non-synonymous amino acid substitutions with respect to the sequence of the hibiscus isolate of HGSV-2. The polyprotein and p10 putatively coded in the RNA1 presented 8 and 1 amino acid substitutions, respectively, which did not structurally align to the original amino acids putatively coded by the hibiscus isolate of HGSV-2. BM1, p64/65, and p39 putatively coded in RNA 2 and 3 possessed 1, 1, and 2 amino acid substitutions, respectively, which did not structurally align to the original amino acids putatively coded by the hibiscus isolate of HGSV-2 (Table 4.3). The sequences of the hibiscus isolate of HGSV-2 and the full-length cDNA clone shared 99.0%, 99.9% and 99.1% nucleotide identities for the RNA 1, 2 and 3, respectively.

Table 4.3 List of amino acid substitutions found in RNA 1, 2 and 3 of the full-length cDNA clone of HGSV-2 (35SRbz-HGSV-2-RNA1/2/3). Amino acid substitutions highlighted in red represent substitutions that did not structurally align to the original amino acid putatively coded in proteins of the hibiscus isolate of HGSV-2.

RNA	Nucleotide differences	Non-synonymous differences	Substitutions
1	84	28	<u>Polyprotein</u> : D147E, A579T, W584R , I698T , G718S, V792I, E801D, K851E, F861L, L1035F, V1072L, G1091S, S1188G, R1223S , S1312F , L1345H , D1395N, Q1424K, I1432R , K1467E, G1608R , I1614V, N1615D, E2043K, D2290G, G2366R , R2399K, Q2571R
		1	<u>p10</u> : L53P
2	3	1	<u>BM1</u> : E2G
3	29	4	<u>p64/65</u> : D48E, K62R, T457A, V540G
		7	<u>p39</u> : M33V, C72W , N130D, H316Q, I329V, A337I , K348N

Proteins putatively coded by the full-length cDNA clone and the hibiscus isolate of HGSV-2 were structurally aligned using the Expresso algorithm implemented in T-Coffee to infer amino acid substitutions not structurally related.

4.3.3 35SRbz-HGSV-2-RNA1/2/3 are infectious in *P. vulgaris*, *N. benthamiana*, *N. tabacum* and *H. arnottianus* plants

To test the infectivity of the hibiscus isolate of the HGSV-2 full-length cDNA clone, 35SRbz-HGSV-2-RNA1/2/3 constructs were transformed into *A. tumefaciens* strain EHA105. Transformed cells were then co-infiltrated into leaves of four host species: *P. vulgaris*, *N. benthamiana*, *N. tabacum* and *H. arnottianus*. After 17-21 dpi, symptoms were obvious in all the 12 agroinfiltrated leaves and were characterized by the presence of chlorotic blotches with a dark green perimeter. Whereas the control leaves did not present any obvious symptom aside from infiltration damage (Figure 4.7 and Table 4.4). After 23-30 dpi, accelerated senescence was observed in some of the inoculated leaves when compared to the non-infiltrated cotyledonary leaves of the same plant which did not present any symptom. Importantly, a hypersensitive-response (HR)-like phenotype was observed in the agroinfiltrated leaves with the full-length cDNA clones (Figure 4.8).



Figure 4.7 Symptoms caused by the full-length cDNA clone of HGSV-2 (35SRbz-HGSV-2-RNA1/2/3) agroinfiltrated into *P. vulgaris* cotyledonary leaves. Observed symptoms included chlorotic blotches surrounded by a dark green perimeter that were obvious at 15-21 dpi. After 20-25 dpi, accelerated senescence and hypersensitive-response-like phenotype were observed in some of the agroinfiltrated leaves (right bottom image and Figure 4.8).



Figure 4.8 Symptoms of the accelerated senescence and hypersensitive-response (HR)-like phenotype observed in the *P. vulgaris* cotyledonary leaves. Leaves were agroinfiltrated with the full-length cDNA clone of HGSV-2 (35SRbz-HGSV-2-RNA1/2/3) after 17-21 dpi (left) and 23-30 dpi (center), and compared to a control leaf inoculated with pJL89 empty vector (right).

In experiment 2, both cotyledonary leaves of 12 *P. vulgaris* plants were agroinfiltrated with 35SRbz-HGSV-2-RNA1/2/3 and both cotyledonary leaves of the same number of plants were agroinfiltrated with pJL89 as a control. After ~21 dpi, 20 of the 24 leaves agroinfiltrated with the full-length cDNA clone presented similar symptoms observed in experiment 1 (Figure 4.7) whereas none of the leaves agroinfiltrated with pJL89 presented symptoms (Table 4.4). In experiment 3, both cotyledonary leaves of eight *P. vulgaris* plants were agroinfiltrated with the full-length cDNA clone whereas both cotyledonary leaves of four plants were agroinfiltrated with pJL89. After ~21 dpi, 14 out of the 16 leaves agroinfiltrated with 35SRbz-HGSV-2-RNA1/2/3 presented similar symptoms to those observed in experiments 1 and 2 (Figure 4.7) while none of the leaves agroinfiltrated with pJL89 showed any obvious symptom (Table 4.4). In all cases, a bacterial OD (A600) of 0.2 was used and the presence of HGSV-2 was confirmed only in the symptomatic leaves using DNase-RT-PCR assays (Table 4.4) and HGSV-2 RNA 1-, 2- and 3-specific primers (Table 4.1). Direct sequencing of the amplicons showed they shared 99% nucleotide identity to the hibiscus isolate of HGSV-2.

Table 4.4 Agroinfiltration experiments of the cotyledonary leaves of *P. vulgaris* plants using the full-length cDNA clone of HGSV-2. Buffer and empty vector (pJL89) were used as inoculation controls. Symptoms on the agroinfiltrated leaves were observed after 17-21 dpi.

Experiment 1							
Inoculum	Plants	Leaves/ plant	Total leaves	Symptomatic/ inoculated	DNase-RT-PCR-positive		
					HGSV-2 RNA1	HGSV-2 RNA2	HGSV-2 RNA3
Buffer	3	2	6	0/6	0/6	0/6	0/6
35SRbz-HGSV- 2-RNA1/2/3	12	1	12	12/12	12/12	12/12	12/12
Experiment 2							
pJL89	12	2	24	0/24	0/24	0/24	0/24
35SRbz-HGSV- 2-RNA1/2/3	12	2	24	20/24	20/24	20/24	20/24
Experiment 3							
pJL89	4	2	8	0/8	0/8	0/8	0/8
35SRbz-HGSV- 2-RNA1/2/3	8	2	16	14/16	14/16	14/16	14/16

Once the infectivity of 35SRbz-HGSV-2-RNA1/2/3 was verified in repeated experiments using the cotyledonary leaves of *P. vulgaris* plants, the true leaves of *N. benthamiana*, *N. tabacum* and *H. arnottianus* plants were used in agroinfiltration experiments. The cotyledonary leaves of the latter host were also agroinfiltrated. Empty vector pJL89 was used as an experimental control in all the experiments. Similar to the experiments performed on *P. vulgaris* plants, none of the cotyledonary or true leaves agroinfiltrated with pJL89 presented symptoms during the course study. However, all the experimental hosts agroinfiltrated with the full-length cDNA clone of HGSV-2 presented symptoms at different time frames. All (18/18) *N. tabacum* leaves presented symptoms after 5-7 dpi. After 15-18 dpi, 15 out of 18 *N. benthamiana* leaves presented symptoms. All (6/6) cotyledonary *H. arnottianus* leaves presented symptoms after 21 dpi (Table 4.5). For both *Nicotiana* spp. and the cotyledonary leaves of *H. arnottianus*, the symptoms were characterized by yellow chlorosis in the agroinfiltrated area (Figure 4.9). Whereas 7 out of the 12 agroinfiltrated true leaves of *H. arnottianus* seedlings presented symptoms after 45 dpi. These symptoms were characterized by green chlorotic lesions in the agroinfiltrated area which turned yellow or necrotic after 90-120 dpi. On the other hand, agroinfiltrated leaves of *N. tabacum* and *N. benthamiana* with the full-length cDNA clone showed some HR-like phenotype after 7-10 and 21-25 dpi, respectively (Figure 4.9). The presence of the genomic RNA segments of HGSV-2 was confirmed only in the symptomatic leaves using DNase-RT-PCR assays (Table 4.5) and HGSV-2 RNA 1-, 2- and 3-specific

primers (Table 4.1). Direct sequencing of the amplicons showed they shared 99% nucleotide identity to the hibiscus isolate of HGSV-2.

Table 4.5 Agroinfiltration results using both the full-length cDNA clone of HGSV-2 (35SRbz-HGSV-2-RNA1/2/3) and pJL89 (control) on the cotyledonary and true leaves of *H. arnottianus*, and the true leaves of *N. benthamiana* and *N. tabacum*. Symptoms on the latter host were observed after 5-7 dpi whereas symptoms on the cotyledonary leaves of *H. arnottianus* and the true leaves of *N. benthamiana* were observed after 18-21 dpi. Symptoms on the true leaves of *H. arnottianus* plants were observed after 45 dpi.

<i>H. arnottianus</i> (cotyledonary leaves)							
Inoculum	Plants	Leaves/ plant	Total leaves	Symptomatic/ inoculated	DNase-RT-PCR assays		
					HGSV- 2 RNA1	HGSV- 2 RNA2	HGSV- 2 RNA3
pJL89	2	2	4	0/4	0/4	0/4	0/4
35SRbz-HGSV- 2-RNA1/2/3	3	2	6	6/6	6/6	6/6	6/6
<i>H. arnottianus</i> (true leaves)							
pJL89	2	3	6	0/6	0/6	0/6	0/6
35SRbz-HGSV- 2-RNA1/2/3	4	3	12	7/12	7/12	7/12	7/12
<i>N. benthamiana</i> (true leaves)							
pJL89	4	3	12	0/12	0/12	0/12	0/12
35SRbz-HGSV- 2-RNA1/2/3	6	3	18	15/18	15/18	15/18	15/18
<i>N. tabacum</i> (true leaves)							
pJL89	2	3	6	0/6	0/6	0/6	0/6
35SRbz-HGSV- 2-RNA1/2/3	6	3	18	18/18	18/18	18/18	18/18

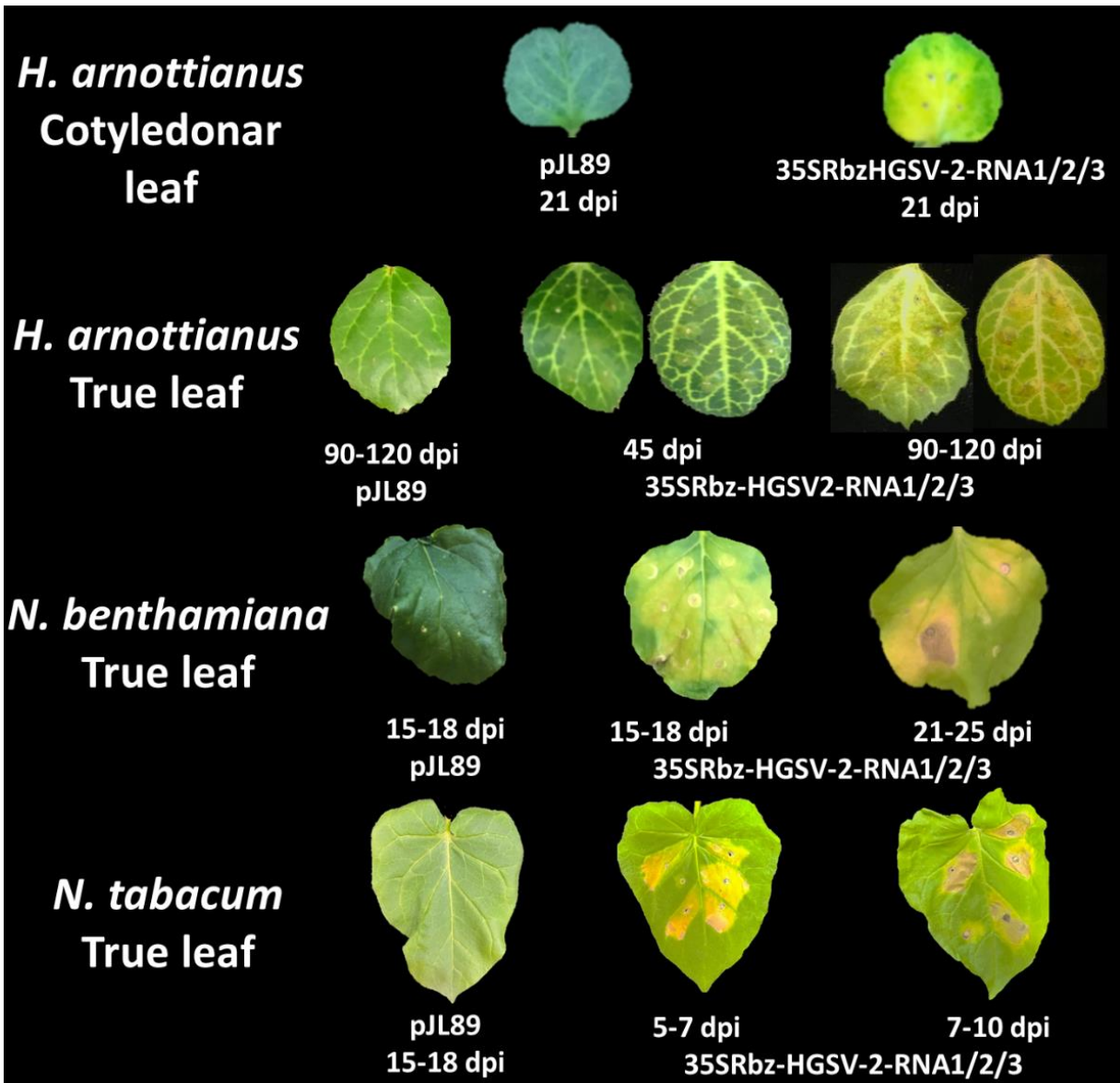


Figure 4.9 Symptoms caused by 35SRbz-HGSV-2-RNA1/2/3 in the cotyledonary and true leaves of *H. arnottianus* and the true leaves of *N. benthamiana* and *N. tabacum*. Symptoms were expressed at different time frames depending on the host and the type of leaf agroinfiltrated. Symptoms in true leaves of both *Nicotiana* species and the cotyledonary leaves of *H. arnottianus* were characterized by yellow chlorosis in the agroinfiltrated area. While the symptoms of the true leaves of *H. arnottianus* were characterized by green chlorotic lesions in the agroinfiltrated area which turned yellow or necrotic after 90-120 dpi.

4.3.4 Further evidence of the infectivity of 35SRbz-HGSV-2-RNA1/2/3

In order to further demonstrate the infectivity of the full-length infectious clone of HGSV-2, two assays were performed. First, partially purified virion preparations, obtained as detailed by Colariccio et al. (2000) from cotyledonary *P. vulgaris* leaf tissue previously agroinfiltrated with 35SRbz-HGSV-2-RNA1/2/3, were negatively stained and observed under the TEM. Electron-dense quasi-spherical

structures with varied sizes from 150 to 250 nm were observed and likely represented the recombinant virions of HGSV-2 (Figure 4.10A). Additionally, DNase-RT-PCR assays on RNA extracted from these partially purified virus preparations tested positive for the presence of HGSV-2 RNA 1, 2 and 3. A water non-template control (NTC) and a positive control tested negative and positive, respectively, in these assays (Figure 4.10B).

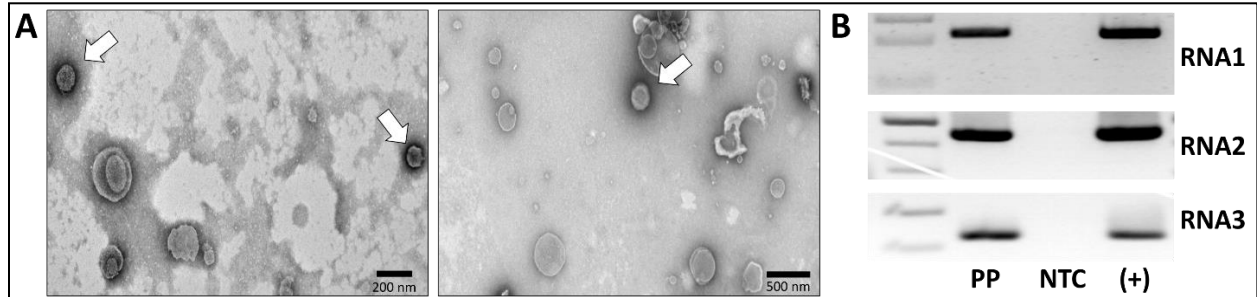


Figure 4.10 Partially purified virion preparations of the virus progeny from the full-length cDNA clone of HGSV-2 and results of diagnostic DNase-RT-PCR assays. A) Electron-dense quasi-spherical structures (150-250 nm) likely represent the recombinant virions of HGSV-2 (white arrows). The putative virions were negatively stained with 1% phosphotungstic acid and observed by transmission electron microscopy. B) DNase-RT-PCR assays on RNA extracted from partially purified virus preps (PP), a water non-template control (NTC), and RNA extracted from HGSV-2 symptomatic leaf tissue of *H. arnottianus* (+).

Second, three leaves per plant of four *N. benthamiana* plants were mechanically inoculated as detailed by Colariccio et al. (1995) using *P. vulgaris* cotyledonary leaves agroinfiltrated with 35SRbz-HGSV-2-RNA1/2/3 as inoculum. Three leaves of one *N. benthamiana* plant were mock inoculated. After 6 dpi, necrotic local lesions were observed in four leaves, 1 leaf per inoculated plant, whereas the mock inoculated leaves were symptomless. The four symptomatic leaves tested positive for the RNA 1, 2 and 3 of HGSV-2 using DNase-RT-PCR assays and HGSV-2-specific primers (Table 4.1). A non-template control (NTC) tested negative in these assays (Figure 4.11). Direct sequencing of the amplicons showed they shared 99% nucleotide identity to the hibiscus isolate of HGSV-2.

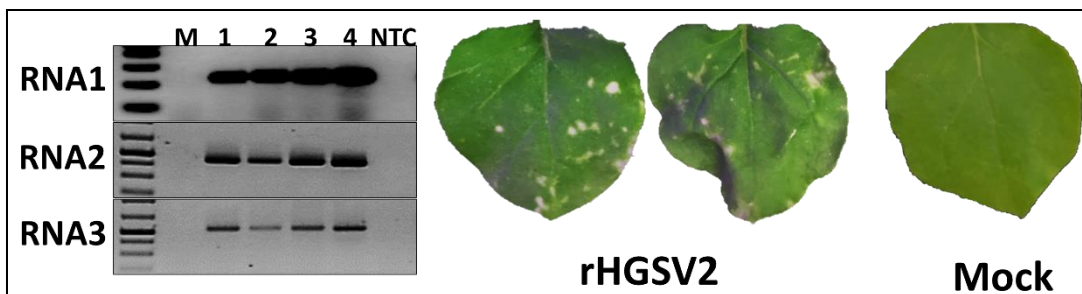


Figure 4.11 Necrotic local lesions putatively caused by recombinant HGSV-2 (rHGSV-2) virions mechanically inoculated on *N. benthamiana* leaves (center). No lesions were observed in any of the leaves of the mock-inoculated plants (right). The local lesions were present in only four (lanes 1-4) mechanically inoculated *N. benthamiana* leaves which tested positive for HGSV-2 RNA 1, 2 and 3 using DNase-RT-PCR assays (left). Lane M, mock inoculated leaf; NTC, non-template control.

4.3.5 Identification of *Brevipalpus* specimens used in transmission assays and virus acquisition status

Three individual *Brevipalpus* specimens that were used in the mite transmission assays were used in DRT-PCR assays for mite barcoding and virus detection. Using 28S rRNA primers, a ~700 bp amplicon of the expected size was produced from each of the three individual mites (Figure 4.12). Direct sequencing of the ~700 bp 28S rRNA amplicon for the three individual mites, and a pairwise nucleotide alignment showed the three sequences were 100% identical. A BLASTn search using the consensus sequence showed it shares 98.9% nucleotide identity to *B. azores* (MK919272) with 92% query coverage. Partial sequences of HGSV-2 RNA 1, RNA 2 and RNA 3 were amplified by DRT-qPCR and DRT-PCR assays in two of these three mites using HGSV-2-specific primers (Figure 4.12). Whereas the *Ubiq* gene was detected from the three *Brevipalpus* specimens using DRT-qPCR and *Brevipalpus*-specific primers (Rogerio et al., 2019) (Figure 4.12). The melting curves in the RT-qPCR assays corroborated the identity of HGSV-2 RNA 1 and RNA 2 when compared to the positive control (data not shown). Furthermore, direct sequencing showed the partial sequence of RNA 3 shared 100% nucleotide identity to the targeted p39 region in RNA 3 of the citrus isolate of HGSV-2.

To aid in the identification of mite species, scanning electron micrographs were taken of the anterior and posterior sides of three *Brevipalpus* specimens that were used in the mite transmission assays. The three specimens showed identical physiological features between one another. In Figure 4.13A and B, a picture of the anterior side and a zoom to the ventral and genital plaques are shown, respectively. On both figures, undulated patterns in the reticulations of the ventral part are observed. These physiological features are typically present in *B. azores* specimens (Figure 4.13C) (Beard et al. 2015; Tassi 2018).

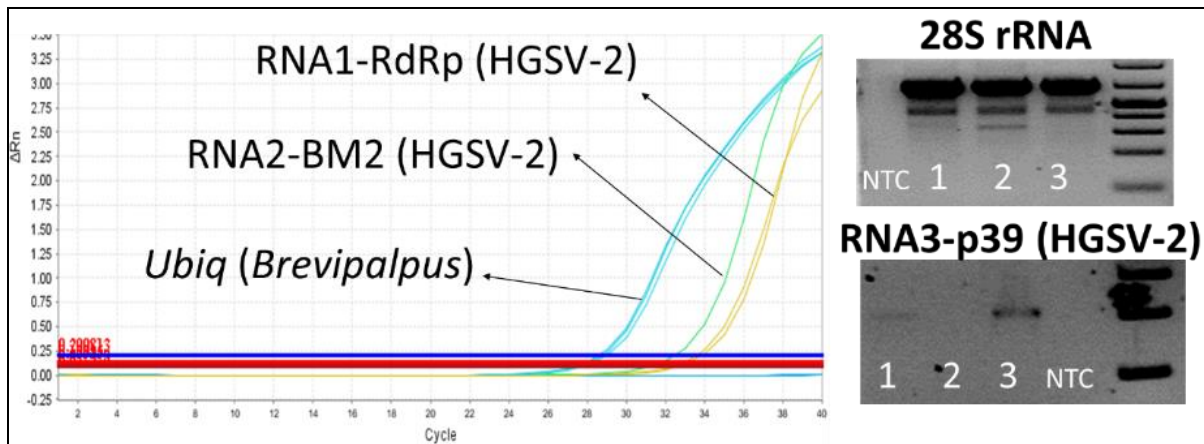


Figure 4.12 DRT-qPCR (left) and DRT-PCR (right) assays for mite barcoding (28S rRNA; upper right) and detection of RNA 1, 2, (left) and 3 (lower right), of HGSV-2. Two mites (lanes 1 and 3) were positive for RNAs 1, 2 and 3 of HGSV-2 while one mite tested negative for the three RNAs of HGSV-2. The *Ubiq* gene was amplified in DRT-qPCR assays and used as an internal control using *brevipalpus*-specific primers.

4.3.6 *B. azores* transmits HGSV-2

Four leaves per plant of *C. reticulata* and *C. sinensis* trees grafted onto C35 rootstocks were each infested with five viruliferous *B. azores* mites while one leaf of the same trees was exposed to five non-viruliferous mites. After 21 dpi, one *C. reticulata* leaf presented a light green chlorotic lesion. This viral-like symptom turned into an irregularly-shaped light green chlorotic lesion after 60 dpi that covered ~40% of the leaf, but did not increase its size after 60 additional days of observation. This symptom putatively caused by HGSV-2 resembled the natural infection of HGSV-2 observed in *C. reticulata* trees growing in Pukalani, Maui (Figure 4.14). None of the other four leaves, including one leaf exposed to non-viruliferous mites, of the same *C. reticulata* tree presented symptoms. Similarly, none of the *C. sinensis* leaves presented any symptom after 120 days of observation. The three RNAs of HGSV-2 were detected in the single *C. reticulata* leaf presenting HGSV-2 symptoms using RT-PCR assays while all the other citrus leaves tested negative (data not shown). Direct sequencing of the amplicons showed they shared 100% nucleotide identity to the citrus isolate of HGSV-2.

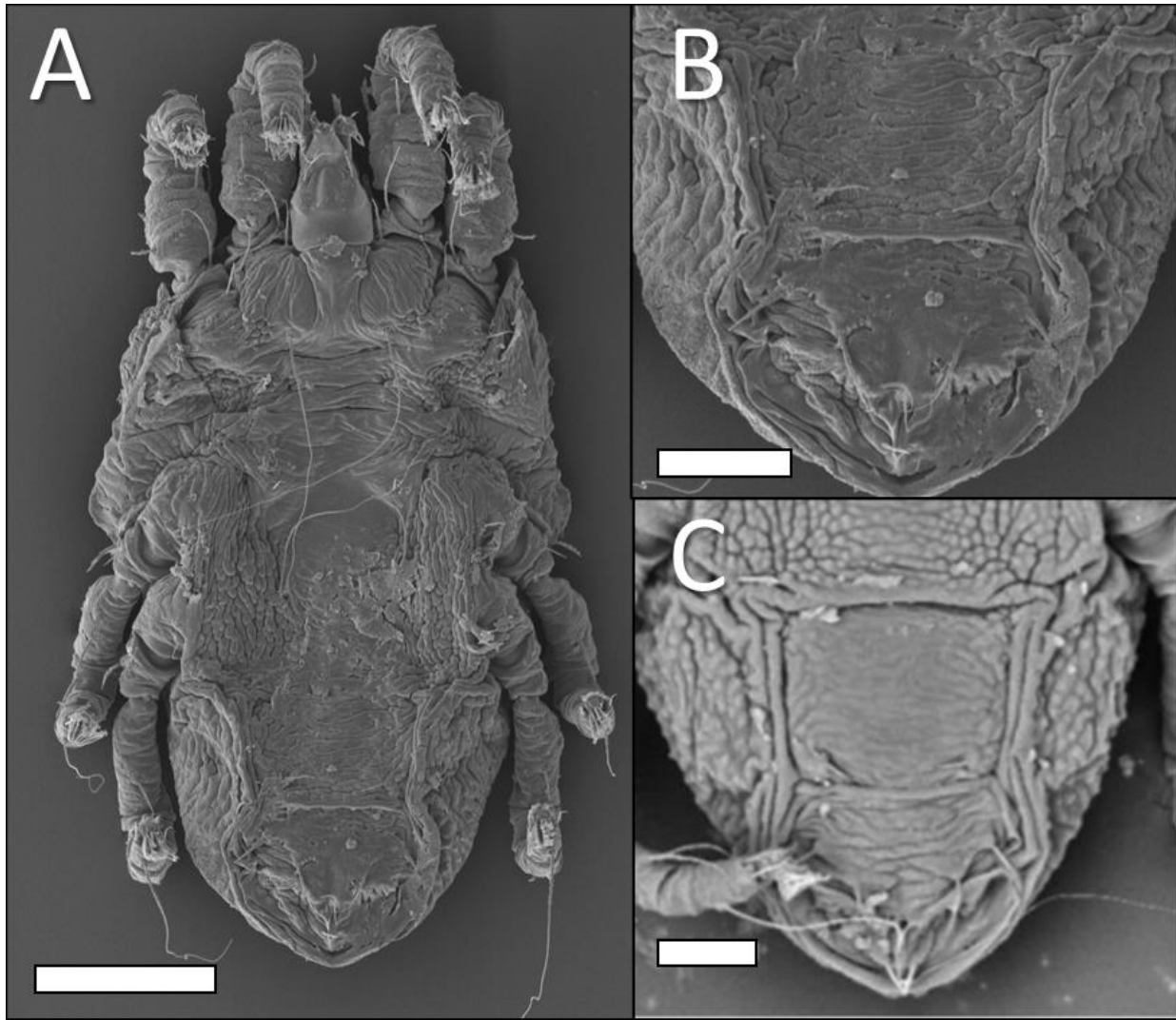


Figure 4.13 Physiological characteristics of *Brevipalpus azores* females used in this study (A and B) and observed with a Hitachi S-4800 Field Emission Scanning Electron Microscope at an accelerating voltage of 5.0 kV. A) Picture of the whole body. B) Zoom to the ventral and genital area. C) SEM zoomed pictured of the ventral part of *B. azores* (Adapted from Tassi 2018). White scale bars: A: 100 µm, B and C: 20 µm.

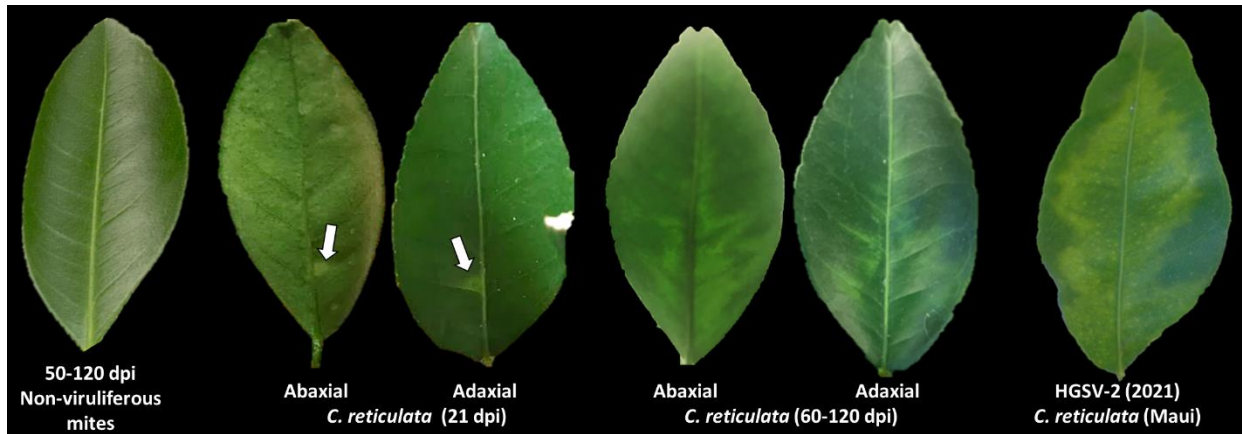


Figure 4.14 Symptoms caused by HGSV-2 on a single *C. reticulata* leaf 21-120 days after exposure to viruliferous *B. azores* mites. A light green chlorotic lesion was initially observed after 21 dpi and this turned into an irregularly shaped light green chlorotic lesion covering ~40% of the leaf after 60 dpi. The size of the chlorotic lesion did not increase its size after 60 additional days of observation. On the far right, a *C. reticulata* leaf from Pukalani, Maui infected with HGSV-2 is displayed. On the far left, a non-symptomatic *C. reticulata* leaf of the same tree exposed to non-viruliferous mites.

To demonstrate the ability of the citrus isolate of HGSV-2 to infect hibiscus, the single *C. reticulata* leaf presenting HGSV-2 symptoms was used as a source for virus acquisition of *B. azores* mites. Two leaves per plant of three *H. arnottianus* seedlings were each infested with five viruliferous *B. azores* mites while two leaves of a single *H. arnottianus* seedling were infested with five non-viruliferous mites. After 50 dpi, two *H. arnottianus* leaves from two different seedlings presented small chlorotic lesions with a red chlorotic center (Figure 4.15). These lesions did not increase in size or change in appearance after 70 days of additional observation. However, one of the symptomatic leaves, which exhibited a greater number of chlorotic lesions, presented accelerated senescence in comparison with the other leaves of the same plant that emerged at a similar time. The two leaves exposed to non-viruliferous mites did not present any symptoms during 120 days of observation (Figure 4.15). The three RNAs of HGSV-2 were detected in the two *H. arnottianus* leaves presenting HGSV-2 symptoms using RT-PCR assays while all the other hibiscus leaves tested negative (data not shown). Direct sequencing of the amplicons showed they shared 100% nucleotide identity to the citrus isolate of HGSV-2.

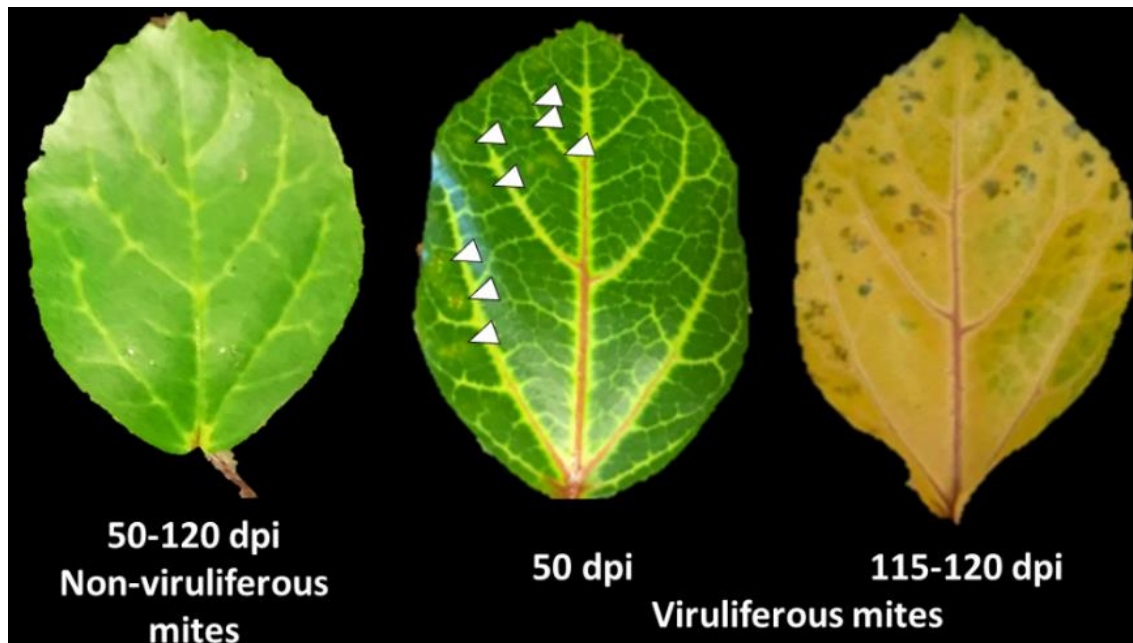


Figure 4.15 Transmission of a citrus isolate of HGSV-2 to *Hibiscus arnottianus* by *Brevipalpus azores*. Chlorotic lesions containing a red chlorotic center caused by HGSV-2 in an *H. arnottianus* leaf (center, arrowheads). Symptoms were obvious after 50 dpi and did not increase their size after 120 dpi. One out of the two leaves presenting HGSV-2 symptoms exhibited accelerated senescence after 115-120 dpi (right) in comparison with the other leaves of the same seedling that emerged at similar time frames. No symptoms were observed on leaves infested with non-viruliferous mites (left).

4.4 DISCUSSION

In this study, the full and near complete genomic sequences of two additional HGSV-2 isolates were obtained using overlapping RT-PCR amplicons (Table 4.1) and Sanger sequencing. The hibiscus and citrus isolates of HGSV-2 were sampled in locations from the islands of Oahu and Maui (Figure 4.1), respectively, where HGSV-2 was previously reported (Roy et al., 2015a). Although low genomic diversity was found within the HGSV-2 isolates (<3%), several key differences were found in the predicted genomic organization of the sequences obtained in this study compared to the genomic organization reported by Melzer et al. (2012) (HQ852052- HQ852052). First, a small ORF of 273 bp was present in the 3' region of RNA 1 of the three isolates analyzed (Figure 4.4) that putatively encodes a protein of 10 kDa. This protein was not previously considered an ORF putatively coding for a protein (Melzer et al., 2012) due to its small size (< 300bp). Although this putative protein shows no similarity to any described proteins (ie. orphan protein), it contains two predicted transmembrane domains and presents low identity levels (20%), and similar genome placement to the p10 protein encoded by the

recently described hibiscus yellow blotch virus (HYBV) (data not shown). HYBV is a new *Kitaviridae* member infecting *H. rosa-sinensis* that was characterized in Chapter III. Interestingly, small ORFs of ~200 bp coding for orphan proteins predicted to contain transmembrane domains have been found in the 5' region of the RNA 2 of cileviruses (Ramos-González et al., 2020). Although previously long overlooked, it has been recently speculated that these orphan proteins coding for transmembrane domains are coded by DNA and RNA viruses and can provide a versatile mechanism for regulating cellular activities by oligomerizing and forming membranes and ion channels (DiMaio, 2014).

Notable changes in the genomic organization of the ORFs putatively encoded by RNA 2 and 3 of HGSV-2 (Figure 4.4) were caused by insertions and deletions (indels) present in the genome of the first citrus isolate of HGSV-2 sequenced (HQ852053 and HQ852054). These indels affected the predicted coding regions of several proteins causing the prediction of longer or shorter ORFs and fusing two ORFs into one (Figures 6.4, 6.5 and 6.6). Considering the same genomic organization was found in the two HGSV-2 isolates that came from different Hawaiian Islands and plant hosts, i.e. citrus and hibiscus from Maui and Oahu, respectively, it is likely that sequence errors detailed in Figures 6.5 and 6.6 were introduced into the original sequence represented by HQ852053 and HQ852054 in Melzer et al. (2012). In the earlier study, traditional low throughput cloning and sequencing were used to assemble the genome, resulting in less coverage depth in comparison to the one generated in this study. Unfortunately, the citrus tree in Oahu where the first citrus isolate of HGSV-2 was characterized from was removed and no plant sample from that tree is available to confirm this possibility.

In-fusion cloning allowed the construction of 35SRbz-HGSV-2-RNA1/2/3, the first reverse genetic system for a kitavirid. A similar procedure implemented for the construction of an infectious clone for CSDaV (Matsumura et al., 2019) allowed the construction of 35SRbz-HGSV-2-RNA1 (Figure 4.2) after several failed attempts to amplify the whole 8,369 bp genomic sequence of RNA 1, including a 15 bp poly-A tail, of the hibiscus isolate of HGSV-2 (data not shown). Several non-synonymous nucleotide differences were found between the full-length cDNA clone and the hibiscus isolate of HGSV-2. Although a few of these resulted in non-structurally related amino acid changes (Table 4.3), the biological activity of the progeny virus derived from the full-length cDNA clones 35SRbz-HGSV-2-RNA1/2/3 was comparable with that of the wild-type virus in *H. arnottianus*, a natural host of HGSV-2 (Figure 4.9). Additionally, the infectious clone of HGSV-2 developed in this study proved suitability to infect the experimental hosts *N. benthamiana* and *N. tabacum* (Figure 4.9) as well as *P. vulgaris* (Figure 4.7), an experimental indicator plant for BTV-C (Garita et al., 2013). The implemented DNase-RT-PCR assays for specific detection of RNA 1, 2 and 3 of HGSV-2 using virus-specific primers (Table 4.1) allowed confirmation of the presence of the recombinant HGSV-2 (rHGSV-2) in most of the agroinfiltrated leaves

of all the plant hosts (Tables 6.4 and 6.5). The DNase digestion step was critical in the diagnostic assays to have certainty that the targeted molecules detected were of RNA origin and not from vector origin.

Because kitavirids cannot establish plant systemic infection naturally, it was not possible to assess if the virus progeny derived from the infectious clone of HGSV-2 colonized systemic non-agroinfiltrated leaves. Therefore, to further support the infectivity of the full-length cDNA clone, rHGSV-2 virions were partially purified following a protocol detailed by Colariccio et al. (2000), negatively stained using 1% phosphotungstic acid and viewed in the TEM. Abundant electro dense quasi-spherical structures were observed and had varied sizes ranging from 150 to 250 nm (Figure 4.10A). Although it was previously speculated that HGSV-2 virions may be short (~30-50 nm) and bacilliform, this was suggested based on the observation of negatively stained ultra-thin sections of HGSV-2 infected leaf tissue (Melzer et al., 2012). Importantly, DNase-RT-PCR assays on RNA extracted from these partially purified virus preparations tested positive for RNA 1, 2 and 3 of HGSV-2 whereas the negative and positive controls tested negative and positive, respectively (Figure 4.10B). This result corroborated the detection of a partial sequence within the genomic RNA that was perhaps coated inside the rHGSV-2 virions which were derived from 35SRbz-HGSV-2-RNA1/2/3. Furthermore, rHGSV-2 virions derived from the full-length cDNA clone were mechanically inoculated onto *N. benthamiana* plants. Although only a few *N. benthamiana* leaves presented necrotic local lesions after 6 days, all the symptomatic leaves tested positive for the RNA 1, 2 and 3 of HGSV-2 using DNase-RT-PCR assays (Figure 4.11). These necrotic local lesions resemble the HR-like phenotype displayed by the local lesions in *N. benthamiana* leaves that were mechanically inoculated using leaf tissue infected by a related kitavirid, citrus leprosis virus C (CiLV-C) (Arena et al., 2020). In addition to the *N. benthamiana* leaves that were mechanically inoculated with rHGSV-2 virions, *P. vulgaris* (Figure 4.8), *N. benthamiana*, and *N. tabacum* (Figure 4.9) that were agroinfiltrated with the infectious clone of HGSV-2 also displayed an HR-like phenotype. These results are congruent with the HR-like phenotype displayed by *Arabidopsis thaliana* and citrus plants upon CiLV-C infection. The outcome of an HR-like response in these plants was corroborated using transcriptomics and biochemical assays (Arena et al., 2016). In conjunction with the HR-like phenotype in the leaves agroinfiltrated with the full-length cDNA clone of HGSV-2, accelerated senescence was also observed in the agroinfiltrated leaves when compared to non-agroinfiltrated leaves or leaves agroinfiltrated with an empty vector of the same plant and same age (Figures 6.8 and 6.9). This same pattern of symptom development upon CiLV-C infection has been previously reported in *A. thaliana* plants (Arena et al., 2013) and conforms to, but on a shorter temporal scale, those observed in citrus trees infected with CiLV-C (Bastianel et al., 2010). It has been recently suggested that p61 is the viral determinant of CiLV-C that causes an HR-like response and therefore leprosis symptoms on citrus (Arena et al., 2020). Even though no p61 homolog is coded by HGSV-2, still an HR-like phenotype was

observed in several plant hosts agroinfiltrated with the full-length cDNA clone of HGSV-2 (Figures 6.8 and 6.9). Further studies are required to determine what HGSV-2 protein may be the viral determinant that leads to an HR-like response. Notwithstanding, all these results taken together provide strong evidence of the infectivity of the reverse genetics system of HGSV-2 developed in this study. This system will be invaluable for future studies on the basic biology of kitavirids and virus-host and virus-vector interactions. Furthermore, evaluation of the response of citrus varieties to HGSV-2 infection can take place once an effective agro-delivery method for citrus is developed. Such a study can be useful for the citrus industry in Hawaii as well as other US states that are threatened by leprosis and other BTV-related diseases.

An isoline population of non-viruliferous mites was established from a single *Brevipalpus* female collected from a mandarin (*C. reticulata*) tree growing at the University of Hawaii at Manoa campus. These non-viruliferous mites were used in transmission assays of HGSV-2 from citrus to citrus and from citrus to hibiscus using AAP and IAP of 3 days. Only one of the four *C. reticulata* leaves exposed to viruliferous mites presented green chlorotic lesions that resemble the natural infection of HGSV-2 in mandarin trees (Figure 4.14) while none of the *C. sinensis* leaves exposed to viruliferous mites presented symptoms. Two out of the six *H. arnottianus* leaves exposed to viruliferous mites presented symptoms resembling to those observed in hibiscus leaves exhibiting BTV symptoms (Kitajima et al., 2003). Congruent with the feeding pattern reported for *B. yothersi* (Tassi et al., 2017), the chlorotic lesions in *H. arnottianus* leaves suggested an aggregated feeding pattern on leaf edges and near veins for the *Brevipalpus* specimens used in these transmission assays (Figure 4.15). DRT-PCR assays on three specimens used in the transmission assays suggested that the identity of the mites was *B. azores* based on a ~700 bp sequence of the 28S rRNA gene. Micrographs of the anterior and posterior sides of three *Brevipalpus* specimens used in the transmission assays were obtained using the SEM. The physiological features of the three specimens were identical among one another. The undulated patterns found in the ventricular part of the ventral side of the mites (Figure 4.13) supported the identity of the mites used in the transmission assays was *B. azores* (Beard et al., 2015; Tassi 2018). *B. azores* and *B. papayensis* share high physiological and molecular resemblance that complicates mite identification (Tassi 2018). Nunes et al. (2018) determined that under experimental conditions *B. papayensis* can transmit CiLV-C to *P. vulgaris* with a low transmission efficiency of 27% perhaps due to the low efficiency of single mite transmission used in that study. In this work, five mites per leaf were used and transmission efficiencies of 33%, 25% and 0% were observed in *H. arnottianus*, *C. reticulata* and *C. sinensis*, respectively. DRT-PCR assays confirmed the viruliferous status in 2 out of the 3 specimens examined (Figure 4.12). These latter results are congruent with those found by Tassi et al. (2017) that reported that 25 to 60% of *B. yothersi* mites feeding on CiLV-C infected tissue acquired the virus. Therefore, the uncertainty of the

viruliferous status of the mites used in the transmission assays may explain the low transmission efficiencies observed in *H. arnottianus* and *C. reticulata* as well as the null transmission of HGSV-2 that was observed in *C. sinensis*. However, additional experiments are required to clarify the acquisition efficiency of HGSV-2 by *B. azores*. Still, the results obtained in the transmission assays in this study clearly demonstrate that *B. azores* is able to transmit HGSV-2 and confirms the BTV nature of higreviruses. Future studies are required to verify if *B. yothersi* or *B. papayensis* can also transmit HGSV-2 and at what transmission efficiency.

4.5 LITERATURE CITED

- Arena, G.D., Bergamini, M.P., Tassi, A.D., Kitajima, E.W., Kubo, K.S., Freitas-Astúa, J. (2013). Citrus leprosis virus C infects *Arabidopsis thaliana*, the model for plant-pathogen interactions. *J. Plant Pathol.* 95, 448. doi: 10.4454/JPP.V95I2.003
- Arena, G.D., Ramos-González, P.L., Falk, B.W., Casteel, C.L., Freitas-Astúa, J. and Machado, M.A. (2020). Plant Immune System Activation Upon Citrus Leprosis Virus C Infection Is Mimicked by the Ectopic Expression of the P61 Viral Protein. *Front. Plant Sci.* 11:1188. doi: 10.3389/fpls.2020.01188
- Arena, G.D., Ramos-González, P.L., Nunes, M.A., Ribeiro-Alves, M., Camargo, L.E.A., Kitajima, E.W., Machado, M.A. and Freitas-Astúa, J. (2016). Citrus leprosis virus C Infection Results in Hypersensitive-Like Response, Suppression of the JA/ET Plant Defense Pathway and Promotion of the Colonization of Its Mite Vector. *Front. Plant Sci.* 7:1757. doi: 10.3389/fpls.2016.01757
- Arif, M. & Ochoa-Corona, F. (2013). Comparative assessment of 5' A/T-rich overhang sequences with optimal and sub-optimal primers to increase PCR yields and sensitivity. *Mol. Biotechnol.* 55, 17-26. doi: 10.1007/s12033-012-9617-5
- Armougom, F., Moretti, S., Poirot, O., Audic, S., Dumas, P., Schaeli, B., et al. (2006). Expresso: automatic incorporation of structural information in multiple sequence alignments using 3D-Coffee. *Nucleic Acids Res.* 34(Web Server issue), W604-W608. doi:10.1093/nar/gkl092
- Beard, J.J., Ochoa, R., Braswell, W.E., Bauchan, G.R. (2015) *Brevipalpus phoenicis* (Geijskes) species complex (Acari: Tenuipalpidae) – a closer look. *Zootaxa* 3944:1-67. doi: 10.11646/zootaxa.3944.1.1.
- Bastianel, M., Novelli, V.M., Kitajima, E.W., Kubo, K.S., Bassanezi, R.B., Machado, M.A., et al. (2010). Citrus Leprosis: Centennial of an unusual mite–virus pathosystem. *Plant Dis.* 94, 284–292. doi: 10.1094/PDIS-94-3-0284
- Chabi-Jesus, C., Ramos-González, P.L., Tassi, A.D., Guerra-Peraza, O., Kitajima, E.W., Harakava, R., Beserra Jr., J.E.A., Salaroli, R.B., Freitas-Astúa, J. (2018). Identification and characterization of citrus chlorotic spot virus, a new Dichorhavirus associated with citrus leprosis-like symptoms. *Plant Dis* 102: 1588-1598.
- Colariccio, A., Lovisolo, O., Boccardo, G., Chagas, C.M., d'Aquilio, M. & Rossetti, V. (2000). Preliminary purification and double stranded RNA analysis of citrus leprosis virus. *Proceedings Conference International Organization of Citrus Virologists*, 14, 159-163.

Colariccio, A., Lovisolo, O., Chagas, C.M., Galleti, S.R., Rossetti, V., Kitajima, E.W. (1995) Mechanical transmission and ultrastructural aspects of citrus leprosis disease. *Fitopatologia Brasileira* 20:208-213.

Cook, G., Kirkman, W., Clase, R., Steyn, C., Basson, E., Fourie, P. H., Moore, S. D., Grout, T.G., Carstens, E., Hattingh, V. (2019). Orchid fleck virus associated with the first case of citrus leprosis-N in South Africa. *Eur J Pl Pathol* 155, 1373-1379. doi:10.1007/s10658-019-01854-4

Cruz-Jaramillo, J.L., Ruiz-Medrano, R., Rojas-Morales, L., Lopez-Buenfill, J.A., Morales-Galvan, O., Chavarin-Palacio, C., Ramirez-Pool, J.A., Xoconostle-Cazares, B. (2014). Characterization of a proposed dichorhavirus associated with the citrus leprosis disease and analysis of the host response. *Viruses* 6(7): 2602-2622. doi: 10.3390/v6072602

Di Tommaso, P., Moretti, S., Xenarios, I., Orobittg, M., Montanyola, A., Chang, J.M., et al. (2011) T-Coffee: a web server for the multiple sequence alignment of protein and RNA sequences using structural information and homology extension. *Nucleic Acids Res.* 39(Web Server issue), W13-W17. doi:10.1093/nar/gkr245

Dimaio, D. (2014). Viral miniproteins. *Annu. Rev. Microbiol.* 68, 21–43. doi: 10.1146/annurev-micro-091313-103727

Druciarek, T., Lewandowski, M. and Tzanetakis, I. (2019). A new, sensitive and efficient method for taxonomic placement in the Eriophyoidea and virus detection in individual eriophyoids. *Exp. Appl. Acarol.* 78, 247-261. Doi:10.1007/s10493-019-00382-4

Garita, L.C., Tassi, A.D., Calegario, R.F., Kitajima, E.W., Carbonell, S.A.M., Freitas-Astúa, J. (2013). Common Bean: Experimental Indicator Plant for Citrus leprosis virus C and Some Other Cytoplasmic-Type Brevipalpus-Transmitted Viruses. *Plant Dis.* 97(10): 1346-1351. doi: 10.1094/PDIS-12-12-1143-RE

Kearse, M., Moir, R., Wilson, A., Stones-Havas, S., Cheung, M., Sturrock, S., Buxton, S., Cooper, A., Markowitz, S., Duran, C., Thierer, T., Ashton, B., Meintjes, P., and Drummond, A. 2012. Geneious Basic: An integrated and extendable desktop software platform for the organization and analysis of sequence data. *Bioinformatics* 28:1647–1649.

Kitajima, E.W., Chagas, C.M., and Rodrigues, J.C.V. (2003). Brevipalpus-transmitted plant virus and virus-like diseases: cytopathology and some recent cases. *Exp. Appl. Acarol.* 30, 135–160.

Kuchibhatla, D.B., Sherman, W.A., Chung, B.Y., Cook, S., Schneider, G., Eisenhaber, B., Karlin, D.G. (2014) Powerful sequence similarity search methods and in-depth manual analyses can identify remote homologs in many apparently “orphan” viral proteins. *J. Virol.* 88(1): 10-20

- Lazareva, E.A., Lezzhov, A.A., Komarova, T.V., Morozov, S.Y., Heinlein, M., Solovyev, A. (2017) A novel block of plant virus movement genes. *Mol Plant Pathol* 18(5): 611-624. doi: 10.1111/mpp.12418.
- Locali-Fabris, E. C., Freitas-Astúa, J., Souza, A. A., Takita, M. A., Astúa-Monge, G., Antonioli-Luizon, R., et al. (2006). Complete nucleotide sequence, genomic organization and phylogenetic analysis of Citrus leprosis virus cytoplasmic type. *J. Gen. Virol.* 87, 2721–2729. doi: 10.1099/vir.0.82038-0
- Lindbo, J. (2007) TRBO: a high-efficiency Tobacco mosaic virus RNA-based overexpression vector. *Plant Physiol.* 145, 1232–1240.
- Matsumura, E.E., Coletta-Filho, H.D., Machado, M.A., Nouri, S., Falk, B.W. (2019) Rescue of Citrus sudden death-associated virus in *Nicotiana benthamiana* plants from cloned cDNA: insights into mechanisms of expression of the three capsid proteins. *Mol. Pl. Pathol.* 20(5): 611-625. doi: 10.1111/mpp.12780
- Melzer, M.J., Sether, D.M., Borth, W.B., Hu, J.S. (2012). Characterization of a virus infecting *Citrus volkameriana* with citrus leprosis-like symptoms. *Phytopathol* 102(1): 122-127. doi: 10.1094/PHYTO-01-11-0013.
- Mironov, S.V., Dabert, J. & Dabert, M. (2012). A new feather mite species of the genus *Proctophylloides* Robin, 1877 (Astigmata: Proctophylloidae) from the long-tailed tit *Aegithalos caudatus* (Passeriformes Aegithalidae)-morphological description with DNA barcode data. *Zootaxa* 3253: 54-61.
- Morris, T.J. and Dodds, J.A. 1979. Isolation and Analysis of Double-Stranded RNA from Virus-Infected Plant and Fungal Tissue. *Phytopathology*, 69:854-858.
- Navarro, B., Minutolo, M., De Stradis, A., Palmisano, F., Alioto, D. & Di Serio, F. (2018). The first phlebo-like virus infecting plants: a case study on the adaptation of negative-stranded RNA viruses to new hosts. *Mol. Plant Pathol.* 19(5), 1075-1089. doi: 10.1111/mpp.12587.
- Nunes, M.A., de Carvalho Mineiro, J.L., Rogério, L.A., Ferreira, L.M., Tassi, A., Novelli, V.M., Kitajima, E.W., Freitas-Astúa, J. (2018). First report of *Brevipalpus papayensis* as vector of coffee ringspot virus and citrus leprosis virus C. *Plant Dis.* 102:1046. doi: 10.1094/PDIS-07-17-1000-PDN
- Pascon, R.C., Kitajima, J.P., Breton, M.C., Assumpcao, L., Greggio, C., Zanca, A.S., Okura, V.K., Alegria, M.C., Camargo, M.E., Silva, G.G., Cardozo, J.C., Vallim, M.A., Franco, S.F., Silva, V.H., Jordao, H., Oliveira, F., Giachetto, P.F., Ferrari, F., Aguilar-Vildoso, C.I., Franchiscini, F.J., Silva, J.M., Arruda, P., Ferro, J.A., Reinach, F. and da Silva, A.C. (2006) The complete nucleotide sequence and genomic organization of citrus leprosis associated virus, cytoplasmic type (CiLV-C). *Virus Genes* 32, 289–298.

- Potter, S.C., Luciani, A., Eddy, S.R., Park, Y., Lopez, R. & Finn, R.D. (2018). HMMER web server: 2018 update. *Nucleic Acids Res.* 46(W1), W200-W204. doi: 10.1093/nar/gky448
- Quito-Avila, D.F., Freitas-Astúa, J., & Melzer, M.J. (2020). “Bluner-, Cile-, and higreviruses (kitaviridae),” in *Reference Module in Life Sciences*, ed. B. D. Roitberg (Amsterdam: Elsevier), 1–5.
- Ramos-González, P.L., Chabi-Jesus, C., Arena, G.D., Tassi, A.D., Kitajima, E.W., & Freitas-Astúa, J. (2018). Leprosis de los cítricos: una enfermedad multietiológica singular. *Citrus leprosis: a unique multietiological disease. Citrus in the Americas* 1(1): 4–19.
- Ramos-González, P.L., Chabi-Jesus, C., Guerra-Peraza, O., Breton, M.C., Arena, G.D., Nunes, M.A., Kitajima, E.W., Machado, M.A., & Freitas-Astúa, J. (2016). Phylogenetic and Molecular Variability Studies Reveal a New Genetic Clade of Citrus leprosis virus C. *Viruses*, 8(6), 153. <https://doi.org/10.3390/v8060153>
- Ramos-González, P.L., Chabi-Jesus, C., Guerra-Peraza, O., Tassi, A.D., Kitajima, E.W., Harakava, R., Salaroli, R.B., Freitas-Astúa, J. (2017). Citrus leprosis virus N: A new dichorhavirus causing citrus leprosis disease. *Phytopathol* 107: 963-976.
- Ramos-González, P.L., Santos, G.F., Chabi-Jesus, C., Harakava, R., Kitajima, E.W. and Freitas-Astúa, J. (2020). Passion Fruit Green Spot Virus Genome Harbors a New Orphan ORF and Highlights the Flexibility of the 5'-End of the RNA2 Segment Across Cileviruses. *Front. Microbiol.* 11:206. doi: 10.3389/fmicb.2020.00206
- Rogério, L.A., Galdeano, D.M., Arena, G.D., Nunes, M.A., Machado, M.A., Novelli, V.M. (2019). Reference genes for gene expression studies by RT-qPCR in *Brevipalpus yothersi* (Acari: Tenuipalpidae), the mite vector of citrus leprosis virus. *Sci Rep* 9, 6536 . <https://doi.org/10.1038/s41598-019-42993-2>
- Roy, A., Choudhary, Leon, M.G., Shao, J., Govindarajulu, A., Achor, D., et al., (2013). A novel virus of the genus Cilevirus causing symptoms similar to citrus leprosis. *Phytopathol* 103(5): 488-500. doi: 10.1094/PHYTO-07-12-0177-R
- Roy, A., Hartung, J.S., Schneider, W.L., Shao, J., Leon, G., Melzer, M.J., Beard, J.J., Otero-Colina, G., Bauchan, G.R., Ochoa, R., Brlansky, R.H. (2015a). Role bending: Complex relationships between viruses, hosts, and vectors related to citrus leprosis, an emerging disease. *Phytopathology* 105(7): 1013-1025. doi: 10.1094/PHYTO-12-14-0375-FI.
- Roy, A., Stone, A.L., Shao, J., Otero-Colina, G., Wei, G., Choudhary, N., Achor, D., Levy, L., Nakhla, M.K., Hartung, J.S., Schneider, W.L., Brlansky, R.H. (2015b). Identification and molecular

characterization of nuclear citrus leprosis virus, a member of the proposed dichorhavirus genus infecting multiple citrus species in Mexico. *Phytopathol* 105(4): 564-575. doi: 10.1094/PHYTO-09-14-0245-R.

Sonnenberg, R., Wolte, A.W., and Tautz, D. 2007. An evaluation of LSU rDNA D1-D2 sequences for their use in species identification. *Front. Zool.* 4:6 (doi: 10.1186/1742-9994-4-6).

Tassi, A.D. (2018). Diversidade morfológica e genética de diferentes espécies de *Brevipalpus* (Acari: Tenuipalpidae) e suas competências como vetores de vírus. 262. Available at: https://teses.usp.br/teses/disponiveis/11/11135/tde-17072018-160552/publico/Aline_Daniele_Tassi_versao_revisada.pdf

Tassi, A.D., Garita-Salazar, L.C., Amorim, L., Novelli, V.M., Freitas-Astúa, J., Childers, C.C., & Kitajima, E.W. (2017). Virus-vector relationship in the Citrus leprosis pathosystem. *Experimental & applied acarology*, 71(3), 227–241. <https://doi.org/10.1007/s10493-017-0123-0>

Untergasser, A., Cutcutache, I., Koressaar, T., Ye, J., Faircloth, B.C., Remm, M., et al. (2012). Primer3 - new capabilities and interfaces. *Nucleic Acids Res.* 40(15): e115

CHAPTER V

THE VIROME OF TENUIPALPID MITES IN HAWAII, WITH AN EMPHASIS ON KITA- AND KITA-LIKE VIRUSES

5.1 INTRODUCTION

There are about 1100 described flat mite species in the family Tenuipalpidae which are further classified into 38 genera (Beard et al., 2013). *Brevipalpus* and *Tenuipalpus* harbor more than 600 species and are the most economically important genera within Tenuipalpidae, however, only some species are major pests causing discernible direct and/or indirect injury and yield impacts by toxin injection and/or plant virus transmission, respectively (Gerson 2008). Perhaps the most important species in the family are *B. californicus*, *B. obovatus*, and *B. phoenicis* species complexes which are the most intercepted tenuipalpid mites and the only known virus vectors, within Tenuipalpidae, that transmit plant viruses of quarantine concern (Freitas-Astúa et al., 2018; Rodrigues and Childers 2013). Among these cryptic species complexes, *B. phoenicis* was recently further subdivided into eight subgroups: *B. ferraguti*, *B. yothersi*, *B. hondurani*, *B. feresi*, *B. phoenicis sensu stricto* (s.s.), *B. tucuman*, *B. papayensis*, and *B. azores* (Beard et al., 2015). Out of all these *Brevipalpus* species, virus vector ability has been confirmed for *B. yothersi*, *B. papayensis*, *B. phoenicis* s.s. and *B. californicus* (Kondo et al., 2003; Roy et al., 2015; Ramos-Gonzalez et al., 2017; Nunes et al., 2018).

Brevipalpus-transmitted viruses (BTVs), different from most plant viruses, do not establish a systemic infection in their host naturally, but rather are confined to localized lesions (Freitas-Astúa et al., 2018; Rodrigues and Childers 2013). Based on the cytopathological effect, i.e. viroplasm, observed in infected tissue using transmission electron microscope (TEM), they can be classified into the cytoplasmic type (BTV-C) and the nuclear type (BTV-N) (Kitajima et al., 2003). BTVs have been found affecting economically important crops such as citrus, coffee, passion fruit, orchids, and numerous other ornamentals. The localized symptoms caused by these viruses are very similar and characterized by chlorotic or green spots and ringspots that may present in leaves, fruits and stems (Freitas-Astúa et al., 2018; Kitajima et al., 2003). BTV-N and BTV-C belong to the genera *Dichorhavirus* (*Rhabdoviridae* family) and *Cilevirus* (*Kitaviridae* family), respectively. Both BTVs group with phylogenetically related insect- and arthropod- viruses: BTV-C with a large number of unclassified viruses that are loosely described as negeviruses, and BTV-N with rhabdovirids. Both BTV-Cs and BTV-Ns cause local lesions only in their plant hosts and both are transmitted in a persistently, perhaps propagative, manner (Nunes et

al., 2017; Ramos-González et al., 2020; Whitfield et al., 2018). Considering these circumstances, it has been speculated that ancestors of BTV-Cs and BTV-Ns colonized arthropods and harbored unsegmented RNA genomes characteristic of negevirus and classical rhabdovirids, respectively (Kondo et al., 2017; Freitas-Astúa et al., 2018; Ramos-González et al., 2020; Quito-Avila et al., 2020). Based on phylogenetic relationships, negevirus can be further classified into at least four groups at the genus level, namely “nelorpivirus”, “sandewavirus” (Kallies et al., 2014), “aphiglyvirus” and “centivirus” (Kondo et al., 2020).

The aim of the present study detailed in this chapter was to characterize BTV-related viruses within the virome present in tenuipalpid mites using high throughput sequencing (HTS). This study will provide a broader perspective of the viruses that may share an evolutionary origin with BTVs and are infecting *Brevipalpus* and other tenuipalpid mites. This study will open new research opportunities to explore the characterization of new BTVs that are found in populations of flat mites from other geographic locations.

5.2 MATERIALS AND METHODS

5.2.1 Flat mite specimen collection

Leaves, twigs, and/or fruits, were collected from several known plant hosts of flat mites (Tenuipalpidae family) (Beard et al. 2013) from several locations across the islands of Oahu and Hawaii (Figure 5.1). The plant material was placed in hermetic bags, transported to the Agrosecurity laboratory at the University of Hawaii at Manoa, and was individually inspected under a dissecting microscope. If present, flat mites were retrieved using a sterile fine needle and placed into a 1.5 mL tube containing 500 µL of 95% ethanol. The needle was flame-sterilized between each individual mite sample collected per plant host per location. Each mite sample consisted of at least 10 flat mites that were collected from the same plant host per location. Capped tubes were securely wrapped with one layer of parafilm and placed at -80°C until nucleic acid extraction was performed.

5.2.2 Nucleic acid extraction

Tubes containing the mites were briefly centrifuged for 30 seconds at 2,000xg to pellet the mites, and the ethanol was carefully removed using a micropipette. The mites were then powdered using liquid nitrogen and a micro-pestle, then homogenized with 100 uL of CTAB buffer containing beta-mercaptoethanol. Total nucleic acids (TNA) were immediately extracted as described by Li et al. (2008), and the

resuspended TNA were further purified using the PureLink RNA mini kit (ThermoFisher Scientific, Waltham, MA), according to the manufacturer’s instructions for liquid samples. TNA were resuspended in 20 μ L of DEPC-treated water and quantified using a NanoDrop 2000 Spectrophotometer (ThermoFisher Scientific, Waltham, MA). To reduce future sequencing costs, the TNA extracts from each sample; i.e. mites from the same hosts, but different locations; were equimolarly pooled to have five final pool samples (Table 5.1).

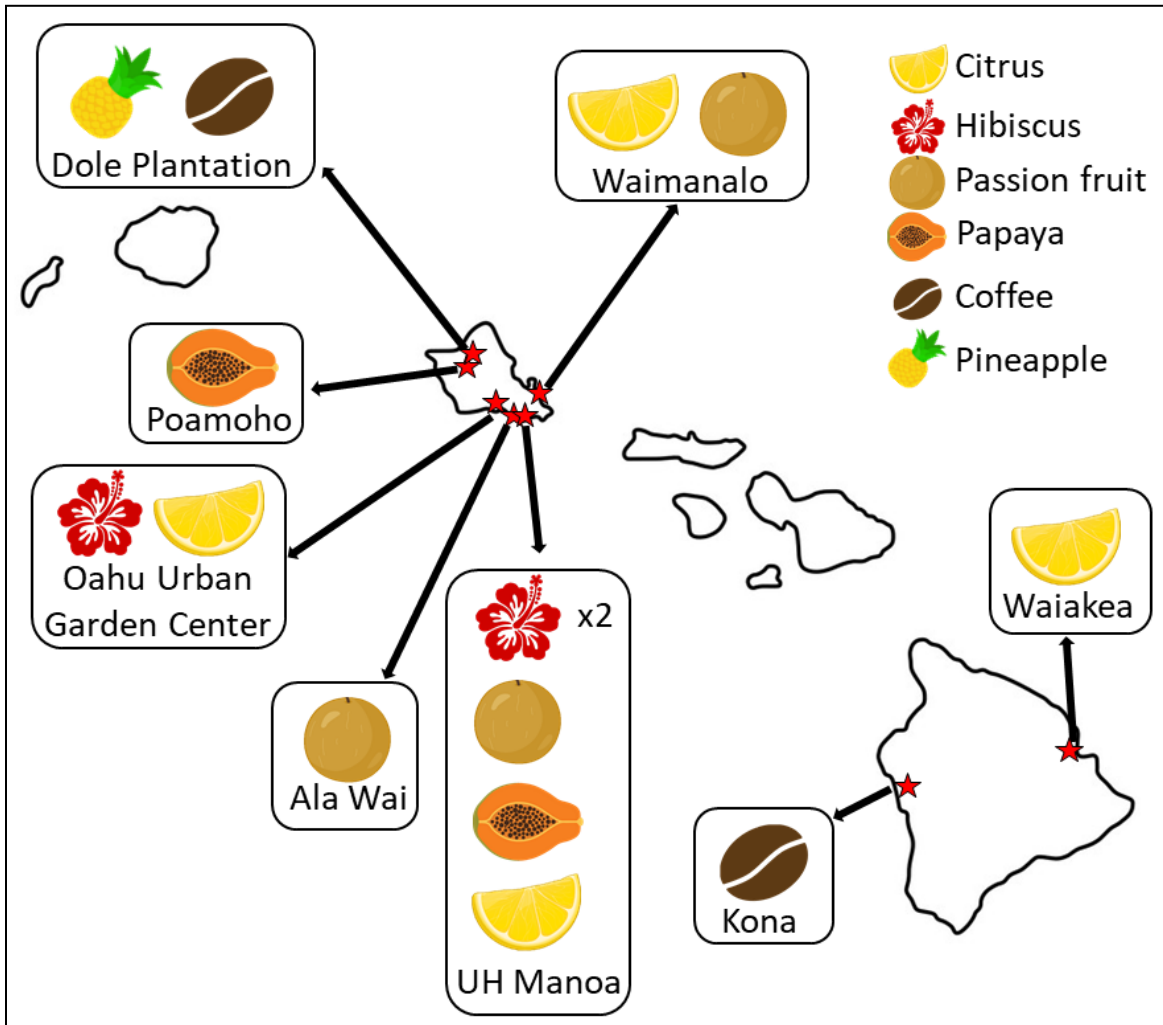


Figure 5.1 Map detailing plant host and growing location and hosts from which flat mite specimens were collected on the islands of Oahu and Hawaii. One individual mite sample was composed of at least 10 tenuipalpid mites collected per location per plant host.

1.2.3 Determination of the virome in the tenuipalpid mite samples

Pools of TNA were stabilized in RNA Stabilization tubes (Genewiz, South Plainfield, NJ) according to the manufacturer's instructions. The tubes containing the stabilized TNA pools were sent to the University of California Irvine Genomics High Throughput Facility. Ribodepletion and libraries construction were performed using the SMARTer Stranded Total RNA-Seq Kit v3 - Pico Input Mammalian kit (Clontech, Mountain View, CA) following the manufacturer's instructions. HTS was performed on an Illumina NovaSeq 6000 platform using an S4 200 cycle kit. Genome assembly and bioinformatic analyses were performed as described (Olmedo-Velarde et al., 2019) with slight modifications. Briefly, paired-end reads were trimmed, and quality filtered using Trimmomatic 0.35.3 (Bolger et al., 2014). Tenuipalpid-specific reads were mapped to the draft genome of *B. yothersi* (https://ftp.ncbi.nih.gov/genomes/GenBank/invertebrate/Brevipalpus_yothersi/) and to any Tenuipalpidae sequences available in GenBank (last accessed on September 20, 2021) using Bowtie 2 (Langmead et al., 2012). The remaining reads were *de novo* assembled using SPAdes (Bankevich et al., 2012). Contigs were annotated using BLASTX search (Altschul et al., 1997) against the viral genome database (<ftp://ftp.ncbi.nih.gov/genomes/Viruses/all.fna.tar.gz>). Contigs with similarity to virus sequences were then used as reference for an iterative mapping approach (Dey et al., 2019) using Geneious mapper plugin implemented in Geneious v. 10.1.3 (Kearse et al., 2012) and the trimmed sequence reads.

1.2.4 Virus nomenclature

Viruses identified in this chapter have been named using the following nomenclature system: I) the first part of the name is the genus of the mite associated with the source of the virus. II) The second part of the name identifies the virus taxonomic group (order, family, or genus) to which the contig was most closely related. This nomenclature system was adopted for this study and does not reflect an official name of the virus or the name that might be proposed to the International Committee on the Taxonomy of Viruses.

1.2.5 Mite barcoding, virus detection and HTS results confirmation in individual mite samples

cDNA was synthesized using individual mite TNA, random and oligo dT primers, and the Maxima-H minus reverse transcription kit (ThermoFisher Scientific, Waltham, MA) using the manufacturer's instructions. Two microliters of two-fold diluted cDNA reactions were used in endpoint PCR for DNA barcoding and internal PCR control using the 28S rRNA primers, D1D2w2: 5'-

ACAAGTACCDTRAGGGAAAGTTG-3', 28Sr0990: 5'-CCTTGGTCCGTGTTTCAAGAC-3' (Sonnenberg et al. 2007; Mironov et al. 2012) that produce an expected amplicon of ~700 bp. The cytochrome oxidase unit I (COI) gene was additionally amplified using the COI primers, DNF: 5'-TACAGCTCCTATAGATAAAAC-3', DNR: 5'-TGATTTTTTGGTCACCCAGAAG-3' (Navajas et al. 1996) that produce an expected amplicon of ~450bp. All DNA barcoding PCR assays were performed using Q5 High Fidelity DNA Polymerase (New England Biolabs, Ipswich, MA). Furthermore, endpoint RT-PCR assays using contig-specific primer sets were performed on the cDNAs of the individual mite samples to determine virus presence and confirm HTS results. Contig-specific primer sets for each Tenuipalpidae-associated virus were designed to target the RdRp, HEL, or MET conserved domains of all the virus-like contigs found. When no viral conserved domain was found in the contigs, primers were designed in the specific regions where the nucleotide sequences presented protein homology to virus sequences present in GenBank using BLASTx searches. Primer3 (Untergasser et al., 2012) was used for the primer design with consideration of thermodynamic primer features (Arif and Ochoa-Corona, 2013). These primer sets were used for specific detection of all the Tenuipalpidae-associated viruses in endpoint RT-PCR assays using 0.5 μ M as the final primer concentration and 55 °C as the annealing temperature. All barcoding amplicons were cloned into pGEM-T-Easy (Promega, Madison, WI) and 3-5 clones were sequenced. Amplicons from all other RT-PCR assays were gel extracted, purified, and bi-directionally sequenced.

1.2.6 Genomic and Proteomic Analyses

Virus contigs presenting similarity to BTVs, i.e. viruses belonging to the *Kitaviridae* family and *Dichorhavirus* genus, were selected for further analysis detailed as follows. The NCBI ORFfinder program (www.ncbi.nlm.nih.gov/orffinder) was used to identify putative open reading frames (ORFs) *in silico*. Conserved domains were predicted using either the NCBI conserved domain search tool (www.ncbi.nlm.nih.gov/Structure/cdd/wrpsb.cgi) or HMMSCAN (www.ebi.ac.uk/Tools/hmmer/search/hmmscan) implemented in HMMER (Potter et al., 2018). HMMSCAN was also used for the prediction of transmembrane helices. BLASTP searches were used to retrieve protein homologs and infer the putative function. Pairwise protein sequence comparisons using orthologous sequences retrieved from GenBank were performed using LALIGN (www.ebi.ac.uk/Tools/psa/lalign) (Huang and Miller, 1991).

1.2.7 Phylogenetic Analyses

Phylogenetic relationships were inferred using the predicted protein sequences encoded by contigs presenting similarity to BTVs, and their respective virus homolog sequences available in GenBank. Multiple protein sequences alignments were performed with ClustalW (Thompson et al., 1994) implemented in MEGA 7.0.25 (Kumar et al., 2016) using the RNA-dependent RNA polymerase (RdRp), methyltransferase (MET), helicase (HEL), and/or coat protein (CP) domains. Ambiguous positions for each alignment were curated using Gblocks 0.91b (<https://ngphylogeny.fr>) (Talavera and Castresana, 2007). The best model of protein evolution for each alignment was used to generate a Maximum Likelihood tree with 1,000 bootstrap repetitions and the best model of protein evolution. Similarly, to corroborate the *Brevipalpus* species identity, phylogenetic relationships were inferred using the partial 28S rRNA and COI genes sequences, and their respective homolog sequences available in GenBank. Multiple nucleotide sequences alignments, alignment curation, and phylogenetic tree construction were performed as detailed above.

5.3 RESULTS

5.3.1 Molecular identification of mite samples

Following the inspection of 35 plant samples comprised of plant species in the genera *Citrus*, *Passiflora*, *Coffea*, *Hibiscus*, *Ananas*, *Ficus*, *Carica*, *Oncidium*, *Phalaenopsis*, *Dendrobium*, *Theobroma*, *Gardenia*, *Areca*, *Anthurium* and *Cordyline*, 15 were found to be infested with flat mites that were collected for this study. Infested host samples included *Citrus* spp. (four samples), *Passiflora edulis* (three samples), *Hibiscus* spp. (three samples), *Coffea* sp. (two samples), *Carica papaya* (two samples), and *Ananas comosus* (one sample) (Figure 5.1 and Table 5.1). Sanger sequencing of the partial sequences of 28S rRNA and COI genes suggested the presence of *B. yothersi*, *B. papayensis*, *B. azores* and *B. obovatus* infesting the collected citrus, hibiscus, coffee, and papaya samples (Table 5.1 and Supplementary Table 5.1). Whereas the flat mites collected from pineapple were predicted to be *Dolichotetranychus* sp (Tenuipalpidae family). Interestingly, two populations of 28S rRNA partial sequences from mite samples citrus O3 and coffee O1 were obtained from 5-6 clones per amplicon. 28S rRNA partial sequences highly identical to *B. azores* and *B. yothersi* sequences were obtained from citrus O3 while two 28S rRNA partial sequences highly identical to *B. papayensis* sequences that shared 98.8% identity between each other were also found. All the sequences obtained from the barcoding assays presented >98% nucleotide identity to their closest GenBank accession (Supplementary Table 5.1).

5.3.2 Analysis of the virome present in tenuipalpid mites

The five libraries (pool 1-5) generated for this study were composed of mites from four citrus samples (pool 1), three hibiscus samples (pool 2), three passionfruit samples (pool 3), two papaya samples (pool 4), and two coffee and one pineapple sample (pool 5). Illumina HTS generated from ~65.2 to ~90.8 M of 100 bp paired-end reads from each library. After trimming, quality control and subtraction of reads of tenuipalpid origin, a variable number between ~21.2 M to ~61.9 M of paired-end reads for the five libraries were *de novo* assembled. The SPAdes *de novo* assembler produced between 415 to 10,908 contigs for the five library datasets. BLASTx searches using all the generated contigs from the five library datasets suggested the presence of between 5 to 24 viral contigs from several distinct taxa in the five datasets (Table 5.1). Viral sequences that were similar to those within the order *Picornavirales* and the family *Kitaviridae* comprised the majority of the viral sequences identified in the tenuipalpid specimens (Figure 5.2). A smaller number of contigs were predicted to have similarities with viruses within the families *Narnaviridae*, *Reoviridae*, *Tombusviridae*, *Solemoviridae*, and the unofficial negevirus taxon (Figure 5.2).

Table 5.1 Location, identity of the tenuipalpid mites, number of HTS reads and contigs generated for determination of the virome present in each mite sample collected from Oahu and Hawaii Islands.

Mite sample ID	Host	Location ¹	Tenuipalpid Identity ³	Pool of TNA	Number of reads (100 bp)	Non-host number of reads	Contigs	Viral contigs
Citrus O1	<i>Citrus</i> spp.	WRS ²	<i>B. azores</i>	1	65.2 M	39.3 M	5,286	13
Citrus O2	<i>Citrus</i> spp.	OUGC ²	<i>B. yothersi</i>	1				
Citrus O3	<i>Citrus reticulata</i>	UH Manoa	<i>B. azores</i> <i>B. yothersi</i>	1				
Citrus H1	<i>Citrus</i> spp.	Waiakea ¹	<i>B. yothersi</i>	1				
Hibiscus O1	<i>Hibiscus arnottianus</i>	UH Manoa	<i>B. papayensis</i>	2	86.5 M	61.9 M	6,255	24
Hibiscus O2	<i>Hibiscus arnottianus</i>	UH Manoa	<i>B. papayensis</i>	2				
Hibiscus O3	<i>Hibiscus rosa-sinensis</i>	OUGC ²	<i>B. obovatus</i>	2				
Passionfruit	<i>Passiflora</i>	AWCG ²	<i>B. yothersi</i>	3	90.8 M	21.9 M	415	11

O1	<i>edulis</i>								
Passionfruit	<i>Passiflora</i>	UH	<i>B. yothersi</i>	3					
O2	<i>edulis</i>	Manoa							
Passionfruit	<i>Passiflora</i>	WRS ²	<i>B. yothersi</i>	3					
O3	<i>edulis</i>								
Papaya	<i>Carica</i>	PRS ²	<i>B. papayensis</i>	4	70.1 M	21.2 M	1,960	20	
O1	<i>papaya</i>								
Papaya	<i>Carica</i>	UH	<i>B. yothersi</i>	4					
O2	<i>papaya</i>	Manoa							
Coffee	<i>Coffea</i> sp.	Kona ¹	<i>B. papayensis</i>	5	81.4 M	37.8 M	10,908	5	
H1									
Coffee	<i>Coffea</i> sp.	Dole	<i>B. papayensis</i>	5					
O1		Plantation							
Pineapple	<i>Ananas</i>	Dole	<i>Dolichotetranychus</i>	5					
O1	<i>comosus</i>	Plantation	sp.						

¹ All the locations where plant samples and mites were collected from correspond to the island of Oahu, except for Waiakea (Citrus H1) and Kona (Coffee H1) that were collected from Hawaii Island.

² OUGC = Oahu Urban Garden Center, AWCG = Ala Wai community garden, WRS = Waimanalo Research Station, PRS = Poamoho Research Station

³ Identity of tenuipalpid mites was inferred using the partial sequences of 28S rRNA and cytochrome oxidase I genes (Supplementary Table 5.1).

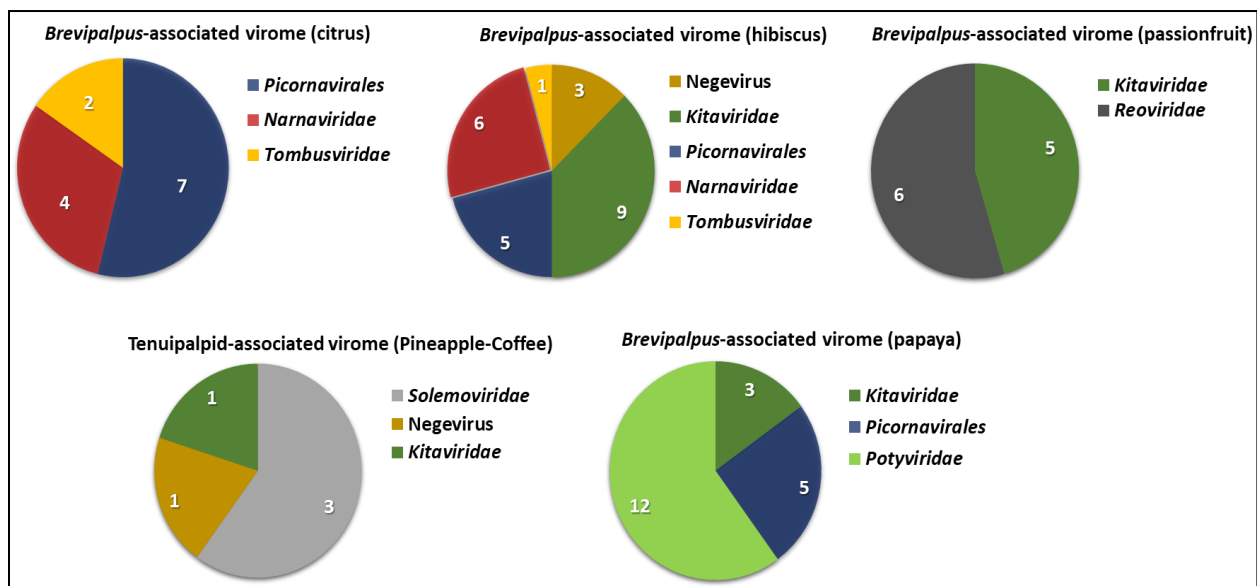


Figure 5.2 SPAdes *de novo* assembled contigs with matches to sequences with putative viral origin organized by taxonomical classification (families and order).

The contigs of putative viral origin that were identified in the five datasets using BLASTx searches had variable lengths between ~1 to ~9 Kbp. Most of these nucleotide sequences likely represented putative new virus species considering the low protein identities (<60%) their inferred protein sequences shared to their closest counterparts in GenBank. Exceptions were contigs whose inferred protein sequences presented >96% protein identity to the hibiscus strain of citrus leprosis virus C2 (CiLV-C2H, KC626783-4), hibiscus green spot virus 2 (HGVS-2, HQ852052-4), both belonging to the *Kitaviridae* family, and papaya ringspot virus (PRSV, MT470188) which belongs to the *Potyviridae* family. Some contigs likely represent near complete genome sequences of the putative new viruses when the genome size and organization were compared to those of their closest relative (data not shown). When the raw reads were mapped to the contig sequences with the putative viral origin, less than 0.5% of the total reads from the five datasets were used. The number of reads that mapped to the virus contigs was 204,669; 104,930; 39,549; 12,760 and 1,403 that corresponded to the passionfruit, citrus, hibiscus, papaya, and pineapple/coffee mite samples, respectively.

For the *Brevipalpus*-associated virome from citrus almost the totality of the viral reads (96%) mapped to contig sequences putatively classified within the order *Picornavirales* order while the remaining reads mapped to contig sequences putatively classified within the *Narnaviridae* and *Tombusviridae* families (Figure 5.3). For the *Brevipalpus*-associated virome from hibiscus, about 42%, 30%, and 18% of viral reads mapped to contigs that presented similarity to viruses within the order *Picornavirales*, *Narnaviridae* family, and hibiscus green spot virus 2 (*Kitaviridae* family), respectively. The remaining reads mapped to virus contig sequences putatively classified within the negevirus taxon (9%) and *Tombusviridae* family (1%). In both viromes associated with *Brevipalpus* mites from passionfruit and papaya, the majority of the reads mapped to virus contig sequences that shared >98% nucleotide sequence identity to the cilevirus CiLVC-C2H (*Kitaviridae* family; KC626783-4) (Figure 5.3). Interestingly, about 19% and 3% of the viral reads mapped to virus contig sequences within the *Reoviridae* and *Potyviridae* families for the mite samples from passionfruit and papaya, respectively. Although the number of viral reads that mapped to the virus contig sequences of potyvirid origin was low (387, Figure 5.3), they mapped to contig sequences that were distributed along the potyvirid homolog genome (data not shown). These contig sequences presented ~96% nucleotide identities to PRSV isolates from Taiwan (MT470188) and Hawaii (EU126128). Also, a low number of reads (695) mapped to virus contigs that presented similarity to viruses within the order *Picornavirales* in the papaya mite samples. Finally, for the tenuipalpid-associated virome from coffee and pineapple, the number of viral reads were almost equally mapped in number to virus contig sequences within the *Sobemoviridae* and *Kitaviridae* families, and the unofficial taxon negevirus (Figure 5.3).

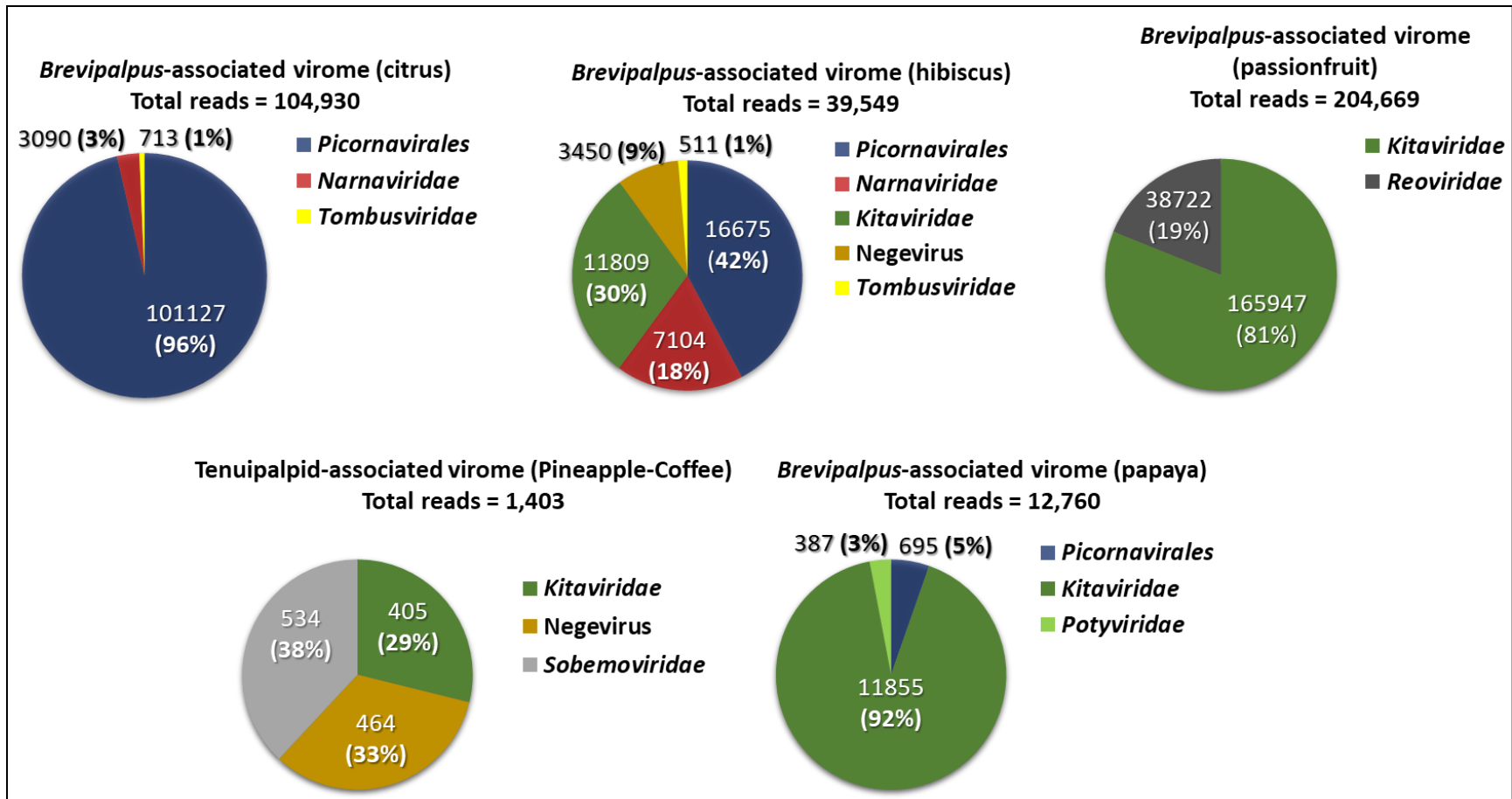


Figure 5.3 Raw sequence reads of viral origin generated from flat mite libraries are organized by taxonomical order or family. The number of reads that mapped to contig sequences putatively classified within the viral families or order *Picornavirales* is detailed, as well as the percentage that these reads represent within the total number of reads that mapped to contig sequences with putative viral origin. In all cases, the number of reads that mapped to virus contig sequences represented less than 0.5% of the total number of reads for each of the five flat mite libraries.

5.3.3 Confirmation of virus presence in individual mite samples

Contig-specific primers were designed in conserved virus domains (RdRp or HEL) or in the specific regions where the nucleotide sequences presented protein homology to the virus sequences in GenBank (Supplementary Table 5.2). These primers were used in RT-PCR assays to validate HTS results and virus presence. Almost all of the contig sequences were detected in at least one of the mite samples prior to pooling, except for the *Brevipalpus*-associated narnavirus contig 2 and *Brevipalpus*-associated picornavirus contig 3 and 4 from citrus which was not detected in any of the citrus mite samples. *Brevipalpus*-associated picornavirus contig 1, 5, and 6 from citrus, and CiLV-C2H RNA 1 and 2 from passionfruit were detected in two individual mite samples. Interestingly, CiLV-C2H RNA 1 and 2 were also detected from mites collected from the mite sample papaya O2. Both papaya O2 and passionfruit O2 mite samples were collected from plants growing in the same garden on the UH Manoa campus. Overall, mite samples citrus O1 and O3, hibiscus O1 and O3, passionfruit O1 and O2, papaya O1 and O2, and pineapple O1 tested positive for at least one virus whereas no virus contigs were detected in the other mite samples. (Table 5.2). Direct sequencing of all the amplicons corroborated the virus identity by showing >99% nucleotide identity to the original contig sequences. Considering the scope of this study, virus contig sequences presenting similarity to members classified within the *Kitaviridae* family and negevirus taxon underwent further analysis.

Table 5.2 RT-PCR assays results for virus presence confirmation. Virus contig sequences were *de novo* assembled using SPAdes and their viral origin was annotated using BLASTx searches.

<i>Brevipalpus</i> -associated virome				
Citrus				
Virus contig name	O1	O2	O3	H1
Brevipalpus-associated narnavirus contig 1	+	-	-	-
Brevipalpus-associated narnavirus contig 2	-	-	-	-
Brevipalpus-associated picornavirus contig 1	+	-	+	-
Brevipalpus-associated picornavirus contig 2	+	-	-	-
Brevipalpus-associated picornavirus contig 3	-	-	-	-
Brevipalpus-associated picornavirus contig 4	-	-	-	-
Brevipalpus-associated picornavirus contig 5	+	-	+	-
Brevipalpus-associated picornavirus contig 6	+	-	+	-
Brevipalpus-associated tombusvirus contig 1	+	-	-	-
Brevipalpus-associated tombusvirus contig 2	+	-	-	-
Hibiscus				
Virus contig name	O1	O2	O3	
Brevipalpus-associated narnavirus contig 1	+	-	-	
Brevipalpus-associated narnavirus contig 2	+	-	-	

Brevipalpus-associated narnavirus contig 3	+	-	-
Brevipalpus-associated narnavirus contig 4	+	-	-
Brevipalpus-associated narnavirus contig 5	+	-	-
Brevipalpus-associated narnavirus contig 6	+	-	-
Brevipalpus-associated picornavirus contig 1	-	-	+
Brevipalpus-associated picornavirus contig 2	-	-	+
Brevipalpus-associated picornavirus contig 3	-	-	+
Brevipalpus-associated picornavirus contig 4	-	-	+
Brevipalpus-associated picornavirus contig 5	-	-	+
Brevipalpus-associated tombusvirus contig 1	+	-	-
Brevipalpus-associated negevirus contig 1	-	-	+
Brevipalpus-associated bluner-like virus contig 1	+	-	-
Brevipalpus-associated bluner-like virus contig 2	+	-	-
Hibiscus green spot virus 2 RNA 1	+	-	-
Hibiscus green spot virus 2 RNA 2	+	-	-
Hibiscus green spot virus 2 RNA 3	+	-	-
Passionfruit			
Virus contig name	O1	O2	O3
Brevipalpus-associated reovirus contig 1	-	-	+
Citrus leprosis virus C2 RNA 1	+	+	-
Citrus leprosis virus C2 RNA 2	+	+	-
Papaya			
Virus contig name	O1	O2	
Brevipalpus-associated picornavirus contig 1	+	-	
Brevipalpus-associated picornavirus contig 2	+	-	
Citrus leprosis virus C2 RNA 1	-	+	
Citrus leprosis virus C2 RNA 2	-	+	
Papaya ringspot virus	-	+	
Tenuipalpid-associated virome			
Pineapple and Coffee			
Virus contig name	Pineapple O1	Coffee O1	Coffee H1
Dolichotetranychus-associated negevirus contig 1	+	-	-
Dolichotetranychus-associated solemovirus contig 1	+	-	-
Dolichotetranychus-associated cile-like virus contig 1	+	-	-

5.3.4 Molecular characterization of virus contig sequences similar to kitavirids and negeviruses

5.3.4.1 Citrus leprosis virus C2H and hibiscus green spot virus 2

Near-complete genomes of the kitavirids CiLV-C2H and HGSV-2 were *de novo* assembled using SPAdes from the datasets originated from passionfruit and papaya, and hibiscus mite datasets, respectively. RT-PCR assays confirmed the presence of CiLV-C2H in the mite samples passionfruit O1, O2, and papaya O2, and HGSV-2 in hibiscus O1 (Table 5.2). The near-complete genomes of CiLV-C2H RNA 1 and 2 that were retrieved from the passionfruit and papaya datasets presented ~99.9% nucleotide identity following pairwise alignment. Both genomic sequences of CiLV-C2H from the passionfruit and papaya mite datasets presented >97% nucleotide identity to CiLV-C2H characterized from hibiscus (KC626783-KC626784). Moreover, the near-complete genome of HGSV-2 from the hibiscus mite dataset presented >98.8% nucleotide identity to HGSV-2 characterized from *C. volkameriana* (HQ852052- HQ852054). The genomic organizations of both CiLV-C2 and HGSV-2 virus sequences were identical to that previously reported (Melzer et al., 2013) and that reported in Chapter IV of this study, respectively (Figure 5.4).

5.3.4.2 Contig sequences representing putative new viruses related to kitavirids

Inferred protein sequences from one contig (2,147 bp) found in the pineapple-coffee mite dataset presented ~51% identity to the kitavirid hibiscus yellow blotch virus (HYBV) described in Chapter III of this study using BLASTx searches. Even though short ORFs were predicted within the nucleotide sequence of this contig (data not shown), an RdRp domain was predicted to encompass a few of these coding regions of the contig. To facilitate representation of this contig and potential contig assembly errors, a continual open ORF was assumed. The presence of this contig was confirmed in the mite sample pineapple O1 using RT-PCR assays (Table 5.2). The contig was designated *Dolichotetranychus*-associated cile-like virus contig (Figure 5.4) considering its origin from *Dolichotetranychus* mites. Moreover, two contig sequences (3,511 and 3,585 bp) found in the hibiscus dataset were predicted to code for single ORFs coding for putative proteins of 126 and 125 kDa, respectively. The putative 126 kDa protein was predicted to contain MET and HEL domains while the putative 125 kDa protein was predicted to contain MET and RdRp domains (Figure 5.4). BLASTx searches revealed that the putative 126 and 125 kDa proteins presented ~30-32% identity to Bemisia tabaci bromo-like virus 3 (QWC36511), and ~42.8% identity to Erysiphe necator associated bluner-like virus 1 (QKS69535),

respectively. Considering the resemblance of these two contigs to RNA 1 and 2 of blunerviruses (Morozov et al., 2020; Figure 5.4), the contigs were named *Brevipalpus*-associated bluner-like virus contig 1 and 2. The presence of the two bluner-like virus contigs was confirmed in the mite sample hibiscus O1 using RT-PCR assays (Table 5.2).

5.3.4.3 Contig sequences representing putative new viruses related to negevirus

Two contig sequences of 9,664 bp and 2,089 bp were *de novo* assembled from the hibiscus and pineapple-coffee mite datasets, respectively. Using RT-PCR assays, the presence of both contig sequences was confirmed in the mite samples hibiscus O3 and pineapple O1, respectively (Table 5.2). BLASTx searches showed that both contig sequences shared 41.9% protein identity with 55% query coverage to Fort Crockett virus (YP_009351834) and 34.3% protein identity with 19% query coverage to Wallerfield virus (AIS40857), respectively. The 9,664 and 2,089 bp sequences, likely representing new virus species, were named *Brevipalpus*-associated negevirus and *Dolichotetranychus*-associated negevirus, respectively. *Brevipalpus*-associated negevirus was predicted to contain three large ORFs putatively coding for 275, 45, and 23kDa proteins, respectively (Figure 5.4). The putative 275 kDa protein was predicted as a replication-associated polyprotein containing multiple protein domains involved in virus replication: MET, methyltransferase FtsJ (FtsJ), HEL and RdRp. The putative 23 kDa protein was predicted to have the virion membrane protein of plant and insect viruses conserved domain (SP24) while no protein domain was found in the putative 45 kDa protein. Also, two small ORFs less than 300 bp in length were found overlapping along the coding region of the putative 275 kDa protein. Both putative proteins of 4-5 kDa contain at least one transmembrane domain.

Moreover, although several small ORFs were predicted in the *Dolichotetranychus*-associated negevirus contig sequence, only a putative protein coded by an 838 bp ORF presented homology to Wallerfield virus using BLASTx searches. To facilitate representation of this contig and potential contig assembly errors, a continual open ORF was assumed. A chroparavirus MET domain (PFAM 19223) was found in this potential ORF (Figure 5.4).

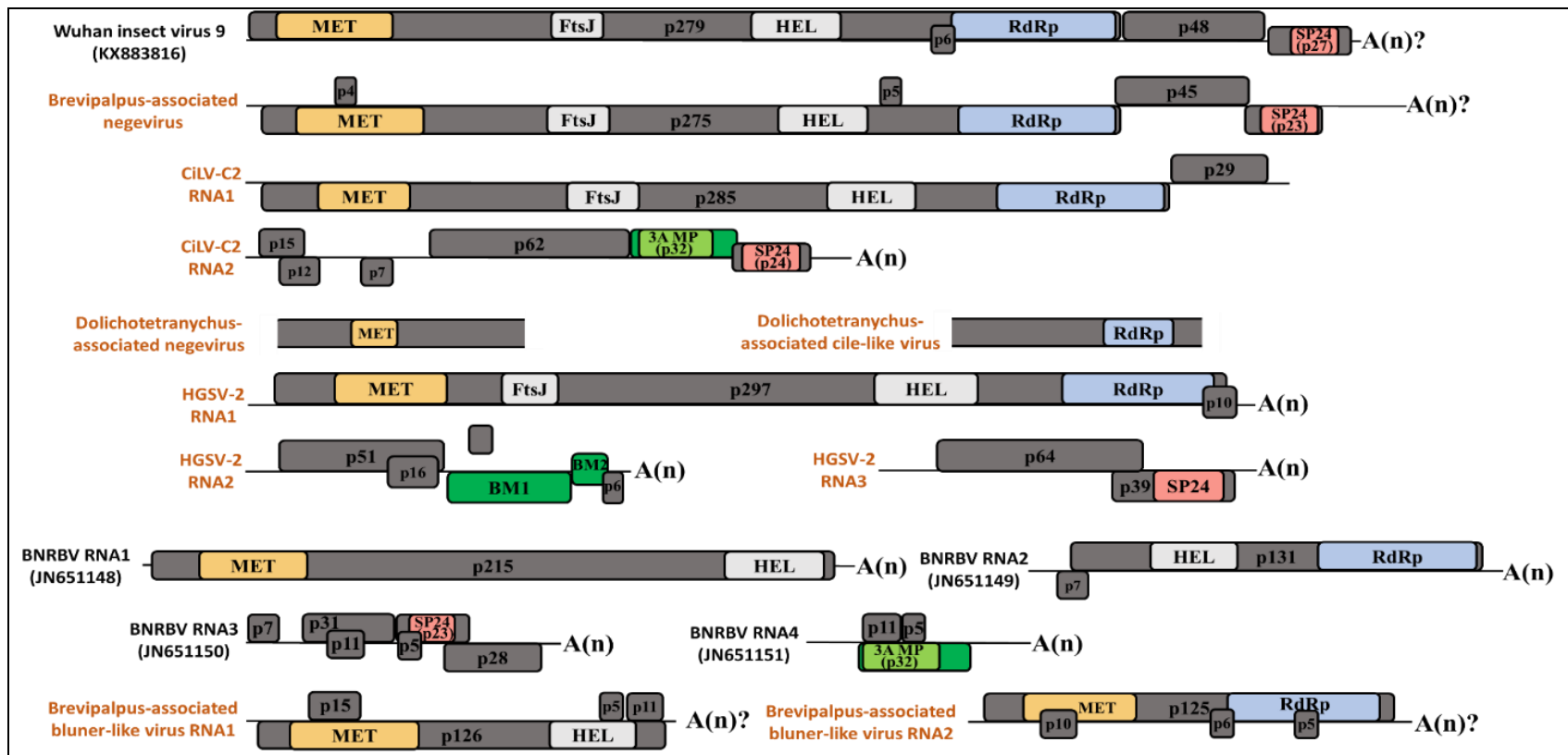


Figure 5.4 Genome organization of the BTVs-C, citrus leprosis virus C2 (CiLV-C2) and hibiscus green spot virus 2 (HGSV-2), and the putative new viruses that show relationship to the *Kitaviridae* family and the unofficial negevirus taxon. The genomes of Wuhan insect virus 9 (unclassified virus within the negevirus taxon) and blueberry necrotic ring blotch virus (BNRBV, Genus *Blunervirus*, *Kitaviridae* family) were included in this figure for genome organization comparisons. The names assigned to the virus contig sequences from this study have an orange font while virus sequences from other studies containing their respective GenBank accession have black font. Open reading frames are represented by gray and green colored boxes. Green colored boxes represent ORFs coding for putative genes associated to virus movement. Small ORFs shorter than 300 bp which putatively code for proteins containing transmembrane domains are also depicted. Protein conserved domains are represented by colored boxes: methyltransferase (MET, light orange and FtsJ, light gray), RNA-dependent RNA polymerase (RdRp, light blue), helicase (HEL, light gray), movement protein 3A (3A MP, light green), and virion membrane protein of plant and insect viruses (SP24, light red). Based on the confirmed existence of poly-A tails [A(n)] in several negeviruses and kitavirids, it is hypothesized the same feature is present in the putative new viruses [A(n)?].

5.3.5 Phylogenetic relationships of the tenuipalpid mite populations and putative new negeviruses and kitavirids found within the tenuipalpid-associated virome

5.3.5.1 Phylogenetic relationships of the tenuipalpid mite populations inferred using the 28S rRNA and COI genes

Phylogenetic relationships of the tenuipalpid mite populations were inferred using multiple nucleotide sequence alignments of the 28S rRNA and COI genes and the Maximum Likelihood algorithm. The phylogenies of both barcoding sequences presented similar topology with few differences. The phylogenies for *B. obovatus* and *B. azores* were identical in both 28S rRNA- and COI-inferred relationships and were placed in single monotypic lineages specific for both *Brevipalpus* species. However, although *B. yothersi* and *B. papayensis* were placed in single monotypic clades in the 28S rRNA phylogeny, two main clades were observed within the lineages specific for both *Brevipalpus* species (Figures 5.5 and 5.6). Importantly, the *B. papayensis* clade was paraphyletic in the COI phylogeny in contrast with the monophyletic *B. papayensis* clade that was observed in the 28S rRNA-inferred phylogeny. The *B. azores* clade comprised the excluded clade that was placed within the paraphyletic *B. papayensis* clade in the COI phylogeny (Figure 5.6). Interestingly, although one partial 28S rRNA gene sequence that was amplified from the coffee O1 mite sample presented 98.48% nucleotide identity to *B. papayensis* (MT664798, Supplementary Table 5.1), this sequence was placed in a clade that was basal from the lineage containing the *B. papayensis*, *B. feresi*, *B. phoenicis* and *B. azores* clades in the 28S rRNA phylogeny (Figure 5.5). Regardless, except for this latter sequence, all the sequences that were amplified from the *Brevipalpus* mite samples used in this study were placed within the *B. yothersi*, *B. papayensis*, *B. azores* and *B. obovatus* clades for both 28S rRNA and COI phylogenies. Furthermore, although no *Dolichotetranychus* homolog was found in the GenBank database for the 28S rRNA phylogeny, the partial COI sequence from the pineapple O1 mite sample was grouped with another accession corresponding to *Dolichotetranychus* specimens retrieved from pineapple (MH606191).

These results corroborate the suggested identities of all the tenuipalpid mites that were inferred using BLASTn searches (Supplementary Table 5.1 and Table 5.2).

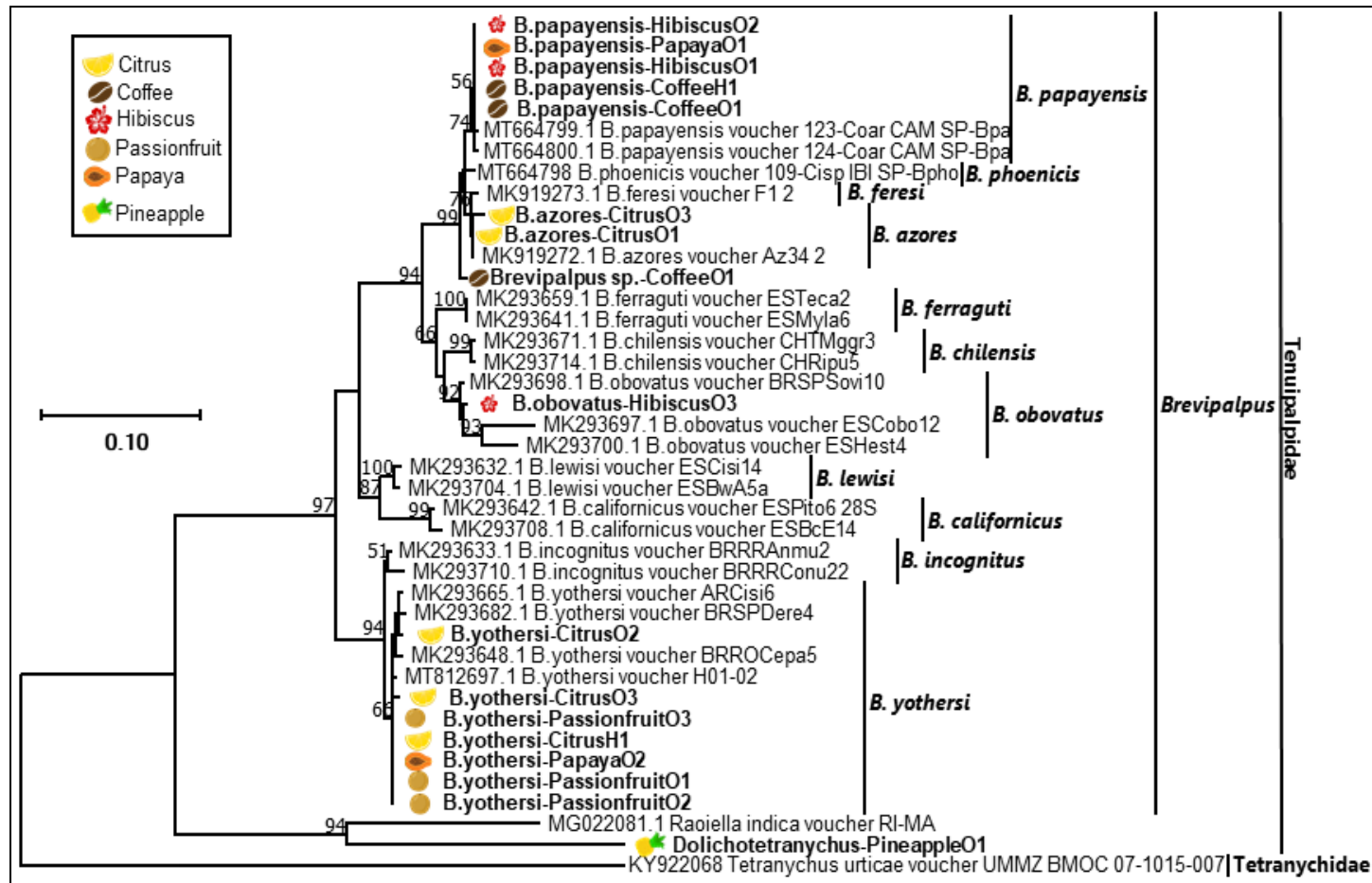


Figure 5.5 Phylogenetic relationships using partial 28S rRNA gene sequences from several tenuipalpid mites classified within *Brevipalpus*, *Raoiella* and *Dolichotetranychus*. Relationships were based on a multiple nucleotide sequence alignment using CLUSTAL and inferred using the Maximum Likelihood algorithm implemented in MEGA 7.0.25. Bootstrap values greater than 50 are shown above the branches after 1,000 repetitions. No *Dolichotetranychus* 28S rRNA sequence was found in the GenBank database. A homolog partial 28S rRNA gene sequence from *Tetranychus urticae* (Tetranychidae) was used as an outgroup. The scale at the left indicates the number of substitutions per given branch length. Tenuipalpid mite samples from in this study are bold and placed next to the respective icon of the plant/fruit from which they were collected.

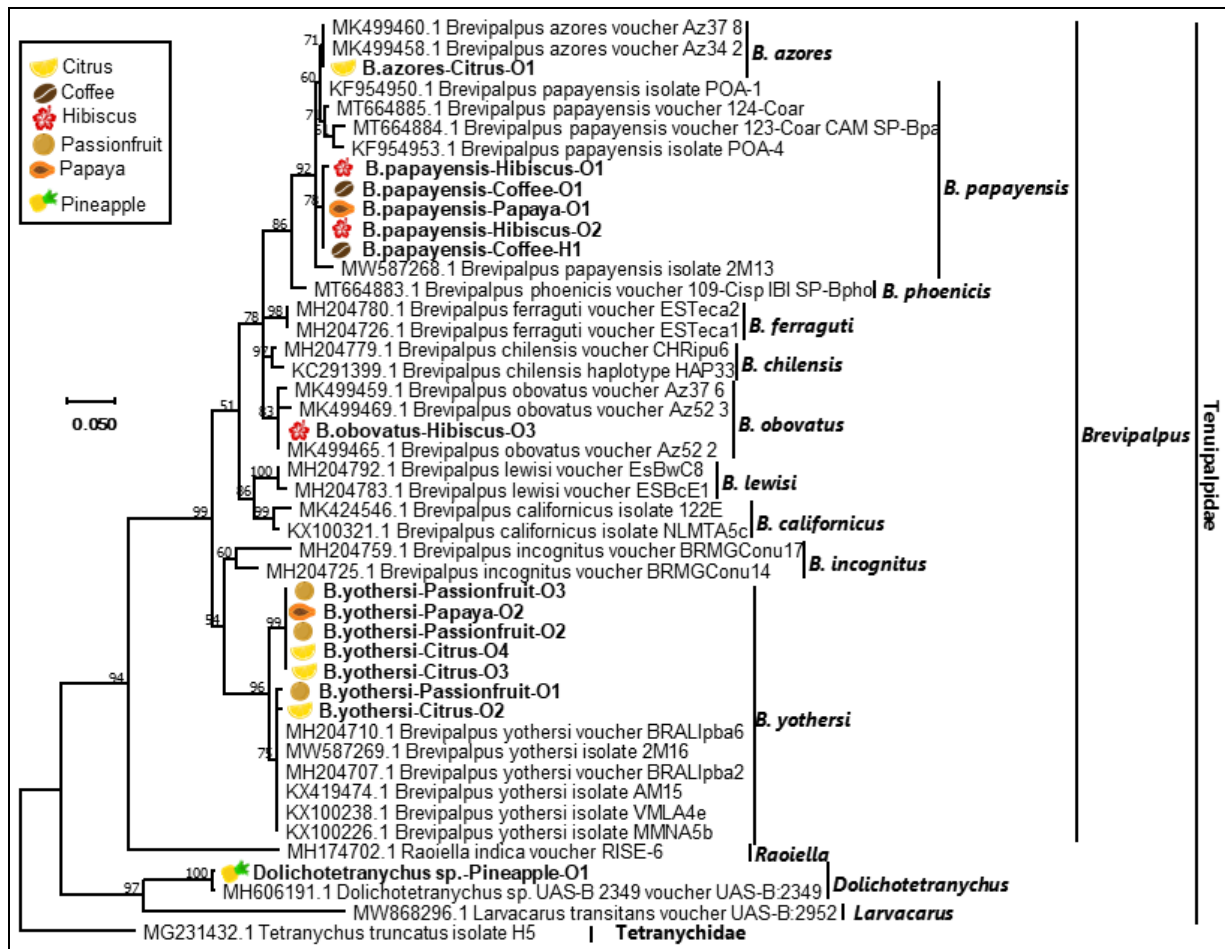


Figure 5.6 Phylogenetic relationships using partial cytochrome oxidase I (COI) gene sequences from several tenuipalpid mites classified as *Brevipalpus*, *Raioella*, *Dolichotetranychus* and *Larvacarus*. Relationships were based on a multiple nucleotide sequence alignment using CLUSTAL and inferred using the Maximum Likelihood algorithm implemented in MEGA 7.0.25. Bootstrap values greater than 50 are shown above the branches after 1,000 repetitions. A homolog partial COI gene sequence from *Tetranychus truncatus* (Tetranychidae) was used as an outgroup. The scale at left indicates the number of substitutions per given branch length. Tenuipalpid mite samples used in this study are bold and placed next to the respective icon of the plant/fruit from which they were collected.

5.3.5.2 Phylogenetic relationships of the putative new negevirus and kitavirids found within the tenuipalpid mite-associated virome

Phylogenetic relationships of the kitavirids and putative new negevirus were inferred using multiple protein sequence alignments of the RdRp, HEL, and MET protein domains. Although similar tree topologies and evolutionary relationships were inferred from these three protein domains (Figures 5.7, 5.8

and 5.9), a few notable differences were found. The kitavirids, CiLV-C2H and HGSV-2, were grouped within a clade containing cileviruses, cile-like viruses and higrevirus, in the three conserved protein domains phylogenies. They were grouped with the previously characterized isolates of the same virus species (CiLV-C2, ATW76030; HGSV-2, AER13445). Similarly, the putative new negevirus found in the mite sample hibiscus O3: *Brevipalpus*-associated negevirus, clustered with Fort Crockett virus (YP009351834) in the three phylogenies. The clade containing the two previously mentioned negevirus shared a common evolutionary origin with the recently reported group ‘aphiglyvirus’ (Kondo et al., 2020) within the unofficial negevirus taxon (Figures 5.7, 5.8 and 5.9).

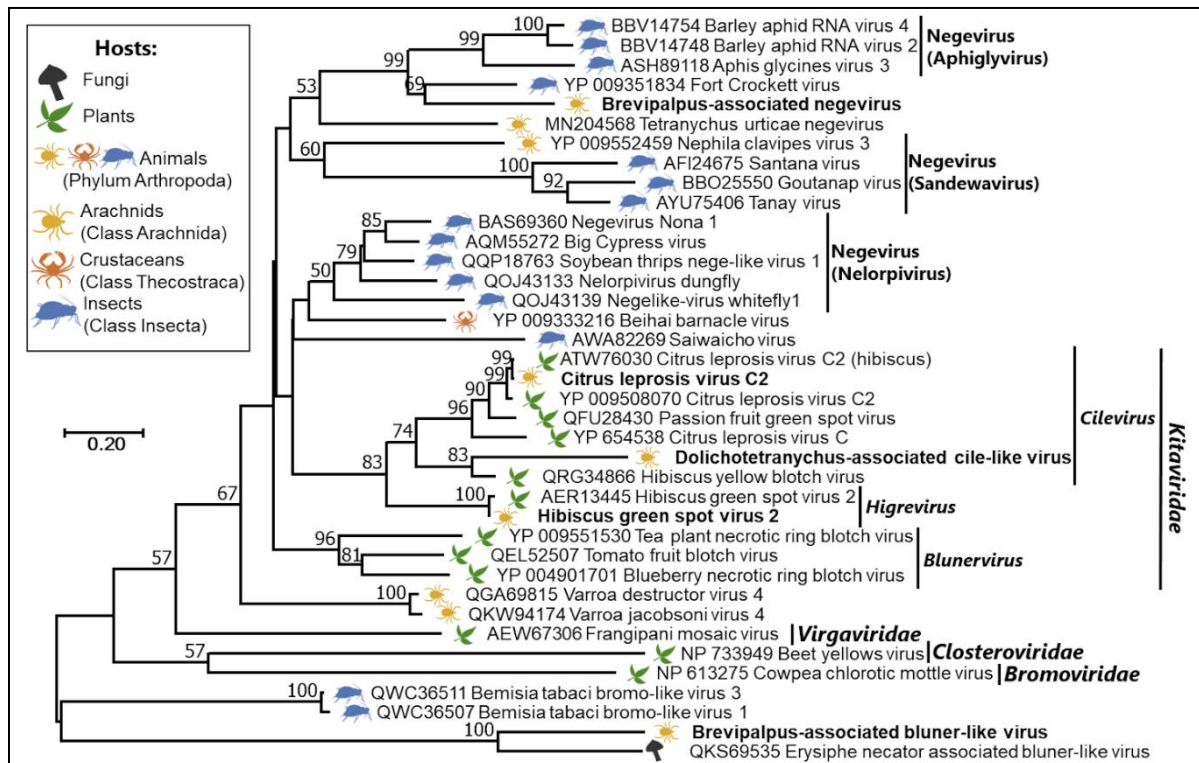


Figure 5.7 Phylogenetic relationships inferred using the RNA-dependent RNA polymerase (RdRp) conserved domain found in the contig sequences of the putative new negevirus and kitavirids in tenuipalpid mite samples. The specific mite sample that each putative new virus was detected from is detailed in Table 5.2. *Brevipalpus*-associated bluner-like virus corresponds to the RdRp domain present in the *Brevipalpus*-associated bluner-like virus contig 2 (RNA 2) (Figure 5.4).

Dolichotetranychus-associated cile-like virus clustered within the polyphyletic *Kitaviridae* clade in the RdRp phylogeny. This virus was grouped with HYBV in a clade outbranching from a clade containing CiLV-C, CiLV-C2 and passion fruit green spot virus (PfGSV) (Figure 5.7). Moreover, the *Dolichotetranychus*-associated negevirus was placed in a divergent monotypic clade that was more related

to bromovirids, virgavirids and to Beihai charybdis crab virus 1 (YP009333242) in the MET phylogeny (Figure 5.9). Finally, no clear evolutionary relationships were inferred for *Brevipalpus*-associated bluner-like virus. The RdRp and MET phylogenies suggested the virus is more closely related to other insect-specific viruses, *Bemisia tabaci* bromo-like viruses and to *Erysiphe necator* associated bluner-like virus, a putative virus infecting the fungus causing grapevine powdery mildew. All these previously mentioned viruses were placed in a clade that outbranched from negevirus and any other virus classified within the order *Martellivirales* that were used in the phylogeny, i.e. kitavirids, bromovirids, closterovirids and virgavirids (Figure 5.7). Whereas the HEL phylogeny indicated that this virus was more related to closterovirids, bromovirids and virgavirids. All these previously mentioned viruses shared an evolutionary origin with nelorpiviruses and blunerviruses (Figure 5.8).

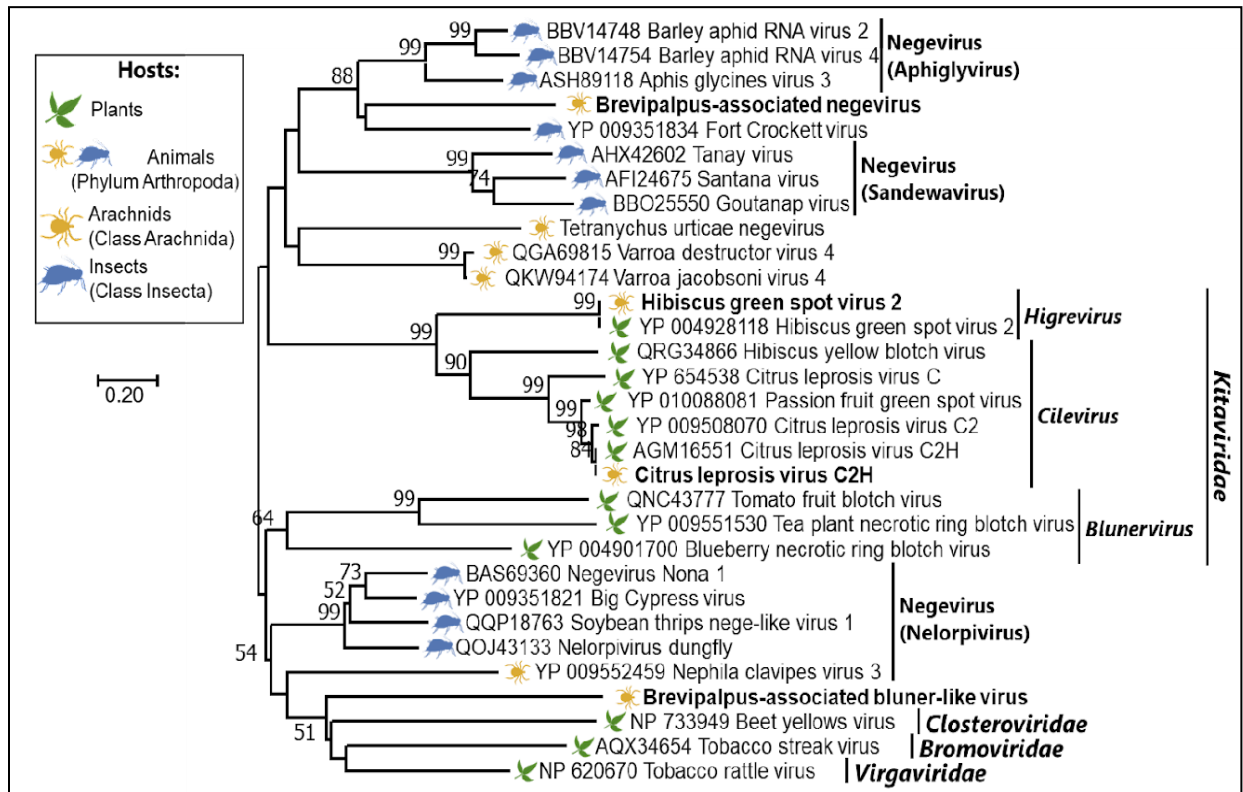


Figure 5.8 Phylogenetic relationships inferred using helicase (HEL) conserved domain found in the contig sequences of the putative new negevirus and kitavirids in tenuipalpid mite samples. The specific mite sample that each putative new virus was detected from is detailed in Table 5.2. *Brevipalpus*-associated bluner-like virus corresponds to the RdRp domain present in the *Brevipalpus*-associated bluner-like virus contig 1 (RNA 1) (Figure 5.4).

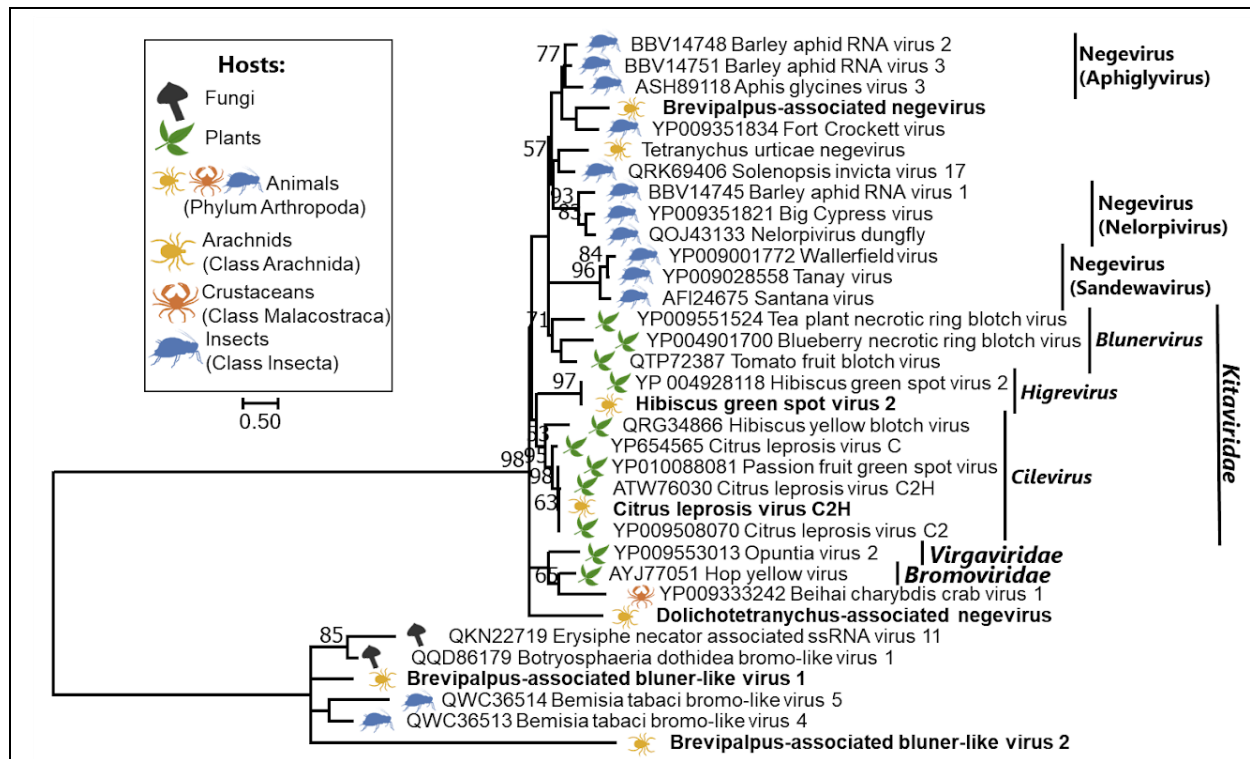


Figure 5.9 Phylogenetic relationships inferred using the methyltransferase (MET) conserved domain found in the contig sequences of the putative new negeviruses and kitavirids in tenuipalpid mite samples. The specific mite sample that each putative new virus was detected from is detailed in Table 5.2. Brevipalpus-associated bluner-like virus 1 and 2 correspond to the MET domains present in the Brevipalpus-associated bluner-like virus contig 1 (RNA 1) and 2 (RNA 2), respectively (Figure 5.4).

5.4 DISCUSSION

This study describes the characterization of kitavirus-related viruses within the virome found in flat mite specimens that were collected from several hosts on Oahu and Hawaii Islands.

Using the TNA extraction protocol described here, TNA was successfully purified from as few as 10 mite specimens. Using a CTAB-based TNA extraction protocol as detailed by Li et al. (2008), with a further purification step using a column-based method was critical for retrieving small amounts of high-quality TNA obtained from the mite samples. Although ribodepleted total RNA is currently considered one of the best templates, if not the best, for transcriptomics and virome studies in plant and arthropod samples (Villamor et al., 2019; Fauver et al., 2019), TNA extracts proved useful for studying the virome present in

the mite samples in this study. Although the kit used in this study for library construction includes a ribodepletion step, abundant rRNA sequences were retrieved from the raw dataset (data not shown). Current ribosomal depletion methods are designed for model animals which may not effectively work on non-model animals. In future studies, ribosomal RNA depletion from RNA or TNA samples from non-model animal hosts may better succeed by using class- or family-specific probes and a reverse-transcription/RNAse-H based protocol (Fauver et al., 2019). Previous HTS studies using ribodepleted total RNA as a template have established the suggested minimum sequencing depth to be between 0.5 – 10 M of reads for virus diagnostics and discovery (Massart et al., 2018; Bester et al., 2021; Huang et al., 2019; Malapi-Wight et al., 2021). Therefore, the high sequencing depth used in this study which ranged from ~65-91 M reads (Table 5.1), may have mitigated the inefficient ribodepletion. Regardless, the library construction method used in this study, the number of raw reads obtained per dataset, and bioinformatic analyses allowed for characterization of the flat mite virome, including the BTV-C and BTV-C-like viruses that were identified.

After the removal of as many reads with tenuipalpid origin as possible, a variable number of non-host reads (~21 – 62 M of reads) were *de novo* assembled (Table 5.1). Although less than 0.5% of the non-host reads had a viral origin, they were *de novo* assembled into contigs that represented, in some cases, the near-complete genome of CiLV-C2H, HGSV-2, PRSV, and several putative new virus species classified within the *Picornavirales* order, *Narnaviridae*, *Tombusviridae*, *Kitaviridae*, *Solemoviridae* and *Potyviridae* families, and the unofficial negevirus taxon, (Figures 5.2, 5.3 and 5.4 and data not shown). Picornavirids, tombusvirids, narnavirids, reovirids, solemovirids, and negevirus have been similarly characterized from other arthropods and insects (Debat 2017; Guo et al., 2021; Huang et al., 2021). The presence of the putative new viruses was validated in at least one mite sample using RT-PCR assays, except for one narnavirus and two picornaviruses which could not be detected in the hibiscus mite samples (Table 5.2). It is possible that the concentration of those putative new viruses was below the sensitivity achieved using RT-PCR assays. Therefore, RT-qPCR assays may have been suitable for detecting the low concentration of these viruses (Osman et al., 2016). Alternatively, it is also possible that the contig sequences of those putative new viruses may be contamination originated during the library preparation process or during the *in-silico* demultiplexing of the raw reads, both of which have been recognized as the common source of contamination in HTS (Lee et al., 2016; Lusk 2014). Although BTV-N related viruses, namely rhabdovirids, have been characterized from other arthropods including ticks and mites (Sameroff et al., 2019; Guo et al., 2021), no rhabdovirid or negative-sense RNA virus was found in any of the datasets generated in this study.

Picornavirid sequences were found in three out of the four *Brevipalpus* derived viral datasets coming from citrus, hibiscus, and papaya hosts (Figures 5.2 and 5.3), and were by far the most abundant source of virus sequence in the citrus dataset. Previously, it was found through data mining that the virome of nephilid spiders was similarly predominated by picornavirids (Debat 2017). Considering picornavirids in arthropods have been reported to cause from no symptom to premature mortality and paralysis (van Oers 2010; Valles et al., 2017), molecular and biological characterization studies of these picornavirids infecting *brevipalpus* mites are required to examine a possible biological control option for these mites.

Near-complete genomes of CiLV-C2H were retrieved from the passionfruit and papaya mite datasets (Figure 5.4). CiLV-C2H presence was confirmed in the papaya O2 and passionfruit O1 and O2 mite samples using RT-PCR assays (Table 5.2). Although viruliferous *B. yothersi* mites carrying CiLV-C2H were collected from papaya leaves, no obvious viral-like symptoms were observed. This suggests the incapability of CiLV-C2H to infect papaya or obvious symptoms may be only visible once leaves senesce. The lack of obvious symptoms in non-senescent tissue has been previously reported for other BTVs infecting passionfruit, hibiscus, and citrus (Ramos-Gonzalez et al., 2020; Melzer et al., 2012; Melzer et al., 2013; Roy et al., 2015). Barcoding of these mite samples using the 28S rRNA and COI genes and phylogenetic analyses suggested their identity to be *B. yothersi* (Table 5.1, Supplementary Table 5.1, and Figures 5.5 and 5.6). It has been previously demonstrated the ability of *B. yothersi* as the natural vector of CiLV-C2 (Roy et al., 2013). Therefore, the detection of CiLV-C2H using RT-PCR assays and HTS suggest the ability of *B. yothersi* to transmit this strain of CiLV-C2 as well. However, proper transmission assays of this divergent strain of CiLV-C2, CiLV-C2H, using *B. yothersi* mites are required.

A near-complete genome of HGSV-2 was retrieved from the hibiscus mite dataset (Figure 5.4). The genomic organization was found to be identical to that obtained from hibiscus and citrus HGSV-2 isolates from Oahu and Maui Islands, respectively (see Chapter IV). The presence of HGSV-2 was confirmed in the hibiscus O1 sample using RT-PCR assays (Table 5.2). Barcoding of this mite sample using the 28S rRNA and COI genes and phylogenetic analyses suggested its identity to be *B. papayensis* mites (Table 5.1, Supplementary 5.1 and Figures 5.5 and 5.6). Transmission assays of HGSV-2 using mites from a *B. azores* colony, which are detailed in Chapter IV, demonstrated the ability of this *Brevipalpus* species to transmit HGSV-2, although with low efficiency. Considering that the *B. papayensis* mites that comprised the hibiscus O1 sample were collected from hibiscus plants with a history of HGSV-2 symptoms at the UH Manoa campus, one can hypothesize that both *Brevipalpus* species may be able to transmit HGSV-2. Considering the close evolutionary relationship between *B. papayensis* and *B. azores*, which are placed in

the same phylogenetic clade of 28S rRNA and COI phylogenies (Figures 5.5 and 5.6), this hypothesis seems plausible. However, proper transmission assays of HGSV-2 using *B. papayensis* mites are required. The molecular relatedness of *B. papayensis* and *B. azores* is further supported by the highly morphological resemblance which complicates mite identification (Beard et al., 2015; Tassi et al., 2018). Interestingly, several contig sequences which encompassed the genome of PRSV were also found in the papaya mite dataset. The presence of PRSV was confirmed in sample papaya O2 using RT-PCR assays (Table 5.2). These results demonstrate, at minimum, PRSV ingestion by *Brevipalpus yothersi* mites. Among members of the *Potyviridae* family, rymoviruses, poaceviruses, and tritimoviruses are transmitted by eriophyid mites in a semi-persistent manner (Wylie et al., 2017). Therefore, it may be worth evaluating the ability of flat mites to transmit PRSV and other potyvirids.

Near-complete genomes of a putative new negevirus, designated Brevipalpus-associated negevirus, and a putative new bluner-like virus, designated Brevipalpus-associated bluner-like virus, were also retrieved from the hibiscus mite dataset. Furthermore, contig sequences representing partial genomic sequences of a putative new negevirus, designated Dolichotetranychus-associated negevirus, and a putative new cile-like virus, designated Dolichotetranychus-associated cile-like virus, were retrieved from the pineapple-coffee mite dataset (Figure 5.4). The presence of these putative new viruses was confirmed using RT-PCR assays. Brevipalpus-associated negevirus (~9.6 Kb), detected in the sample hibiscus O3 (Table 5.2), presented the genomic organization and protein conserved domains typical of negeviruses (Vasilakis et al., 2013; Nunes et al 2017). Considering the low protein identity inferred using BLASTx searches, and the divergence from other negeviruses, including Fort Crocket virus and aphiglyviruses in the RdRp, HEL and MET phylogenies (Figures 5.7 - 5.9), Brevipalpus-associated negevirus is a new negevirus that most closely resembles aphiglyviruses. Negevirus genomes typically contain 3 ORFs that code for a replication-associated polyprotein, a putative glycoprotein, and a membrane-bound protein containing the SP24 conserved domain. The replication-associated polyprotein and the SP24 protein show sequence and evolutionary relationships to the protein homologs encoded by kitavirids. Furthermore, the putative glycoprotein possesses structural features including transmembrane domains and signal peptides which are also present in the putative glycoprotein of the cilevirus p61 (Kuchibhatla et al., 2014). Although it has been speculated that negeviruses and kitavirids share a common ancestor that may have colonized flat mites (Freitas-Astúa et al., 2018; Ramos-González et al., 2020; Quito-Avila et al., 2020), no negevirus had been found infecting *Brevipalpus* to date. Therefore, the identification and partial characterization of Brevipalpus-associated negevirus in this study support this hypothesis considering this virus and kitavirids share a putative common ancestor in the RdRp, HEL, and MET phylogenies (Figures 5.7 - 5.9). Kitavirid ancestors may have originated from arthropod-infecting nege-like viruses through genome

segmentation, recombination, and acquisition of genes for plant cell movement and viral suppression of gene silencing from plant viruses. Gene acquisitions most likely came from plant RNA viruses within the order *Martellivirales* (Ramos-González et al., 2021; Dolja et al., 2020).

Brevipalpus-associated bluner-like virus (RNA 1, 3,511 bp; RNA 2, 3,585 bp), detected in the sample hibiscus O1 (Table 5.2), presented a genomic organization that resembles that of blunerviruses with one notable difference. RNA 1 and RNA 2 of blunerviruses encode for polyproteins required for virus replication. RNA 1-coded polyproteins contain MET and HEL conserved domains while RNA 2-coded polyproteins contain HEL and RdRp conserved domains (Figure 5.4) (Quito-Avila et al., 2020). Similar to the replication-associated polyproteins of blunerviruses, the replication-associated polyproteins of Brevipalpus-associated bluner-like virus contained MET, HEL, and RdRp conserved domains. However, the RNA 2-coded polyprotein of Brevipalpus-associated bluner-like virus contains a MET rather than a HEL conserved domain (Figure 5.4). Considering the low protein identity inferred using BLASTx searches, and the divergence from any other virus classified within the *Martellivirales* order in the RdRp, HEL and MET phylogenies (Figures 5.7 - 5.9), Brevipalpus-associated bluner-like virus is a new virus likely representing a new clade within *Martellivirales*. Considering the speculated transmission of blunerviruses by eriophyid mites (Burkle et al., 2012; Robinson et al., 2012), examination of the virome present in eriophyid mites is necessary to evaluate the presence of negevirus and bluner-like viruses to further corroborate the evolutionary scenario described above. Recently, Koonin et al. (2021) defined the virosphere, “a dynamic entity with extensive evolutionary traffic across its boundaries”, to be composed of the orthovirosphere and perivirosphere. The former is composed of viral agents coding for replication-associated components and structural proteins encapsidating their genome whereas the latter is composed of viral agents coding only for replication-associated components. It is possible that Brevipalpus-associated bluner-like virus is part of the perivirosphere within the *Martellivirales* order considering no CP gene was found within its genome. However, it cannot be discarded that an additional genomic segment coding for a putative CP gene, but not presenting homology detectable with the methods used in this study may have also been present in the HTS data. Remarkably, abundant small ORFs encoding orphan proteins containing transmembrane domains have been found among the genomes of negevirus and kitavirids (Kuchibhatla et al., 2014; Ramos- González et al., 2021). This same scenario was evident in the genomes of Brevipalpus-associated negevirus and Brevipalpus-associated bluner-like virus (Figure 5.4). The hypothesized function of these orphan transmembrane-located small proteins might be to provide flexible mechanisms to regulate cellular activities and increase virus fitness (Dimaio, 2014).

Finally, the partial sequences of Dolichotetranychus-associated negevirus and Dolichotetranychus-associated cile-like virus, both detected in the sample pineapple O1 (Table 5.2), contained MET and RdRP conserved domains, respectively (Figure 5.4). Although the low protein identity to negevirus and kitavirid homologs and the evolutionary relationships that were inferred from the MET and RdRp phylogenies (Figures 5.7 and 5.9) suggest these sequences may be originated from putative new viruses, further work is required that fully characterizes these viruses. Considering the low read number that mapped to the sequences of both of these putative new viruses (Figure 5.3), it is possible these viruses were rather infecting a small number of *Dolichotetranychus* mites that comprised sample pineapple O1. The characterization of Dolichotetranychus-associated cile-like virus and evaluation of virus colonization in pineapple tissue is of great interest for the pineapple industry considering the cile-like virus nature and the importance of cileviruses in causing plant diseases of economic significance. Last, this study established a baseline for a surveillance method on flat mites and look for potential BTVs that might become agriculturally important pathogens. Considering the limited number of samples, very limited number of hosts, and broad host range of flat mites, tremendous opportunities exist to characterize other BTVs and BTV related viruses in populations of flat mites around the world.

5.5 LITERATURE CITED

- Altschul, S.F., Madden, T.L., Schäffer, A.A., Zhang, J., Zhang, Z., Miller, W., and Lipman, D.J. 1997. Gapped BLAST and PSI-BLAST: a new generation of protein database search programs. *Nucleic Acids Res.* 25:3389–3402.
- Arif, M. & Ochoa-Corona, F. (2013). Comparative assessment of 5' A/T-rich overhang sequences with optimal and sub-optimal primers to increase PCR yields and sensitivity. *Mol. Biotechnol.* 55, 17-26. doi: 10.1007/s12033-012-9617-5
- Bankevich, A., Nurk, S., Antipov, D., Gurevich, A. A., Dvorkin, M., Kulikov, A. S., Lesin, V. M., Nikolenko, S. I., Pham, S., Prjibelski, A. D., Pyshkin, A. V., Sirotkin, A. V., Vyahhi, N., Tesler, G., Alekseyev, M. A., & Pevzner, P. A. (2012). SPAdes: a new genome assembly algorithm and its applications to single-cell sequencing. *Journal of computational biology: a journal of computational molecular cell biology*, 19(5), 455–477. <https://doi.org/10.1089/cmb.2012.0021>
- Beard, J. J., Ochoa, R., Bauchan, G. R., Trice, M. D., Redford, A. J., Walters, T. W., et al. (2013). *Flat Mites of the World*, 2 Edn. Fort Collins, CO: CPHST.
- Beard, J. J., Ochoa, R., Braswell, W. E., and Bauchan, G. R. (2015). *Brevipalpus phoenicis* (Geijskes) species complex (Acari: Tenuipalpidae)-a closer look. *Zootaxa* 3944:1-67.
- Bester, R., Cook, G., Breytenbach, J.H.J., Steyn, C., De Bruyn, R., Maree, H.J. (2021). Towards the validation of high-throughput sequencing (HTS) for routine plant virus diagnostics: measurement of variation linked to HTS detection of citrus viruses and viroids. *Virology* 18, 61. <https://doi.org/10.1186/s12985-021-01523-1>
- Bolger, A. M., Lohse, M., & Usadel, B. (2014). Trimmomatic: a flexible trimmer for Illumina sequence data. *Bioinformatics (Oxford, England)*, 30(15), 2114–2120. <https://doi.org/10.1093/bioinformatics/btu170>
- Burkle, C., Olmstead, J.W., Harmon, P.F. (2012). A potential vector of Blueberry necrotic ring blotch virus and symptoms on various host genotypes. *Phytopathol* 102:S4.17.
- Debat, H.J. (2017). An RNA Virome Associated to the Golden Orb-Weaver Spider *Nephila clavipes*. *Front. Microbiol.* 8:2097. doi: 10.3389/fmicb.2017.02097
- Dey, K.K., Sugikawa J., Kerr, C., Melzer, M.J. (2019) Air potato (*Dioscorea bulbifera*) plants displaying virus-like symptoms are co-infected with a novel potyvirus and a novel ampelovirus. *Virus Genes* 55(1):117-121. doi: 10.1007/s11262-018-1616-6.
- Dimaio, D. (2014). Viral miniproteins. *Annu. Rev. Microbiol.* 68, 21–43. doi: 10.1146/annurev-micro-091313-103727
- Dolja, V.V., Krupovic, M., Koonin, E.V. (2020). Deep Roots and Splendid Boughs of the Global Plant Virome. *Annu. Rev. Phytopathol.* 58(1). doi:10.1146/annurev-phyto-030320-041346
- Fauver, J. R., Akter, S., Morales, A., Black, W. C., 4th, Rodriguez, A. D., Stenglein, M. D., Ebel, G. D., & Weger-Lucarelli, J. (2019). A reverse-transcription/RNase H based protocol for depletion of mosquito ribosomal RNA facilitates viral intrahost evolution analysis, transcriptomics and pathogen discovery. *Virology* 528, 181–197. <https://doi.org/10.1016/j.virol.2018.12.020>

- Freitas-Astúa, J., Ramos-González, P.L., Arena, G.D., Tassi, A.D., & Kitajima, E.W. (2018). *Brevipalpus*-transmitted viruses: parallelism beyond a common vector or convergent evolution of distantly related pathogens? *Curr Opin Virol* 33: 66–73. <https://doi.org/10.1016/j.coviro.2018.07.010>
- Gerson, U. (2008). The Tenuipalpidae: an under-explored family of plant-feeding mites. *Systematic and Applied Acarology*, 13(2), 83. doi:10.11158/saa.13.2.1
- Guo, L., Lu, X., Liu, X., Li, P., Wu, J., Xing, F., Peng, H., Xiao, X., Shi, M., Liu, Z., Li, X.-D., Guo, D. (2021). Metatranscriptomic analysis reveals the virome and viral genomic evolution of medically important mites. *J Virol*. 95(7):e01686-20. doi: 10.1128/JVI.01686-20.
- Huang, B., Jennison, A., Whiley, D. McMahon, M., Hewitson, G., Graham, R., De Jong, A., Warrilow, D. (2019). Illumina sequencing of clinical samples for virus detection in a public health laboratory. *Sci Rep* 9, 5409. <https://doi.org/10.1038/s41598-019-41830-w>
- Huang, X. & Miller, W. (1991). A time-efficient, linear-space local similarity algorithm. *Adv. Appl. Math.* 12, 337-357.
- Huang, H.J., Ye, Z.X., Wang, X. Yan, X.-T., Zhang, Y., He, Y.-J., Qi, Y.-H., Zhang, X.-D., ... Li, J.-M. (2021). Diversity and infectivity of the RNA virome among different cryptic species of an agriculturally important insect vector: whitefly *Bemisia tabaci*. *npj Biofilms Microbiomes* 7, 43 <https://doi.org/10.1038/s41522-021-00216-5>
- Kallies, R., Kopp, A., Zirkel, F., Estrada, A., Gillespie, T. R., Drosten, C., Junglen, S. (2014). Genetic characterization of goutanap virus, a novel virus related to negeviruses, cileviruses and higreviruses. *Viruses* 6, 4346–4357. doi: 10.3390/v6114346
- Kearse, M., Moir, R., Wilson, A., Stones-Havas, S., Cheung, M., Sturrock, S., Buxton, S., Cooper, A., Markowitz, S., Duran, C., Thierer, T., Ashton, B., Meintjes, P., and Drummond, A. 2012. Geneious Basic: An integrated and extendable desktop software platform for the organization and analysis of sequence data. *Bioinformatics* 28:1647–1649.
- Kitajima, E.W., Chagas, C.M., Rodrigues, J.C.V. (2003). *Brevipalpus*-transmitted plant virus and virus-like diseases: cytopathology and some recent cases. *Exp Appl Acarol* 30: 135-160.
- Kondo, H., Fujita, M., Hisano H, Hyodo K, Andika IB and Suzuki N (2020) Virome Analysis of Aphid Populations That Infest the Barley Field: The Discovery of Two Novel Groups of Nege/Kita-Like Viruses and Other Novel RNA Viruses. *Front. Microbiol.* 11:509. doi: 10.3389/fmicb.2020.00509
- Kondo, H., Maeda, T., & Tamada, T. (2003). Orchid fleck virus: *Brevipalpus californicus* mite transmission, biological properties and genome structure. *Experimental and Applied Acarology* 30(1-3): 215-223. <https://doi.org/10.1023/B:APPA.0000006550.88615.10>
- Koonin, E.V., Dolja, V.V., Krupovic, M., Kuhn, J.H. (2021). Viruses Defined by the Position of the Virosphere within the Replicator Space. *Microbiol Mol Biol Rev.* 85(4):e0019320. doi: 10.1128/MMBR.00193-20.
- Krogh, A., Larsson, B., von Heijne, G., & Sonnhammer, E.L.L. (2001). Predicting transmembrane protein topology with a hidden Markov model: Application to complete genomes. *J. Mol. Biol.* 305(3), 567-580.

- Kubo, K.S., Novelli, V.M., Bastianel, M., Locali-Fabris, E.C., Antonioli-Luizon, R., Machado, M.A., Freitas-Astúa, J. (2011). Detection of Brevipalpus-transmitted viruses in their mite vectors by RT-PCR. *Exp Appl Acarol.* 54(1):33-9. doi: 10.1007/s10493-011-9425-9.
- Kuchibhatla, D.B., Sherman, W.A., Chung BY, Cook S, Schneider G, Eisenhaber B, Karlin DG. (2014). Powerful sequence similarity search methods and in-depth manual analyses can identify remote homologs in many apparently "orphan" viral proteins. *J Virol.* 88(1):10-20. doi: 10.1128/JVI.02595-13.
- Kumar, S., Stecher, G. & Tamura, K. (2016). MEGA 7: Molecular Evolutionary Genetics Analysis version 7.0 for bigger datasets. *Mol. Biol. Evol.* 33, 1870-1874.
- Langmead, B., Salzberg, S. (2012). Fast gapped-read alignment with Bowtie 2. *Nat Methods* 9, 357–359. <https://doi.org/10.1038/nmeth.1923>
- Lee, H., Lee, C., Tang, J.T., Loh, T.P., Koay, E.S.-C. (2016). Contamination-controlled high-throughput whole genome sequencing for influenza A viruses using the MiSeq sequencer. *Sci Rep* 6, 33318 <https://doi.org/10.1038/srep33318>
- Li, R., Mock, R., Huang, Q., Abad, J., Hartung, J., and Kinard, G. (2008). A reliable and inexpensive method of nucleic acid extraction for the PCR-based detection of diverse plant pathogens. *J. Virol. Methods* 154, 48–55. doi: 10.1016/j.jviromet.2008.09.008
- Lusk, R.W. (2014). Diverse and Widespread Contamination Evident in the Unmapped Depths of High Throughput Sequencing Data. *PLoS ONE* 9(10): e110808. <https://doi.org/10.1371/journal.pone.0110808>
- Malapi-Wight, M., Adhikari, B., Zhou, J., Hendrickson, L., Maroon-Lango, C.J., McFarland, C., Foster, J.A., Hurtado-Gonzales, O.P. (2021). HTS-Based Diagnostics of Sugarcane Viruses: Seasonal Variation and Its Implications for Accurate Detection. *Viruses* 13(8):1627. doi: 10.3390/v13081627.
- Massart, S., Chiumenti, M., De Jonghe, K., Glover, R., Haegeman, A., Koloniuk, I., Kominek, P., Kreuze, J., ... Candresse, T. (2018). Virus detection by high-throughput sequencing of small RNAs: large scale performance testing of sequence analysis strategies. *Phytopathology*. doi:10.1094/phyto-02-18-0067-r
- Melzer, M.J., Sether, D.M., Borth, W.B., Hu, J.S. (2012). Characterization of a virus infecting *Citrus volkameriana* with citrus leprosis-like symptoms. *Phytopathol* 102(1): 122-127. doi: 10.1094/PHYTO-01-11-0013.
- Melzer, M. J., Simbajon, N., Carillo, J., Borth, W. B., Freitas-Astúa, J., Kitajima, E. W., Neupane, K. R., & Hu, J. S. (2013). A cilevirus infects ornamental hibiscus in Hawaii. *Archives of virology* 158(11), 2421–2424. <https://doi.org/10.1007/s00705-013-1745-0>
- Mironov, S. V., Dabert, J., and Dabert, M. (2012). A new feather mite species of the genus *Proctophyllodes* Robin, 1877 (Astigmata: Proctophyllodidae) from the long-tailed tit *Aegithalos caudatus* (Passeriformes Aegithalidae)-morphological description with DNA barcode data. *Zootaxa* 3253, 54–61.
- Navajas, M., Fournier, D., Lagnel, J., Gutierrez, J., and Boursot, P. (1996). Mitochondrial COI sequences in mites: evidence for variations in base composition. *Insect Mol. Biol.* 5, 281–285. doi: 10.1111/j.1365-2583.1996.tb00102.x
- Nunes, M.R.T., Contreras-Gutierrez, M.A., Guzman, H., Martins, L.C., Barbirato, M.F., Savit, C., Balta, V., ... Tesh, R.B. (2017). Genetic characterization, molecular epidemiology, and phylogenetic

relationships of insect-specific viruses in the taxon Negevirus. *Virology* 504:152-167. doi: 10.1016/j.virol.2017.01.022.

Nunes, M. A., de Carvalho Mineiro, J. L., Rogerio, L. A., Ferreira, L. M., Tassi, A., Novelli, V. M., Kitajima, E.W., Freitas-Astúa, J. (2018). First Report of *Brevipalpus* papayensis as Vector of Coffee ringspot virus and Citrus leprosis virus C. *Plant Dis* 102(5): 1046–1046. doi:10.1094/pdis-07-17-1000-pdn

Olmedo-Velarde, A., Park, A.C., Sugano, J., Uchida, J.Y., Kawate, M., Borth, W.B., Hu, J.S., Melzer, M.J. (2019) Characterization of Ti Ringspot-Associated Virus, a Novel Emaravirus Associated with an Emerging Ringspot Disease of *Cordyline fruticosa*. *Plant Dis*. 103(9):2345-2352. doi: 10.1094/PDIS-09-18-1513-RE.

Osman, F., Al Rwahnih, M., Rowhani, A. (2016). Real-time RT-qPCR detection of cherry rasp leaf virus, cherry green ring mottle virus, cherry necrotic rusty mottle virus, cherry virus A and apple chlorotic leaf spot virus in stone fruits. *J. Plant Pathol.* 99, 279–285.

Potter, S.C., Luciani, A., Eddy, S.R., Park, Y., Lopez, R. & Finn, R.D. (2018). HMMER web server: 2018 update. *Nucleic Acids Res.* 46(W1), W200-W204. doi: 10.1093/nar/gky448

Quito-Avila, D.F., Freitas-Astúa, J., and Melzer, M.J. (2021). Bluner-, Cile-, and Higreviruses (Kitaviridae). *Encycl. Virol.* 2021, 247–251. doi: 10.1016/B978-0-12-809633-8.21248-X

Ramos-González, P.L., Chabi-Jesus, C., Guerra-Peraza, O., Tassi, A.D., Kitajima, E.W., Harakava, R., Salaroli, R.B., Freitas-Astúa, J. (2017) Citrus leprosis virus N: A New Dichorhavirus Causing Citrus Leprosis Disease. *Phytopathol* 107(8):963-976. doi: 10.1094/PHYTO-02-17-0042-R.

Ramos-González, P.L. Dos Santos, G.F., Chabi-Jesus, C., Harakava, R., Kitajima, E.W., Freitas-Astúa, J. (2020). Passion Fruit Green Spot Virus Genome Harbors a New Orphan ORF and Highlights the Flexibility of the 5'-End of the RNA2 Segment Across Cileviruses. *Front. Microbiol.* 11:206. doi: 10.3389/fmicb.2020.00206.

Ramos-González, P.L., Pons, T., Chabi-Jesus, C., Arena, G.D. and Freitas-Astua, J. (2021). Poorly Conserved P15 Proteins of Cileviruses Retain Elements of Common Ancestry and Putative Functionality: A Theoretical Assessment on the Evolution of Cilevirus Genomes. *Front. Plant Sci.* 12:771983. doi: 10.3389/fpls.2021.771983

Robinson, T.S., Brannen, P.M., Deom, C.M. (2012). Blueberry necrotic ring blotch: A new disorder of southern highbush blueberries. *Phytopathol* 102:S4.101.

Rodrigues, J.C.V., Childers, C.C. (2013). *Brevipalpus* mites (Acari: Tenuipalpidae): vectors of invasive, non-systemic cytoplasmic and nuclear viruses in plants. *Exp Appl Acarol* 59: 165-175.

Roy, A., Choudhary, N., Guillermo, L.M., Shao, J., Govindarajulu, A., Achor, D., Wei, G., Picton, D.D., Levy, L., Nakhla, M.K., Hartung, J.S., Brlansky, R.H. (2013). A novel virus of the genus Cilevirus causing symptoms similar to citrus leprosis. *Phytopathol* 103(5):488-500. doi: 10.1094/PHYTO-07-12-0177-R. PMID: 23268581.

Roy, A., Hartung, J. S., Schneider, W. L., Shao, J., Leon, M. G., Melzer, M. J., Beard, J. J., Otero-Colina, G., Bauchan, G. R., Ochoa, R., and Brlansky, R. H. (2015) Role bending: Complex relationships between viruses, hosts, and vectors related to citrus leprosis, an emerging disease. *Phytopathol* 105:1013-1025.

- Sameroff, S., Tokarz, R., Charles, R.A. Jain, K., Oleynik, A., Che, X., Georges, K., Carrington, C.V., Lipkin, W.I., Oura, C. (2019). Viral Diversity of Tick Species Parasitizing Cattle and Dogs in Trinidad and Tobago. *Sci Rep* 9, 10421. <https://doi.org/10.1038/s41598-019-46914-1>
- Sonnenberg, R., Wolte, A. W., and Tautz, D. (2007). An evaluation of LSU rDNA D1-D2 sequences for their use in species identification. *Front. Zool.* 4:6. doi: 10.1186/1742-9994-4-6
- Talavera, G., and Castresana, J. (2007). Improvement of phylogenies after removing divergent and ambiguously aligned blocks from protein sequence alignments. *Syst. Biol.* 56, 564–577. doi: 10.1080/10635150701472164
- Tassi, A.D. (2018). Diversidade morfológica e genética de diferentes espécies de *Brevipalpus* (Acari: Tenuipalpidae) e suas competências como vetores de vírus. 262. Available at: https://teses.usp.br/teses/disponiveis/11/11135/tde-17072018-160552/publico/Aline_Daniele_Tassi_versao_revisada.pdf
- Thompson, J.D., Higgins, D.G., and Gibson, T.J. 1994. CLUSTAL W: improving the sensitivity of progressive multiple sequence alignment through sequence weighting, position-specific gap penalties and weight matrix choice. *Nucleic Acids Res.* 22:4673–4680.
- Untergasser, A., Cutcutache, I., Koressaar, T., Ye, J., Faircloth, B.C., Remm, M., et al. (2012). Primer3 - new capabilities and interfaces. *Nucleic Acids Res.* 40(15): e115
- Valles S.M., Chen, Y., Firth, A.E., Guerin, D.M.A., Hashimoto, Y., Herrero, S., de Miranda, J.R., Ryabov, E. (2017). ICTV Virus Taxonomy Profile: Dicistroviridae. *J Gen Virol.* 98:355–6.
- van Oers, M.M. (2010). Genomics and Biology of Iflaviruses. In K. Johnson, & S. . Agari (Eds.), *Insect Virology* (pp. 231-250). Caister Academic Press.
- Vasilakis, N., Forrester, N.L., Palacios, G., Nasar, F., Savji, N., Rossi, S.L., Guzman, H., Wood, T.G., ... Tesh, R. B. (2013). Negevirus: a proposed new taxon of insect-specific viruses with wide geographic distribution. *Journal of virology*, 87(5), 2475–2488. <https://doi.org/10.1128/JVI.00776-12>
- Villamor, D.E.V., Ho, T., Al Rwahnih, M., Martin, R.R., Tzanetakis, I.E. (2019). High Throughput Sequencing For Plant Virus Detection and Discovery. *Phytopathol.* 109(5): 716-725. <https://doi.org/10.1094/PHYTO-07-18-0257-RVW>
- Whitfield, A.E., Huot, O.B., Martin, K.M., Kondo, H., Dietzgen, R.G. (2018). Plant rhabdoviruses—their origins and vector interactions. *Current Opinion in Virology* 33: 198-207.
- Wylie, S. J., Adams, M., Chalam, C., Kreuze, J., López-Moya, J. J., Ohshima, K., Praveen, S., Rabenstein, F., Stenger, D., Wang, A., Zerbini, F. M., & Ictv Report Consortium (2017). ICTV Virus Taxonomy Profile: Potyviridae. *J. Gen. Virol.* 98(3), 352–354. <https://doi.org/10.1099/jgv.0.000740>

5.6 Supplementary Material

Supplementary Table 5.1. BLASTn searches results of the partial 28S rRNA and COI sequences amplified from the mite samples used in this study.

Mite Sample ID	Host	Location ³	28S rRNA			Cytochrome oxidase I (COI)		
			Nucleotide identity	GenBank Accession	Query coverage	Nucleotide identity	GenBank Accession	Query coverage
Citrus O1	<i>Citrus</i> spp.	WRS ²	<i>B. azores</i> 100%	MK91927 2	96%	<i>B. azores</i> 99.72%	MK49946 0	87%
Citrus O2	<i>Citrus</i> spp.	OUGC ²	<i>B. yothersi</i> 99.66%	MK29368 3	96%	<i>B. yothersi</i> 99.4%	KX100285	85%
Citrus O3	<i>Citrus</i>	UH Manoa	<i>B. azores</i> 98.86%	MK91927 2	92%	<i>B. yothersi</i> 99.71%	KF954967	90%
	<i>reticulata</i>		<i>B. yothersi</i> 99.66%	MK29363 0	93%			
Citrus H1	<i>Citrus</i> spp.	Waiakea ³	<i>B. yothersi</i> 100%	MK29367 8	93%	<i>B. yothersi</i> 99.71%	KF954967	84%
Hibiscus O1	<i>Hibiscus arnottianus</i>	UH Manoa	<i>B. papayensis</i> 99.33%	MT664800	94%	<i>B. papayensis</i> 98.55%	KF954950	84%
Hibiscus O2	<i>Hibiscus arnottianus</i>	UH Manoa	<i>B. papayensis</i> 99.33%	MT664800	94%	<i>B. papayensis</i> 99.02%	KF954950	82%
Hibiscus O3	<i>Hibiscus rosa-sinensis</i>	OUGC ²	<i>B. obovatus</i> 100%	MK29369 4	90%	<i>B. obovatus</i> 100%	MK49946 5	86%
Passionfruit O1	<i>Passiflora edulis</i>	AWCG ²	<i>B. yothersi</i> 100%	MK29363 0	94%	<i>B. yothersi</i> 99.74%	MH60506 8	100%
Passionfruit O2	<i>Passiflora edulis</i>	UH Manoa	<i>B. yothersi</i> 100%	MK29363 0	93%	<i>B. yothersi</i> 99.71%	KF954967	89%
Passionfruit O3	<i>Passiflora edulis</i>	WRS ²	<i>B. yothersi</i> 100%	MK29363 0	93%	<i>B. yothersi</i> 99.71%	KF954967	89%
Papaya O1	<i>Carica papaya</i>	PRS ²	<i>B. papayensis</i> 99.33%	MT664800	94%	<i>B. papayensis</i> 98.84%	KF954950	89%
Papaya O2	<i>Carica papaya</i>	UH Manoa	<i>B. yothersi</i> 99.52%	MT812697	100%	<i>B. yothersi</i> 99.71%	KF954967	89%
Coffee H1	<i>Coffea</i> sp.	Kona ³	<i>B. papayensis</i> 99.33%	MT664800	94%	<i>B. papayensis</i> 98.84%	KF954950	84%
Coffee O1	<i>Coffea</i> sp.	Dole plantation	<i>B. papayensis</i> 98.49-99.16%	MT664798 MT664800	94%	<i>B. papayensis</i> 98.84%	KF954950	89%
Pineapple O1	<i>Ananas comosus</i>	Dole plantation	<i>Raioella indica</i> 78.62%	JF928445	93%	<i>Dolichotetranychus</i> sp. 99.73%	MH60619 1	95%

Supplementary Table 5.2. Primer sequences used in RT-PCR assays for virus presence confirmation from the different mite samples used in this study.

Virome	Virus contig name	Forward (5' - 3')	Reverse (5' - 3')	Product size (bp)
<i>Brevipalpus</i> -associated virome (citrus)	Brevipalpus-associated narnavirus contig 1	CATCAACGCCCTGGAGTACC	CCTAATTGCCGGCCTTCACT	551
	Brevipalpus-associated narnavirus contig 2	CCCATCGGACTTCCTCTCCT	AGTCTCCCTCCGTTGCCTAA	251
	Brevipalpus-associated narnavirus contig 3	CAAGCGTTTGGGACCTAGCA	AAGCGCTCATTACAAGGGT	292
	Brevipalpus-associated picornavirus contig 1	CAATGGAGTGCGTGGATGGA	ATGTCTCTCGGGCTCACAGA	656
	Brevipalpus-associated picornavirus contig 2	TGACACGGAAGAGCAGAGGT	TTCGTGGTCATTTGCGTGCA	566
	Brevipalpus-associated picornavirus contig 3	CGTGTTGGACACCGTAGTT	GGGCACGAAAGGTTCCCTGAT	427
	Brevipalpus-associated picornavirus contig 4	AGATCCTTCCGAGCCACCTT	CAGGAGACAGTCGAGTTGGC	246
	Brevipalpus-associated picornavirus contig 5	ACAGGAAATGGCAAAGGTGTC	ACTGCTGCATCGACAAATTGG	176
	Brevipalpus-associated picornavirus contig 6	ACTCCGATACAATCATTGCAGG A	GTACGTGGGAGTTGGTTCGG	243
	Brevipalpus-associated tombusvirus contig 1	TGCGCGAACCTCTTTATGCT	TCACATCAAACGCCAGCTCA	255
Brevipalpus-associated tombusvirus contig 2	CCAACCATGTCCCGTCAACA	CGATTTCAACACCGGCCTTG	353	
<i>Brevipalpus</i> -associated virome (hibiscus)	Brevipalpus-associated bluner-like virus RNA 1	GGTTGATGCATGGTGAGGGT	CCCAACGCCCTAACCAACAT	430
	Brevipalpus-associated bluner-like virus RNA 2	TCATGGTTGGCAGGCTTTGT	TTCCACAGTCTCTCGCAACG	409
	Brevipalpus-associated negevirus contig 1	ACCCTAGATGTGTCCTCGGT	GCGTCACATCATCGTAGGCT	511
	Brevipalpus-associated negevirus contig 2	CGCCAACCAACTGTACTCGT	GGGCATGGTTCCGGAAGGTAT	438
	Brevipalpus-associated narnavirus contig 1	AACGCGTTCCTTCGACTCTC	CTAAGCGACCGTCCTCCAC	666
	Brevipalpus-associated narnavirus contig 2	TAAACGGTTGGGCAGCAGAG	GCTCTTCGGGTGCCTTATCG	213
	Brevipalpus-associated narnavirus contig 3	GTACTIONGCAAGCTCAAGGT	AGCAAGAGATCATCGCCGTT	200
	Brevipalpus-associated narnavirus contig 4	CAAGCGTTTGGGACCTAGCA	AAGCGCTCATTACAAGGGT	292
	Brevipalpus-associated narnavirus contig 5	GCGGGATTGACGGTTACCTC	AAGACTCGCGAATCCAGCTC	321
	Brevipalpus-associated narnavirus contig 6	GGTCAACTCATGGGTTCGCT	TTTCTTGGGTGCCTGTGTCC	675
	Brevipalpus-associated picornavirus contig 1	CCCTGAACGCCGAATCCATT	ATGTGTGGGCTGAGGTCATG	329
	Brevipalpus-associated picornavirus contig 2	GGTAGTCCCTCAGGTAGTGCT	GAGCCTGAACGTCGAATCCA	398
	Brevipalpus-associated picornavirus contig 3	CCTAGCTGCAGACGGGAAAG	CATGGCAGAGAAACCGGACA	470
	Brevipalpus-associated picornavirus contig 4	TCTGGGAGTGACTTGTGGACT	GCCACTCCAACCTCCACATTTG	405
	Brevipalpus-associated picornavirus contig 5	AGTCGCAGGTGTAGCATTCCG	GGACAATAACATTCCCGAAGTGC	226
	Brevipalpus-associated tombusvirus contig 1	CCCTCAAGTTCGGCCATGAA	AGGCACAAATCCCTCCGTTG	293

	Hibiscus green spot virus 2 RNA 1	TGTATGGTGCCCGTGTGTGTC	CGTCACACCACTCAGCAACA	232
	Hibiscus green spot virus 2 RNA 2	GCTGAACGGTGTTCCTGGTG	CCCGTGCATGAACAAGTCGA	450
	Hibiscus green spot virus 2 RNA 3	CTCGGTGCTCTTGTGTGTGTC	GCAAAGACACGAACCCAAGC	526
<i>Brevipalpus</i> - associated virome (papaya)	Brevipalpus-associated picornavirus contig 1	TACGAGGATGATGGCGGTGA	TGCCGGACGAGGGTAATCTA	267
	Brevipalpus-associated picornavirus contig 2	AGTTAGTTTACCCTCGCGTGT	AGAGGCCTCACGTTGCTCTA	160
	Citrus leprosis virus C2 RNA 1	ACAAGATGGCGGACGAACTG	AGCCATGTCATCGGGATCCA	386
	Citrus leprosis virus C2 RNA 2	GATCACCGTAGTTTCATGCG	CCAACGCGGTTAACAACCTC	129
	Papaya ringspot virus	TGACGGCTGGGTGTACTGT	TGCCGCTGTGATTGCCTC	596
<i>Brevipalpus</i> - associated virome (passionfruit)	Citrus leprosis virus C2 RNA 1	ACAAGATGGCGGACGAACTG	AGCCATGTCATCGGGATCCA	
	Citrus leprosis virus C2 RNA 2	GATCACCGTAGTTTCATGCG	CCAACGCGGTTAACAACCTC	129
	Brevipalpus-associated reovirus contig 1	CGGCCGGATTAACCTGAAGAACA	GGATGTCCTGTAGCCATTAATCC T	358
Tenuipalpid- associated virome (pineapple-coffee)	Brevipalpus-associated negevirus contig 1	AGCCGTGATTCAATGCGAGA	ATAACGCCGACACCCACTTC	266
	Brevipalpus-associated solemovirus contig 1	ATGTTGTCTGGGCGGATCAC	TTAAGTTCGGCTGCCTGAC	545
	Brevipalpus-associated cile-like virus contig 1	ACTCCGTTGGTTGTGGGTTTC	CCCTTCCAACCAATCAGCCA	465

CHAPTER VI

MOLECULAR AND BIOLOGICAL CHARACTERIZATION OF A NEW EMARAVIRUS INFECTING CORDYLINE FRUTICOSA IN HAWAII

6.1 INTRODUCTION

Ti (*Cordyline fruticosa* L.) is a common ornamental and landscaping plant in Hawaii that also has great importance in the Hawaiian culture. Its foliage is commonly used in both the food and cut flower industries. Given the diverse use of the ti plant, a small commercial ti industry persists in Hawaii. Ti ringspot is an emerging disease of ti reported by commercial ti growers on the island of Oahu in 2009 (Melzer et al. 2011). Since then, the disease incidence has increased throughout the last decade and is rapidly spreading throughout the Hawaiian Islands. The hallmark of ti ringspot is the presence of chlorotic rings that can be 0.5 to 1 cm in diameter (Melzer et al. 2013a; 2013b). Occasionally, these rings may become necrotic and coalesce into larger, amorphous lesions. New leaves emerge asymptomatic and can remain asymptomatic for weeks before developing ringspot symptoms which suggests that the causal agent is either not systemic or symptoms are only expressed in the mature foliage. Green-leaved varieties are most afflicted by ti ringspot, although red-leaved ornamental varieties with ringspot symptoms have been also observed (Melzer et al. 2013b).

Previous studies have found abundant presence of at least four velariviruses (Family: *Closteroviridae*) in ti plants which were not associated to ti ringspot disease (Melzer et al., 2011; 2013a; 2013b). A putative new emaravirus has been associated to ti ringspot disease, for which the name ‘ti ringspot-associated virus’ (TiRSaV) has been proposed (Melzer et al., 2014). Emaraviruses are multi-segmented negative-sense ssRNA viruses that are transmitted by eriophyid mites (Elbeaino et al., 2018). *Emaravirus* members can possess between four to up to ten genomic RNA segments with sizes ranging from ~1 Kbp to ~ 7 kbp (Elbeaino et al., 2018; Kubota et al., 2020). Each genomic segment codes for a single protein. RNA segments 1-4 are considered the core segments coding for RNA-dependent RNA polymerase (RdRp), glycoprotein precursor (GP), nucleocapsid protein (NC) and movement protein (MP), respectively (Figure 1.4A, Chapter I) (Elbeaino et al., 2018; Mühlbach and Mielke-Ehret 2012). RNA segments 5-10 from different members show no clear homology and their functions are yet to be determined (Zheng et al., 2017) which may lead to hypothesize the plasticity of their genome and existence of more than ten genomic segments (Stewart 2016). Both 5’ and 3’ termini of all the genomic segments have 13-20 nt

(depending on the segment) that are conserved and complementary between each other (5'-AGUAGUGUUCUCC-3' at the 5'-end, 5'-GGAGUUCACUACU-3' at the 3'-end) (Elbeaino et al., 2018).

Park (2016) attempted to characterize TiRSaV using HTS on randomly-primed cDNA libraries constructed from dsRNA extracted from ti ringspot symptomatic plants. Unfortunately, very few emaravirus sequences were recovered using this approach and the number of reads obtained in that study. Fully characterization of TiRSaV infecting ti plants and further association studies to ti ringspot disease is needed in Hawaii to provide nurseries and ti plant farms adequate integrated pest management approaches. An unidentified species of eriophyid mite has consistently observed on both symptomatic and symptomatic ti plants and represents a candidate vector for the putative new *Emaravirus* member infecting ti plants.

This chapter describes the full molecular characterization of TiRSaV, describes its herbaceous host range, determines the multiple TiRSaV segments presence in symptomatic ti plants only and evaluates the possibility of the role of the eriophyid mites found on ti plants as candidate vectors of the new virus.

6.2 MATERIALS AND METHODS

6.2.1 Tissue collection and virus source

The primary sources of common green ti plants with symptoms of ti ringspot (Figure 6.1) were the University of Hawaii at Manoa campus, and Makiki neighborhood, both in Honolulu on the island of Oahu. These samples were used for virus detection, and genomic sequencing.



Figure 6.1 Ringspot symptoms on the leaves of common green ti variety (*Cordyline fruticosa*).

6.2.2 Emaravirus and TiRSaV detection

Total RNA was isolated from ti tissues using a NucleoSpin RNA Plus kit (Macherey-Nagel, Duren, Germany) and reverse transcribed into cDNA using random primers and the M-MLV reverse transcription kit (Promega, Madison, WI). The cDNA was used as template in a conventional RT-PCR assay using emaravirus-specific degenerate primers (Motif A-sense/Motif C-antisense) targeting RdRp gene motifs (Elbeaino et al. 2013). Amplification products were cloned using pGEM-T Easy (Promega) and sequenced at the University of Hawaii Advanced Studies in Genomics, Proteomics, and Bioinformatics Laboratory. Primers targeting the *rbcL* of *C. fruticosa* were used to ensure the quality of template used in the RT-PCR assay (Melzer et al. 2013a). For specific detection of TiRSaV and association of this virus with the observed symptoms, a conventional RT-PCR detection assay was developed. Primers TiRSaV forward (F) and TiRSaV reverse (R) targeted a portion of the RdRp of TiRSaV, and RBC L3 and RBC R3 targeted a portion of the *rbcL* of *C. fruticosa* and served as an internal positive control for the detection assay (Table 6.1). The PCR cycling conditions were initial denaturation for 5 min at 95°C, followed by 40 cycles of 95°C for 30 s, 55°C for 30 s, and 72°C for 30 s. A 7-min final extension was conducted at 72°C. PCR products were resolved on a 2% (w/v) agarose gel and visualized with ethidium bromide over ultraviolet light.

6.2.3 Double-stranded RNA isolation and sequencing

Double-stranded RNA (dsRNA) was isolated from symptomatic tissues from ti plants located at the University of Hawaii at Manoa campus using either CF-11 (Whatman, Maidstone, UK) or Sigmacell

Type 101 (Sigma, St. Lois, MO) cellulose chromatography following the procedure of Morris and Dodds (1979). These dsRNAs were used to amplify the multiple emaravirus segments, except for RNA 1, by taking advantage of the 13 conserved bases present on all emaravirus terminal sequences. Briefly, 200-300 ng of dsRNAs and 1 pmol/liter of primer “Emara-terminus,” were denatured at 95°C for 5 min, quickly chilled on ice for 2 min, and reverse transcribed with the M-MLV reverse transcription kit (Promega) at 42°C for 1 h. The resulting cDNA was subjected to conventional PCR with primer “Emara terminus” using Phusion High-Fidelity DNA Polymerase (New England Biolabs, Ipswich, MA). The final volume of the reaction was 50 µl with cycling parameters consisting of an initial denaturation at 98°C for 30 s, followed by 40 cycles of denaturation at 98°C for 10 s, annealing at 45°C for 20 s, and extension at 72°C for 2 min. A final extension was performed for 3 min at 72°C. The size of the PCR products was checked using agarose gel electrophoresis, and the PCR products were cleaned and concentrated using Amicon ultra filter YM-30 (Millipore, Darmstadt, Germany) and underwent HTS using an Illumina MiSeq 2 × 300 bp (V2) platform at the University of Hawaii Advanced Studies in Genomics, Proteomics, and Bioinformatics Laboratory.

6.2.4 Genome assembly

The single-end and individual paired-end read files from HTS were filtered using Trimmomatic 0.35.3 (Bolger et al. 2014) and reads with phred quality scores lower than 20 were discarded. A quality control check was run with FastQC 0.69 (Babraham Bioinformatics) for the single-end read file and individual paired-end read files, and MultiQC 1.0 (Ewels et al. 2016) was used to merge the quality control files from the individual paired-end reads files. The reads were *de novo* assembled using Trinity 2.2.0 with default parameters (Grabherr et al. 2011) and Velvet 1.2.10 (Zerbino and Birney 2008) with default parameters and kmer sizes ranging from 35 to 65, respectively. Assembled contigs were sorted by length, and duplicates and those with lengths shorter than 100 nucleotides (nt) were discarded using Geneious version 10.1.3 (Kearse et al. 2012). Residual contigs were searched against the nonredundant viral protein database available in GenBank using BlastX (Altschul et al. 1997). Contigs showing resemblance to emaraviruses were identified and saved for further analysis. Using Bowtie 2 (Langmead et al. 2009) and Geneious mappers plug-ins implemented in Geneious version 10.1.3, the 5' and 3' ends of partial segments were extended and sequence corrected in some of the contigs, and the genome coverage and read counts were obtained. For bridging sequence gaps, contig-specific primers were used in RT-PCR assays employing dsRNA as template. Amplification products were cloned and sequenced as above. To determine whether contigs putatively representing TiRSaV genomic RNA segments all belonged to the same virus, RT-PCR assays with specific primers to each segment were conducted on seven symptomatic

and seven asymptomatic ti plants collected on Oahu. The termini of the viral RNAs 1 to 5 were verified by rapid amplification of cDNA ends (RACE). For both ends, dsRNA was poly(A) tailed using the *Escherichia coli* poly(A) polymerase (New England Biolabs, Ipswich, MA). Polyadenylated dsRNAs were reverse transcribed using the primer poly(dT) tail RACE and amplified with primers designed to anneal within 450 nt of the terminus. Amplified products were cloned and sequenced as above. All the bioinformatic tools used, except those implemented in Geneious version 10.1.3, were accessed through the Galaxy platform (Afgan et al. 2016).

6.2.5 Sequence and phylogenetic analyses

The NCBI ORFfinder program (<https://www.ncbi.nlm.nih.gov/orffinder/>) was used to search for putative open reading frames (ORFs), and the proteins they encoded, in the TiRSaV RNAs identified by HTS. Global pairwise sequence comparisons (amino acid) of the RdRp, GP, NC, MP, and p5 sequences with orthologs from other emaraviruses were performed using LALIGN (Huang and Miller 1991). The RdRp, GP, NC, and MP amino acid sequences were aligned with their respective orthologs using the MEGA 7.0.25 (Kumar et al. 2016) ClustalW algorithm (Thompson et al. 1994). The best model of protein evolution for each alignment, partial deletion, and moderate branch swap filter were used to generate a Maximum Likelihood tree with supporting bootstrap values following 1,000 repetitions. Bayesian phylogeny was inferred using BEAST version 2.4.6 (Bouckaert et al. 2014) and the best evolution model with three Markov chain Monte Carlo runs of 100,000,000 generations sampling every 10,000 trees. The process was performed at the CIPRES Science Gateway (<http://www.phylo.org>). The three runs were combined using LogCombiner in BEAST, discarding 10% of the sample trees as burn-in. Effective sample sizes were calculated using Tracer version 1.6 and were >200 for all the parameters. The maximum clade credibility tree and posterior probabilities annotations were calculated using TreeAnnotator in BEAST. An output tree was visualized in FigTree version 1.4.3.

6.2.6 Mechanical transmission to experimental herbaceous hosts

Leaf tissue (2 g) from a symptomatic *C. fruticosa* plant was ground with 20 mL of 0.05 M phosphate buffer, pH 7.5. The homogenate was used to mechanically inoculate the leaves of two groups of plants using carborundum. The first group of plants consisted of four *Nicotiana benthamiana* and four *N. tabacum* plants. For serial inoculations, TiRSaV-infected *N. benthamiana* and *N. tabacum* leaves were used as inoculum to mechanically inoculate six *N. benthamiana* and six *N. tabacum* plants, respectively. The second group consisted of seven plants each of cucumber [*Cucumis sativus* L. ‘Boston Pickling’],

watermelon [*Citrullus lanatus* (Thunb.) Matsum. & Nakai ‘Jubilee’], pumpkin [*Cucurbita melo* L. ‘Connecticut Field’], squash [*Cucurbita melo* ‘Dark Green Zucchini’], and pea [*Pisum sativum* L. ‘SugarSnap’]. For both inoculation experiments, mock-inoculated plants (buffer only) were included as negative controls. The first group of plants were maintained in a growth room at ~25°C and a 16h/8h light/dark photoperiod for 1 to 3 months. The second group of plants were maintained in an air-conditioned glasshouse under natural light conditions. Inoculated plants were observed for symptom development and tested for TiRSaV infection on systemic leaves by RT-PCR assays using the primer pairs TiRSaV-RdRp F/R and/or TiRSaV-NC F2/R2 (Table 6.1) following the protocols described above. Amplification products were cloned and sequenced as described above.

6.2.7 Detection of TiRSaV in eriophyid mites

The internal transcribed spacer (ITS) region and 28S ribosomal RNA sequences and virus status of eriophyid mites recovered from symptomatic ti plants were determined following the approach of Druciarek et al. (2018). Briefly, a single and a group of six eriophyid mites collected from a symptomatic ti leaf were placed into PCR tubes containing random primers (5 mM) and dNTPs (2 mM each) in a volume of 14.5 µL. The mixture was heat-denatured at 90°C for 7 min and quickly chilled on ice for 2 min. M-MLV-RT (160 U), rRNAsin (28 U), and M-MLV-RT 1× buffer (Promega) were added to complete a final volume of 20 µL. The mixture was incubated at 37°C for 1 h and diluted fourfold, eightfold, and 16-fold. The primer sets MITS1 (5’-CCGTAGGTGAACCTGCGGAAGG-3’)/MITS4 (5’-CCACCGTTAATTGTGATTTATTTTGTC-3’) (Fenton et al. 1997; Kumar et al. 2001) and D1D2fw2 (5’-ACAAGTACCDTRAGGGAAAGTTG-3’)/ 28Sr0990 (5’-CCTTGGTCCGTGTTTCAAGAC-3’) (Mironov et al. 2012; Sonnenberg et al. 2007) were used in subsequent PCR reactions with 1 µL of each cDNA dilution as template. For TiRSaV detection, RT-PCR assays were performed using the primer pairs TiRSaV-RdRp F/R, TiRSaV-GP F1/R1, TiRSaV-NC F2/R2, TiRSaV-MP F1/R1, and TiRSaV-P8like F1/R1 (Table 6.1) as described above.

6.3 RESULTS

6.3.1 Genome sequencing

HTS using an Illumina platform was performed on two libraries originating from different starting materials to draft the TiRSaV genome. The first library originated from a degenerate oligo-primed PCR library using dsRNA from symptomatic leaf tissue as template (Park 2016). A total of 490,503 single-end

reads assembled into 3,036 contigs. Following database comparisons, it was determined that most of the viral contigs were derived from the velariviruses known to infect ti. Only three contigs shared highest similarity to emaraviruses and potentially the TiRSaV genome: two contigs (378 and 561 nt) corresponded to regions of the RdRp (RNA 1) and one contig (303 nt) corresponded to a region of the NC (RNA 3). The second library originated from RT-PCR amplification products utilizing a single primer targeting the conserved terminal sequence of emaraviruses. A total of 2,484,124 paired-end reads assembled into 1,952 contigs, of which six (970 to 2,399 nt) possessed significant homology to different emaravirus genomic RNAs. These six contigs, when combined with the three contigs generated from the first library, and degenerate RT-PCR products produced a draft genome of TiRSaV consisting of five genomic RNAs designated as RNA1 to RNA5 (GenBank accessions MH223635 to MH223639). The viral termini of RNAs 1 to 5 were verified by RACE and both 5' and 3' ends of the three RNAs contained the 13 nt conserved in all emaraviruses. Virus-specific primers (Table 6.1) were used to bridge sequence gaps and clarify ambiguous regions. Very high depth of coverage was achieved for RNAs 2 to 5, but not RNA 1 (Table 6.2). To complete the sequence of RNA 1 (RdRp), degenerate primers targeting conserved motifs A and C of the RdRp (Elbeaino et al. 2013) and other internal conserved regions (EMARA F7 5'-TCTTGTGGTGATCCATGIARRCCYTTATTWCC-3', EMARA R8 5'-CCGCGCAGATAATCTTATARAIGAYAARYTRGAAT-3') (Olmedo-Velarde et al. unpublished) were used in conjunction with TiRSaV RNA 1-specific primers to bridge the sequence gaps.

Table 6.1 Primers designed and used in this study for symptom association, specific detection of the 5 ti ringspot-associated virus (TiRSaV) RNAs, bridging sequence gaps and RACE.

Name	Sequence ¹ (5' to 3')	Target	Purpose
TiRSaV FWD	CGCTAAATACTGTCAGTTGGTTTC	RdRp- RNA1	TiRSaV Detection
TiRSaV REV	AGTTATAAGGGTGCTAGCCAGT		
RBC L3	TGGGTTTCTATGCCAGGTGT	<i>C. fruticosa</i>	Host plant internal positive control
RBC R3	AGCAAGATCACGTGGGTGAT	rubisco	
TiRSaV-RdRp F	CAACTGATTACAGTTCTGTCTTATACC	RdRp- RNA1	Detection of
TiRSaV-RdRp R	CCTCATGTTGTTTATGCTCAATTCT		TiRSaV RNA 1
TiRSaV-GP F1	TGATCCTGTGAATTGACTGTACCA	GP-RNA2	Detection of
TiRSaV-GP R1	TCTCAATCATTTCATGGTGTGTAGTCA		TiRSaV RNA 2
TiRSaV-NC F2	TGTCGTTGCTATCACTTCAATGG	NC-RNA3	Detection of
TiRSaV-NC R2	AGATGAACCGTGCAAAGAAAGC		TiRSaV RNA 3

TiRSaV-MP F1	GTTGCTTCACCTGGGACTGT	MP-RNA4	Detection of TiRSaV RNA 4		
TiRSaV-MP R1	AGCCACACACTGATTCTTGCA				
TiRSaV-P8like F1	TCACCTTAAGCACAACCAGATCCT	p5-RNA5	Detection of TiRSaV RNA 5		
TiRSaV-P8like R1	GTAAAGCTGTTCAATCGTCATCTGA				
Emara terminus	GCCGACCAGTAGTGWWTCC	Emaravirus termini	Complete genome amplification		
TiRSaV RdRp 700R	GCATGATGACGAAATTGAGGGA	RdRp- RNA1			
Emara RdRp 550F	GCTCAGGYTCYAAATWMATRATTTC				
TiRSaV RdRp 1370R	TTTGACAGATCCGAATGTTGCAT				
TiRSaV RdRp 3730F	CAACATCATATCTCTTGCTGACCAT				
TiRSaV RdRp 4840R	AGGATACTGGCTTTGATTCTTC				
TiRSaV RdRp 5180F	CCAAGTACAGTATTTAGCGAAGGA				
TiRSaV RdRp 5600R	ACACTACTAAGTTGAAGCCAACACT				
Emara RdRp 6500F	TGAGGAARARKATATCWGGNGT				
TiRSaV GP 200F	GACTGTCATGAATCCATTATCCTCA			GP-RNA2	TiRSaV sequence confirmation and/or bridge sequence gaps
TiRSaV GP 1306R	TGTTATGATGATCTTGAGGCTCTC				
TiRSaV GP 951F	GACTTTGAGGGTGATGAACATATGT				
TiRSaV GP 2236R	GTCAGCAAGATGAAGCCAAGTTA				
TiRSaV NC 270R	CAATAACTGTCAAGAAGACCACTGATTTC	NC-RNA3			
TiRSaV NC 260F	CAGTGGTCTTCTTGACAGTTATTG				
TiRSaV NC 1140R	GGTGTCTTAAGGGTTCAAGTCGT				
TiRSaV NC 840F	CTTCTTTGCACGGTTCATCTT				
TiRSaV MP 141R	AAGCAATACCAGGAAAGGAAAAGCTTGCTG	MP-RNA4			
TiRSaV MP 5F	GTGATCTCCAATGCTATTGTCTTCA				
TiRSaV 1014R	CCTTTGCTGTCGAATCAAATGGA				
TiRSaV P5 61F	TCTGGTAATCTGTAAATCAAAGCCA	p5-RNA5			
TiRSaV P5 1250R	TGATGAAGCACGAGATTAACCGA				
Poly dT_RACE	GACCACGCGACGTGTCGAVTTTTTTTTTTTTTTTT				
TiRSaV P3 RACE_F	GCCATGGATGTTGACTTCTCTG	NC-RNA3	RACE		
TiRSaV P3 RACE_R	GTGAGAGCAACAGCATCCCA				
TiRSaV P4 RACE_F	GACAGCAAAGGAAACAGCCA	MP-RNA4			
TiRSaV P4 RACE_R	AGCATTTCCAGAGCCTTGATGA				

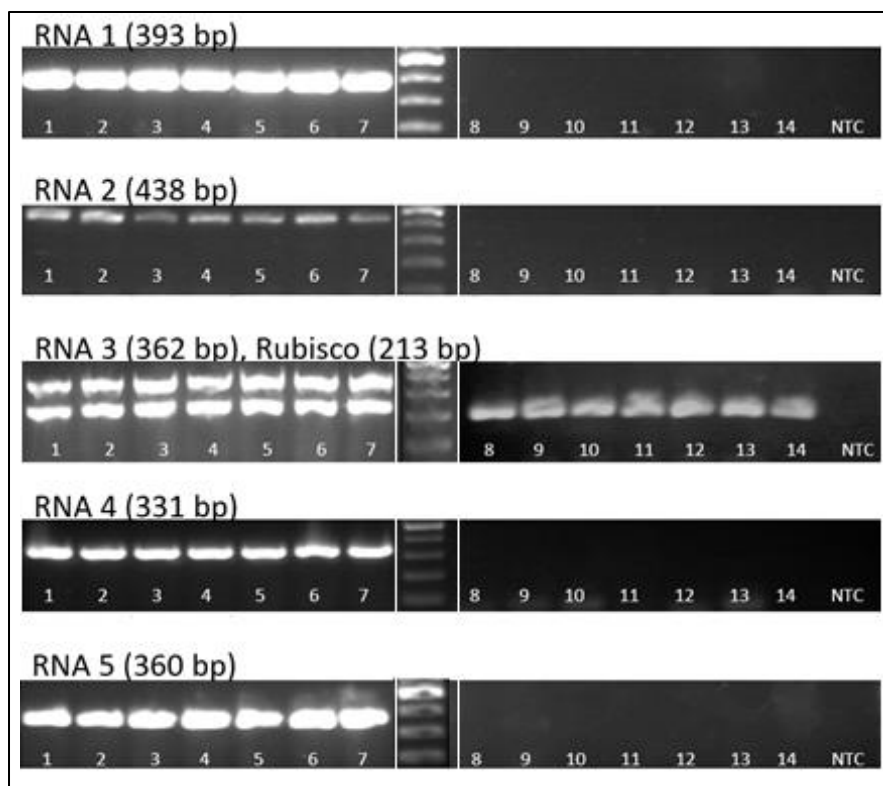


Figure 6.2 Agarose gel electrophoresis of RT-PCR products using primer set specific to putative TiRSaV RNAs (see Table 6.1) to determine if these RNAs were associated with Ti ringspot symptoms and TiRSaV infection. Assays were performed on seven symptomatic (1-7) and seven asymptomatic (8-14) Ti plants and a non-template control (NTC). The quality of the cDNA of each sample was evaluated with RBC L3/R3 (Table 6.1) that was co-loaded the RNA 3 product during electrophoresis. A 100bp ladder (ThermoFisher Scientific, Waltham, MA) is in the center lane. The lanes in panels corresponding to RNA 3 and RNA 5 have been re-arranged for consistency.

6.3.2 Genome organization and phylogenetic analyses

Five negative sense RNA segments predicted to encode proteins with homology to emaraviruses were found to comprise the TiRSaV genome, with each RNA segment encoding a single ORF (Figure 6.3) on the complementary strand. TiRSaV RNA 1 was 7,217 nt in length with one ORF (ORF1, CAU7161-UAA139) coding for a putative RdRp (p1) of 2,340 amino acids (aa) and had a predicted molecular mass of 272 kDa. Pairwise comparisons of the deduced RdRp sequence revealed identities with orthologous proteins of emaraviruses ranging from 37 to 45% (Table 6.3). TiRSaV RNA 2 was 2,399 nt in length with one ORF (ORF2, CAU2341-CUA188) coding for a putative GP (p2) of 717 aa and had a predicted molecular mass of 83 kDa. The GP shared identities with orthologs from emaraviruses ranging from 23 to

38% (Table 6.3). TiRSaV RNA 3 was 1,106 nt in length encoding one ORF (ORF3, CAU978-UUA118) coding for a putative NC (p3) of 286 aa and had a predicted molecular mass of 32 kDa. The NC shared identity levels of 28 to 39% with the orthologs of emaraviruses (Table 6.3). TiRSaV RNA 4 was found to be 1,342 nt in length with a single ORF (ORF4, CAU1261-UUA263) coding for a putative MP (p4) of 332 aa and had a predicted molecular mass of 38 kDa. The identity levels with orthologs of emaraviruses ranged from 20 to 51% (Table 6.3). TiRSaV RNA 5 was 1,323 nt in length and found to encode one ORF (ORF5, CAU1254-CUA739) coding for a putative protein with unknown function (p5) of 171 aa and had a predicted molecular mass of 21 kDa. The identity levels with orthologs from emaraviruses ranged from 29 to 32% (Table 6.3).

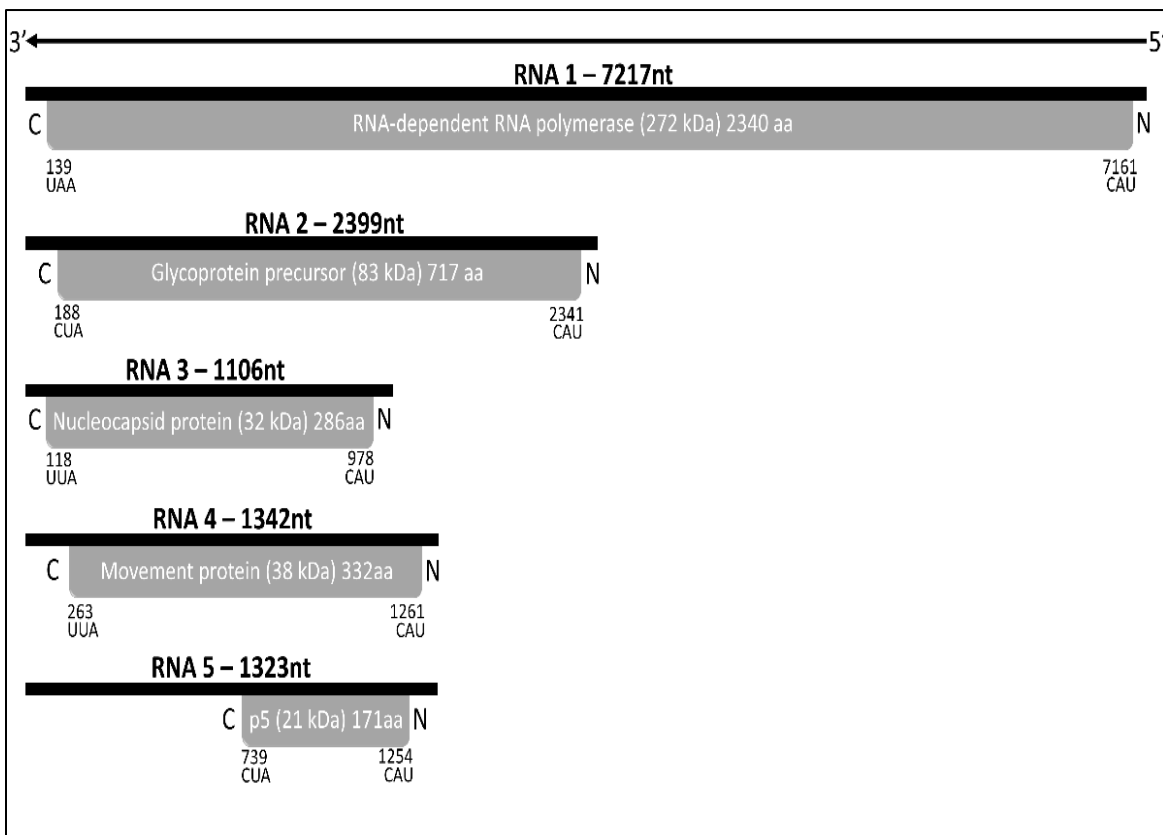


Figure 6. 3 Genome organization of Ti ringspot associated virus. Shaded boxes represent the predicted open reading frame (ORF) for each RNA. The putative protein product for each ORF, start and stop codons, function (if known), and estimated molecular weight are provided. For the purpose of clarity, the genomic RNAs are not drawn to scale.

Table 6.3 Percent amino acid identities between orthologous proteins of ti ringspot-associated virus (TiRSaV) and members and putative members of the genus *Emaravirus*. Raspberry leaf blotch virus (RLBV), High Plains wheat mosaic virus (HPWMoV), palo verde broom virus (PVBV), fig mosaic virus (FMV), European mountain ash ringspot-associated virus (EMARaV), redbud yellow ringspot-associated virus (RYRSaV), Actinidia chlorotic ringspot-associated virus (AcCRaV), blackberry leaf mottle-associated virus (BLMaV), pigeon pea sterility mosaic virus 1 (PPSMV 1), PPSMV 2, rose rosette virus (RRV).

<i>Emaravirus</i> member	TiRSaV protein				
	p1	p2	p3	p4	p5*
RLBV	45	38	39	48	32
HPWMoV	44	36	37	51	29
PVBV	44	31	33	50	-
FMV	39	23	33	20	-
EMARaV	38	24	29	-	-
RYRSaV	38	26	31	22	-
AcCRaV	38	27	29	22	-
BLMaV	38	26	34	20	-
PPSMV 2	38	24	34	21	-
RRV	37	25	31	23	-
PPSMV 1	37	25	28	23	-

* The orthologs of TiRSaV p5 have been designated p8 for HPWMoV and RLBV.

The putative TiRSaV proteins p1, p2, p3, and p5 shared the highest identity levels with orthologs from raspberry leaf blotch virus (RLBV), ranging from 32 to 45%. In contrast, the putative TiRSaV p4 shared the highest identity level (51%) with the HPWMoV ortholog (Table 6.3). Phylogenetic analyses were performed with two character-based algorithms (Maximum Likelihood and Bayesian inference) employing LG+G as the best model of protein evolution. Both algorithms predicted similar relationships between members and putative members of the genus *Emaravirus*. Three distinct clades with similar topologies were formed with both methods and in the four phylogenetic trees: one clade was composed of FMV, PPSMV 2, RRV, blackberry leaf mottle-associated virus (BLMaV), and PPSMV 1; the next clade was composed of Actinidia chlorotic ringspot-associated virus (AcCRaV), EMARaV, and redbud yellow

ringspot-associated virus (RYRSaV); and the third clade was composed of HPWMoV, palo verde broom virus (PVBV), RLBV, and TiRSaV (Figure 6.4).

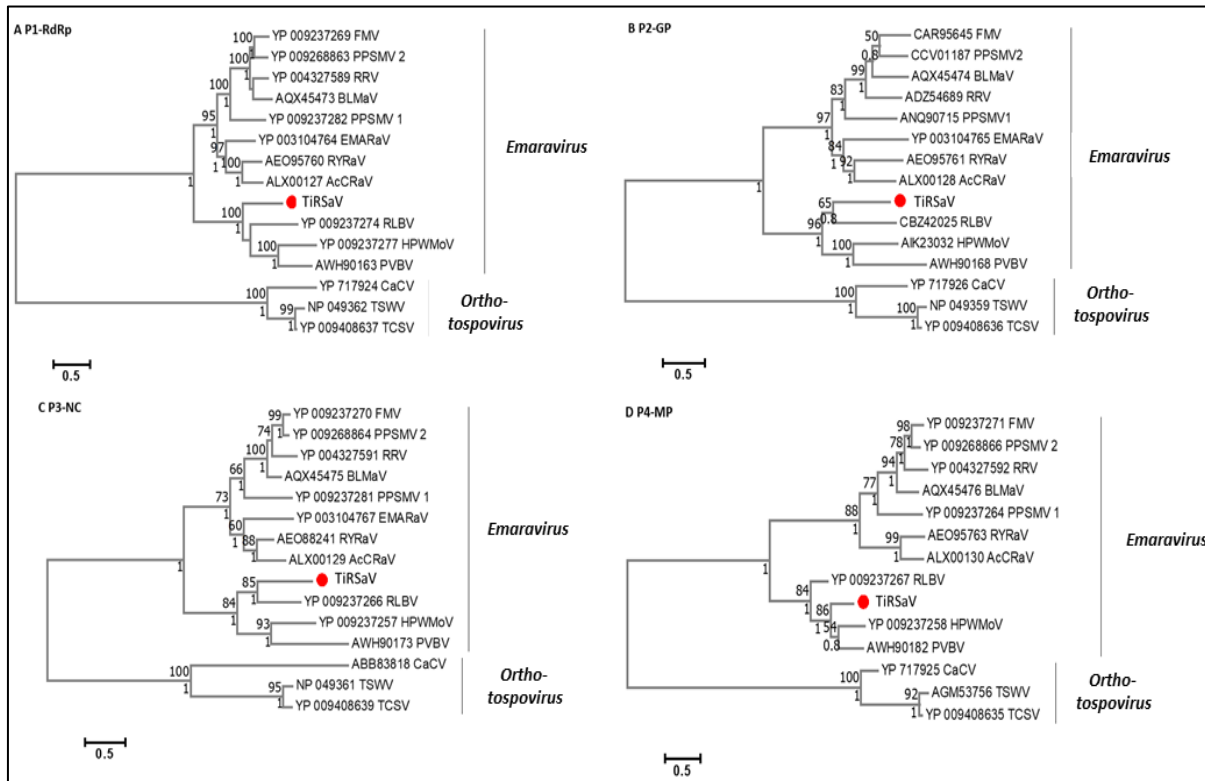


Figure 6.4 Phylogenetic placement of Ti ringspot-associated virus (TiRSaV) within the genus Emaravirus using the A) RNA-dependent RNA polymerase (RdRp), B) glycoprotein precursor (GP), C) nucleocapsid (NC), and D) movement protein (MP) sequences. The phylogenetic tree was generated using the Maximum Likelihood method with 1000 bootstrap to estimate branch support. The numbers above the nodes represent bootstrap values greater than 50, and those under the node represent posterior probabilities greater than 0.7 generated with Bayesian inference with 3 Markov chains Monte Carlo and 100,000,000 generations per chain. The scale represents the number of substitutions per unit branch length. Raspberry leaf blotch virus (RLBV), High Plains wheat mosaic virus (HPWMoV), palo verde broom virus (PVBV), fig mosaic virus (FMV), European mountain ash ringspot-associated virus (EMARaV), redbud yellow ringspot-associated virus (RYRSaV), Actinidia chlorotic ringspot-associated virus (AcCRaV), blackberry leaf mottle-associated virus (BLMaV), pigeon pea sterility mosaic virus 1 (PPSMV 1), PPSMV 2, rose rosette virus (RRV). The GenBank accession numbers for each sequence used in the analyses are provided. Capsicum chlorosis orthotospovirus (CaCV), tomato spotted wilt orthotospovirus (TSWV) and tomato chlorotic spot orthotospovirus (TCSV) were used as an outgroup.

6.3.3 Mechanical transmission to experimental herbaceous hosts

Around 30 days post-inoculation (dpi), systemic leaves from all inoculated plants in the first group were tested by RT-PCR using the specific primer set TiRSaV-RdRp F/R (Table 6.1). PCR products of expected size were obtained from two *N. benthamiana* plants and two *N. tabacum* plants (Figure 6.5).

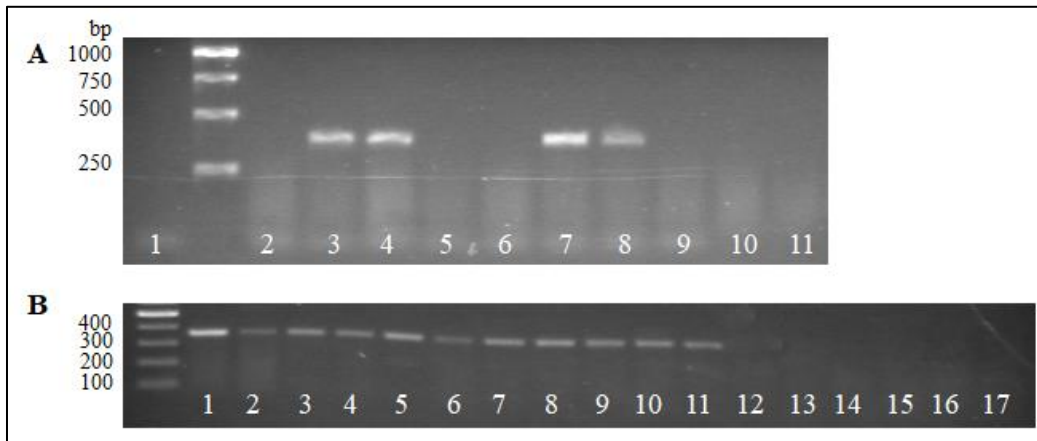


Figure 6.5 RT-PCR assays using TiRSaV-RdRp F/R and TiRSaV-NC F2/R2 on systemic leaves of *Nicotiana benthamiana* and *N. tabacum* mechanically inoculated with ti ringspot-associated virus (TiRSaV) 30 dpi. (A) RT-PCR using TiRSaV-RdRp F/R on *N. benthamiana* and *N. tabacum* mechanically inoculated with sap of TiRSaV-infected *C. fruticosa* leaves. 1) Non-template control. 2) Mock-inoculated *N. benthamiana*. 3-6) TiRSaV-inoculated *N. benthamiana*. 7-10) TiRSaV-inoculated *N. tabacum*. 11) Mock-inoculated *N. tabacum*. (B) RT-PCR using TiRSaV-NC F2/R2 on *N. benthamiana* and *N. tabacum* serially inoculated with sap of TiRSaV-infected *N. benthamiana* and *N. tabacum*, respectively. 1) TiRSaV-positive *N. benthamiana* from first bioassay. 2) TiRSaV-positive *N. tabacum* from first bioassay. 3-8) TiRSaV-inoculated *N. benthamiana*. 9-14) TiRSaV-inoculated *N. tabacum*. 15) Mock-inoculated *N. benthamiana*. 16) Mock-inoculated *N. tabacum*. 17) Non-template control.

Sequencing of the amplicons confirmed the identity of TiRSaV showing the partial fragment of TiRSaV RNA 1 from both *N. benthamiana* and *N. tabacum* plants sharing 99% identity to the TiRSaV RNA 1 from *C. fruticosa*, thus demonstrating mechanical transmission of TiRSaV to experimental herbaceous hosts. Both *N. benthamiana* plants remained asymptomatic for 3 months, but one *N. tabacum* plant presented mild veinal chlorosis at 30 dpi (Figure 6.6). All six *N. benthamiana* plants and three of the six *N. tabacum* plants serially inoculated with TiRSaV tested positive for the virus using the specific primer set TiRSaV-NC F2/R2 that amplifies a region of the NC (RNA 3). Sequencing of the amplicons confirmed that TiRSaV can be mechanically transmissible to *N. benthamiana* and *N. tabacum*, eliciting

mild veinal chlorosis in some *N. tabacum* plants. In the second group of plants, amplification products of the expected size were obtained from 3 of 7 (43%) cucumber plants, 1 of 7 (14%) watermelon plants, 1 of 7 (14%) pumpkin plants, and 1 of 7 (14%) squash plants (data not shown). In all the RT-PCR assays, the non-template control and mock-inoculated plants tested negative. All inoculated plants remained asymptomatic during 3 months of observation.



Figure 6.6 Symptoms on leaves of *Nicotiana tabacum* infected by ti ringspot-associated virus (TiRSaV). Left, mild veinal chlorosis on a systemic leaf from TiRSaV-infected *N. tabacum*. Right, healthy systemic leaf of mock-inoculated *N. tabacum*.

6.3.4 Eriophyid mites and detection of TiRSaV

Primer sets MITS1/ MITS4 (ITS region) and D1D2fw2/28Sr0990 (28S region) generated amplicons of ~620 and ~640 bp, respectively. For both primer sets, amplicons were obtained only when cDNA synthesized from six mites was used as template (Figure 6.7).

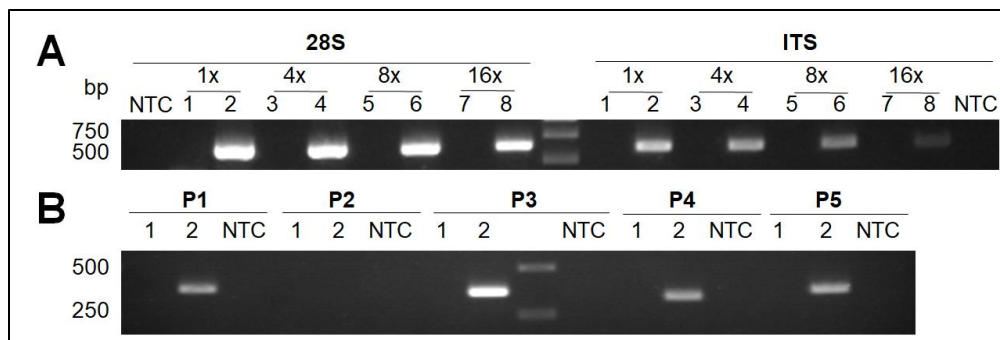


Figure 6.7 28S, ITS regions and TiRSaV genome partial segments amplification from mite cDNA.

(A) RT-PCR using D1D2fw2/28Sr0990 (28S region) and MITS1/MITS4 (ITS region). cDNA synthesized from one mite and its respective 4-fold (4X), 8-fold (8X) and 16-fold (16X) dilution: 1, 3, 5 and 7. cDNA synthesized from six mites and its respective 4-fold (4X), 8-fold (8X) and 16-fold (16X) dilution: 2, 4, 6 and 8. NTC: non-template control. (B) RT-PCR using primers TiRSaV-RdRp F/R targeting the polymerase (P1) of TiRSaV, TiRSaV-GP F1/R1 targeting the glycoprotein (P2) of TiRSaV, TiRSaV-NC F2/R2 targeting the nucleocapsid (P3) of TiRSaV, TiRSaV-MP F1/R1 targeting the movement protein (P4) of TiRSaV and TiRSaV-P8like F1/R1 targeting the putative protein coded by RNA5 (P5) of TiRSaV. 1) 4-fold dilution of cDNA synthesized from one mite. 2) 4-fold dilution of cDNA synthesized from six mites.

After cloning and sequencing four clones of each amplicon, a BLAST search revealed that the ITS sequence (MH796797) was 83% identical to the ITS region from *Aceria parapopuli* (KF782488) with a query coverage of only 41%. For the 28S rDNA region, two groups of sequences were obtained, sharing only 77% of identity between each other. One group (MH796799) shared 87% identity to *Acaphyllisa* sp. (KF782488) and *Neolitaculus* sp. (KM111069), whereas the other group (MH796800) shared 88% identity to *Calacarus carinatus* (KM111063), both with complete query coverage. Using cDNA from the group of six mites diluted fourfold, RT-PCR products of the correct size were generated for four of the five TiRSaV RNAs. Only RNA 2 encoding the glycoprotein was not detected. This RT-PCR detection of TiRSaV indicates ingestion and perhaps acquisition of the virus by eriophyid mites.

6.4 DISCUSSION

The common green ti variety was introduced into Hawaii centuries ago by early Polynesian voyagers. Its pollen and seeds are not viable (Hinkle 2007) and it has therefore been propagated exclusively by vegetative cuttings since its introduction, making it prone to infection by systemic pathogens such as viruses. Indeed, individual ti plants in Hawaii can be co-infected with at least four species in the genus

Velarivirus (Melzer et al. 2013b). None of these velariviruses, however, were associated with ti ringspot (Melzer et al. 2013a). The presence of eriophyid mites on ti plants and the similarity in symptoms between ti ringspot and those caused or associated with *Emaravirus* infection (Figure 6.1) led to the testing of symptomatic ti plants for the presence of an *Emaravirus* member (Melzer et al. 2014). Cloning and sequencing of this product suggested that an undescribed *Emaravirus* member showing low sequence identity with sequences in GenBank was present in symptomatic ti plants. The name ‘ti ringspot-associated virus’ (TiRSaV) was suggested for this ti pathogen (Melzer et al. 2014). Similar to asymptomatic newly emerging ti leaves from TiRSaV-infected plants, it has been observed newly emerged leaves of *Ficus carica* plants in Hawaii are often free of symptoms of fig mosaic, whereas mature leaves display symptoms, suggesting the delayed onset of foliar symptoms is not unique to ti ringspot.

In the first approach adopted by Park (2016) to characterize the genome of TiRSaV, HTS of a dsRNA library generated by a shotgun approach derived from symptomatic ti plant produced relatively little sequence information on the new virus. Conversely, HTS generated a large amount of sequence information on the previously characterized velariviruses that co-infected the plant. This may be a reflection on the relative titers of velariviruses and emaraviruses in ti plants but may also be due to different amounts of dsRNA produced by +ssRNA and –ssRNA viruses during replication and/or transcription. However, in the second approach adopted in this study, HTS performed on PCR products generated using the emaravirus conserved terminal primer together with conventional sequencing allowed the determination of the complete sequences of four of the five segments of the TiRSaV genome, whose molecular features are consistently related to those of emaraviruses (Figure 6.3). The inability of different polymerases to amplify the complete sequence of the RdRp of emaraviruses using the emaravirus consensus terminal primer has been previously reported (Hassan et al. 2017), so the use of degenerate primers located in the *Emaravirus* RdRp motifs and partial fragments generated by the shotgun library addressed this issue and allowed the complete sequence of RNA 1 to be obtained. The phylogenetic relationships inferred from the protein sequences of the emaraviruses, putative emaraviruses, and TiRSaV clearly places the latter within the genus *Emaravirus*, specifically in a clade with RLBV, HPWMoV and PVBV (Figure 2.4). Four of the TiRSaV proteins, p1, p2, p3, and p5, showed the highest homology to RLBV, while p4 showed the highest homology to HPWMoV (Figure 6.4 and Table 6.3).

The genomes of RLBV and HPWMoV have both been reported to consist of eight genomic segments (McGavin et al. 2012; Tatineni et al. 2014; Lu et al. 2015). These viruses belong to a phylogenetically distinct clade in the genus (Figure 6.4) and are characterized by the presence of the four core segments and an additional four segments coding for putative proteins with unknown function and no apparent homology with other emaravirus proteins. However, TiRSaV genome consisted of the four core segments of the emaraviruses and an additional segment coding for putative protein with unknown function and similarity to the p8 of RLBV and HPWMoV (Figure 6.3). Attempts to identify additional TiRSaV genome segments using RT-PCR and a deep exploration in the HTS dataset failed, but we cannot exclude the existence of additional TiRSaV segments, as additional segments in other emaraviruses remained elusive until further studies were undertaken (Lu et al. 2015; Di Bello et al. 2016; Elbeaino et al. 2012). PVBV is a putative *Emaravirus* member infecting blue palo verde trees in Arizona, likely to be vectored by the eriophyid mite *Aculus cercidi*, and closely associated to witches broom disease of the trees. This virus has been reported to have four RNA segments coding for the core proteins of emaraviruses that show the highest homology to HPWMoV proteins (Ilyas et al. 2018). Both PVBV and TiRSaV were characterized using HTS approaches and belong to the same clade in the phylogeny of emaraviruses. This may suggest the four core segments of emaraviruses are enough to cause infection and disease in their hosts and additional segments may help to enhance virulence or pathogenicity (or perhaps transmissibility?). Recently, Verchot et al. (2020) demonstrated that the four core segments of RRV are enough to establish infection on both rose and *N. benthamiana* plants using a RRV reverse genetics system based on the anti-genome delivery of the virus to the plants.

A lack of consistent homology has been reported among the proteins p5-p10 coded by emaraviruses (Tatineni et al. 2014; Hassan et al. 2017) suggesting that some emaraviruses have more than 10 RNA segments (Stewart 2016). Recently, Gupta et al. (2018) reported that HPWMoV p7 and p8 are suppressors of RNA silencing. In contrast, Lu et al. (2015) demonstrated that RLBV p6 and p7 are related to RLBV pathogenicity, although they could not detect RNA silencing suppression in RLBV p2-p8. Further characterization of the function of these putative proteins may help researchers better understand the evolution of emaraviruses and the apparent discrepancy in the number of genomic RNA segments between species.

Eriophyid mites have been identified as the vectors of other emaraviruses (McGavin et al. 2012; Mielke-Ehret et al. 2010; Caglayan et al. 2012). In Hawaii, both symptomatic and asymptomatic ti plants have been found to be infested with these mites. A preliminary molecular examination of mites collected in this study suggest at least two species coexist on symptomatic leaves and based on the low sequence identities

between each other and with current accessions in GenBank, these both may represent previously undescribed species. Four out of five segments of the TiRSaV genome were detected in this mixed sample, making these mites candidates for future taxonomic and virus transmission efforts.

TiRSaV was successfully transmitted mechanically to multiple experimental herbaceous plants including *Nicotiana* and cucurbit species. Zheng et al (2017) were similarly able to mechanically transmit AcCRaV to *N. benthamiana*, although not all AcCRaV-infected plants showed symptoms. The ability of TiRSaV to systemically infect these experimental hosts will facilitate any future virus purification experiments for the purpose of antibody production.

At present, ti ringspot has not been reported outside of Hawaii. Since ti is a globally popular ornamental grown both indoors and outdoors, the strong association of ti ringspot with TiRSaV and the different assays implemented to detect the virus and its RNA segments are relevant for preventing the further spread of the disease in Hawaii and other locations where the disease is not yet present.

6.5 LITERATURE CITED

- Afgan, E., Baker, D., van den Beek, M., Blankenberg, D., Bouvier, D., Čech, M., Chilton, J., Clements, D., Coraor, N., Eberhard, C., Grüning, B., Guerler, A., Hillman-Jackson, J., Von Kuster, G., Rasche, E., Soranzo, N., Turaga, N., Taylor, J., Nekrutenko, A., and Goecks, J. 2016. The Galaxy platform for accessible, reproducible and collaborative biomedical analyses: 2016 update. *Nucleic Acids Res.* 44:W3–W10 (doi:10.1093/nar/gkw343).
- Altschul, S.F., Madden, T.L., Schäffer, A.A., Zhang, J., Zhang, Z., Miller, W., and Lipman, D.J. 1997. Gapped BLAST and PSI-BLAST: a new generation of protein database search programs. *Nucleic Acids Res.* 25:3389–3402.
- Bolger, A.M., Lohse, M., and Usadel, B. 2014. Trimmomatic: a flexible trimmer for Illumina sequence data. *Bioinformatics* 30:2114–2120.
- Bouckaert, R., Heled, J., Kühnert, D., Vaughan, T., Wu, C.-H., Xie, D., Suchard, M.A., Rambaut, A., and Drummond, A.J. 2014. BEAST 2: A Software Platform for Bayesian Evolutionary Analysis. *PLoS Comput. Biol.* 10:e1003537 (doi:10.1371/journal.pcbi.1003537).
- Caglayan, K., Elci1, E., Ulubas Serce, C., Kaya, K., Gazel, M., and Medina, V. 2012. Detection of fig mosaic virus in viruliferous eriophyid mite *Aceria ficus*. *J. Plant Pathol.* 94:629-634.
- Di Bello, P.L., Laney, A.G., Druciarek, T., Ho, T., Gergerich, R.C., Keller, K.E., Martin, R.R., and Tzanetakis, I.E. 2016. A novel emaravirus is associated with redbud yellow ringspot disease. *Virus Res.* 222:41–47.
- Druciarek, T., Lewandowski, M., and Tzanetakis, I. 2018. Direct RT-PCR assay for virus detection and eriophyoid species identification. Poster presented at: International Congress of Plant Pathology 2018, Plant Health in a Global Economy. July 29-August 3, 2018. Boston, MA.
- Elbeaino, T., Digiario, M., and Martelli, G.P. 2012. RNA-5 and -6, two additional negative-sense RNA segments associated with fig mosaic virus. *J. Plant Pathol.* 94:421-425.
- Elbeaino, T., Whitfield, A., Sharma, M., and Digiario, M. 2013. Emaravirus-specific degenerate PCR primers allowed the identification of partial RNA-dependent RNA polymerase sequences of Maize red stripe virus and Pigeonpea sterility mosaic virus. *J Virol. Methods* 188:37–40.
- Ewels, P., Magnusson, M., Lundin, S., and Käller, M. 2016. MultiQC: summarize analysis results for multiple tools and samples in a single report. *Bioinformatics* 32:3047–3048.

- Fenton, B., Malloch, G., and Moxey, E. 1997. Analysis of eriophyid mite rDNA internal transcribed spacer sequences reveals variable simple sequence repeats. *Insect Mol. Biol.* 6:23-32.
- Grabherr, M.G., Haas, B.J., Yassour, M., Levin, J. Z., Thompson, D. A., Amit, I., Adiconis, X., Fan, L., Raychowdhury, R., Zeng, Q., Chen, Z., Mauceli, E., Hacohen, N., Gnirke, A., Rhind, N., di Palma, F., Birren, B.W., Nusbaum, C., Lindblad-Toh, K., Friedman, N., and Regev, A. 2011. Full-length transcriptome assembly from RNA-Seq data without a reference genome. *Nat. Biotechnol.* 29:644–652.
- Gupta, A.K., Hein, G.L., Graybosch, R.A., and Tatineni, S. 2018. Octapartite negative-sense RNA genome of High Plains wheat mosaic virus encodes two suppressors of RNA silencing. *Virology*, 518:152–162.
- Hassan, M., Di Bello, P.L., Keller, K.E., Martin, R.R., Sabanadzovic, S., and Tzanetakis, I.E. 2017. A new, widespread emaravirus discovered in blackberry. *Virus Res.* 235:1–5.
- Hinkle, A.E. 2007. Population structure of Pacific *Cordyline fruticosa* (Laxmanniaceae) with implications for human settlement of Polynesia. *Am. J. Bot.* 94:828–839.
- Huang, X. and Miller, W. 1991. A time-efficient, linear-space local similarity algorithm. *Adv. Appl. Math.* 12:337–357.
- Ilyas, M., Avelar, A.S., Schuch, U., and Brown, J.K. 2018. First report of an emaravirus associated with witches broom disease and eriophyid mite infestations of the blue palo verde tree in Arizona. *Plant Dis.* 102:1863.
- Kearse, M., Moir, R., Wilson, A., Stones-Havas, S., Cheung, M., Sturrock, S., Buxton, S., Cooper, A., Markowitz, S., Duran, C., Thierer, T., Ashton, B., Meintjes, P., and Drummond, A. 2012. Geneious Basic: An integrated and extendable desktop software platform for the organization and analysis of sequence data. *Bioinformatics* 28:1647–1649.
- Kumar, P.L., Fenton, B., Duncan, G., Jones, A., Sreenivasulu, P., and Reddy, D. 2001. Assessment of variation in *Aceria cajani* using analysis of rDNA ITS regions and scanning electron microscopy: implications for the variability observed in host plant resistance to pigeonpea sterility mosaic disease. *Ann. Appl. Biol.* 139:61-73.
- Kumar, P.L., Jones, A.T., and Reddy, D.V.R. 2003. A novel mite-transmitted virus with a divided RNA genome closely associated with pigeonpea sterility mosaic disease. *Phytopathology* 93:71–81.
- Kumar, S., Stecher, G., and Tamura, K. 2016. MEGA7: Molecular Evolutionary Genetics Analysis Version 7.0 for Bigger Datasets. *Mol. Biol. Evol.* 33:1870–1874.

- Langmead, B., Trapnell, C., Pop, M., and Salzberg, S.L. 2009. Ultrafast and memory-efficient alignment of short DNA sequences to the human genome. *Genome Biol.* 10:R25 (doi:10.1186/gb-2009-10-3-r25).
- Lu, Y., McGavin, W., Cock, P.J.A., Schnettler, E., Yan, F., Chen, J., and MacFarlane, S. A. 2015. Newly identified RNAs of raspberry leaf blotch virus encoding a related group of proteins. *J. Gen. Virol.* 96:3432–3439.
- McGavin, W.J., Mitchell, C., Cock, P.J.A., Wright, K.M., and MacFarlane, S.A. 2012. Raspberry leaf blotch virus, a putative new member of the genus Emaravirus, encodes a novel genomic RNA. *J. Gen. Virol.* 93:430–437.
- Melzer, M.J., Sether, D.M., Borth, W.B., Mersino, E.F., and Hu, J.S. 2011. An assemblage of closteroviruses infects Hawaiian ti (*Cordyline fruticosa* L.). *Virus Genes* 42:254–260.
- Melzer, M., Ayin, C., Sugano, J., Uchida, J., Kawate, M., Borth, W., and Hu, J. 2013a. Differentiation and Distribution of Cordyline Viruses 1–4 in Hawaiian ti Plants (*Cordyline fruticosa* L.). *Viruses* 5:1655–1663.
- Melzer, M.J., Sugano, J.S., Uchida, J.Y., Borth, W.B., Kawate, M.K., and Hu, J.S. 2013b. Molecular characterization of closteroviruses infecting *Cordyline fruticosa* L. in Hawaii. *Front. Microbiol.* 4:39 (doi:10.3389/fmicb.2013.00039).
- Mielke-Ehret, N. and Mühlbach, H.-P. 2012. Emaravirus: a novel genus of multipartite, negative strand RNA plant viruses. *Viruses* 4:1515–1536.
- Mielke-Ehret, N., Thoma, J., Schlattermund, N., and Mühlbach, H.P. 2010. Detection of European mountain ash ringspot-associated virus-specific RNA and protein P3 in the pear leaf blister mite *Phytoptus pyri* (Eriophyidae). *Arch. Virol.* 155:987–991.
- Mironov, S.V., Dabert, J., and Dabert, M. 2012. A new feather mite species of the genus *Proctophyllodes* Robin, 1877 (Astigmata: Proctophylloidea) from the long-tailed tit *Aegithalos caudatus* (Passeriformes: Aegithalidae)-morphological description with DNA barcode data. *Zootaxa* 3253:54–61.
- Morris, T.J. and Dodds, J.A. 1979. Isolation and Analysis of Double-Stranded RNA from Virus-Infected Plant and Fungal Tissue. *Phytopathology*, 69:854-858.
- Mühlbach, H.-P. and Mielke-Ehret, N. 2012. Emaravirus. In *Virus Taxonomy: Classification and Nomenclature of Viruses, Ninth Report of the International Committee on Taxonomy of Viruses*; King, A.M.Q., Adams, M.J., Carstens, E.B, Lefkowitz, E.J., Eds.; Elsevier Academic Press: London, UK, 2012; pp. 767–769, ISBN 0123846846.

- Olmedo-Velarde, A., Ochoa-Corona, F.M., and Elbeaino, T. 2016. Towards a broad detection of emaraviruses: Endpoint RT-PCR. *Phytopathology* 106:S4.118
- Park, A. (2016). Molecular Characterization of Ti Ringspot Associated Emaravirus and the Development of Assays for Its Detection. M.S. thesis. University of Hawaii at Manoa.
- Sonnenberg, R., Wolte, A.W., and Tautz, D. 2007. An evaluation of LSU rDNA D1-D2 sequences for their use in species identification. *Front. Zool.* 4:6 (doi: 10.1186/1742-9994-4-6).
- Stewart, L.R. 2016. Sequence diversity of wheat mosaic virus isolates. *Virus Res.* 213:299–303.
- Tatineni, S., McMechan, A.J., Wosula, E.N., Wegulo, S.N., Graybosch, R.A., French, R., and Hein, G. L. 2014. An eriophyid mite-transmitted plant virus contains eight genomic RNA segments with unusual heterogeneity in the nucleocapsid protein. *J. Virol.* 88:11834–11845.
- Thompson, J.D., Higgins, D.G., and Gibson, T.J. 1994. CLUSTAL W: improving the sensitivity of progressive multiple sequence alignment through sequence weighting, position-specific gap penalties and weight matrix choice. *Nucleic Acids Res.* 22:4673–4680.
- Zerbino, D.R. and Birney, E. 2008. Velvet: Algorithms for de novo short read assembly using de Bruijn graphs. *Genome Res.* 18:821–829.
- Zheng, Y., Navarro, B., Wang, G., Wang, Y. Yang, Z., Xu, W., Zhu, C., Wang, L., Di Serio, F., and Hong, N. 2017. Actinidia chlorotic ringspot-associated virus: a novel emaravirus infecting kiwifruit plants. *Mol. Plant Pathol.* 18:569-581.

CHAPTER VII

CONCLUSIONS AND FUTURE RESEARCH DIRECTIONS

Passion fruit was found as a new host for citrus leprosis virus C2 (CiLV-C2). Considering the widespread presence of the passion fruit and hibiscus, another host of the virus in Hawaii, and the absence of natural infection of CiLV-C2 in citrus hosts in the state, it is worth examining the ability of different isolates of the virus to infect citrus hosts under experimental conditions. An orchid strain of orchid fleck virus (OFV) was found, causing citrus leprosis in a semi-abandoned orchard on Hawaii Island. Although eradication efforts are ongoing where OFV was found, delimiting surveys are needed to evaluate how widespread OFV is in citrus elsewhere in the state and evaluate its presence in other hosts, including orchids, ti plants, and other ornamentals that might be unreported hosts of the virus. Hibiscus yellow blotch virus (HYBV), a new *Brevipalpus*-transmitted virus (BTV), was characterized from symptomatic hibiscus plants. Considering its close relationship with cileviruses and temporary placement within the *Cilevirus* clade, it is worth evaluating the ability of HYBV to infect citrus hosts under experimental conditions using *Brevipalpus yothersi* mites which is a possible vector of the virus.

Although low genetic diversity was found among citrus and hibiscus isolates of hibiscus green spot virus 2 (HGSV-2), a few differences were found at the protein level that may impact virus-host or virus-vector interactions. It was also demonstrated that *B. azores* can transmit HGSV-2 from citrus to citrus and from citrus to hibiscus. However, *B. papayensis* mites have been associated with HGSV-2 symptomatic hibiscus plants. Therefore, evaluating the potential vector ability of *B. papayensis* and other *Brevipalpus* species is required to understand further how HGSV-2 may move from host to host. Moreover, the basis of a reverse genetics system for HGSV-2 was developed in the form of an infectious clone of the virus. This genetic tool can be used to perform fundamental studies and further our knowledge of kitavirid interactions with their plant and mite hosts. The addition of a green fluorescent protein (GFP) fusion protein will help monitor the movement of the infectious clone of HGSV-2 *in planta*. Two good candidate genes for expressing the fusion protein can be the two proteins coded in RNA 2, which are suspected to be involved in the virus movement. Perhaps the factors that prevent systemic movement in their plant host can then be elucidated. Once a suitable agrodelivery method is developed, this tool can also be used to assess the susceptibility of different citrus hosts to HGSV-2.

The virome of tenuipalpid mites collected from several hosts from two Hawaiian Islands was comprised of several putative new virus species but was predominated by picornavirids. Further molecular and biological characterization of these picornavirids with possible biological control options for these mites

should be examined. These results also established a baseline method to investigate the presence of BTVs in populations of flat mites from more hosts and additional geographic locations. Considering the economic losses, some BTVs can cause in several crops, and that a putative new BTV-like virus was found in tenuipalpid mites collected from pineapple, it is necessary to fully characterize the genome of this virus, evaluate its ability to infect pineapple and assess its impact to the crop.

The genome of ti ringspot-associated virus (TiRSaV) was fully characterized and found to consist of five RNAs, which is congruent with the genomic composition of other emaraviruses. All these genomic segments were found only in plants presenting ringspot symptoms. Considering that at least two uncharacterized eriophyid mite species were found on ti plants that tested positive for TiRSaV, future work to describe these two mite species and determine their role in transmitting TiRSaV is warranted.

This study has expanded our knowledge of mite-associated viruses present in Hawaiian agroecosystems. Several new and known mite-associated viruses were characterized at the molecular and biological levels. Due to the emergence and federal actionable pest status for some of these viruses, this knowledge will be essential for growing healthy commodities in Hawaii and the US.